

1-1-1970

Static and dynamic light scattering study of crystalline polymer films.

Takeji Hashimoto
University of Massachusetts Amherst

Follow this and additional works at: https://scholarworks.umass.edu/dissertations_1

Recommended Citation

Hashimoto, Takeji, "Static and dynamic light scattering study of crystalline polymer films." (1970).
Doctoral Dissertations 1896 - February 2014. 584.
<https://doi.org/10.7275/vvkh-j974> https://scholarworks.umass.edu/dissertations_1/584

This Open Access Dissertation is brought to you for free and open access by ScholarWorks@UMass Amherst. It has been accepted for inclusion in Doctoral Dissertations 1896 - February 2014 by an authorized administrator of ScholarWorks@UMass Amherst. For more information, please contact scholarworks@library.umass.edu.



312066 0015 4482 2

STATIC AND DYNAMIC LIGHT SCATTERING STUDY
OF
CRYSTALLINE POLYMER FILMS

A Dissertation Presented

by

Takeji Hashimoto

Submitted to the Graduate School of the
University of Massachusetts in
Partial fulfillment of the requirements for the degree of

DOCTOR OF PHILOSOPHY

October 1970

Major Subject: Polymer Science and Engineering

STATIC AND DYNAMIC LIGHT SCATTERING STUDY

OF


CRYSTALLINE POLYMER FILMS

A Dissertation Presented

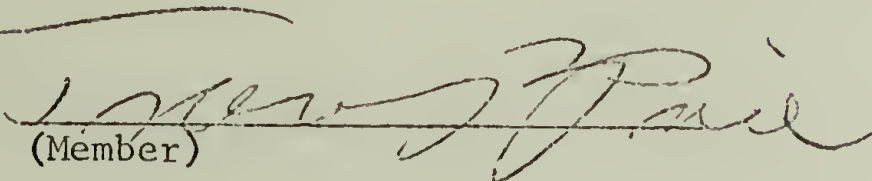
by

Takeji Hashimoto

Approved as to style and content by:


(Chairman of Committee)


(Member)


(Member)

October

1970

To

Setsuko Hashimoto

A C K N O W L E D G E M E N T

The author wishes to express his appreciation to the Petroleum Research Fund of American Chemical Society and to the Office of Naval Research for financial assistance.

The author wishes to express his sincere appreciation to Professor Richard S. Stein, thesis director, for his guidance, encouragement and many helpful discussions throughout the course of this work. The helpful suggestions of Professors Roger S. Porter and Fraser P. Price, the other members of the thesis committee are also gratefully acknowledged.

The author wishes to express his sincere appreciations to Professor Hiromichi Kawai, his former advisor in Kyoto University, Kyoto, Japan for his guidance and encouragement throughout the course of development of the dynamic light scattering technique.

Acknowledgement and thanks go to a number of coworkers at the Polymer Research Insititute, particularly for the assistance of Mr. D. A. Keedy in the design and construction of the dynamic light scattering apparatus.

The author thanks to Mrs. Sophia Kinney and Miss Helen Piekarski for providing secretarial work during the course of the work.

Computer calculations were carried out at the University of Massachusetts Research Computing Center.

The support of the Fulbright Commission for a Visting Scholarship at University of Massachusetts is appreciated.

The author thanks to his wife, Setsuko for typing the finished copy.

T A B L E O F C O N T E N T S

INTRODUCTION	1
PART I THE LIGHT SCATTERING STUDIES ON SYSTEMS HAVING NON-RANDOM ORIENTATION	
CHAPTER I INTRODUCTION AND PREVIOUS WORK	9
CHAPTER II NON-RANDOM THEORY FOR UNORIENTED SYSTEM	
II-1 The Model	17
II-2 Delta Function Approximation	22
II-3 Numerical Calculation	24
II-4 Conclusions	29
CHAPTER III NON-RANDOM THEORY FOR ORIENTED SYSTEM	
III-1 General Descriptions of the Scattering from System Based upon Harmonic Expansion Approach	30
III-2 Delta Function Approximation	41
III-3 Gaussian Correlation Functions	42
III-4 Numerical Calculations	46
PART II THE LIGHT SCATTERING STUDIES ON SPHERULITIC POLYMERS	
CHAPTER I INTRODUCTION	52
CHAPTER II THE SCATTERING OF LIGHT BY UNDEFORMED DISORDERED SPHERULITES	
II-1 The Effect of Disorder in the Magnitude of the Anisotropy	59
II-2 Case of Combined Disorder in Orientation and Anisotropy	68
II-3 The V_V Component of Scattering and the Separation of Density and Orientation Fluctuations	72

CHAPTER III	THE SCATTERING OF LIGHT BY DEFORMED DISORDERED SPHERULITES	
III-1	Introduction	78
III-2	The Calculation	79
III-3	Case of Angular Disorder	82
III-4	Results	87
III-5	Conclusions	91
PART III THE DYNAMIC LIGHT SCATTERING STUDIES ON SPHERULITIC POLYMERS		
CHAPTER I	INTRODUCTION AND PREVIOUS WORK	93
CHAPTER II	THE APPARATUS	
II-1	Light Source Part	97
II-2	Deformation Apparatus	99
II-3	Detecting Part	100
II-4	Variation of Temperature and Frequency	109
CHAPTER III	PRINCIPLE OF THE DLS MEASUREMENTS AND SOME PRELIMINARY RESULTS	
III-1	Principle of the Measurements	111
III-2	Some Preliminary Results	117
CHAPTER IV	ANGULAR DEPENDENCE OF THE DLS	
IV-1	Introduction	124
IV-2	Some Static Experimental Results	127
IV-3	Ω Dependence of the DLS at Small Scattering Angle	131
IV-4	Ω Dependence of the DLS at High Scattering Angle	136

IV-5	Some Conclusions of the Study on the Angular Dependence of the DLS	139
CHAPTER V	TEMPERATURE DEPENDENCE OF THE DLS	
V-1	Dynamic Mechanical Properties of the Sample	142
V-2	Temperature Dependence of the DLS	143
CHAPTER VI	A THEORETICAL STUDY ON THE DLS ARISING FROM THE DEFORMATION OF SPHERULITES	
VI-1	Introduction	149
VI-2	Application to the DLS	155
VI-3	Results of Numerical Calculations and Comparison with the Experimental Results	158
CHAPTER VII	RELATIONSHIP TO OTHER OPTICAL AND MECHANICAL STUDY	166
VII-1	Relationship to Static X-ray Study	167
VII-2	Relationship to Dynamic X-ray Study and Dynamic Mechanical Properties	173
VII-3	A Simple Mechanical Model Treatment for Rheo-Optical Properties	179
PART IV	FUTURE WORK	
	Theoretical	188
	Experimental	192
	BIBLIOGRAPHY	197
	CAPTIONS FOR FIGURES	204

I N T R O D U C T I O N

The light scattering from crystalline polymer films has been used to characterize crystalline superstructures such as spherulites, rods and disks which are usually found in crystalline polymer films prepared from melts and cast or molded from concentrated solutions. The scattering has been shown to arise principally from internal heterogeneities of both density and orientation of optic axes of scattering elements occurring in polymer films over distances comparable with the wavelength of the light¹⁻³. It is possible by analyzing and separating the heterogeneities to evaluate the size, shape and type of the superstructures as a whole as well as the internal perfection of such superstructures in terms of both density and orientation. However the separation of the density and orientation heterogeneities, and the separation of the internal heterogeneities occurring in such superstructures from the properties related to the superstructure as a whole are still not completely successful at this moment.

The light scattering technique has been also applied to elucidate deformation mechanism of such superstructures⁴⁻⁷. In principle, one can analyze the deformation of the superstructures as a whole from the change of the entire scattering intensity distribution at low scattering angles and the change of the internal heterogeneities within the superstructures by that at high scattering angles. Such sort of analysis in terms of deformation mechanisms can again be carried out, in principle, from the point of view of both density and orientation. The change of the density

heterogeneities may give additional information about the interpretation of the deformation mechanism over that obtained from the orientational heterogeneities. The other optical techniques such as wide angle x-ray, birefringence, UV-, Visible- and IR-dichroism are only associated with orientation of individual crystallites, amorphous chains or special chemical groups. The cooperative change in orientation of these structural units gives rise to the change of the orientation heterogeneities related to the light scattering technique.

The change of the internal heterogeneities may not necessarily occur uniformly throughout the superstructure but may be quite angularly dependent with respect to the stretching direction. In case of spherulitic superstructure, the portion of the structure located parallel to the stretching direction (polar part) is deformed in a different manner to that in a perpendicular direction to stretching (equatorial part)⁸⁻¹³. Such angular dependence of the spherulite deformation may be quite temperature dependent. Just as the angular dependence of the deformation has been interpreted by using the reciprocity principle between the small angle x-ray scattering and its objects^{12,13}, a similar interpretation may be also applied to the light scattering. The light scattering technique may see the intra- and inter-lamellar deformations in different angular portions of the spherulite. The angular dependence of the deformation may be more directly studied by using the light scattering technique than the other optical techniques mentioned above since all methods except the small angle x-ray technique cannot distinguish the structure units located in the polar part from those in the equatorial part except the case where

a microbeam technique is employed for those methods^{14,15}.

The light scattering technique can also be applied to dynamic studies where the change of the scattered intensity upon deformation is observed as a function of the time-scale of the experiments. The technique can be combined with dynamic mechanical experiments under transient loading patterns as employed in creep and stress relaxation experiments and with periodic or dynamic loading. From such experiments one may obtain informations about the time dependent response of the superstructure as a whole and that of the internal structures as well in terms of both density and orientation. The time dependent response of the internal structures may be, in general, angularly dependent. The technique may be connected to dynamic mechanical experiments to understand the mechanical properties of bulk crystalline polymers.

It should be emphasized here that the light scattering technique by itself does not provide enough informations but that it must be combined with other optical techniques mentioned above in order to elucidate the relationship between the deformation mechanism and the mechanical properties of the crystalline polymers.

On the basis of the concepts discussed above this work has been carried out in order to study the relationship between the morphology and deformation mechanism of the crystalline superstructures by means of static and dynamic light scattering.

An outline of the thesis is briefly explained as follows.

In Part I, a statistical description of the light scattering from the crystalline superstructures is discussed on the basis of the general

harmonic expansion approach and its special case, the delta function approach in order to describe the nature of the non-random orientation fluctuations found in such systems. In Chapter II [adapted in part from J. Polymer Sci., A2, 8, 1127 (1970) with R. S. Stein], the theory is developed for unorientated systems and in Chapter III [adapted in part from J. Polymer Sci., A2 (in press) with R. S. Stein] the theory is extended to oriented systems. Although the general approach can explain the whole spectrum of experimental systems ranging from the structure composed of random arrays of crystallites (random orientation fluctuations), through rod or disk like superstructure to perfect spherulitic superstructure (one of extreme case of non-random orientation fluctuations), such a general theory is complex and the association of the higher order expansion coefficients with physically visualizable structural variables is difficult. The extensions of the theory to three dimensional case and to oriented systems would compound this complexity. Because of such complexity, the delta function approximation is introduced in the general theory, which restricts the theory to systems having rod and disk-like crystalline superstructures. The scattering from such systems are described in terms of the various properties of such superstructures, i. e., (1) size and perfection, (2) type (for examples rod, disk and so on), and (3) mutual packing of superstructures in space. In case of oriented systems, the scattering also depends upon (4) orientation of the superstructure and (5) angular dependences of perfection and mutual packing of superstructures with respect to stretching direction.

In Part II, the scattering is discussed for the system having spherulitic superstructure of crystalline materials with some degree of internal imperfection. The over-all symmetry of the spherulitic structure is treated by assuming a model of the anisotropic sphere³ and the internal imperfections are treated in terms of the magnitude and correlation function for the internal heterogeneities by using a statistical approach.

In Chapter II [adapted from a paper to be published with R. S. Stein] effects of such internal heterogeneities in terms of density, anisotropy and orientation on the scattering intensity distributions are discussed for undeformed spherulites. In Chapter III [adapted from a paper submitted for publication with R. S. Stein] the theory is extended to the deformed spherulites. The effects of angular dependence of the internal orientation heterogeneities on the scattering patterns are discussed.

In Part III, the static light scattering studies are applied to the dynamic light scattering (DLS) in which the variation of the light scattering intensity from a sample subjected to stationery sinusoidal strain is studied as a function of frequency and temperature of the experiment. In Chapter II [presented in part in the APS meeting at Philadelphia, March 1969 with M. Motegi, H. Kawai and R. S. Stein, and in part in the IUPAC meeting at Leiden, the Netherlands, 1970 with R. S. Stein and P. J. Phillips] the apparatus constructed for the DLS measurements are described. In Chapter III a principle and some preliminary experiments of the DLS for medium density polyethylene (MDPE) are discussed. In Chapter IV [presented in part in the IUPAC meeting, Leiden, the Netherlands, 1970

with R. S. Stein and P. J. Phillips] and Chapter V, the experimental results on angular dependence (Ω) and temperature dependence of the DLS are discussed qualitatively for the MDPE. Some speculations on the deformation of the equatorial part of the spherulite involves time and temperature dependent deformation processes to the bulk strain. In Chapter VI [presented in part in the IUPAC meeting, Leiden, the Netherlands, 1970 with R. S. Stein and P. J. Phillips] some theoretical interpretations are discussed on the experimental angular dependences of the DLS under cross-polarizers based upon the deformation model of the spherulite proposed by van Aartsen and Stein⁵. The experimental results are explained in terms of time-dependent internal reorientation processes, i. e., (1) twisting of crystallites around their crystallographic b-axes occurring predominantly in the equatorial part of the spherulites and (2) tilting of the crystallites around their a-axes occurring predominantly in the polar part. In Chapter VII, the results of the DLS study shall be briefly discussed in relation to other type of experiments, especially to the dynamic experiments such as dynamic mechanical, x-ray and birefringence experiments.

Finally in Part IV some other interesting studies which cannot be carried out through this work shall be proposed as a future work.

P A R T I

THE LIGHT SCATTERING STUDIES ON SYSTEMS
HAVING NON-RANDOM ORIENTATION

In this part we shall discuss the scattering of light from systems having so called non-random orientation fluctuations for both unoriented and oriented systems. The scattering theories will be developed by using a statistical approach in which the scattering is described in terms of the magnitude of statistical fluctuations of orientation of the optic axes of optically anisotropic scattering elements and their correlations. For simplicity, the theories will be restricted to the two-dimensional case with optic axes confined to lie in the plane perpendicular to incident beam.

In most of the crystalline polymer films the crystallites generally tend to form more or less crystalline domains rather than randomly distributed arrays of crystallites. In such cases the orientation correlations may become strongly anisotropic in a sense that the correlations are greater along the extension direction. Namely, the orientation correlations are non-random in such cases. The theory based upon this concept may be applicable to structures having non-random orientation fluctuations such as rod- and disk-like structures as well as structures composed of random arrays of crystallites (i. e. structures having random orientation fluctuations) as an extreme case of the theory. However an application of such statistical theories to spherulitic polymers may be rather poor except the theory based upon the general harmonic expansion

approach which will be discussed in following chapters. The scattering from spherulitic systems shall be discussed in Part II.

C H A P T E R I

INTRODUCTION AND PREVIOUS WORK

The theory for the scattering of light for polymer films having both random¹⁶ and non-random^{2,17} orientation correlations has been discussed previously. In both cases, scattering arises principally because of the correlation in orientation between the optic axes of anisotropic scattering volume elements. The variation of the scattered intensity with the scattering angle θ (Fig. I-1) depends upon the variation of the orientation correlation with the distance r between volume elements (Fig. I-2). The larger the distance over which the correlation persists, the more rapidly will the scattered intensity decrease with increasing θ .

For the case of random orientation correlations, the orientation correlation was assumed to be independent of the angle β (Fig. I-2) between one of the optic axes and the vector r but only dependent upon the magnitude of r . This led to region of correlation which were spherically symmetrical in shape and to scattering patterns which (at small values of θ) were cylindrically symmetrical about the incident beam. Two types of scattering experiments were proposed for unoriented systems; one in which the intensity was designated as $I_{||}$ in which the polarizer angle ψ_1 and analyzer angle ψ_2 (Fig. I-1) were changed simultaneously so that $\psi = \psi_1 = \psi_2$, and a second where the intensity was designated as I_{\perp} in which the polarizer and analyzer angles were kept crossed so that $\psi = \psi_1 = \psi_2 + 90^\circ$. It was shown that at small values of θ , the values of $I_{||}$

and I_+ were independent of ψ and at larger values, the variation occurred in a predictable manner. The experimental results on polypropylene films were shown to confirm to this model¹⁸. Recently, Prins and coworkers²¹ have proposed a slightly different relationship between ψ_1 and ψ_2 for $I_{||}$ and I_+ experiments leading to constancy of intensity even at large values of θ and I_+ intensity is independent of density fluctuations. The newly proposed relationship between ψ_1 and ψ_2 for $I_{||}$ and I_+ experiments shall be discussed in Appendix I.

Non-random orientation correlations are defined as those for which the orientation correlation is dependent upon β . Special cases of scattering from spherulites^{6,19}, rods and disks²⁰ have been treated where it is shown that $I_{||}$ and I_+ become highly dependent upon ψ . Such dependence is found for spherulitic polymers in agreement with theory^{2,17}.

Most crystalline polymers are intermediate between these extremes. A ψ dependence of scattering has been found for many polymers possessing spherulite type order but the dependence is less than that predicted on the basis of theories for scattering from perfect spherulites. This indicates that there is a greater degree of randomness of correlation than for perfect spherulites. One method for describing such systems employed by Keijzers, van Aartsen and Prins (KVP)²¹ is in terms of a "two-phase model" in which the scattering is thought to consist of two components, one characteristic of the scattering from perfect spherulites and one arising from the random structure

$$I = \phi_S I_S + \phi_R I_R \quad (1)$$

The previous theories for I_S and I_R are used, and ϕ_S and ϕ_R are the fractions of the two components. Since most of the systems are completely filled with spherulites, the random component consists of less perfectly ordered material within the spherulite. An alternate approach to such a system might be to consider it in terms of a single phase completely spherulitic system with density fluctuations within spheres by Stein, Wilson and Stidham²². Treatments of orientational disorder and anisotropy disorder within spherulites shall be discussed in Part II.

These spherulite type theories are best for treating high degrees of non-randomness where the symmetry of spherulitic order dominates. For systems that are fairly random, a more reasonable approach is to consider perturbations of the random theory. Two approaches of this type have been described:

(a) A rod-disk interpolation theory² has been described involving an interpolation parameter ϵ . For $\epsilon = 0$, the scattering is random but as ϵ approaches $+1$, the scattering approaches that characteristic of an assembly of isolated rods while as ϵ approaches -1 , the scattering is like that of disks. While the theory predicts some features of the observed scattering, it is semi-empirical, mathematically unappealing and requires modifications leading to an unreasonable number of parameters in order to fit data.

(b) A "harmonic expansion theory"^{2,17} in which the correlation

functions are expanded in Fourier series in β in two-dimensions or in spherical harmonics in three has been proposed in which each of the coefficients of expansion are functions of r and serve as additional correlation functions describing the non-randomness. The theory is general and is capable of describing all stages of order ranging from random to perfect spherulitic. Such a general theory is complex and while it is capable of exactly describing data, the association of these higher order correlation functions with physically visualizable structural variables is difficult. The extension of the theory to the description of three-dimensional order, oriented systems would compound this complexity.

Thus there is still need for a theory intermediate in complexity between that of the KVP and the harmonic expansion approach as a perturbation of random fluctuation theory to describe the properties of slightly non-random systems. An approximate theory of this sort is described in this part both for unoriented (in Chapter II) and for oriented systems (in Chapter III).

In case of oriented polymers the scattering of light has been shown^{26,27,28} to depend also upon the angle Ω which the principal axis of orientation makes with regard to the normal to the scattering plane as well as upon the scattering angle θ and the polarization angles ψ_1 and ψ_2 (Fig. I-1). Usually, measurements are made under conditions designated as $I_{||}$ where $\psi = \psi_1 = \psi_2$ and I_{\perp} when $\psi = \psi_1 = \psi_2 + 90^\circ$. While an arbitrary relationship between the values of ψ and Ω is possible, the birefringence occurring in oriented systems will affect the scattering pattern so as to make interpretation difficult²⁹⁻³³. The birefringence effect is minimized when measurements are made under the condition that the stretching

direction is parallel to the polarizer or analyzer^{32,33}.

Intensities measured under these conditions will be designated $I_{||}(\Omega)$ for $I_{||}$ when $\Omega = \psi_1 = \psi_2$, $I_{+}(\Omega)$ for I_{+} when $\Omega = \psi_1 = \psi_2 - 90^\circ$, $I_{= }(\Omega)$ for $I_{= }$ when $\psi_1 = \psi_2 = \Omega + 90^\circ$. It is noted that this definition of $I_{||}$ and I_{+} differs from the definition proposed by Keijzers, van Aartsen and Prins²¹ as a result of their more elaborate and correct definition of the vector \underline{Q} . While a formulation in terms of their definition is preferable, the results are stated in terms of the definition described above to facilitate comparison with our earlier work. In practice, the numerical differences resulting from our treatment quoted in this part will differ negligibly from those obtained using their definition as shown in Appendix I. These three intensities, $I_{||}(\Omega)$, $I_{+}(\Omega)$ and $I_{= }(\Omega)$ are functions of θ and Ω and are equivalent to photographic patterns corresponding to $V_V(\mu = 90^\circ - \Omega)$, H_V or $V_H(\mu = 90^\circ - \Omega)$ and $H_H(\mu = 90^\circ - \Omega)$, respectively. Under these conditions of measurement, the effect of birefringence on the light scattering pattern will be neglected, even though there will be some effect resulting from the retardation of the scattered ray which becomes more important at larger values of θ .

The statistical calculation of the scattering from a heterogeneous medium involves the evaluation of the integral

$$I = C_1 \int_{\underline{r}} (\underline{M}_i \cdot \underline{O}) (\underline{M}_j \cdot \underline{O}) \cos k(\underline{r} \cdot \underline{s}) d\underline{r} \quad (2)$$

where C_1 is a constant of proportionality, \underline{M}_i and \underline{M}_j are the induced

dipoles in the i^{th} and j^{th} scattering elements separated by vector distance \underline{r} (Fig. I-2), k is the wave number ($2\pi/\lambda$) in the scattering medium and \underline{s} is the scattering vector defined by $\underline{s} = \underline{s}_1 - \underline{s}_0$ where \underline{s}_1 and \underline{s}_0 are unit vectors along the scattered and incident ray. The unit vector \underline{o} lies along the direction of the polarization passed by the analyzer in the scattered ray. For unoriented systems at small values of the scattering angle, θ , this leads to the result¹⁶

$$I_+ = C_2 \delta^2 \int f(r) \cos[k (\underline{r} \cdot \underline{s})] dr \quad (3)$$

for the case of random orientation fluctuations in which the correlation in orientation of the optic axes of elements i and j (represented by the unit vectors \underline{a}_i and \underline{a}_j in Fig. I-2) depends only upon \underline{r} and is independent of the angle β which \underline{a}_i makes with \underline{r} . Here δ is the anisotropy in polarizability of the scattering element, $\delta = \alpha_1 - \alpha_2$, where α_1 and α_2 are polarizabilities along and perpendicular to the principal axis. The orientation correlation function $f(r)$ is defined as

$$f(r) = [3 \langle \cos^2 \theta_{ij} \rangle_r - 1] / 2 \quad (4)$$

where θ_{ij} is the angle between \underline{a}_i and \underline{a}_j . The symbol $\langle \rangle_r$ designates an average over all pairs of scattering elements separated by distance r .

This function, which may be determined by Fourier inversion, describes the size of the region over which the orientation of optic axes is correlated and is related to the structure of the polymer.

The $I_{||}$ component of scattering has been shown to also depend upon a density correlation function $\gamma(r)$ defined by

$$\gamma(r) = \langle \Delta\alpha_i \Delta\alpha_j \rangle_r / \langle (\Delta\alpha_i)^2 \rangle_{av} \quad (5)$$

where $\Delta\alpha_i$ is the deviation of the local average polarizability of the i^{th} element from the macroscopic average. It has been shown how the correlation functions can be separated from a combination of $I_{||}$ and I_+ measurement.

The random orientation function approach was generalized to oriented systems. For uniaxial orientation, this led for example to the result (at small θ)³⁴

$$I_+(\Omega = 0^\circ) = C_3 \delta^2 \langle \sin^2 \theta_i \cos^2 \theta_i \rangle_{av} \int f(\underline{r}) \cos k(\underline{r} \cdot \underline{s}) d\underline{r} \quad (6)$$

where θ_i is the angle between \underline{a}_i and the stretching direction. This expression deviates from Eq. (3) in two respects:

- (1) The expression contains an orientation factor $\langle \sin^2 \theta_i \cos^2 \theta_i \rangle_{av}$ which changes as the optic axes become oriented upon stretching a sample. This, for example, leads to a decrease in scattered intensity upon stretching a sample so that θ_i approaches 0° .
- (2) The scalar correlation function $f(r)$ is replaced by a vector function $\underline{f}(\underline{r})$. This means that the probability of optic axes being parallel depends upon direction within the oriented sample. A consequence is that

while I_+ for unoriented samples is independent of Ω , I_+ for oriented sample varies with Ω as has been experimentally demonstrated^{26,28}.

The use of the random orientation correlation approximation in this analysis is an oversimplification. Evidence for this comes from the prediction with this approximation that for example, at small θ , I_+ should be independent of ψ for unoriented samples. Experimentally, appreciable ψ dependence is found for many crystalline polymers. It is intuitively apparent that if non-randomness of correlations is important for unoriented polymers, the effect should become more significant for oriented systems where the dependence of correlations upon β should be more important. The random orientation fluctuation theory for oriented systems will be generalized in Chapter III to the system having non-random orientation correlations with macroscopic orientation of optic axes.

C H A P T E R II

NON-RANDOM THEORY FOR UNORIENTED SYSTEM

II-1. The Model

The calculation will be carried out for the same system discussed in our previous non-random theories^{2,17}. The scattering volume elements will be assumed to be uniaxially polarizable with principal polarizabilities α_1 and α_2 along and perpendicular to the optic axis of the i^{th} scattering element lying in the direction of the unit vector, \underline{a}_i . The anisotropy $\delta = \alpha_1 - \alpha_2$ will be assumed identical for all volume elements so that the scattering arises only from correlation in the direction of \underline{a}_i . For simplicity, the calculation is restricted to two-dimensions with \underline{a}_i confined to lie in the YZ plane perpendicular to the incident beam (in the X direction). The scattering angle, θ , is measured in the horizontal (XY) plane. No macroscopic orientation is considered so that all values of α , the angular coordinate of \underline{r} , are equally probable.

As shown in the previous paper¹⁷, the scattering from two dimensional system is given, in general, by

$$I_+ = C' \delta^2 \left\{ \begin{aligned} & \sin^2 \psi \cos^2 \psi (K_1 + K_2 \cos^2 \theta - [K_3 + K_3'] \cos \theta \\ & + K_4 (\cos^2 \psi \cos \theta - \sin^2 \psi)^2 - ([K_5 + K_5'] - [K_6 + K_6'] \cos \theta) \\ & (\cos^2 \psi \cos \theta - \sin^2 \psi) \sin \psi \cos \psi + K_7 \sin^2 \psi \cos^2 \psi \\ & (1 - \cos \theta)^2 \end{aligned} \right\} \quad (1)$$

and

$$I_{||} = C' \left\{ \delta^2 [K_1 \cos^4 \psi + K_2 \cos^2 \theta \sin^4 \psi + 2K_3 \cos \theta \sin^2 \psi \cos^2 \psi + 2K_5 \cos^3 \psi \sin \psi (1 + \cos \theta) + 2K_6 \sin^3 \psi \cos \psi \cos \theta (1 + \cos \theta) + K_4 (1 + \cos \theta)^2 \sin^2 \psi \cos^2 \psi] + K_7 (\cos^2 \psi + \cos \theta \sin^2 \psi)^2 \right\} \quad (2)$$

where

$$K_1 = \int \langle (\tilde{a}_i \cdot \tilde{k})^2 (\tilde{a}_j \cdot \tilde{k})^2 \rangle_{\tilde{r}} \cos k (\tilde{r} \cdot \tilde{s}) d\tilde{r} \quad (3)$$

$$K_2 = \int \langle (\tilde{a}_i \cdot \tilde{j})^2 (\tilde{a}_j \cdot \tilde{j})^2 \rangle_{\tilde{r}} \cos k (\tilde{r} \cdot \tilde{s}) d\tilde{r} \quad (4)$$

$$K_3 = \int \langle (\tilde{a}_i \cdot \tilde{k})^2 (\tilde{a}_i \cdot \tilde{j})^2 \rangle_{\tilde{r}} \cos k (\tilde{r} \cdot \tilde{s}) d\tilde{r} \quad (5)$$

$$K_4 = \int \langle (\tilde{a}_i \cdot \tilde{j}) (\tilde{a}_i \cdot \tilde{k}) (\tilde{a}_j \cdot \tilde{j}) (\tilde{a}_j \cdot \tilde{k}) \rangle_{\tilde{r}} \cos k (\tilde{r} \cdot \tilde{s}) d\tilde{r} \quad (6)$$

$$K_5 = \int \langle (\tilde{a}_i \cdot \tilde{k})^2 (\tilde{a}_j \cdot \tilde{j}) (\tilde{a}_j \cdot \tilde{k}) \rangle_{\tilde{r}} \cos k (\tilde{r} \cdot \tilde{s}) d\tilde{r} \quad (7)$$

$$K_6 = \int \langle (\tilde{a}_i \cdot \tilde{j})^2 (\tilde{a}_j \cdot \tilde{j}) (\tilde{a}_j \cdot \tilde{k}) \rangle_{\tilde{r}} \cos k (\tilde{r} \cdot \tilde{s}) d\tilde{r} \quad (8)$$

$$K_7 = \int \langle \alpha_i \alpha_j \rangle_{\tilde{r}} \cos k (\tilde{r} \cdot \tilde{s}) d\tilde{r} \quad (9)$$

upon solving these equation by using a harmonic expansion approach, it was shown that the scattered intensity for unoriented systems is finally given by

$$\begin{aligned}
 I_{+} = C \int_0^{\infty} \left\{ 2 \langle (\Delta \alpha_i)^2 \rangle J_0(w) \gamma(r) \phi_1 \right. \\
 + (\delta^2/4) [T_0 J_0(w) \phi_2 + (T_2 - S_2) J_2(w) \phi_3 \\
 + \frac{1}{2} (T_4 - S_4) J_4(w) \phi_4 + (Z_2 + R_2) J_2(w) \phi_{12} \\
 \left. + (Z_4 + R_4) J_4(w) \phi_{13}] \right\} r dr
 \end{aligned} \tag{10}$$

and

$$\begin{aligned}
 I_{||} = C \int_0^{\infty} \left\{ 2 \langle (\Delta \alpha_i)^2 \rangle J_0(w) \gamma(r) \phi_5 \right. \\
 + (\delta^2/4) [T_0 J_0(w) \phi_6 + (T_2 - S_2) J_2(w) \phi_7 \\
 + \frac{1}{2} (T_4 - S_4) J_4(w) \phi_8 + (Z_2 + R_2) J_2(w) \phi_9 \\
 \left. + (Z_4 + R_4) J_4(w) \phi_{10}] \right\} r dr
 \end{aligned} \tag{11}$$

where $w = 2\pi (r/\lambda) \sin \theta$ and λ is the wavelength of light in the medium.

In these equations C is a physical constant related to the absolute intensity which is immaterial to these considerations. The ϕ_1 terms are trigonometric functions of the scattering angles θ and ψ and are defined as before by

$$\Phi_0 = \sin^2 \psi \cos^2 \psi (1 + \cos \theta)^2$$

$$\Phi_1 = \sin^2 \psi \cos^2 \psi (1 - \cos \theta)^2$$

$$\Phi_2 = \Phi_0 + (\cos^2 \psi \cos \theta - \sin^2 \psi)^2$$

$$\Phi_3 = \sin^2 \theta \sin^2 \psi \cos^2 \psi$$

$$\Phi_4 = \Phi_0 - (\cos^2 \psi \cos \theta - \sin^2 \psi)^2$$

$$\Phi_5 = (\cos^2 \psi + \cos \theta \cdot \sin^2 \psi)^2$$

$$\Phi_6 = \Phi_0 + (\cos^2 \psi - \cos \theta \sin^2 \psi)^2$$

$$\Phi_7 = \cos^4 \psi - \sin^4 \psi \cos^2 \theta$$

$$\Phi_8 = \Phi_0 - (\cos^2 \psi - \cos \theta \sin^2 \psi)^2$$

$$\Phi_9 = (\Phi_5)^{\frac{1}{2}} \sin \psi \cos \psi (1 + \cos \theta)$$

$$\Phi_{10} = (\cos^2 \psi - \sin^2 \psi \cos \theta) \sin \psi \cos \psi (1 + \cos \theta)$$

$$\Phi_{11} = (\sin^2 \psi - \cos^2 \psi \cos \theta) \sin \psi \cos \psi$$

$$\phi_{12} = \phi_{11} (1 - \cos \theta)$$

$$\phi_{13} = \phi_{11} (1 + \cos \theta) \quad (12)$$

The term $\langle (\Delta \alpha_i)^2 \rangle$ is the mean-squared fluctuation in the spacial average refractive index and $\gamma(r)$ is the correlation function describing these "density" fluctuations defined by eq. (5) in Chapter I.

The correlation in orientation between optic axes of scattering elements i and j is described in terms of two correlation functions

$$F_1(r, \beta) = \langle \cos 2\theta_{ij} \rangle_{r, \beta} \quad (13)$$

and

$$F_2(r, \beta) = \langle \sin 2\theta_{ij} \rangle_{r, \beta} \quad (14)$$

where θ_{ij} is the angle between the optic axes of elements i and j . The averages are taken over all pairs of elements at constant r and with the vector r making a constant angle with respect to the i^{th} optic axis.

For random orientation correlations, positive and negative values of θ_{ij} are equally likely so $F_2(r, \beta) = 0$. Also, correlations depend only upon r so that

$$F_1(r, \beta) = F_1(r) = \langle \cos 2\theta_{ij} \rangle_r = 2 \langle \cos^2 \theta_{ij} \rangle_r - 1 = f(r) \quad (15)$$

and is identical with the single orientation function introduced in the theory of random orientation correlations. This has been shown to give rise to scattering which is independent of ψ at small θ and is characteristic of correlated regions which are circular in shape.

When correlation depends upon β , the correlation function was expanded in Fourier series in β giving

$$F_1(r, \beta) = T_0(r) + \sum_n [T_n(r) \cos(n\beta) + Z_n(r) \sin(n\beta)] \quad (16)$$

and

$$F_2(r, \beta) = R_0(r) + \sum_n [R_n(r) \cos(n\beta) + S_n(r) \sin(n\beta)] \quad (17)$$

defining the coefficients T_n , Z_n , R_n and S_n of eqns. (10) and (11). The random orientation correlation case corresponds to $T_0(r) = f(r)$ with all of the other coefficients being zero. The scattering was shown to only depend upon coefficients corresponding to values of n of 0, 2 and 4.

II-2. Delta Function Approximation

As a simplification of this general treatment we shall consider a special type of correlation somewhat like that introduced in the rod-disk interpolation theory. We shall assume that it is more probable that optic axes are parallel at some particular value of β designated as β_0 and the probability of parallelness is less and equal at all other values of β . When $\beta_0 = 0^\circ$, the correlation is rod-like while when it is

90°, it is disk-like. This will be mathematically represented by

$$F_1(r, \beta) = f_0(r) \delta(\beta - \beta_0) + [1 - \delta(\beta - \beta_0)] f(r) \quad (18)$$

and

$$F_2(r, \beta) = g_0(r) \delta(\beta - \beta_0) + [1 - \delta(\beta - \beta_0)] g(r) \quad (19)$$

The term $\delta(\beta - \beta_0)$ is a delta function defined such that for an arbitrary function of β , $\mu(\beta)$

$$\int_{\beta=0}^{2\pi} \mu(\beta) \delta(\beta - \beta_0) d\beta = \mu(\beta_0) \quad (20)$$

The correlation function $f_0(r)$ is that in the direction of strong correlation whereas $f(r)$ is that in any other direction. For a discrete object such as a rod immersed in an isotropic medium, $f(r) = 0$ for finite r .

Since the coefficients of the Fourier expansion can be given, for example, by

$$T_n = \frac{1}{\pi} \int_0^{2\pi} F_1 \cos n\beta d\beta \quad (21)$$

substitution of eq. (18) for F_1 yields

$$\begin{aligned}
T_n &= \frac{1}{\pi} \left\{ f_0(r) \int_0^{2\pi} \delta(\beta - \beta_0) \cos(n\beta) d\beta \right. \\
&\quad \left. + f(r) \int_0^{2\pi} [1 - \delta(\beta - \beta_0)] \cos(n\beta) d\beta \right\} \\
&= [f_0(r) - f(r)] \cos(n\beta_0) / \pi
\end{aligned} \tag{22}$$

In the particular case when $n = 0$, an extra term enters to give

$$T_0 = f(r) + [f_0(r) - f(r)] / 2\pi \tag{23}$$

Similarly

$$Z_n = \frac{1}{\pi} [f_0(r) - f(r)] \sin(n\beta_0) \tag{24}$$

In this manner, all of the Fourier coefficients are related to $f_0(r)$, $f(r)$ and β_0 . When $f_0(r)$ and $f(r)$ are identical, the angularly dependent terms vanish and the theory reduces to the random correlation case. $f_0(r)$ may be related to the size and perfectness of the crystalline domains in terms of orientation, while $f(r)$ may be related to mutual arrangement of these domains in space. β_0 is related to the type of these domains.

II-3. Numerical Calculation

For purposes of numerical illustration, we consider first the case where at any β_j , correlation at $+\theta_{ij}$ and $-\theta_{ij}$ are equally probable. This is a situation where there is no "handedness" so that optic axes

are arranged symmetrically about some symmetry axis of the correlated region. Also correlations at $+\beta$ and $-\beta$ will be considered equally probable. Under these conditions $F_2 = 0$, $Z_n = 0$ so, for example, eqns. (10) and (11) reduce to

$$I_+ = C \int_0^\infty \left\{ 2 \langle (\Delta \alpha_i)^2 \rangle J_0(w) \gamma(r) \phi_1 + (\delta^2/4) \left(f(r) J_0(w) \phi_2 + (1/\pi) [f_0(r) - f(r)] \left[\frac{1}{2} J_0(w) \phi_2 + \cos 2\beta_0 J_2(w) \phi_3 + \frac{1}{2} \cos 4\beta_0 J_4(w) \phi_4 \right] \right) \right\} r dr \quad (25)$$

$$I_{||} = C \int_0^\infty \left\{ 2 \langle (\Delta \alpha_i)^2 \rangle J_0(w) \gamma(r) \phi_5 + \frac{\delta^2}{4} \left(f(r) J_0(w) \phi_6 + (1/\pi) [f_0(r) - f(r)] \left[\frac{1}{2} J_0(w) \phi_6 + \cos 2\beta_0 J_2(w) \phi_7 - \frac{1}{2} \cos 4\beta_0 J_4(w) \phi_8 \right] \right) \right\} r dr \quad (26)$$

The integrals over r were evaluated by assuming the Gaussian functions

$$f_0(r) = \exp(-r^2 / a_0^2) \quad (27)$$

$$f(r) = \exp(-r^2 / a^2) \quad (28)$$

and

$$\gamma(r) = \exp(-r^2 / a_d^2) \quad (28)$$

for which the integrations may be readily performed. In the case where the correlation is asymmetric in β , additional terms associated with the coefficient Z_n must be added to eqns. (25) and (26). For I_+ intensity this is given by

$$\frac{C}{\pi} \frac{\delta^2}{4} \int_0^\infty [f_0(r) - f(r)] [\sin 2\beta_o \cdot J_2(w) \phi_{12} + \sin 4\beta_o \cdot J_4(w) \phi_{13}] r dr$$

and for case of $I_{||}$ intensity

$$\frac{C}{\pi} \frac{\delta^2}{4} \int_0^\infty [f_0(r) - f(r)] [\sin 2\beta_o \cdot J_2(w) \phi_9 + \sin 4\beta_o \cdot J_4(w) \phi_{10}] r dr$$

Some numerical results of such calculations are shown in Figs. I-3 through I-7 for the case where $a_0 = 2\mu$, $a = 1\mu$ and $a_d = 4\mu$ using $\lambda = 0.364$ in the medium. δ^2 and $\langle(\Delta \alpha_i)^2\rangle$ are assumed to be 9×10^{-6} and 9×10^{-8} , respectively. The contour lines represent equal levels of logarithmic intensity which are shown in table I-1.

TABLE I-1

The Designation of Constant Intensity Contours

<u>Contour No.</u>	<u>Relative Intensity*</u>	<u>Contour No.</u>	<u>Relative Intensity*</u>
1	60	1'	48
2	35	2'	30
3	20	3'	15
4	10	4'	7
5	6	5'	4
6	3.5	6'	2.5
7	2	7'	1.5
8	11		

* In arbitrary unit.

It is seen from Fig. I-3 that the I_+ scattering pattern for $\beta_0 = 90^\circ$ has four-fold symmetry with maximum intensity for values of ψ being odd multiples of 45° . This pattern is somewhat like that of a spherulite with optic axes parallel or perpendicular to the radius except that the intensity decreases monotonically with θ rather than exhibiting a maximum at some θ as for a spherulite^{6,19}. This prediction of ψ variation for disk-like correlation is in better agreement with experiment than the earlier rod-disk interpolation theory².

The $I_{||}$ pattern for $\beta_0 = 0^\circ$ is shown in Fig. I-4. The pattern is seen to have two-fold symmetry at small values of θ but shows four-fold symmetry at larger θ . The two-fold symmetry arises from the T_2 term of

eqns. (10) and (11) whereas the fourfold symmetry comes from the T_4 term. The coefficient ϕ_7 multiplying the T_2 term decreases with θ more rapidly than ϕ_8 multiplying the T_4 term.

The I_+ pattern for $\beta_0 = 0^\circ$ is identical with that for $\beta_0 = 90^\circ$. This occurs because the coefficient ϕ_3 multiplying the $\cos 2\beta_0$ term of eq. (25) approaches zero at small θ and the $\cos 4\beta_0$ term is identical at $\beta_0 = 0^\circ$ and 90° . The $I_{||}$ pattern for $\beta_0 = 90^\circ$ exhibits two-fold symmetry and is rotated through 90° from the $\beta_0 = 0^\circ$ pattern.

The I_+ pattern for $\beta_0 = 45^\circ$ is shown in Fig. I-5. It is noted that the simplified eqns. (25) and (26) cannot be used in this case because of the asymmetry in β and the additional terms associated with Z_2 and Z_4 must be included. The pattern shows four-fold symmetry with maximum scattering at $\psi = 0^\circ$ and 90° and is rotated through 45° with respect to Fig. I-3.

The $I_{||}$ pattern for $\beta_0 = 45^\circ$ in Fig. I-6 is seen to be skewed and has two-fold symmetry about $\psi = -45^\circ$. For $\beta_0 = -45^\circ$ the pattern is the same but the $I_{||}$ pattern is skewed in the opposite direction to $\psi = +45^\circ$. Most real systems have overall symmetry and consist of equal numbers of regions within the scattering volume corresponding to positive and negative values of β_0 . Thus, one might observe an $I_{||}$ pattern shown in Fig. I-7 obtained by summing $\beta_0 = +45^\circ$ and $\beta_0 = -45^\circ$ pattern. The result has four-fold symmetry with maxima at odd multiples of 45° . Such patterns have been obtained experimentally for poly(tetrafluoroethylene)²⁴ and poly(chlorotrifluoroethylene)²⁵ and had

been explained on the basis of scattering from rods with optic axes at 45° to the rod axis. The present explanation in terms of non-random orientation correlations is more physically reasonable.

II-4. Conclusions

This special case of the non-random orientation correlation theory is more easy to visualize than the more general case and yields predictions of scattering patterns that correspond to experimental situations. It is suggested that this simplification may be fruitful in extension of the theory to three-dimensions and to oriented systems. The approach is thought to be more general and realistic than the earlier rod-disk interpolation theory. The monotonic decrease of scattering with θ predicted by this theory is too simple, as a maximum intensity at some value of θ is often found experimentally. This oversimplification is a consequence of the assumptions of eqs. (27) and (28) of Gaussian correlation functions. The appropriate correlation functions for real systems retain some spherulitic character and exhibit maxima and minima. It is presently felt that this behavior is more readily described by introducing disorder into spherulite scattering theories, which will be discussed in Part II.

C H A P T E R I I I

NON-RANDOM THEORY FOR ORIENTED SYSTEMS

In the previous chapter a statistical theory for the scattering of light from unoriented polymer films was discussed on the basis of a general harmonic expansion approach and numerical calculations have been made for a special case of the approach by using the delta function approach.

In this chapter, the theory is first extended to oriented polymer films on the basis of the general harmonic expansion approach and then as in the case of unoriented systems, the delta function approach is adopted to the general results in order to make numerical calculations. The theory is also confined to two dimensional case. For oriented systems the scattering depends upon two types of distributions describing (1) the orientation distribution of optic axes of scattering elements and (2) the angular dependence of correlation in orientation between pairs of optic axes. These distributions are expanded in Fourier series (in the two-dimensional treatment), the coefficients of which are functions of elongation and describe the elongation dependence of the scattering patterns.

III-1. General Descriptions of the Scattering from
the System Based upon Harmonic Expansion Approach

In case of oriented systems one must start from eqns. (1) to (9) in Chapter II and derive equations by taking into account 1) macroscopic orientation of optic axes and 2) the angular dependence of general orientation correlation functions.

We shall discuss first the evaluation of K_1 term in eq. (3) in Chapter II for an oriented system. The evaluations of the other K_i terms given by eqns. (4) to (8) are carried out in a similar manner. Now

$$\begin{aligned} \langle (\underline{a}_i \cdot \underline{k})^2 (\underline{a}_j \cdot \underline{k})^2 \rangle_{\underline{r}} &= \langle \cos^2 \theta_i \cos^2 \theta_j \rangle_{\underline{r}} \\ &= (1/4) \{ 1 + \langle \cos 2\theta_i \rangle_{\underline{r}} + \langle \cos 2\theta_j \rangle_{\underline{r}} \\ &\quad + \langle \cos 2\theta_i \cos 2\theta_j \rangle_{\underline{r}} \} \end{aligned} \quad (1)$$

Now $\langle \cos 2\theta_i \rangle_{\underline{r}}$ is equal to $\langle \cos 2\theta_i \rangle_{av}$ since this is independent of \underline{r} and β as it does not depend upon the location of element j . The angle θ_i may be expressed in terms of the angle η between \underline{a}_i and the stretching direction Z' as shown in Fig. I-8 so that it follows that

$$\begin{aligned} \langle \cos 2\theta_i \rangle_{av} &= \langle \cos [2(\eta + \Omega)] \rangle_{av} \\ &= \langle \cos 2\eta \rangle_{av} \cos 2\Omega - \langle \sin 2\eta \rangle_{av} \sin 2\Omega \end{aligned} \quad (2)$$

The distribution in orientation of the optic axes about Z' may be expanded in a Fourier series such that the probability of a given orientation $p(\eta)$ is

$$p(\eta) = \rho_0 [1 + 2(\rho_2 \cos 2\eta + \rho_4 \cos 4\eta + \dots)] \quad (3)$$

where for example, ρ_2 is given by

$$\rho_2 = \langle \cos 2\eta \rangle_{av} = \frac{\int_0^{2\pi} p(\eta) \cos 2\eta \, d\eta}{\int_0^{2\pi} p(\eta) \, d\eta} \quad (4)$$

and is the second moment of the orientation distribution. Only even cosine terms are retained in eq. (3) so as to impose the reasonable symmetry requirements that $p(\eta) = p(-\eta) = p(\eta + \pi)$. It follows that $\langle \sin 2\eta_i \rangle = 0$ so that

$$\langle \cos 2\theta_i \rangle_{av} = \rho_2 \cos 2\Omega \quad (5)$$

We shall assume that at low degrees of orientation, it will suffice to retain terms only up to ρ_2 .

To evaluate $\langle \cos 2\theta_j \rangle_r$ we will first evaluate the average at a given β , $\langle \cos 2\theta_j \rangle_{r,\beta}$, and then average this over all β . If we realize that $\theta_j = \theta_i + \theta_{ij}$, it follows that

$$\langle \cos 2\theta_j \rangle_{r,\beta} = (\cos 2\theta_i) F_1 - (\sin 2\theta_i) F_2 \quad (6)$$

For simplicity, we shall restrict our treatment to cases which imply that for any β , the probability of finding θ_{ij} at $+\theta_{ij}$ and $-\theta_{ij}$ is the same. Then $F_1(r, \beta)$ may be expanded in an even cosine term Fourier series in θ to give

$$F_1(r, \beta) = \sum_{n=0}^{\infty} T_{2n}(r) \cos 2n\beta \quad (7)$$

Now introducing the angle ξ between r and the stretching direction, eq. (7) becomes

$$\langle \cos 2\theta_j \rangle_{r,\beta} = \cos [2(\eta + \Omega)] \sum_{n=0}^{\infty} T_{2n}(r) \cos [2n(\eta - \xi)] \quad (8)$$

The average over β is equivalent to averaging over η . Thus one obtains

$$\begin{aligned}
\langle \cos 2\theta_j \rangle_{\tilde{r}} &= \int_0^{2\pi} p(\eta) \langle \cos 2\theta_j \rangle_{\tilde{r}, \beta} d\eta / \int_0^{2\pi} p(\eta) d\eta \\
&= \left(\frac{1}{2\pi}\right) \sum_{n=0}^{\infty} T_{2n}(\tilde{r}) \int_0^{\infty} \left\{ [1 + 2\rho_2 \cos 2\eta] [\cos 2\Omega \cos 2\eta \right. \\
&\quad \left. - \sin 2\Omega \sin 2\eta] [\cos 2n\xi \cos 2n\eta + \sin 2n\xi \sin 2n\eta] \right\} d\eta
\end{aligned}
\tag{9}$$

$$\begin{aligned}
\langle \cos 2\theta_j \rangle_{\tilde{r}} &= \frac{1}{2} \left\{ 2\rho_2 \cos 2\Omega \cdot T_0(\tilde{r}) + \cos [2(\Omega + \xi)] \cdot T_2(\tilde{r}) + \right. \\
&\quad \left. \rho_2 \cos [2(\Omega + 2\xi)] \cdot T_4(\tilde{r}) \right\}
\end{aligned}
\tag{10}$$

The last term of eq. (1) is evaluated in a similar manner to give

$$\begin{aligned}
\langle \cos 2\theta_i \cos 2\theta_j \rangle_{\tilde{r}} &= \frac{1}{2} \langle (1 + \cos 4\theta_i) \cos 2\theta_{ij} - \sin 4\theta_i \sin 2\theta_{ij} \rangle_{\tilde{r}} \\
&= (1/4\pi) \int_0^{2\pi} p(\eta) [1 + \cos 4(\Omega + \eta)] F_1(\tilde{r}, \eta) d\eta \\
&= \frac{1}{4} \left\{ 2 T_0(\tilde{r}) + \rho_2 [2\cos 2\xi + \cos 2(2\Omega + \xi)] T_2(\tilde{r}) \right. \\
&\quad \left. + \cos 4(\Omega + \xi) \cdot T_4(\tilde{r}) + \rho_2 \cos 2(2\Omega + 3\xi) \cdot T_6(\tilde{r}) \right\}
\end{aligned}
\tag{11}$$

Thus, by combining eqns. (1), (5), (10) and (11) we obtain

$$\begin{aligned}
\langle (a_{\tilde{i}} \cdot k)^2 (a_{\tilde{j}} \cdot k)^2 \rangle_{\tilde{r}} &= \frac{1}{4} (1 + \rho_2 \cos 2\Omega) \\
&+ \frac{1}{16} [(4 \rho_2 \cos 2\Omega + 2) T_0(\tilde{r}) + (2 \cos 2(\Omega + \xi) \\
&+ \rho_2 [2 \cos 2\xi + \cos (4\Omega + 2\xi)] T_2(\tilde{r}) \\
&+ (2 \rho_2 \cos (2\Omega + 4\xi) + \cos 4(\Omega + \xi)) T_4(\tilde{r}) \\
&+ \rho_2 \cos (4\Omega + 6\xi) T_6(\tilde{r})] \quad (12)
\end{aligned}$$

This expression is then substituted into eq. (3) in Chapter II in order to evaluate K_1 . It is apparent that

$$\cos [k(\tilde{r} \cdot \tilde{s})] d\tilde{r} = \cos (w \sin \alpha) r dr d\alpha \quad (13)$$

It is necessary to express the Fourier coefficients $T_{2n}(\tilde{r})$ in terms of the angular coordinates of \tilde{r} . This is done by expansion of each of these coefficients in an even cosine series in ξ to obtain

$$\begin{aligned}
T_{2n}(\tilde{r}) &= T_{2n}(\tilde{r}, \xi) = \sum_{m=0}^{\infty} t_{2n,2m}(\tilde{r}) \cos (2m\xi) \\
&= \sum_{m=0}^{\infty} t_{2n,2m}(\tilde{r}) [\cos (2m\Omega) \cos (2m\alpha) + \sin (2m\Omega) \sin (2m\alpha)] \quad (14)
\end{aligned}$$

For unoriented systems $T_{2n}(r)$ is independent of ξ and only the $m = 0$ term remains. The higher order coefficients describe the dependence of orientation correlation upon direction within the oriented sample. A typical integral encountered in substituting (12) and (13) into (3) in Chapter II is

$$P_3 = \int \cos 2(\Omega + \xi) T_2(r) \cos k(r \cdot s) dr \quad (15)$$

This is evaluated using Jacobi's expansion

$$\cos(w \sin \alpha) = J_0(w) + 2 \sum_{k=1}^{\infty} J_{2k}(w) \cos 2k\alpha \quad (16)$$

to give

$$\begin{aligned} P_3 &= \int_{r=0}^{\infty} \int_{\alpha=0}^{2\pi} \left\{ \sum_{m=0}^{\infty} t_{2,2m} [\cos 2m\Omega \cos 2m\alpha \cos 2\alpha \right. \\ &\quad \left. + \sin 2m\Omega \sin 2m\alpha \cos 2\alpha] [J_0(w) + 2 \sum_{k=1}^{\infty} J_{2k}(w) \cos 2k\alpha] \right\} d\alpha dr \\ &= \int_{r=0}^{\infty} \left\{ \pi t_{2,2} J_0(w) \cos 2\Omega + 2 \sum_{m=0}^{\infty} \sum_{k=1}^{\infty} t_{2,2m} \int_0^{2\pi} \right. \\ &\quad \left. [\cos 2m\Omega \cos 2m\alpha \cos 2\alpha + \sin 2m\Omega \sin 2m\alpha \cos 2\alpha] \right. \\ &\quad \left. J_{2k}(w) \cos (2k\alpha) d\alpha \right\} r dr \\ &= \int_{r=0}^{\infty} \left\{ \pi t_{2,2} J_0(w) \cos 2\Omega + \sum_{m=0}^{\infty} \sum_{k=1}^{\infty} t_{2,2m} \int_0^{2\pi} \right. \\ &\quad \left. [\cos 2m\Omega (\cos 2(m-1)\alpha \right. \\ &\quad \left. + \cos 2(m+1)\alpha) + \sin 2m\Omega (\sin 2(m+1)\alpha + \sin 2(m-1)\alpha)] \right\} r dr \end{aligned}$$

$$\begin{aligned}
& \left. J_{2k}^{(w)} \cos (2k\alpha) d\alpha \right\} r dr \\
& = \pi \sum_{m=0}^{\infty} \int_{r=0}^{\infty} t_{2,2m}(r) \cos 2m\Omega \cdot [J_{2|m-1|}^{(w)} + J_{2(m+1)}^{(w)}] r dr
\end{aligned} \tag{17}$$

The other terms are evaluated in a similar manner to give

$$\begin{aligned}
K_1 &= \frac{1}{4} \left(\frac{1}{2} + \rho_2 \cos 2\Omega \right) P_2 + \frac{1}{16} [2P_3 + \rho_2 (2P_4 + P_5) \\
&+ 2 \rho_2 P_6 + P_7 + \rho_2 P_8]
\end{aligned} \tag{18}$$

where

$$P_2 = 2\pi \sum_{m=0}^{\infty} \int_{r=0}^{\infty} t_{0,2m}(r) \cos [2m\Omega] \cdot J_{2m}^{(w)} r dr \tag{19}$$

$$\begin{aligned}
P_4 &= \pi \sum_{m=0}^{\infty} \int_{r=0}^{\infty} t_{2,2m}(r) \left\{ \cos [2(m-1)\Omega] \cdot J_{2|m-1|}^{(w)} \right. \\
&\quad \left. + \cos [2(m+1)\Omega] \cdot J_{2(m+1)}^{(w)} \right\} r dr
\end{aligned} \tag{20}$$

$$\begin{aligned}
P_5 &= \pi \sum_{m=0}^{\infty} \int_{r=0}^{\infty} t_{2,2m}(r) \left\{ \cos [2(m+1)\Omega] \cdot J_{2|m-1|}^{(w)} \right. \\
&\quad \left. + \cos [2(m-1)\Omega] \cdot J_{2(m+1)}^{(w)} \right\} r dr
\end{aligned} \tag{21}$$

$$\begin{aligned}
P_6 &= \pi \sum_{m=0}^{\infty} \int_{r=0}^{\infty} t_{4,2m}(r) \left\{ \cos [2(m-1)\Omega] \cdot J_{2|m-2|}^{(w)} \right. \\
&\quad \left. + \cos [2(m+1)\Omega] \cdot J_{2(m+2)}^{(w)} \right\} r dr
\end{aligned} \tag{22}$$

and

$$P_8 = \pi \sum_{m=0}^{\infty} \int_{r=0}^{\infty} t_{6,2m} \left\{ \cos [2(m-1)\Omega] \cdot J_{2|m-3|}(w) \right. \\ \left. + \cos [2(m+1)\Omega] \cdot J_{2(m+3)}(w) \right\} r dr \quad (23)$$

The other K_i terms can be evaluated similarly and be given by

$$K_2 = \frac{1}{16} [2(1 - 2\rho_2 \cos 2\Omega) P_2 + 2\rho_2 P_4 + \rho_2 P_5 - 2P_3 \\ + P_7 - 2\rho_2 P_6 + \rho_2 P_8] \quad (24)$$

$$K_3 = \frac{-1}{16} [(4\rho_2 \cos 2\Omega + 2) P_2 + 2P_3 + \rho_2(2P_4 + P_5) \\ + 2\rho_2 P_6 + P_7 + \rho_2 P_8] \quad (25)$$

$$K_3' = \frac{1}{16} [(4\rho_2 \cos 2\Omega - 2) P_2 + 2P_3 - \rho_2(2P_4 + P_5) \\ + 2\rho_2 P_6 - P_7 - \rho_2 P_8] \quad (26)$$

$$K_4 = \frac{1}{16} [2\rho_2 + 2\rho_2 P_4 - \rho_2 P_5 - P_7 - \rho_2 P_8] \quad (27)$$

$$K_5 = \frac{1}{16} [4\rho_2 \sin 2\Omega \cdot P_2 + 2P_9 + \rho_2 P_{10} + 2\rho_2 P_{11} \\ + P_{12} + \rho_2 P_{13}] \quad (28)$$

$$K_5' = \frac{1}{16} [\rho_2 P_{10} + P_{12} + \rho_2 P_{13}] \quad (29)$$

$$K_6 = \frac{1}{16} [4\rho_2 \sin 2\Omega \cdot P_2 + 2P_9 - \rho_2 P_{10} + 2\rho_2 P_{11} - P_{12} - \rho_2 P_{13}] \quad (30)$$

$$K_6' = \frac{-1}{16} [\rho_2 P_{10} + P_{12} + \rho_2 P_{13}] \quad (31)$$

where

$$P_7 = \pi \sum_{m=0}^{\infty} \int_{r=0}^{\infty} t_{4,2m}(r) \cos [2m\Omega] \cdot \left\{ J_{2|m-2|}^{(w)} + J_{2(m+2)}^{(w)} \right\} r dr \quad (32)$$

$$P_9 = \pi \sum_{m=0}^{\infty} \int_{r=0}^{\infty} t_{2,2m}(r) \sin[2m\Omega] \cdot \left\{ J_{2|m-1|}^{(w)} - J_{2(m+1)}^{(w)} \right\} r dr \quad (33)$$

$$P_{10} = \pi \sum_{m=0}^{\infty} \int_{r=0}^{\infty} t_{2,2m}(r) \left\{ \sin[2(m+1)\Omega] \cdot J_{2|m-1|}^{(w)} - \sin[2(m-1)\Omega] \cdot J_{2(m+1)}^{(w)} \right\} r dr \quad (34)$$

$$P_{11} = \pi \sum_{m=0}^{\infty} \int_{r=0}^{\infty} t_{4,2m}(r) \left\{ \sin[2(m-1)\Omega] \cdot J_{2|m-2|}^{(w)} - \sin[2(m+1)\Omega] \cdot J_{2(m+2)}^{(w)} \right\} r dr \quad (35)$$

$$P_{12} = \pi \sum_{m=0}^{\infty} \int_{r=0}^{\infty} t_{4,2m}(r) \sin[2m\Omega] \cdot \left\{ J_{2|m-2|}^{(w)} - J_{2(m+2)}^{(w)} \right\} r dr \quad (36)$$

$$P_{13} = \pi \sum_{m=0}^{\infty} \int_{r=0}^{\infty} t_{6,2m}(r) \left\{ \sin[2(m-1)\Omega] \cdot J_{2|m-3|}^{(w)} - \sin[2(m+1)\Omega] \cdot J_{2(m+3)}^{(w)} \right\} r dr \quad (37)$$

Substituting K_i terms into eq. (1) in Chapter II, one obtains

$$\begin{aligned}
 I_+(\psi, \Omega, \theta) = & C_4 K_7 \Phi_1 + \frac{\pi}{16} C_4 \delta^2 \int_0^\infty \left\{ A_{0,0} t_{0,0} J_0(w) \right. \\
 & + A_{0,2} t_{0,2} J_2(w) + A_{2,0} t_{2,0} J_2(w) + A_{2,2} t_{2,2} J_0(w) \\
 & + A_{2,2}' t_{2,2} J_4(w) + A_{4,0} t_{4,0} J_4(w) + A_{4,2} t_{4,2} J_2(w) \\
 & + A_{4,2}' t_{4,2} J_6(w) + A_{6,0} t_{6,0} J_6(w) + A_{6,2} t_{6,2} J_4(w) \\
 & \left. + A_{6,2}' t_{6,2} J_8(w) + \dots \right\} r dr \quad (38)
 \end{aligned}$$

where the $A_{i,j}$ terms are functions of ψ , Ω and θ given by

$$A_{0,0} = 4 [\Phi_2 + 2\rho_2 (\Phi_3 \cos 2\Omega - \Phi_{12} \sin 2\Omega)]$$

$$A_{0,2} = A_{0,0} \cos 2\Omega$$

$$A_{2,0} = 2 [2\Phi_3 + \rho_2 (2\Phi_0 + \Phi_2) \cos 2\Omega - 2\rho_2 \Phi_{13} \sin 2\Omega]$$

$$A_{2,2} = 2\rho_2 \Phi_2 + 2(\Phi_3 \cos 2\Omega - \Phi_{12} \sin 2\Omega) + \rho_2 [\Phi_4 \cos 4\Omega - 2\Phi_{13} \sin 4\Omega]$$

$$A_{2,2}' = \rho_2 \Phi_4 + 2(\Phi_3 \cos 2\Omega + \Phi_{12} \sin 2\Omega) + 2\rho_2 \Phi_2 \cos 4\Omega$$

$$A_{4,0} = 2[\Phi_4 + 2\rho_2 (\Phi_3 \cos 2\Omega + \Phi_{12} \sin 2\Omega)]$$

$$A_{4,2} = 2\rho_2 \Phi_3 + \Phi_4 \cos 2\Omega - 2\Phi_{13} \sin 2\Omega$$

$$A_{4,2} = \phi_4 \cos 2\Omega + 2\phi_{13} \sin 2\Omega + 2\rho_2(\phi_3 \cos 4\Omega + \phi_{12} \sin 4\Omega)$$

$$A_{6,0} = 2[\rho_2\phi_4 \cos 2\Omega + 2\rho_2\phi_{13} \sin 2\Omega]$$

$$A_{6,2} = \rho_2\phi_4$$

$$A_{6,2} = \rho_2\phi_4 \cos 4\Omega + 2\rho_2\phi_{13} \sin 4\Omega \quad (39)$$

The ϕ_i terms are functions of ψ and θ which have been previously defined in Chapter II. The K_7 term arises from density fluctuations which will be neglected in this treatment. For unoriented systems $\rho_2 = 0$ and

$$t_{0,2} = t_{2,2} = t_{4,2} = 0 \text{ and}$$

$$I_+ = (\pi/4) C_4 \delta^2 \int_0^\infty \left\{ \phi_2 t_{0,0} J_0(w) + \phi_3 t_{2,0} J_2(w) + \frac{1}{2} \phi_4 t_{4,0} J_4(w) \right\} r dr \quad (40)$$

which agrees with the previously reported result¹⁷ for which the scattering is independent of Ω . For random orientation fluctuations in oriented systems, only the $t_{0,2m}$ terms are non-vanishing, and the result is the two-dimensional equivalent of the Stein-Hotta result²⁷.

The scattering from an oriented system may be generally described by specifying the dependence of all of the $t_{m,n}$ terms upon r . Such characterization would require a large number of parameters that could not be easily related to structural features of the polymer. A more comprehensible description may be formulated by extending the delta function

approximation which has been useful for describing non-random correlations in unoriented systems as shown in Chapter II.

III-2. Delta Function Approximation

As in the Chapter II, we shall assume that correlation is strong in some particular direction β_0 and describable by a correlation function $f_0(r)$. Thus

$$F_1(r, \beta) = \delta(\beta - \beta_0) f_0(r) + [1 - \delta(\beta - \beta_0)] f(r) \quad (41)$$

where $\delta(\beta - \beta_0)$ is a delta function. We shall assume that each of these correlation functions may be expanded in an even cosine series in ξ to give

$$f_0(r) = f_0(r, \xi) = \sum_{m=0}^{\infty} f_{2m}^0(r) \cos(2m\xi) \quad (42)$$

$$f(r) = f(r, \xi) = \sum_{m=0}^{\infty} f_{2m}(r) \cos(2m\xi) \quad (43)$$

If one considers the structure to consist of an assembly of substructures within which correlation occurs, then the difference between f_0^0 and f_0 functions determines the anisotropy of shape of the domain and the difference between f_{2m}^0 and f_{2m} describes the orientation of this domain in the stretched sample. Now the $t_{2n,2m}$ coefficients in eq. (14) may be related to the f functions to give

$$t_{0,2\ell}(r) = \frac{1}{2\pi} [f_{2\ell}^0(r) + f_{2\ell}(r)] + f_{2\ell}(r) \quad (44)$$

$$t_{2m,2\ell}(r) = \frac{1}{\pi} [f_{2\ell}^o(r) - f_{2\ell}(r)] \cos(2m\beta_o) \quad (45)$$

III-3. Gaussian Correlation Functions

In previous discussions of random and non-randomly correlated systems, a Gaussian correlation function was used as a good approximation^{16,26,27,33} for less ordered systems

$$f(r) = \exp[-r^2 / a^2] \quad (46)$$

where there was a correlation distance serving as a measure of the distance over which optic axis orientation was correlated. In delta function approximation, a similar function was assumed for $f_o(r)$ with a different correlation distance a_o in the direction of β_o . The difference between a_o and a is a measure of the anisotropy in shape of the correlated domain.

For oriented systems, an ellipsoidally symmetrical correlated domain was assumed^{17,26,27} so that

$$f(r) = \exp \left\{ -[(y'/a)^2 + (z'/c)^2] \right\} \quad (47)$$

where c and a are correlation distances along and perpendicular to the orientation direction (z'). This may be expressed in polar coordinates as

$$\begin{aligned} f(r, \xi) &= \exp \left[-\frac{r^2}{d^2} (1 + b \cos 2\xi) \right] \\ &= e^{-r^2/d^2} [1 + (r^2 b/d^2) \cos 2\xi + \dots] \end{aligned} \quad (48)$$

and

$$\begin{aligned} (b/d^2) &= \frac{1}{2} [(1/a^2) - (1/c^2)] \\ 1/d^2 &= \frac{1}{2} [(1/a^2) + (1/c^2)] \end{aligned} \quad (49)$$

If we compare this with the first two terms of eq. (43), we see that

$$f_0(r) = \exp [-r^2/d^2] \quad (50)$$

and

$$f_2(r) = \sigma r^2 \exp [-r^2/d^2] \quad (51)$$

where $\sigma = b/d^2$. For purposes of numerical calculation we shall assume this form of correlation function is characterized by the parameters d , an average correlation distance, and σ , a correlation orientation parameter. Similar types of functions will be assumed for $f_0^0(r)$ within the domain with parameters d_0 and σ_0 . More complex types of orientation could be described by retaining additional terms in eq. (43), but this would involve introducing more parameters than could be experimentally characterized. Also domains of more complex shape, in principle, be described through use of other than Gaussian correlation functions, but again, the complexity is not warranted.

With the use of such correlation functions the integrals over r required in eq. (38) may be obtained. For example, noticing that

$$\int_{x=0}^{\infty} e^{-a^2 x^2} x^{\mu-1} J_{\nu}(bx) dx = \frac{\Gamma\left(\frac{\mu+\nu}{2}\right) b^{\nu}}{2^{\nu+1} a^{\mu+\nu} \Gamma(\nu+1)} {}_1F_1\left(\frac{\mu+\nu}{2}; \nu+1; \frac{-b^2}{4a}\right)$$

for positive real part of $(\mu + \nu)$, the third term gives

$$\int_0^{\infty} t_{2,0} J_2(w) r dr = \frac{1}{\pi} \cos 2\beta_0 \cdot \frac{h^2}{16} \left\{ d_0^4 {}_1F_1(2; 3; -u_0^2/4) - d_1^4 {}_1F_1(2; 3; -u^2/4) \right\} \quad (52)$$

where $u = kd \sin \theta$, $u_0 = kd_0 \sin \theta$, ${}_1F_1(\alpha; \gamma; z)$ is a Kummer's function which is a special case of a generalized hypergeometric function and is designated hereafter as $F(\alpha, \gamma; z)$.

$$F(\alpha, \gamma; z) = \frac{\Gamma(\gamma)}{\Gamma(\alpha)} \sum_{n=0}^{\infty} \frac{\Gamma(\alpha+n)}{\Gamma(\gamma+n)} \frac{z^n}{n!} \quad (53)$$

The other integrals over r are carried out similarly and as a final result one obtains,

$$\begin{aligned} I_+ = & C_4 K_7 \phi_1 + \frac{1}{16} C_4 \delta^2 \left\{ \frac{1}{2} A_{0,0} Q_1 + A_{2,0} Q_2 \cos 2\beta_0 \right. \\ & + A_{4,0} Q_3 \cos 4\beta_0 + A_{6,0} Q_4 \cos 6\beta_0 + \frac{1}{2} A_{0,2} Q_5 + A_{2,2} Q_6 \cos 2\beta_0 \\ & + A_{2,2}' Q_7 \cos 2\beta_0 + A_{4,2} Q_5 \cos 4\beta_0 + A_{4,2}' Q_7' \cos 4\beta_0 \\ & \left. + A_{6,2} Q_7 \cos 6\beta_0 + A_{6,2}' Q_8 \cos 6\beta_0 + \pi A_{0,0} Q_9 + \pi A_{0,2} Q_{10} + \dots \right\} \end{aligned} \quad (54)$$

where

$$Q_1 = \frac{1}{2} \left[d_o F(1, 1; -u_o^2/4) - d^2 F(1, 1; -u^2/4) \right] \quad (55)$$

$$Q_2 = \frac{h^2}{16} \left[d_o^4 F(2, 3; -u_o^2/4) - d^4 F(2, 3; -u^2/4) \right] \quad (56)$$

$$Q_3 = \frac{h^4}{384} \left[d_o^4 F(3, 5; -u_o^2/4) - d^6 F(3, 5; -u^2/4) \right] \quad (57)$$

$$Q_4 = \frac{h^6}{2^7 \cdot 120} \left[d_o^8 F(4, 7; -u_o^2/4) - d^8 F(4, 7; -u^2/4) \right] \quad (58)$$

$$Q_5 = \frac{h^2}{8} \left[\sigma d^6 F(3, 3; -u^2/4) - \sigma_o d_o^6 F(3, 3; -u_o^2/4) \right] \quad (59)$$

$$Q_6 = \frac{1}{2} \left[\sigma d^4 F(2, 1; -u^2/4) - \sigma_o d_o^4 F(2, 1; -u_o^2/4) \right] \quad (60)$$

$$Q_7 = \frac{h^4}{128} \left[\sigma d^8 F(4, 5; -u^2/4) - \sigma_o d_o^8 F(4, 5; -u_o^2/4) \right] \quad (61)$$

$$Q_7' = \frac{h^6}{2^7 \cdot 30} \left[\sigma d^{10} F(5, 7; -u^2/4) - \sigma_o d_o^{10} F(5, 7; -u_o^2/4) \right] \quad (62)$$

$$Q_8 = \frac{h^8}{336 \cdot 2^9} \left[\sigma d^{12} F(6, 9; -u^2/4) - \sigma_o d_o^{12} F(6, 9; -u_o^2/4) \right] \quad (63)$$

$$Q_9 = \frac{d^2}{2} F(1, 1; -u^2/4) \quad (64)$$

$$Q_{10} = -\frac{\sigma h^2 d^6}{8} F(3, 3; -u^2/4) \quad (65)$$

by using a recursion relationship of Kummer's function

$$\alpha F(\alpha + 1, \gamma + 1; z) = (\alpha - \gamma) F(\alpha, \gamma + 1; z) + \gamma F(\alpha, \gamma; z)$$

$$(\gamma - \alpha) z F(\alpha, \gamma + 1; z) = \gamma (z + \gamma - 1) F(\alpha, \gamma; z)$$

$$+ \gamma (1 - \gamma) F(\alpha, \gamma - 1; z) \quad (66)$$

the terms Q_i are described in terms of more elementary Kummer's function like $F(1, \gamma; z)$ which in turn is described in terms of more fundamental analytical functions. For example

$$F(1, 2; z) = (e^z - 1) / z \quad (67)$$

$$F(1, 3; z) = (e^z - 1 - z) \cdot 2/z^2 \quad (68)$$

III-4. Numerical Calculations

The effect of the various parameters upon the I_+ scattering patterns was explored by performing numerical calculations using the CDC 3600 computer of the University of Massachusetts Research Computing Center. Calculations are carried out for the H_V patterns (I_+ where $\Omega = \psi$) as a function of the parameters β_0 , d_0 , d , σ , σ_0 and ρ_2 . The significance of these parameters is as follows:

β_0 is the angle which the direction of maximum correlation of orientation makes with the optic axis of the domains. For rod-like domains extended in the optic axis direction $\beta_0 = 0^\circ$ while for disk-like domains, $\beta_0 = 90^\circ$.

d_0 is the correlation distance in the direction of β_0 whereas d is the correlation distance in any other direction. For random correlations, $d = d_0$.

σ_0 is a measure of how the correlation distance in the β_0 direction depends upon direction in the oriented film, whereas σ is a measure of this dependence in other than the β_0 direction. σ_0 may be taken as a measure of the orientation of correlations within the domain while σ is related to

the interdomain correlations. While d_o and σ_o are measures of the angular dependence of size and perfection of the domains, d and σ are associated with the mutual packing of these domains in space. For random correlations, $\sigma = \sigma_o$ while for unoriented systems, $\sigma = \sigma_o = 0$.

The parameter ρ_2 is an orientation function for optic axes which is zero if these are randomly oriented parallel to the orientation axis of the sample. The ρ_2 parameter differs from the σ parameters in that ρ_2 deals with the orientation of the optic axes of the individual elements while the σ 's are associated with the orientation of the correlated domain containing many scattering elements.

The numerical calculations are carried out for values of the parameters which are summarized in Table I-2. A comparison of Figs. I-9 and I-10 reveals the effect of orienting the optic axes without orienting the disk shaped region of correlation. Without orientation, the I_+ intensity distribution shows symmetrical maxima at odd multiples of $\psi = 45^\circ$ as previously discussed. With increase in ρ_2 , the pattern is oriented toward $\psi = 0^\circ$ at larger scattering angles and $\psi = 90^\circ$ at smaller. This would correspond to a shift of the lobes of the photographic pattern toward the equator ($\mu = 90^\circ$).

One may see the effect of change in the orientation of the correlation direction for a given degree of optic axis orientation by comparing Figs. I-10 and I-11. There appears to be little effect on the scattering pattern. It should be noted that while $\sigma = \sigma_o = 1/16$ for these two cases $(c_o/a_o) = 1.3$ and $(c/a) = 1.06$ so that orientation of correlation

within the domain is greater than that between domains.

The effect of a further increase in optic axis orientation function for a given degree of domain orientation may be seen by comparing Figs. I-11 and I-12. This is seen to result in a greater asymmetry of the pattern about $\psi = 45^\circ$.

The effect of orientation of correlations between domains without having such orientation within the domain may be seen by comparison with Fig. I-14 where $\sigma_0 = 0$ ($c_0/a_0 = 1$) but $\sigma = 0.385$ (corresponding to $c/a = 1.5$) where a build-up of intensity in the equatorial region of the pattern is evident so that splitting into four lobes is less pronounced. An increase in σ_0 to $1/16$ (in Fig. I-15) with σ held at 0.385 produces little change indicating that the orientation of intradomain correlation has less effect than that of interdomain correlation.

A change from disk to rod-like correlation is seen by comparing Fig. I-12 where $\beta_0 = 90^\circ$ with Fig. I-13 where $\beta_0 = 0^\circ$ for the same value of other parameters. It is noted that for rod-like correlation, the pattern is oriented toward the meridian rather than the equator. This may be compared with the H_V patterns for unoriented systems where there is no difference between patterns corresponding to β_0 of 0° and 90° .

Considerations of V_V and H_H patterns would of course have been possible using this same approach, but it was felt that the H_V patterns adequately served to illustrate some of the features of the scattering from oriented systems.

It is noted that the theory is rather poor in describing the scatter-

ing from systems where the domains are organized in well-ordered morphology as found in spherulitic structures. Under such conditions, the correlation functions vary in a more complex manner with r than the assumed Gaussian form¹⁷ and dependence of correlation upon β is more complex than that represented by the delta-function. Also the change in orientation and correlation with strain depends upon the mechanics of the spherulite deformation so that higher terms in the Fourier expansion in orientation angles would be needed.

This theory may, however, be a good approximation for systems with less ordered arrangement of the domains in which there is a small deviation from random orientation correlations leading to rod or disk like character. As has been discussed in the previous treatment for unoriented system, this theory has some advantages over model calculations for the scattering from oriented rods⁷ in that one may include effects due to interparticle interference as well as those related to fluctuations within the domains.

TABLE I-2

Values of Parameters for Numerical Calculations*

<u>Fig. No.</u>	<u>$d_o(\mu)$</u>	<u>$d(\mu)$</u>	<u>σ_o</u>	<u>c_o/a_o</u>	<u>σ</u>	<u>c/a</u>	<u>ρ_2</u>	<u>β_o</u>
I-9	2	1	0	1.0	0	1.0	0	90°
I-10	2	1	0	1.0	0	1.0	1/4	90°
I-11	2	1	1/16	1.3	1/16	1.06	1/4	90°
I-12	2	1	1/16	1.3	1/16	1.06	1/2	90°
I-13	2	1	1/16	1.3	1/16	1.06	1/2	0°
I-14	2	1	0	1.0	0.385	1.5	1/2	90°
I-15	2	1	1/16	1.3	0.385	1.5	1/2	90°

* (σ_o , σ) and (c_o/a_o , c/a) are not independent to each other but dependent upon in a manner as shown in eqns. (49), (50) and (51).

TABLE I-3

The Designation of Constant Intensity Contours

<u>Contour No.</u>	<u>Relative Intensity*</u>
1	200
2	100
3	50
4	20
5	10
6	5
7	2

* In arbitrary unit.

P A R T II

THE LIGHT SCATTERING STUDIES
OF SPHERULITIC POLYMERS

In this part we shall discuss the scattering of light from spherulitic superstructures having internal heterogeneities in density, anisotropy and orientation. The effect of such internal heterogeneities on the scattering patterns shall be analyzed for undeformed (in Chapter II) and deformed (in Chapter III) two-dimensional spherulites for mathematical simplicity.

The theories based upon the two-dimensional treatment are not realistic and general because most experimental systems are composed of three-dimensional spherulites. However they appear to explain most of the fundamental features of the scattering from polyethylene films.

C H A P T E R I

INTRODUCTION

In the previous part (Part I), the theory of light scattering has been statistically described for systems having non-random orientation fluctuations by using a correlation function approach. It was pointed out there that although a general harmonic expansion approach is capable of exactly describing the scattering from spherulitic systems, it is complex even for the case of the unoriented two-dimensional case, and the extension of the theory to the description of three-dimensional and oriented systems would compound the complexity to an extent where the application of the theory would be impractical.

Most of the complexity in such a statistical approach arise from the difficulty in describing statistically the high degree of geometrical symmetry found in the crystalline superstructures. For systems having such high symmetry, a model approach has been used to avoid this complexity.

The theory of scattering of light from spherulites has been developed based upon the model approach³⁻⁶ in which the spherulites are assumed to be homogeneous anisotropic disks or spheres (for the case of two-⁶ and three-dimensional³ undeformed spherulites, respectively) or elliptical disks⁶ and ellipsoids^{4,5} (for the case of two- and three-dimensional deformed spherulites, respectively) having different polarizabilities along and perpendicular to radii of spherulites. Spherulites are assumed

to be perfect in that there are no internal fluctuations of density, anisotropy and orientation.

Such perfect spherulite theories predict quite well the qualitative features of low angle light scattering patterns. The predicated patterns, however, differ quantitatively from experiments in three important aspects as shown in Chapter IV of Part III and in reference (35): (1) the theoretical patterns show a more rapid intensity decrease with the scattering angle at larger scattering angles than do the experimental patterns, (2) the theory predicts a greater azimuthal angle dependence of scattered intensity than is experimentally found and (3) a "background intensity" is always found for H_V scattering patterns along $\mu = 0^\circ$ and 90° and at very small scattering angles close to zero.

Such background scattering has been subtracted from the experimental data to facilitate comparison with the perfect spherulite theory^{4,6}. It is our feeling, however, that this background scattering conveys important information about the internal arrangement of the structure within spherulites so that its study is warranted. The background intensity is believed to be primarily associated with the internal heterogeneities of the spherulites which arises from three kinds of imperfectness of spherulites: (1) intralamellar imperfections such as chain ends, short branches or chain links, (2) imperfections on the surface of the lamellae such as large loops, longer branches or chain ends and (3) interlamellar imperfections such as non crystalline part. It should be noted here that incomplete spherulite scattering such as from sheaf-like sectors^{37,38}

and truncations³⁹ also contribute to the background scattering. However it appears that the internal disorders may make a principal contribution to the background scattering in polyethylene films slowly cooled from melts or isothermally crystallized at high temperature than the disorders in spherulite shape. This is because the latter type of disorders are relatively insensitive to intensity of the background scattering compared with the former and require a fairly large amount of truncations and a fairly thin sectors in order to produce an appreciable background intensity. At $\mu = 0^\circ$ or 90° , the H_V scattering from the perfect spherulite is negligible in which case the experimental intensity yields direct information about the background. Such measurements are quite pertinent in studies of the spherulite morphology and the dynamics of spherulite deformation where it is believed that the time scales for the spherulite deformation itself and the rearrangement of the internal structure are different, as shown in Part III.

Two type of the theories have been developed in order to take into account the background scattering.

1. Composite model

The model has been proposed by Keijzers, van Aartsen and Prins²¹ (KVP). As discussed in Part I, this model assumes the total scattering intensity to be a sum of the intensity from the two components, one from perfect spherulites and the other from structures having random orientation fluctuations. The model is verified experimentally for isotactic polypropylene and polystyrene²¹. However in the case of polyethylene,

deviations of the theory from experiments have been observed by Chu³⁵, and also in this work for medium density polyethylene (see Chapter IV in Part III). The deviations occur especially at high scattering angles where the experimental H_V intensity distributions show greater azimuthal angle (μ or ψ) dependence than those of the theory. The deviations are attributed to the non-randomness in orientation fluctuations within the spherulite. A modified composite model is proposed³⁵ to account for these deviations. In this approach too, it is assumed that the total scattering intensity is a sum of the scattered intensity from two different structure components, one from the perfect spherulite as KVP and the other from structures having non-random orientation fluctuations. For the scattering from the latter component, the theory based upon the delta function approximation shown in Chapter I of Part I is adapted. The theory is more general than that of KVP and capable of taking into account for the deviations although it is somewhat complicated compared with the KVP theory.

In either case, however, the assumptions on the presence of the two phases and on the incoherence of the scattering from each phase limit the generality and the applicability of the theory. In the case of polyethylene, spherulites fill the sample space and impinge to each other³⁷, and the heterogeneities are built in within the spherulite or in boundaries between adjacent spherulites. In such a case the assumptions introduced to the composite models may not hold but the scattering should be described in terms of a single phase model (Disordered Spherulite

Model) allowing internal perturbations of the spherulite in terms of density, anisotropy and orientation.

2. Disordered spherulite model

The disordered spherulite theory has been recently proposed²³ for two dimensional spherulites. The H_V scattering intensity distribution was calculated for the case of orientational disorder in which the orientation angle (β) of the optic axes of scattering elements with respect to the spherulite radii varies from place to place within the spherulite, while the anisotropy of the spherulite (δ) is kept constant. Therefore

$$\beta = \beta(r, \alpha)$$

$$\delta = \text{constant} \tag{1}$$

where r and α specify the position of the scattering elements within the spherulite and are defined in Fig. II-1.

For mathematical simplicity two extreme case are considered: (1) case of radial disorders, in which β depends only upon r but not upon α , i. e., $\beta = \beta(r)$. (2) case of angular disorders, in which $\beta = \beta(\alpha)$. It should be noted here that such a kind of one dimensional disorder would overestimate the non-randomness in the internal orientation heterogeneities (cf, in the KVP approach orientation fluctuations are assumed to be random). The real system should be described in terms of combined radial and angular disorder. The orientational disorder is statistically described in terms of the magnitude and correlation distance of the orientation fluctuations. In the case of radial disorder, the correlation

function ($f(r_{12})$) is defined as

$$f(r_{12}) = \langle \cos 2\beta_{12} \rangle_{r_{12}}$$

and assumed to be

$$f(r_{12}) = \exp (-r_{12}/a) \quad (2)$$

where a is the correlation distance for the radial disorder and r_{12} is the radial separation distance of the two scattering elements. $\beta_{12} = \Delta\beta_2 - \Delta\beta_1$, and $\Delta\beta_1$ and $\Delta\beta_2$ are the fluctuations in β at r_1 and r_2 from their average (β_0). $\langle \rangle_{r_{12}}$ stands for the average under constant r_{12} .

Similarly in case of the angular disorder

$$\begin{aligned} G(\gamma_{12}) &= \langle \cos 2\beta_{12} \rangle_{\gamma_{12}} \\ &= \exp [-|\gamma_{12}| / c] \end{aligned} \quad (3)$$

where $G(\gamma_{12})$ is the angular correlation function and $\gamma_{12} = \alpha_{12} = \alpha_1 - \alpha_2$, which is an angular separation of two scattering elements. c is the angular correlation distance. The absolute value $|\gamma_{12}|$ is defined such that if $|\gamma_{12}| > \pi$ its supplement $[2\pi - |\gamma_{12}|]$ is used. The magnitude of the orientation fluctuations is expressed by $\langle \cos^2 2\Delta\beta_1 \rangle_{av}$ for both cases.

The theory can take into account the scattering from systems ranging from perfect spherulitic order (in which c or a is large and $\langle \cos^2 2\Delta\beta_1 \rangle_{av} = 1$) to highly disordered systems (in which $\langle \cos^2 2\Delta\beta_1 \rangle_{av} = \langle \sin^2 2\Delta\beta_1 \rangle_{av} = 1/2$ and c or a is small compared with size of the spherulites, which

leads to the prediction that H_V intensity is independent of azimuthal angle μ or ψ .). The numerical calculations have been made for case of intermediate order. The results indicate that (1) the radial disorder principally affects the scattering at scattering angles greater than that of maximum scattering, θ_{\max} , and that (2) the angular disorder principally affects the scattering at the scattering angle less than θ_{\max} . It is also indicated that (3) a build-up of the intensity at $\theta < \theta_{\max}$ or at $\theta > \theta_{\max}$ is increased with a decrease of a or c , that is with an increase of the internal disorders, and that (4) the disorder can take into account the background scattering at $\mu = 0^\circ$ and 90° .

In this part, theories for the scattering of light by spherulitic polymers shall be developed both for undeformed and deformed spherulites on the basis of the disordered spherulite model.

C H A P T E R I I

THE SCATTERING OF LIGHT BY UNDEFORMED DISORDERED SPHERULITES

In this chapter we shall first discuss the simplest case of disorder in the magnitude of the anisotropy in section II-1 and then in section II-2, a case of combined disorder in orientation and anisotropy. Finally in section II-3 we shall discuss the V_V component of scattering and a separation of density and orientation fluctuations occurring within the spherulites. Numerical calculations have been made for the simplest case only and the effect of anisotropy disorder on the H_V scattering shall be discussed in detail.

II-1. The Effect of Disorder in the Magnitude of the Anisotropy

In Chapter I of this part and in previous work²³, the scattering of light from a disordered two-dimensional spherulite was analyzed where the anisotropy, δ of the scattering volume element was held constant but the orientation of its optic axis vector \underline{a} (see Fig. II-1) was allowed to deviate from its average orientation angle, β_0 , with respect to the spherulite radius. In this section (II-1) we shall consider the consequence of holding the optic axis orientation angle β constant at β_0 but allowing the magnitude of the anisotropy to fluctuate from its average value δ_0 . The treatment discussed here is also thought to be an extension of the theory on the isotropic sphere with internal density fluctuations⁴⁰ to the anisotropic disk with internal anisotropy fluctuations.

The Calculation

For a two-dimensional spherulite of radius R lying in a plane perpendicular to the incident beam with optic axes lying in the plane of the spherulite and at a constant angle, β_0 , to the radius, the amplitude of H_V scattering is given by⁶

$$E_{H_V} = \frac{1}{2} C_2 \cos \rho_2 \int_{r=0}^R \int_{\alpha=0}^{2\pi} \delta(r, \alpha) \cos 2\beta_0 \sin 2\alpha \cos k(r, s) d\alpha r dr \quad (4)$$

The term C_2 is a constant related to C of the previous work²³ by $C = C_2 \delta$, and α and r are the circular coordinate of a scattering volume element.

The angle ρ_2 is given by⁶

$$\cos \rho_2 = \cos \theta / [\cos^2 \theta + \sin^2 \theta \sin^2 \mu]^{1/2} \quad (5)$$

As before $k = 2\pi/\lambda$, λ is the wavelength in the medium, and $\underline{s} = \underline{s}_0 - \underline{s}_1$ where \underline{s}_0 and \underline{s}_1 are unit incident and scattered ray vectors. The anisotropy $\delta(r, \alpha)$ must be included within the integral because it is a function of position in the disordered spherulite. As in the previous work²³, we shall use the correlation function approach to evaluate the scattered intensity, which involves squaring eq. (4) prior to integration. Since the general case would lead to a four-fold integral whose numerical calculation would be prohibitive, we shall consider only special cases where $\delta(r, \alpha)$ is only a function of α or of r but not both together.

Case of Radial Disorder

If $\delta(r, \alpha)$ only varies with r but not α , then eq. (4) may be integrated

over α to give

$$E_{H_V} = C_2 \pi \cos \rho_2 \sin 2\xi_0 \cdot \int_{r=0}^R \delta(r) J_2(x) r dr \quad (6)$$

where $\xi_0 = \mu + \beta_0$, $x = kr \sin \theta$, and $J_2(x)$ is the second order Bessel function of x . Therefore, upon squaring,

$$I_{H_V} = K \cos^2 \rho_2 \sin^2 2\xi_0 \cdot \int_{r_1=0}^R \int_{r_2=0}^R \delta(r_2) \delta(r_1) J_2(x_2) J_2(x_1) r_1 r_2 dr_1 dr_2 \quad (7)$$

where K is a proportional constant related to C_2 . We shall now consider $\delta(r_i)$ to fluctuate from its average value by an amount $\Delta(r_i)$ defined by

$$\delta(r_i) = \delta_0 + \Delta(r_i) \quad (8)$$

Then

$$\langle \delta(r_1) \delta(r_2) \rangle_{r_{12}} = \delta_0^2 + 2\delta_0 \langle \Delta(r_1) \rangle_{r_{12}} + \langle \Delta(r_1) \Delta(r_2) \rangle_{r_{12}} \quad (9)$$

where the average is found at constant $r_{12} = r_2 - r_1$. Now, since positive and negative fluctuations are equally probable, it follows that

$$\langle \Delta(r_1) \rangle_{r_{12}} = 0 \quad (10)$$

Let us define a correlation function of anisotropy like, that introduced by Stein and Wilson¹⁶

$$\Psi_r(r_{12}) = \langle \Delta(r_1) \Delta(r_2) \rangle_{r_{12}} / \langle (\Delta(r_1))^2 \rangle_{av} \quad (11)$$

Then eq. (4) becomes

$$I_{H_V} = K \cos^2 \rho_2 \cdot \sin^2 2\xi_o \cdot \delta_o^2 \left\{ \int_{r=0}^R \int_{r=0}^R J_2(x_1) J_2(x_2) r_1 r_2 dr_1 dr_2 \right. \\ \left. + \frac{\langle (\Delta(r_i))^2 \rangle_{av}}{\delta_o^2} \int_{r_1=0}^R \int_{r_2=0}^R \Psi_r(r_{12}) J_2(x_1) J_2(x_2) r_1 r_2 dr_1 dr_2 \right\} \quad (12)$$

The first term represents the scattering from a perfect spherulite, whereas the second term represents the excess scattering from the anisotropy fluctuations. Thus

$$I_{H_V} = k \cos^2 \rho_2 \cdot \sin^2 2\xi_o \cdot \delta_o^2 \left\{ \frac{R^4}{w^4} [2 - J_0(w) - w J_1(w)]^2 \right. \\ \left. + \frac{\langle (\Delta(r_i))^2 \rangle_{av}}{\delta_o^2} \int_{r_1=0}^R \int_{r_2=0}^R \Psi_r(r_{12}) J_2(x_1) J_2(x_2) r_1 r_2 dr_1 dr_2 \right\} \quad (13)$$

where $w = kR \sin\theta$. As in the previous work²³, an exponential correlation function is assumed of the form

$$\Psi_r(r_{12}) = \exp [-|r_{12}|/a] \quad (14)$$

where a is a radial correlation distance of anisotropy disorder. The integral in the second term of eq. (12) is identical with that appearing in the previous work²³ for radial disorder of orientation so that the results of the numerical integrations of the previous work may be employed here.

Numerical results have been obtained for $\beta_o = 90^\circ$ (or 0°), $R = 3\mu$, $\lambda = 0.364\mu$, and for $a = 1,000 \text{ \AA}$, $6,000 \text{ \AA}$ and $15,000 \text{ \AA}$. The arbitrary constant in the scattering intensity equation is chosen such that $K\delta_o^2 = 10^5$. A plot of the H_V intensity at $\mu = 45^\circ$ is given in Fig. II-2 for $a = 15,000 \text{ \AA}$ and $\langle(\Delta(r_i))^2\rangle_{av}/\delta_o^2$ of 0 , 1×10^{-5} , 5×10^{-5} , 1×10^{-4} and 1×10^{-3} . It is seen that with an increasing amplitude of anisotropy fluctuation, the fine structure of the higher order intensity variation with θ is lost, and also there is an increasing intensity of scattering at larger values of θ . The even order intensity maxima tend to smear out while the odd order tend to be broadened and enhanced in intensity.

As with orientation fluctuations in the radial direction, the zero intensity at $\theta = 0$ which arises from the angular symmetry is preserved. The intensity varies with $\sin^2 2\xi_o$ so that the variation of intensity with the azimuthal angle μ characteristic of a perfect spherulite remains.

Plots of the variation of the scattered H_V intensity at $\mu = 45^\circ$ for a variety of values of $\langle(\Delta(r_i))^2\rangle_{av}/\delta_o^2$ are given in Fig. II-3 for $a = 6,000 \text{ \AA}$ and in Fig. II-4 for $a = 1,000 \text{ \AA}$. It is noted that as the correlation distance becomes shorter, the build-up of intensity at larger scattering angles becomes greater.

Case of Angular Disorder

In this case, $\delta(r, \alpha)$ only varies with α but not r , so that eq. (4) may be integrated over r to give

$$E_{H_V} = \frac{1}{2} C_{2\pi} \cos \rho_2 R^2 \int_{\alpha=0}^{\pi} \delta(\alpha) \cdot \sin(2\alpha + 2\beta_0) \cdot f(\gamma) \cdot d\alpha \quad (15)$$

where $\gamma = \alpha - \mu$ and

$$f(\gamma) = \frac{\cos(w \cos \gamma) - 1}{(w \cos \gamma)^2} + \frac{\sin(w \cos \gamma)}{(w \cos \gamma)} \quad (16)$$

Thus if $\beta_0 = 0^\circ$ or 90° ,

$$I_{H_V} = K' \cdot \cos^2 \rho_2 \cdot R^4 \int_{\alpha_1=0}^{2\pi} \int_{\alpha_2=0}^{2\pi} \delta(\alpha_1) \delta(\alpha_2) \sin 2\alpha_1 \cdot \sin 2\alpha_2 \cdot f(\gamma_1) f(\gamma_2) d\alpha_1 d\alpha_2 \quad (17)$$

where $K' = (1/4)K$. As in the previous work²³, we assume that

$\langle \delta(\alpha_1) \delta(\alpha_2) \rangle_{\alpha_1, \alpha_2}$ depends only upon the angular separation of the scattering elements and is random and we define a fluctuation in $\delta(\alpha)$ by

$$\delta(\alpha_i) = \delta_0 + \Delta(\alpha_i) \quad (18)$$

so that

$$\langle \delta(\alpha_1) \delta(\alpha_2) \rangle_{\alpha_1, \alpha_2} = \delta_0^2 + \langle \Delta(\alpha_1) \Delta(\alpha_2) \rangle_{\alpha_{12}} \quad (19)$$

where $\alpha_{12} = \alpha_2 - \alpha_1$. We may define an angular correlation function

$$\Psi_\alpha(\alpha_{12}) = \langle \Delta(\alpha_1) \Delta(\alpha_2) \rangle_{\alpha_{12}} / \langle (\Delta(\alpha_1))^2 \rangle_{av} \quad (20)$$

So that eq. (17) becomes, as before

$$I_{H_V} = K' \cdot \cos^2 \rho \cdot R^4 \delta_o^2 \left\{ \frac{1}{w^4} [2 - 2J_0(w) - w J_1(w)]^2 \sin^2 2\mu \right. \\ \left. + \frac{\langle (\Delta(\alpha_i))^2 \rangle_{av}}{\delta_o^2} [\sin^2 2\mu \cdot I_1 + \cos^2 2\mu \cdot I_2] \right\} \quad (21)$$

where

$$I_1 = \int_{\gamma_2=0}^{2\pi} \int_{\gamma_1=0}^{2\pi} \Psi_\alpha(\gamma_{12}) \cos 2\gamma_1 \cdot \cos 2\gamma_2 \cdot f(\gamma_1) f(\gamma_2) d\gamma_1 d\gamma_2 \quad (22)$$

and

$$I_2 = \int_{\gamma_2=0}^{2\pi} \int_{\gamma_1=0}^{2\pi} \Psi_\alpha(\gamma_{12}) \sin 2\gamma_1 \cdot \sin 2\gamma_2 \cdot f(\gamma_1) f(\gamma_2) d\gamma_1 d\gamma_2 \quad (23)$$

where $\gamma_{12} = \gamma_2 - \gamma_1 = \alpha_{12}$. The angular correlation function may be represented by an exponential function as before

$$\Psi_\alpha(\gamma_{12}) = \exp [-|\gamma_{12}|/c] \quad (24)$$

where $|\gamma_{12}|$ is the absolute value of γ_{12} ($= \alpha_{12}$) with the additional restriction that if $\gamma_{12} > 180^\circ$, $\Psi_\alpha(\gamma_{12}) = \Psi_\alpha(\gamma_{12} - 180^\circ)$.

The results of the numerical calculations of the previous work²³ for I_1 and I_2 may then be used. A calculated variation of I_{H_V} with θ at $\mu = 45^\circ$ is given in Fig. II-5 for a 3μ spherulite and $\lambda = 0.364$ for $c = 0.7$ and various values of $\langle (\Delta(\alpha_i))^2 \rangle_{av} / \delta_o^2$. The arbitrary constant is chosen such that $K' \delta_o^2 R^4 = 10^5$. Similar plots are given in Fig. II-6

for $\langle (\Delta(\alpha_i))^2 \rangle_{av} / \delta_o^2 = 5 \times 10^{-3}$ and $c = \pi, 0.7\pi$ and 0.5π . It is evident from the figures that angular disorder produces a somewhat similar effect as does radial disorder, with the higher order maxima and minima becoming more diffuse with an increase in the mean-squared amplitude of the anisotropy fluctuation, $\langle (\Delta(\alpha_i))^2 \rangle_{av} / \delta_o^2$, and with a decrease in the correlation distance, c . An important difference between the effects of radial and angular disorder is that with angular disorder, there is an increasing intensity at angles less than that of the maximum intensity, θ_{max} , with increasing amplitude or decreasing correlation distance for the anisotropy disorder whereas this region is not affected much by radial disorders. On the other hand, the intensity at angles greater than θ_{max} is more affected by radial disorder.

While the azimuthal dependence of H_V intensity is not affected by radial disorder of anisotropy, so that the intensity remains zero at $\mu = 0^\circ$ and $\mu = 90^\circ$ (for $\beta_o = 0^\circ$ or 90°), there is an appreciable effect on this μ dependence by angular disorder of anisotropy. Thus it is possible to distinguish between such radial and angular disorder from an examination of this μ dependence. It is noted that radial disorder of orientation of optic axes does affect the dependence of scattered intensity, which differs from the results for radial disorder in the magnitude of the anisotropy.

The effect of angular disorder in anisotropy is demonstrated in the contour diagram of Fig. II-7 where a perfect spherulite is compared with disordered spherulites having an angular correlation distance of 0.7π radians and mean-squared fluctuations of anisotropy characterized by

$\langle (\Delta(\alpha_i))^2 \rangle_{av} / \delta_o^2$ of 0.005 and 0.01. It is seen that increasing disorder leads to patterns of the "tennis-racquet" type described by Kawai and coworkers³⁶. The numbers on the contour lines refer to relative intensities given in Table I. With increasing disorder, there is a build-up of a connecting link of scattered intensity between the center of the pattern and the typical H_V scattering maximum.

TABLE II-1

The Designation of Contour
Lines of Constant Intensity

<u>Line No.</u>	<u>Relative Intensity</u>
1	4×10^3
2	3×10^3
3	2×10^3
4	1×10^3
5	5×10^2
6	2×10^2
7	1×10^2

Summary

The contribution to the disorder scattering by imperfect spherulites resulting from fluctuations in the magnitude of the anisotropy is analyzed for two-dimensional spherulites. The fluctuations are described in terms of a parameter characterizing the mean-squared amplitude of the fluctuations and correlation function describing the distance over which the correlation occurs. Cases considered are those where the correlation

depends on either the radial or the angular separation of the scattering volume elements. Numerical calculations have been made for H_V scattering. As with the case of disorder in orientation, one finds that disorder in anisotropy results in (1) a non-zero value of intensity at $\mu = 0^\circ$ and 90° , (2) a decrease in the higher order variation of scattered intensity with θ , and (3) an increase in the intensity of scattering at higher values of θ over that for a perfect spherulite. In addition, (4) disorder in the angular direction leads to an increase in the scattered intensity at small values of θ as compared with the zero intensity of scattering from a perfect spherulite at $\theta = 0^\circ$.

II-2. Case of Combined Disorder in Orientation and Anisotropy

Radial Disorder

If both the angle β and the anisotropy δ are dependent upon r , one must use, instead of eq. (6), the equation

$$E_{H_V} = C_2 \pi \cos \rho_2 \int_{r=0}^{\infty} \sin 2\xi(r) \cdot \delta(r) J_2(x) r dr \quad (25)$$

where $\xi(r) = \mu + \beta(r)$ and is a function of r which must be included in the integral. The intensity is then

$$I_{H_V} = K \cos^2 \rho_2 \int_{r_1=0}^R \int_{r_2=0}^R \langle \delta(r_1) \delta(r_2) \sin 2\xi(r_1) \cdot \sin 2\xi(r_2) \rangle_{r_1, r_2} J_2(x_1) J_2(x_2) r_1 r_2 dr_1 dr_2 \quad (26)$$

It is then assumed that fluctuations in angle, β are independent of fluctuations in the magnitude of the anisotropy. Thus it follows that

$$\begin{aligned}
& \langle \delta(r_1) \delta(r_2) \sin 2\xi(r_1) \cdot \sin 2\xi(r_2) \rangle_{r_1, r_2} \\
& = \langle \delta(r_1) \delta(r_2) \rangle_{r_1, r_2} \langle \sin 2\xi(r_1) \cdot \sin 2\xi(r_2) \rangle_{r_1, r_2} \quad (27)
\end{aligned}$$

Now from eqns. (9), (10) and (11)

$$\langle \delta(r_1) \delta(r_2) \rangle_{r_1, r_2} = \delta_o^2 + \langle (\Delta(r_i))^2 \rangle_{av} \Psi_r(r_{12}) \quad (28)$$

We may adopt the procedure of the previous work²³ to show that

$$\begin{aligned}
\langle \sin 2\xi(r_1) \cdot \sin 2\xi(r_2) \rangle_{r_1, r_2} = f(r_{12}) & \left\{ \sin^2 2\xi_o \cdot \langle \cos^2 2\Delta\beta_1 \rangle_{av} \right. \\
& \left. + \cos^2 2\xi_o \langle \sin^2 2\Delta\beta_1 \rangle_{av} \right\} \quad (29)
\end{aligned}$$

where

$$f(r_{12}) = \langle \cos 2\beta_{12} \rangle_{r_{12}} \quad (30)$$

and, as before²³, $\Delta\beta_1 = \beta(r_1) - \beta_o$ and $\beta_{12} = \beta(r_2) - \beta(r_1)$. Therefore from eqns. (26) to (30), one obtains

$$\begin{aligned}
I_{H_V} = K \cos^2 \rho_2 & \left\{ \sin^2 2\xi_o \langle \cos^2 2\Delta\beta_1 \rangle_{av} + \cos^2 2\xi_o \langle \sin^2 2\Delta\beta_1 \rangle_{av} \right\} \\
& \delta_o^2 \int_{r_1=0}^R \int_{r_2=0}^R \left[1 + \frac{\langle (\Delta(r_i))^2 \rangle_{av}}{\delta_o^2} \Psi_r(r_{12}) \right] f(r_{12}) \\
& J_2(x_1) J_2(x_2) r_1 r_2 dr_1 dr_2 \quad (31)
\end{aligned}$$

This equation reduces to eq. (28) of the previous paper²³ when $\langle (\Delta(r_i))^2 \rangle_{av} = 0$ and when an exponential correlation function is assumed for $f(r_{12})$, and to eq. (13) of this part when $\Delta\beta_1 = 0$ and $f(r_{12}) = 1$.

If there is a large amplitude fluctuation $\langle \cos^2 2\Delta\beta_1 \rangle_{av}$ and $\langle \sin^2 2\Delta\beta_1 \rangle_{av}$ both approach 1/2. Also, under these conditions, the correlation distances associated with the correlation function $f(r_{12})$ and $\psi_r(r_{12})$ will be small as compared with the radius of the spherulite, so that the limits of integration may be extended to infinity without appreciable error to give

$$I_{H_V} = \frac{1}{2} K \cos^2 \rho_2 \cdot \delta_o^2 \int_{r_1=0}^{\infty} \int_{r_2=0}^{\infty} \left[1 + \frac{\langle (\Delta(r_i))^2 \rangle_{av}}{\delta_o^2} \psi_r(r_{12}) \right] f(r_{12}) J_2(x_1) J_2(x_2) r_1 r_2 dr_1 dr_2 \quad (32)$$

This result is a two-dimensional analog of the Stein-Wilson random orientation correlation theory¹⁶. In this case there is sufficient randomness so that the effect of the spherulitic superstructure is smeared out, and the scattered intensity becomes independent of azimuthal angle μ and is cylindrically symmetrical about the incident beam. Furthermore, the scattering pattern becomes independent of the spherulite radius, R but depends only upon the correlation distances associated with the disorder in anisotropy and orientation.

Angular Disorder

An analogous treatment applies to case of a combination of anisotropy and orientational disorder in the angular direction which leads to the

equation

$$I_{H_V} = K' \cos^2 \rho_2 R^4 \delta_o^2 \left\{ [\sin^2 2\xi_o \langle \cos^2 2\Delta\beta_1 \rangle_{av} + \cos^2 2\xi_o \langle \sin^2 2\Delta\beta_1 \rangle_{av}] I_3 + [\sin^2 2\xi_o \langle \sin^2 2\Delta\beta_1 \rangle_{av} + \cos^2 2\xi_o \langle \cos^2 2\Delta\beta_1 \rangle_{av}] I_4 \right\} \quad (33)$$

where

$$I_3 = \int_{\gamma_1=0}^{2\pi} \int_{\gamma_2=0}^{2\pi} \left[1 + \frac{\langle (\Delta(\alpha_i))^2 \rangle_{av}}{\delta_o^2} \Psi_\alpha(\gamma_{12}) \right] G(\gamma_{12}) \cos 2\gamma_1 \cos 2\gamma_2 f(\gamma_1) f(\gamma_2) d\gamma_1 d\gamma_2 \quad (34)$$

and

$$I_4 = \int_{\gamma_1=0}^{2\pi} \int_{\gamma_2=0}^{2\pi} \left[1 + \frac{\langle (\Delta(\alpha_i))^2 \rangle_{av}}{\delta_o^2} \Psi_\alpha(\gamma_{12}) \right] G(\gamma_{12}) \sin 2\gamma_1 \sin 2\gamma_2 f(\gamma_1) f(\gamma_2) d\gamma_1 d\gamma_2 \quad (35)$$

where $G(\gamma_{12})$ is an orientation correlation function in the angular direction defined by

$$G(\gamma_{12}) = \langle \cos 2\beta_{12} \rangle_{\gamma_{12}} \quad (36)$$

the average being evaluated for all pairs of scattering elements at the same radial distance from the center of the spherulite but at a fixed angular separation γ_{12} . As with the case of radial disorder, it is seen that the intensity is the sum of two terms one of which arises from

orientational disorder and the other of which arises from both orientational and anisotropy disorder.

II-3. The V_V Component of Scattering and the Separation of Density and Orientation Fluctuations

In previous work on the scattering from media with random fluctuations¹⁶, it was shown that the H_V scattering arises primarily from orientation fluctuations but that the V_V scattering also contains a contribution from density (or average refractive index) fluctuations. Thus from a combination of measurements of V_V and H_V scattering, it is possible to separate the two contributions. For a perfect spherulite, the H_V scattering arises from the anisotropy of the spherulite, δ_o , whereas the V_V scattering also depends upon the refractive index of the surroundings³. Thus it is expected that the H_V scattering from a disordered spherulite will depend upon the anisotropy of the spherulite and upon the fluctuations of anisotropy and optic axis orientation, while the V_V scattering also depends upon the refractive index of the environment and upon the fluctuation of the density of the spherulite from the average.

From previous results⁶, one obtains the expression for the amplitude of the V_V scattering,

$$E_{V_V} = C_2 \cos \rho_1 \left\{ \int_{r=0}^R \int_{\alpha=0}^{2\pi} \alpha_2(r, \alpha) \cos[x \cos(\mu - \alpha)] d\alpha r dr + \int_{r=0}^R \int_{\alpha=0}^{2\pi} \delta(r, \alpha) \cos^2 \gamma \cos[x \cos(\mu - \alpha)] d\alpha r dr \right\} \quad (37)$$

where $\cos \rho_1$ is given by⁶

$$\cos \rho_1 = \cos \theta / [\cos^2 \theta + \sin^2 \theta \cos^2 \mu]^{\frac{1}{2}} \quad (38)$$

We shall first consider the case of only radial disorder where eq. (37) may be integrated over angle α to give

$$E_{V_V} = - C_2 \pi \cos \rho_1 \left\{ 2 \int_{r=0}^R \alpha_2(r) J_0(x) r dr + \int_{r=0}^R \delta(r) [J_0(x) - J_2(x) \cos 2\xi] r dr \right\} \quad (39)$$

Upon squaring to calculate the intensities, one obtains

$$I_{V_V} = K \cos^2 \rho_1 [4 I_5 + 4 I_6 + I_7] \quad (40)$$

where

$$I_5 = \int_{r_1=0}^R \int_{r_2=0}^R \langle \alpha_2(r_1) \alpha_2(r_2) \rangle_{r_1, r_2} J_0(x_1) J_0(x_2) r_1 r_2 dr_1 dr_2 \quad (41)$$

$$I_6 = \int_{r_1=0}^R \int_{r_2=0}^R \langle \alpha_2(r_1) \delta(r_2) \rangle_{r_1, r_2} J_0(x_1) [J_0(x_2) - J_2(x_2) \langle \cos 2\xi(r_2) \rangle_{r_1, r_2}] r_1 r_2 dr_1 dr_2 \quad (42)$$

and

$$I_7 = \int_{r_1=0}^R \int_{r_2=0}^R \langle \delta(r_1) \delta(r_2) \rangle_{r_1, r_2} [J_0(x_1) J_0(x_2) - 2 J_0(x_2) J_2(x_1) \langle \cos 2\xi(r_1) \rangle_{r_1, r_2} + \langle \cos 2\xi(r_1) \cos 2\xi(r_2) \rangle_{r_1, r_2} J_2(x_1) J_2(x_2)] r_1 r_2 dr_1 dr_2 \quad (43)$$

It has been assumed that anisotropy and density fluctuations are independent of orientation fluctuations. The integral I_5 depends only upon density fluctuations, I_7 depends upon anisotropy and orientation fluctuations, while I_6 depends upon cross correlations of density and anisotropy fluctuations.

In eq. (42), $\langle \cos 2\xi(r_2) \rangle_{r_1, r_2}$ depends only upon r_2 and

$$\begin{aligned} \langle \cos 2\xi(r_2) \rangle_{r_1, r_2} &= \langle \cos 2\xi(r_2) \rangle_{av} = \langle \cos(2\mu + 2\beta_2) \rangle_{av} \\ &= \langle \cos(2\mu + 2\beta_0 + 2\Delta\beta_2) \rangle_{av} = \langle \cos(2\xi_0 + 2\Delta\beta_2) \rangle_{av} \\ &= \cos 2\xi_0 \langle \cos 2\Delta\beta_2 \rangle_{av} - \sin 2\xi_0 \langle \sin 2\Delta\beta_2 \rangle_{av} = 0 \end{aligned} \quad (44)$$

Since $\langle \sin 2\Delta\beta_2 \rangle_{av} = \langle \cos 2\Delta\beta_2 \rangle_{av} = 0$ as positive and negative values of $\Delta\beta_2$ are equally probable. Here β_2 is defined by $\beta_2 = \beta(r_2)$. Similarly, in eq. (43), $\langle \cos 2\xi(r_1) \rangle_{r_1, r_2} = 0$ thus it follows that

$$I_6 = \int_{r_1=0}^R \int_{r_2=0}^R \langle \alpha_2(r_1) \delta(r_2) \rangle_{r_1, r_2} J_0(x_1) J_0(x_2) r_1 r_2 dr_1 dr_2 \quad (45)$$

and

$$\begin{aligned} I_7 &= \int_{r_1=0}^R \int_{r_2=0}^R \langle \delta(r_1) \delta(r_2) \rangle_{r_1, r_2} [J_0(x_1) J_0(x_2) \\ &\quad + \langle \cos 2\xi(r_1) \cos 2\xi(r_2) \rangle_{r_1, r_2} J_2(x_1) J_2(x_2)] r_1 r_2 dr_1 dr_2 \end{aligned} \quad (46)$$

As before one may use

$$\begin{aligned} \langle \cos 2\xi(r_1) \cos 2\xi(r_2) \rangle_{r_1, r_2} &= [\cos^2 2\xi_0 \cdot \langle \cos^2 2\Delta\beta_1 \rangle_{av} \\ &\quad + \sin^2 2\xi_0 \cdot \langle \sin^2 2\Delta\beta_1 \rangle_{av}] f(r_{12}) \end{aligned} \quad (47)$$

In the Stein-Wilson theory¹⁶, it was assumed that density and anisotropy fluctuations were independent. We shall not make this assumption here since we consider that density and anisotropy fluctuations both arise from the same origin, that is the fluctuation in the number of crystals per cm³. It is conceivable, of course that anisotropy fluctuations could arise, in part from fluctuations in the amorphous orientation but we shall not consider this possibility.

To interconnect the fluctuations in density and anisotropy, we shall consider the fluctuations in $\rho(r)$, the number of crystals at distance r from the origin (assuming only radial fluctuations). If the principal polarizabilities of the crystals are α_1 and α_2 , the polarizability per unit volume at radius r is

$$\alpha_1(r) = \rho(r)\alpha_1$$

$$\alpha_2(r) = \rho(r)\alpha_2 = (\alpha - \delta/3)\rho(r)$$

so

$$\delta(r) = \alpha_1(r) - \alpha_2(r) = \rho(r) (\alpha_1 - \alpha_2) = \rho(r)\delta \quad (48)$$

where δ is anisotropy of the crystal itself and $\delta = \alpha_1 - \alpha_2$ and the average polarizability of the crystal is $(\alpha_1 + 2\alpha_2)/3$. Thus

$$\langle \alpha_2(r_1)\alpha_2(r_2) \rangle_{r_1, r_2} = (\alpha - \delta/3)^2 \langle \rho(r_1)\rho(r_2) \rangle_{r_1, r_2} \quad (49)$$

Now since $\rho(r_1) = \rho_0 + \Delta\rho_1$ where ρ_0 is the average number of crystals per cm³, it follows that

$$\langle \rho(r_1)\rho(r_2) \rangle_{r_1, r_2} = \rho_0^2 + \langle (\Delta\rho)^2 \rangle_{av} \gamma(r_{12}) \quad (50)$$

where $\gamma(r_{12})$ is a correlation function defined as

$$\gamma(r_{12}) = \langle \Delta\rho_1 \Delta\rho_2 \rangle_{r_1, r_2} / \langle (\Delta\rho)^2 \rangle_{av} \quad (51)$$

Thus we see that

$$\langle \alpha_2(r_1) \alpha_2(r_2) \rangle_{r_1, r_2} = (\alpha - \delta/3)^2 \rho_o^2 \left[1 + \frac{\langle (\Delta\rho)^2 \rangle_{av}}{\rho_o^2} \gamma(r_{12}) \right] \quad (52)$$

Similarly, it follows that

$$\langle \delta(r_1) \delta(r_2) \rangle_{r_1, r_2} = \delta^2 \rho_o^2 \left[1 + \frac{\langle (\Delta\rho)^2 \rangle_{av}}{\rho_o^2} \gamma(r_{12}) \right] \quad (53)$$

Upon substituting these quantities into eqns. (41), (42) and (43) for I_5 , I_6 and I_7 , one obtains

$$\begin{aligned} I_{VV} = & K \cos^2 \rho_1 \cdot \rho_o^2 \left\{ (4\alpha^2 + (4/3)\alpha\delta + (1/9)\delta^2) \right. \\ & \int_{r_2=0}^R \int_{r_1=0}^R \left[1 + \frac{\langle (\Delta\rho)^2 \rangle_{av}}{\rho_o^2} \gamma(r_{12}) \right] J_0(x_1) J_0(x_2) r_1 r_2 dr_1 dr_2 \\ & + \delta^2 [\cos^2 2\xi_o \langle \cos^2 2\Delta\beta_1 \rangle_{av} + \sin^2 2\xi_o \langle \sin^2 2\Delta\beta_1 \rangle_{av}] \\ & \left. \int_{r_2=0}^R \int_{r_1=0}^R \left[1 + \frac{\langle (\Delta\rho)^2 \rangle_{av}}{\rho_o^2} \gamma(r_{12}) \right] f(r_{12}) J_2(x_1) J_2(x_2) r_1 r_2 dr_1 dr_2 \right\} \quad (54) \end{aligned}$$

The first term is associated with density fluctuations while the second term is associated with both density and orientation fluctuations. The first term is μ independent while the second term is dependent upon μ .

The eq. (31) may be written in terms of these same variables as

$$I_{H_V} = K \cos^2 \rho_2 \left\{ \sin^2 2\xi_o \langle \cos^2 2\Delta\beta_1 \rangle_{av} + \cos^2 2\xi_o \langle \sin^2 2\Delta\beta_1 \rangle_{av} \right\} \delta^2 \rho_o^2$$

$$\int_{r_2=0}^R \int_{r_1=0}^R \left[1 + \frac{\langle (\Delta\rho)^2 \rangle_{av}}{\rho_o^2} \gamma(r_{12}) \right] f(r_{12}) J_2(x_1) J_2(x_2) r_1 r_2 dr_1 dr_2$$

(55)

It is possible to separate the contribution to scattering arising from density and orientation fluctuations by measurement of I_V and I_{H_V} at appropriate angles. Thus it might be possible to obtain the parameters $\langle \cos^2 2\Delta\beta_1 \rangle_{av}$ and $\langle (\Delta\rho)^2 \rangle_{av} / \rho_o^2$ and the correlation functions $\gamma(r_{12})$ and $f(r_{12})$ required to specify the disorder in a given system.

A similar but more complex analysis may be made for systems with disorder in the angular direction.

C H A P T E R I I I

THE SCATTERING OF LIGHT BY
DEFORMED DISORDERED SPHERULITES

In this chapter the change in the light scattering patterns upon deforming two-dimensional disordered spherulites is shown to arise from three effects occurring upon stretching: (1) the change in shape of the spherulite, (2) the change in deviation of the optic axis orientation angle from its average value, and (3) the change in the distance over which this deviation is correlated. The effects of these contributions upon the experimental scattering patterns are analyzed.

III-1. Introduction

The change in light scattering patterns upon deforming perfect spherulites has been considered in two⁶ and three dimensions^{4,5}. The theories are based upon a model of affine deformation of an anisotropic sphere (or circle) to an ellipsoid (or ellipse) and lead to predicted scattering patterns which change shape with deformation in a manner which is approximately in agreement with experiment. The results are somewhat dependent upon the assumptions concerning the way in which the optic axes of the anisotropic elements constituting the spherulite change their orientation as the spherulite is deformed.

It has been shown in previous chapters of this part that the scattered intensity from spherulites is superposed on a background intensity, and that the background intensity arises from internal heterogeneities of the spherulites in terms of density, anisotropy and orientation. Such background scattering has been also observed with deformed spherulites^{4,6}.

The change of background scattering upon stretching the spherulite is believed to be associated with the change of the internal heterogeneities resulting from the internal rearrangement of structure within the deformed spherulites. Thus the background scattering is believed to convey important information on the deformation mechanism of the spherulites. Direct information about the background may be obtained by measurements of H_V scattering at $\mu = 0^\circ$ and 90° where spherulitic contribution vanishes.

In this chapter, a similar analysis is carried out for the effect of disorder in orientation from deformed spherulites.

III-2. The Calculation

Consider a two-dimensional spherulite with the optic axes \tilde{a} lying in the plane of the spherulite (in YZ-plane) at an angle β to the radius (Fig. II-1). The plane of the spherulite lies perpendicular to the incident beam. The angular coordinates of the radial vector \tilde{r} to a given scattering element are r and α . The H_V scattered intensity is given by

$$E_{H_V} = K \cos \rho_2 \int N_o \sin [2 (\alpha + \beta)] \cos [k (\tilde{r} \cdot \tilde{s})] d\tilde{r} \quad (1)$$

where as before, $\cos \rho_2 = \cos \theta / [\cos^2 \theta + \sin^2 \theta \sin^2 \mu]^{1/2}$, θ and μ are the scattering angles, $k = 2\pi/\lambda$ and $\tilde{s} = \tilde{s}_0 - \tilde{s}_1$ where \tilde{s}_0 and \tilde{s}_1 are unit incident and scattered ray vectors. N_o is the density of scattering material at position \tilde{r} in the spherulite. K is a proportional constant associated with C_2 in the previous chapter of this part. Upon deformation, this becomes

$$E_{H_V} = K \cos \rho_2 \int N (r', \alpha') \sin[2(\alpha' + \beta')] \cos[k(\tilde{r}' \cdot \tilde{s})] d\tilde{r} \quad (2)$$

where the primed quantities designate the deformed state. The scattering density $N(r', \alpha')$ is generally a function of position in the spherulite as is the angular orientation of the optic axis with respect to the radius.

As before⁶, we shall assume an affine deformation such that all parts of the spherulite deform with the same strain with an extension ratio λ_3 in the stretching direction (vertical and parallel to the direction of polarization of the incident light) and λ_2 in the transverse direction. It is usual but not necessary to assume that these spherulite extension ratios correspond to the sample extension ratios. This affine deformation results in the following transformations⁶.

$$r' = r [\lambda_2^2 \sin^2 \alpha + \lambda_3^2 \cos^2 \alpha]^{1/2} \quad (3)$$

$$\sin \alpha' = \frac{\lambda_2 \sin \alpha}{[\lambda_2^2 \sin^2 \alpha + \lambda_3^2 \cos^2 \alpha]^{1/2}} \quad (4)$$

and

$$\cos \alpha' = \frac{\lambda_3 \cos \alpha}{[\lambda_2^2 \sin^2 \alpha + \lambda_3^2 \cos^2 \alpha]^{1/2}} \quad (5)$$

It is then convenient to define an angle γ such that

$$\sin \gamma = \frac{\lambda_2 \sin \mu}{[\lambda_2^2 \sin^2 \mu + \lambda_3^2 \cos^2 \mu]^{1/2}} \quad (6)$$

and

$$\cos \gamma = \frac{\lambda_3 \cos \mu}{[\lambda_2^2 \sin^2 \mu + \lambda_3^2 \cos^2 \mu]^{1/2}} \quad (7)$$

and a variable q such that

$$q = kr \sin \theta [\lambda_2^2 \sin^2 \mu + \lambda_3^2 \cos^2 \mu]^{1/2} \quad (8)$$

in which case

$$k (\tilde{r}' \cdot \tilde{s}) = q \cos \psi \quad (9)$$

where $\psi = \alpha - \gamma$. It also follows that $rdr = (R^2/X^2) qdq$ where $X = kR \sin \theta [\lambda_2^2 \sin^2 \mu + \lambda_3^2 \cos^2 \mu]^{1/2}$ and R is the initial (undeformed) radius of the spherulite.

We shall also adopt the assumption of Case I of the previous paper⁶ that the total density of scattering material remains constant at every point within the spherulite so that $N_0 r dr d\alpha = N(\alpha', r') r' dr' d\alpha'$. Upon substituting eqns. (3) through (9) into eq. (2) one obtains

$$E_{H_V} = K_1 \int_{q=0}^X \int_{\psi=0}^{2\pi} \{B(\alpha) \cos 2\beta' + C(\alpha) \sin 2\beta'\} \cos [q \cos \psi] d\psi q dq \quad (10)$$

where $K_1 = (1/2)K \cos \rho_2 N_0 (R^2/X^2)$ and

$$B(\alpha) = \frac{\lambda_2 \lambda_3 \sin 2\alpha}{[\lambda_2^2 \sin^2 \alpha + \lambda_3^2 \cos^2 \alpha]} \quad (11)$$

$$C(\alpha) = \frac{\lambda_3^2 \cos^2 \alpha - \lambda_2^2 \sin^2 \alpha}{[\lambda_2^2 \sin^2 \alpha + \lambda_3^2 \cos^2 \alpha]} \quad (12)$$

and

$$X = kR \sin \theta [\lambda_2^2 \sin^2 \mu + \lambda_3^2 \cos^2 \mu]^{1/2} \quad (12a)$$

III-3. Case of Angular Disorder

We shall assume that at a given polar angle α' within the deformed spherulite, the optic axis angle β' is independent of r and hence of q . In this case, eq. (10) may be integrated over q holding ψ constant. Let us define a function $f(\psi)$ by

$$\begin{aligned} f(\psi) &= \frac{1}{X^2} \int_{q=0}^X \cos [q \cos \psi] q dq \\ &= \frac{\cos [X \cos \psi] - 1}{[X \cos \psi]^2} + \frac{\sin [X \cos \psi]}{X \cos \psi} \end{aligned} \quad (13)$$

Then eq. (10) becomes

$$E_{H_V} = K_1 X^2 \int_{\psi=0}^{2\pi} [B(\alpha) \cos 2\beta' + C(\alpha) \sin 2\beta'] f(\psi) d\psi \quad (14)$$

If β' is constant, this integral may be evaluated numerically to give results equivalent to those previously published⁶ (for $\beta' = 0^\circ$) for uniform spherulites. Numerical integration can also be carried out for the case where β' is a function of α in the deformed state.

The case of interest here is that where there is heterogeneity in β' in the deformed state. As in the earlier paper²³, we shall adopt the correlation function approach involving squaring eq. (14) prior to integration to obtain for the scattered intensity

$$\begin{aligned}
I_{H_V} &= K_2 K_1^2 \int_{\psi_2=0}^{2\pi} \int_{\psi_1=0}^{2\pi} [B(\alpha_1) \cos 2\beta_1' + C(\alpha_1) \sin 2\beta_1'] \\
&\quad [B(\alpha_2) \cos 2\beta_2' + C(\alpha_2) \sin 2\beta_2'] f(\psi_1) f(\psi_2) d\psi_1 d\psi_2 \\
&= K_2 K_1^2 [I_1 + I_2 + 2I_3]
\end{aligned} \tag{15}$$

where

$$I_1 = \int_{\psi_2=0}^{2\pi} \int_{\psi_1=0}^{2\pi} B(\alpha_1) B(\alpha_2) \cos 2\beta_1' \cos 2\beta_2' f(\psi_1) f(\psi_2) d\psi_1 d\psi_2 \tag{16}$$

$$I_2 = \int_{\psi_2=0}^{2\pi} \int_{\psi_1=0}^{2\pi} C(\alpha_1) C(\alpha_2) \sin 2\beta_1' \sin 2\beta_2' f(\psi_1) f(\psi_2) d\psi_1 d\psi_2 \tag{17}$$

and

$$I_3 = \int_{\psi_2=0}^{2\pi} \int_{\psi_1=0}^{2\pi} B(\alpha_1) C(\alpha_2) \cos 2\beta_1' \sin 2\beta_2' f(\psi_1) f(\psi_2) d\psi_1 d\psi_2 \tag{18}$$

We may now assume, as before, that $\beta_1' = \beta_{01}' + \Delta\beta_1'$ where β_{01}' is the average value of β_1' in the deformed state at the angular location corresponding to α_1 , and $\Delta\beta_1'$ is the fluctuation from the average at this position. Then

$$\begin{aligned}
\cos 2\beta_1' \cos 2\beta_2' &= \cos 2\beta_{01}' \cos 2\beta_{02}' \cos(2\Delta\beta_1') \cos(2\Delta\beta_2') \\
&\quad + \sin 2\beta_{01}' \sin 2\beta_{02}' \sin(2\Delta\beta_1') \sin(2\Delta\beta_2') \\
&\quad - 2\sin 2\beta_{01}' \cos 2\beta_{02}' \sin(2\Delta\beta_1') \cos(2\Delta\beta_2')
\end{aligned} \tag{19}$$

Now if $\Delta\beta_{12}' = \Delta\beta_2' - \Delta\beta_1'$, then

$$\begin{aligned} \cos(2\Delta\beta_1') \cos(2\Delta\beta_2') &= \cos^2(2\Delta\beta_1') \cos(2\Delta\beta_{12}') \\ &\quad - \sin(2\Delta\beta_1') \cos(2\Delta\beta_1') \sin(2\Delta\beta_{12}') \end{aligned} \quad (20)$$

We shall adopt the previous assumptions that (1) the fluctuation $\Delta\beta_{12}'$ is independent of $\Delta\beta_1'$ and (2) positive and negative fluctuations of $\Delta\beta_1'$ are equally probable. Thus, for a given ψ_1 and ψ_2 , eq. (20) becomes

$$\langle \cos(2\Delta\beta_1') \cos(2\Delta\beta_2') \rangle_{\psi_1, \psi_2} = \langle \cos^2(2\Delta\beta_1') \rangle_{\psi_1} \langle \cos(2\Delta\beta_{12}') \rangle_{\psi_1, \psi_2} \quad (21)$$

Similarly, it follows that

$$\langle \sin(2\Delta\beta_1') \sin(2\Delta\beta_2') \rangle_{\psi_1, \psi_2} = \langle \sin^2(2\Delta\beta_1') \rangle_{\psi_1} \langle \cos(2\Delta\beta_{12}') \rangle_{\psi_1, \psi_2} \quad (22)$$

and

$$\langle \sin(2\Delta\beta_1') \cos(2\Delta\beta_2') \rangle_{\psi_1, \psi_2} = 0 \quad (23)$$

We shall now define a correlation function

$$G(\psi_1, \psi_2) = \langle \cos(2\Delta\beta_{12}') \rangle_{\psi_1, \psi_2} = G(\psi_1, \psi_{12}) \quad (24)$$

Then eq. (19) becomes

$$\begin{aligned} \langle \cos(2\beta_1') \cos(2\beta_2') \rangle_{\psi_1, \psi_2} &= [\cos 2\beta_{01}' \cos 2\beta_{02}' \langle \cos^2(2\Delta\beta_1') \rangle_{\psi_1} \\ &\quad + \sin 2\beta_{01}' \sin 2\beta_{02}' \langle \sin^2(2\Delta\beta_1') \rangle_{\psi_1}] G(\psi_1, \psi_{12}) \end{aligned} \quad (25)$$

Similarly

$$\begin{aligned} \langle \sin(2\beta_1') \sin(2\beta_2') \rangle_{\psi_1, \psi_2} &= [\sin 2\beta_{o1}' \sin 2\beta_{o2}' \langle \cos^2(2\Delta\beta_1') \rangle \\ &+ \cos(2\beta_{o1}') \cos(2\beta_{o2}') \langle \sin^2(2\Delta\beta_1') \rangle] G(\psi_1, \psi_{12}) \end{aligned} \quad (26)$$

and

$$\begin{aligned} \langle \sin(2\beta_1') \cos(2\beta_2') \rangle_{\psi_1, \psi_2} &= \{ \sin 2\beta_{o1}' \cos 2\beta_{o2}' [\langle \cos^2(2\Delta\beta_1') \rangle_{\psi_1} \\ &- \langle \sin^2(2\Delta\beta_2') \rangle_{\psi_2}] \} G(\psi_1, \psi_{12}) \end{aligned} \quad (27)$$

The evaluation of the integrals I_1 , I_2 and I_3 then depends upon the way in which quantities such as β_{o1}' , $\langle \sin^2(2\Delta\beta_1') \rangle$ and $G(\psi_1, \psi_2)$ depend upon angular position within the spherulite. Let us consider a simple case first where $\beta_{o1}' = \beta_o'$ and is independent of position within the spherulite. Then for the simple case where $\beta_o' = 0^\circ$, the integrals become

$$I_1 = \int_{\psi_2=0}^{2\pi} \int_{\psi_1=0}^{2\pi} B(\alpha_1) B(\alpha_2) \langle \cos^2(2\Delta\beta_1') \rangle_{\psi_1} G(\psi_1, \psi_{12}) f(\psi_1) f(\psi_2) d\psi_1 d\psi_2 \quad (28)$$

$$I_2 = \int_{\psi_2=0}^{2\pi} \int_{\psi_1=0}^{2\pi} C(\alpha_1) C(\alpha_2) \langle \sin^2(2\Delta\beta_1') \rangle_{\psi_1} f(\psi_1) f(\psi_2) G(\psi_1, \psi_{12}) d\psi_1 d\psi_2 \quad (29)$$

and $I_3 = 0$. The integration next depends upon the way in which terms like $\langle \sin^2(2\Delta\beta_1') \rangle_{\psi_1}$ depend upon ψ_1 and upon the functional form of $G(\psi_1, \psi_{12})$. A simple assumption to study first is that where the angular dependence of disorder is not affected by the deformation so that these terms are

independent of ψ_1 in which case

$$I_1 = \langle \cos^2(2\Delta\beta_1') \rangle \int_{\psi_2=0}^{2\pi} \int_{\psi_1=0}^{2\pi} B(\alpha_1) B(\alpha_2) f(\psi_1) f(\psi_2) G(\psi_{12}) d\psi_1 d\psi_2 \quad (30)$$

$$I_2 = \langle \sin^2(2\Delta\beta_1') \rangle \int_{\psi_2=0}^{2\pi} \int_{\psi_1=0}^{2\pi} C(\alpha_1) C(\alpha_2) f(\psi_1) f(\psi_2) G(\psi_{12}) d\psi_1 d\psi_2 \quad (31)$$

One may assume that $G(\psi_{12})$ may be represented exponentially as in the previous work so that

$$G(\psi_{12}) = \exp [-|\psi_{12}|/c] \quad (32)$$

where c is an angular correlation distance. It is noted that $\psi_{12} = \alpha_{12}$.

The quantity $|\psi_{12}|$ is defined such that if $|\psi_{12}| > \pi$, its supplement $(2\pi - |\psi_{12}|)$ is used.

If disorder is dependent upon deformation quantities like $\langle \sin^2(2\Delta\beta_1') \rangle_{\psi_1}$ depend upon position within the spherulite. A simple assumption is that it varies ellipsoidally with the angle α so that

$$\langle \cos^2(2\Delta\beta_1') \rangle_{\psi_1} = g_o (1 + \sigma \sin^2 \alpha_1) \quad (33)$$

so that it increases from g_o in the polar part of the spherulite to $g_o(1 + \sigma)$ in the equatorial part. When $\sigma = 0$, this reduces to the previous case.

Similarly, the correlation distance varies with α so that as a simple assumption

$$G(\gamma_1, \gamma_{12}) = \exp [-|\gamma_{12}|/c(1 + \rho \sin^2 \alpha_1)] \quad (34)$$

These equations may then be used in the evaluation of the integrals in eqns. (28) and (29) where σ and ρ are parameters describing the effect of orientation on the random contribution to the scattering. These parameters each vary with elongation.

III-4. Results

Calculations of H_V intensities for various values of the parameters have been carried out using the CDC 3600 computer of the University of Massachusetts Research Computing Center. The calculations were made for uniaxial deformation at constant volume so that $\lambda_3 = \lambda_s$ and $\lambda_2 = \lambda_s^{-1}$. Values of the undeformed spherulite radius $R = 3\mu$ and wavelength of light in the medium $\lambda = 0.364\mu$ were chosen (corresponding to the mercury green line in air $\lambda_0 = 0.546\mu$ with refractive index $n = 1.5$). The angular disorder correlation distance, c , was assumed to be independent of angle and elongation and was taken to be 0.7 radians. The proportionality constant $K_1^2 K_2^2 / \cos^2 \rho_2$ was arbitrarily set at 10^5 . The values of parameters corresponding to the various figures are summarized in Table II-2. The intensity contours are indicated by numbers which are relative intensities as shown in Table II-3.

TABLE II-2

A Summary of Parameters for Scattering Calculations

λ_s	g_o	σ	Fig. No.	Comments
1.0	1.0	0.0	II-9(a)	Contour Diagrams
1.0	0.9	0.0	II-9(b)	Contour Diagrams
1.0	0.7	0.0	II-9(c)	Contour Diagrams
1.0	0.9	0.0	II-10	θ Dependence
1.5	0.8	0.0	II-12(a)	Contour Diagrams
1.5	1.0	0.0	II-12(b)	Contour Diagrams
1.5	1.0	-0.2	II-12(c)	Contour Diagrams
1.5	1.0	-0.5	II-12(d)	Contour Diagrams
1.5	0.5	1.0	II-12(e)	Contour Diagrams
1.5	1.0	0.0 to -0.5	II-13	θ Dependence at $\mu = 0^\circ$
1.5	1.0	0.0 to -0.5	II-14	θ Dependence at $\mu = 90^\circ$

TABLE II-3

The Designation of Constant Intensity Contours

<u>Contour No.</u>	<u>Relative Intensity</u>
1	1.4×10^5
2	1.0×10^5
2'	8.0×10^4
3	7.0×10^4
3'	6.0×10^4
4	5.0×10^4
5	4.0×10^4
6	3.0×10^4
7	2.0×10^4
8	1.0×10^4

It is seen from a comparison of the undeformed perfect two-dimensional spherulite pattern of Fig. II-8 with the patterns of Fig. II-9 for the undeformed disordered spherulite that, as has previously been pointed out²³, the effect of disorder is to give a "tennis racquet" type pattern where there is a build-up of intensity toward the center of the pattern as disorder increases. This is further seen in the plot of Fig. II-10 for the variation of intensity with θ . The absolute intensity of scattering tends to decrease with increasing disorder*. For the perfect spherulite, the scattered intensity is zero at $\theta = 0$ and at all values of θ along $\mu = 0^\circ$ and 90° . For the disordered spherulite, there is a build-up of intensity at these values of μ .

The next set of figures are for the case of a spherulite which is deformed by an elongation ratio $\lambda_s = 1.5$. In Figs. II-12a and 12b, $\sigma = 0$ designating an angular variation of $\langle \cos^2(2\Delta\beta_1') \rangle_{av}$ which is independent of direction in the film. The disorder parameter in II-12a is 0.8 while it is 1.0 in II-12b.

It is seen that the patterns undergo a characteristic change in shape with deformation as previously pointed out⁶, with the intensity maxima moving toward higher values of μ and θ . For the undeformed spherulite, the maximum occurs at $\mu = 45^\circ$ and $\theta = 4.4^\circ$ while at an elongation ratio of 1.5, it occurs at $\mu = 60^\circ$ and $\theta = 4.8^\circ$ for $g_o = 1.0$. It is seen

* It should be noted that in case of angular disorder of the anisotropy, the absolute intensity is increased with increasing disorder. The reason of the difference may be easily seen by comparing eqns. (20) to (22) with eqns. (15), (25) and (26) under $\lambda_2 = \lambda_3 = 1$.

with increasing disorder, as g_o goes from 1.0 to 0.8, the pattern assumes a more "deformed tennis racquet" appearance with an increase in intensity at small values of θ and at $\mu = 0^\circ$ and 90° .

The effect of an angular dependence of $\langle \cos^2 2\Delta\beta_1' \rangle$ is seen in Figs. II-12c and II-12d where σ is allowed to assume values of -0.2 and -0.5 while g_o is kept constant at 1.0. The variation of $\langle \cos^2 2\Delta\beta_1' \rangle$ corresponding to these values of σ is shown in Fig. II-11. These negative values of σ correspond to spherulites in which the disorder is greater in the lateral region than the polar region. Fig. II-12e corresponds to $g_o = 0.5$ and $\sigma = 1.0$ which, as shown in Fig. II-11, is where the disorder is greatest in the polar region of the spherulite.

It is noted that the μ and θ at which the maximum scattering occurs is rather insensitive to the disorder parameters. As the amplitude of the orientation fluctuations becomes larger in the equatorial regions of the spherulites, there is a build-up of intensity in the polar region of the scattering pattern (at $\mu = 0^\circ$). This may be seen in Fig. II-13 representing a plot of the variation of H_V scattered intensity with θ at $\mu = 0^\circ$ for a deformed spherulite with $\lambda_s = 1.5$, $g_o = 1.0$ and σ changing from 0.0 to -0.5 which may be compared with Fig. II-14, the corresponding variation in the equatorial region of the scattering pattern at $\mu = 90^\circ$. The changes in the equatorial region of the pattern are more complex. The effect of such angular dependence of disorder is greater at $\mu = 0^\circ$ and 90° than at the μ corresponding to the intensity maximum.

Similarly, a comparison of Figs. II-12b and II-12e reveals that an increase in the amplitude of the orientation fluctuation in the polar

region of the spherulite leads to a pronounced increase in intensity at the equator of the scattering pattern (at $\mu = 90^\circ$).

Experimental scattering patterns from deformed polyethylene more closely resemble theoretical patterns like Fig. II-12c suggesting that larger fluctuations occur in the equatorial region of the deformed spherulite.

In these calculations, the angular correlation distance was kept constant. An angular variation of this is expected to have similar effects as produced by an angular variation of the amplitude of the fluctuation. Also, it has been assumed that the average optic axis tilt angle, β_o' , is independent of angle in the deformed state. A more thorough analysis would allow this to vary with α , perhaps in the manner of the empirical equation of van Aartsen, et.al.⁵. These additional variations are not included in this paper because of the desire to avoid introducing an unmanageable number of empirical parameters.

III-5. Conclusions

The introduction of non-randomness into the theory of the scattering from deformed spherulites produces changes in the predicted scattering patterns analogous to those predicted for undeformed spherulites. The disorder results in an increase in scattered intensity at small values of the scattering angle θ as well as non-zero intensities at $\mu = 0^\circ$ and 90° . The relative effect on the intensity at $\mu = 0^\circ$ and 90° depends upon the angular dependence of the amplitude and correlation distance associated with the fluctuations from orientational order within the spherulite.

The experimental observations of scattering patterns from stretched polyethylene indicate that a greater degree of disorder occurs in the equatorial part of the spherulite.

P A R T I I I

THE DYNAMIC LIGHT SCATTERING
STUDIES ON SPHERULITIC POLYMERS

C H A P T E R I

Introduction and Previous Works

The light scattering from crystalline polymer films has been used to characterize the crystalline superstructure and has been shown to arise principally from correlations in orientation of crystals occurring over distances comparable with the wavelength of light^{16,34}. Procedures for the separation of the contributions to scattering from density and orientation fluctuations were described for systems containing random orientation correlations. Most crystalline polymer systems have non-random orientation correlations represented by such structures as spherulites. Scattering patterns from uniform two and three dimensional spherulites have been calculated theoretically^{3,6} and found to qualitatively agree with experiment. Such spherulite theories predict scattering patterns characteristic of a greater degree of order than is experimentally found. Deviations are described in terms of disorder of orientation of crystals within spherulites²³ and disorder in the shape³⁹. The scattered intensity at higher angles is usually found to exceed that predicted by the uniform spherulite theories and results from heterogeneity of crystal orientation within the spherulite which may be characterized by orientation functions.

Upon deformation of the sample the scattering patterns change in a

manner characteristic of the orientation of the crystalline superstructures and can be approximately described by assuming that the spherulites become ellipsoidal when the samples are stretched⁴⁻⁶. Details depend upon the specific model employed for describing the change in orientation of the crystals within a spherulite when the spherulite deforms^{4,5}.

Dynamic mechanical, birefringence⁴¹, and x-ray diffraction experiments^{45,46} have been employed to study polymer deformation mechanisms associated with molecular orientation changes. These confirm previous proposals that the alpha mechanical loss peak consists of at least two components, the lower temperature one (α_1) being related to lamellar slip accompanying the twisting of the lamellae about their b axis which lies along the spherulite radius, while the higher temperature component (α_2) is related to molecular motion within the crystalline lattice. The mechanism which is proposed supposes that a rapid spherulite deformation accompanies the stretching of the sample and that this is followed by a slower orientation change of the crystals within the spherulite occurring by the α_1 and α_2 processes. Previous evidence for the rapid spherulite deformation comes from high speed light scattering motion pictures in which the fast change in the low angle light scattering pattern is demonstrated⁴⁴.

It is proposed that the variation of the light scattering intensity accompanying the vibration of a sample may further characterize the deformation processes. Earlier works of photometric dynamic light scattering studies have been carried out by LeGrand et. al. for polyethylene under stress relaxation⁴³ and sinusoidal tensile loading process⁴⁷. One significant results of those studies may be in the fact that the variation of V_V

intensity when the stretching direction is perpendicular to the scattering plane occurs appreciably for a time scale of 1 second to 1000second during the stress relaxation process while the variation of the H_V intensity under the same condition is hardly observable for that time scale⁴³. The fact may then suggest a significant factor underlying deformation process of crystalline polymers that a relaxation process associated with the change of density fluctuations may occur at longer time scale than that associated with crystalline reorientation processes.

The above discussion may be just an example to illustrate applications of the dynamic light scattering (DLS) technique. The DLS intensity depends upon i) static (ϵ_s) and dynamic (ϵ_d) strain, ii) time and temperature of the measurements, iii) stretching direction of the sample (Ω), iv) scattering angle (θ) and v) polarization conditions for polarizer and analyzer as well as iv) samples being studied. The studies of the DLS as a function of these variables may give us much informations for characterizing deformation processes occurring in crystalline superstructures. For example, in the case of polyethylene spherulites the deformation of the spherulites is, more or less, heterogeneous and is shown indirectly by x-ray orientation studies¹¹ to be quite different in the polar and equatorial part of the spherulites in terms of the orientation of the crystallographic axes. Such angular dependence of spherulite deformation with respect to the stretching axis may be studied more directly in terms of both orientation and density fluctuations by observing the DLS intensities as a function of the azimuthal angle Ω and the polarization conditions. One can also study the DLS as a function of scattering angle θ .

At small θ the DLS depends upon the response of the average spherulitic contour to the applied strain, while at large θ the DLS depends upon the response of the heterogeneities correlated over shorter distances than the spherulite size. Therefore the dependence of the DLS may provide additional information over those determined by the Ω dependence.

The DLS may also be measured as a function of other variables as discussed above to confirm a proposed deformation mechanism. For this purpose, a DLS apparatus has been constructed. The apparatus is designed to observe the DLS intensities from samples subjected to sinusoidal tensile strain.

C H A P T E R II

The Apparatus

An outline of the apparatus is schematically shown in Fig. III-1. A mercury vapor lamp (General Electric Supply Company, Type H100A4/T) has been used as a light source. The lamp is fired by a 110 volt AC power supply through a ballast transformer (General Electric Supply Company, Type 89G182). An incident beam from the mercury arc is monochromatized by a combination of a narrow band pass filter (Type No. 90-50550, Bausch & Lomb Incorporated) and a color glass filter for mercury green light, 546 m μ . The half width of the band pass filter is about 50 m μ . The incident beam is collimated by a set of lenses which will be shown later. The collimated monochromatic incident beam with wavelength 546 m μ is passed through a polarizer. The plane polarized incident beam irradiates the sample which is subjected to a sinusoidal tensile strain. The variation of scattered beam intensity due to the sample vibration, after passing through an analyzer under certain polarization conditions, is detected synchronously with the phase of strain by a detecting system composed of a photomultiplier(PM) tube, preamplifier, integrator, electronic counter and an oscilloscope. In the following, each part of the apparatus shall be discussed in more detail.

II-1. Light Source Part

Fig. III-2 shows a schematic diagram of an optical arrangement of the light source part. The lenses L1, L2, L3 and a pinhole P are used to collimate the incident beam. The pinhole P is placed at the front focus

point of the lens L3 to make the beam from L3 parallel. The size of the pinhole determines the divergence (or parallelness) of the incident beam. By using a pinhole with 1 mm diameter a divergence of about 30 minutes is obtained. The lens L1 is chosen to be such one that collects a relatively large flux of energy of the incident beam by using a lens with a relatively large diameter. The lenses L2 and L3 are chosen to satisfy a condition that the size of the output beam from the lens L3 is as small as the desired beam area (about 8 mm in diameter) which irradiates the sample. Therefore in this system, a diaphragm D is primarily used to cut off the diffused stray light in the incident beam but not to determine the size of the output beam diameter. By this way a part of the loss of the incident beam energy accompanying the process to determine the incident beam area is avoided.

The collimated monochromatic incident beam is finally passed through a polarizer P (whose polarization direction (ψ_1) can be rotated through 360°) to produce a plane polarized incident beam.

A part of the incident beam is reflected by a slide glass and is detected by a PM tube (RCA 1P21) to monitor fluctuations of the incident beam intensity. Because of the reflection at the slide glass, the final incident beam after the slide glass G is partially polarized and has degree of polarization about 21%. The correction for this effect is shown on Fig. III-3.

Pictures of the light source part are shown in the right hand side of Figs. III-4(a) and III-5. The symbols of A, B, F and PM stand for the same meaning as those of Fig. III-2.

II-2. Deformation Apparatus

Pictures of the deformation apparatus are shown in the left hand side of Figs. III-4(a) and III-5 and in the right hand side of Fig. III-4(b). The picture in Fig. III-4(b) is taken from the left hand side of the picture in Fig. III-4(a) and includes the detecting part of the DLS apparatus (which will be described in later) in the left hand side. The picture in Fig. III-5 is taken from the right hand side of the picture in Fig. III-4(a). The apparatus was designed by professor H. Kawai, Department of Polymer Chemistry, Kyoto University, Kyoto, Japan, and constructed by Iwamoto Machinery Company, Limited, Kyoto, Japan. In Fig. III-4(a), a sinusoidal tensile strain is mechanically imposed on the sample by using a set of eccentric cams (E). The static and dynamic strain can be changed almost continuously by using cams with various eccentricity and by adjusting initial sample length. The stretching of the sample is done simultaneously from both ends so that the part of the sample irradiated by the incident beam stays in the same position during the stretching process. The stretching direction of the sample (Ω) can be rotated from the vertical ($\Omega = 0^\circ$) to the horizontal ($\Omega = 90^\circ$) direction by rotating a worm gear D (Fig. III-4(a)). One can also change the tilting angle (ϕ) of the sample normal with respect to direction of the incident beam propagation by rotating a worm gear F (Fig. III-4(a)). Therefore the apparatus can be used for the study of biaxially oriented systems as well as uniaxially oriented systems. Two holders for PM tubes can be set on the disk D1 and D2 and can be rotated through 180° to vary the scattering angles, θ_1 and θ_2 (Fig. III-4(a)).

Frequency of the sample vibration can be changed from about 10 Hz to any lower frequency desired.

II-3. Detecting Part

The detecting part of the scattered beam intensity is composed of two part; one for the optical and the other for the electronic part.

a) Optical Part

Details of the optical part for detecting the scattered beam are schematically shown in Fig. III-6(a). The scattered beam is observed through an analyzer A (A in Fig. III-4(a)) whose polarization direction can be rotated through 360° . A diaphragm D is set at the back focus point of the lens L so that only a parallel flux of the scattered beam which occurs at some scattering angle θ can be passed through the diaphragm D and detected by a PM tube (RCA 1P21). The diameter of the pinhole in the diaphragm determines the angular resolution of the scattered intensity distribution with respect to θ .

The system has advantages in the following points compared with a conventional system shown in Fig. III-6(b) in which the angular resolution is directly determined by the size of the pinhole D, an irradiated area of the sample and a distance between sample and the pinhole D;

- i) The system in Fig. III-6(a) requires no correction for the change of irradiated volume of the sample when the scattering angle is changed, while in the conventional system the correction⁴² is needed.
- ii) It is possible in this system to increase the scattered beam energy without losing the angular resolution by increasing the

irradiated volume of the sample. On the other hand, in the conventional system, one cannot increase the irradiated volume of the sample without decreasing the angular resolution.

b) Electronic Part

In this section we shall discuss the electronic problems for detecting the DLS signals and the electronic system which has been used in the DLS experiments.

b-1) The electronic problems for detecting the DLS signals

As we shall discuss in later, the DLS signal is generally (1) quite small compared with static scattering intensity and therefore (2) fluctuations of static scattering intensity, even though they are very small, produce a baseline drift (of the DLS signal) which is comparable or even greater than the DLS signal itself. The DLS signal is generally less than 10% and quite often even less than 1% of the static scattering intensity and (3) noisy especially at high scattering angles. In order to achieve an amplification of the small DLS signals to a satisfactory level, one has to block off the large baseline signal corresponding to the static scattering intensity by some means because of the factor (1). Otherwise a power saturation will occur in the preamplifier before a satisfactory amplification is achieved to the DLS signals.

The baseline drift pointed out by the factor (2) may arise from i) fluctuations of the incident beam intensity, ii) fluctuations of high voltage power supply for PM tubes, iii) drift of electronics which are used, iv) random noise from PM tubes and v) sample vibrations. The drift and noise problem seem to be the most important. For example if there is

a 1% fluctuations of the baseline due to incident beam intensity fluctuations, for example and if the magnitude of the DLS signal is 1% of the baseline signal, then DLS signal is of the same magnitude as the baseline drift. Because of this noise and drift problem, the DLS signals are detected by using a signal averaging technique.

b-2) The electronic system

An outline of apparatus is shown in Fig. III-1. An output of the monitor and the detector PM tube are matched to each other in voltage by adjusting the supply voltage for monitor PM tube. The dynode string resistors for the PM tubes are wired in a manner shown in Fig. III-7. The detector PM tube is cooled for operation with high stability and minimized noise by using a refrigerated PM tube chamber (Model TE-109TS, Products for Research Inc., Mass.) R in Fig. III-4(b). The cooling may not be necessary for the measurements at low scattering angles but may be useful at high scattering angles.

The two outputs matched to each other are then fed to a differential preamplifier where the outputs are differentiated and then amplified. In this manner a large baseline signal accompanied with the DLS signals are cancelled out and only the small DLS signals are subjected to the preamplification, so that the power saturation problems are not encountered. (The amount of voltage change supplied for monitor PM tube in order to bring the two signals into balance is associated with the static scattering intensity.) At the same time the fluctuations of the baseline signals may be effectively cancelled out through the process of the differentiation

because two outputs are matched to each other. An offset voltage arising from the DLS signal is amplified by the differential preamplifier, and the DLS signal after the differential preamplifier is then fed to an integrator (Type CW-1 Box Car Integrator, Princeton Applied Research Corporation, N. J.) where further amplification and signal averaging can be carried out.

As an ideal stable preamplifier, a differential amplifier which is built in a 502 Dual Beam Oscilloscope (Textronix Inc. Oregon) has been used. The preamplifier has a variety of functions and can be used as a simple D.C and A.C preamplifier or a differential D.C and A.C preamplifier. An output of the preamplifier is taken from a point shown in Fig. III-8. The preamplifier has a wide range of input attenuation so that it can be used for a wide range of input signals.

In Fig. III-9 a block diagram of a part of CW-1 Box Car Integrator which has been used in these experiments is shown. As seen from the figure an input signal is amplified in the A.C or D.C coupling mode of the integrator with a range of time constants. The amplification of the signal can be carried out either in a continuous manner or in a manner determined by an external gate controlling signal. In the case of static light scattering measurements, the amplifier is operated in continuous mode by using D.C coupling and the noise of the signals accompanying the static scattering intensity is averaged out with an appropriate time constant.

In the case of DLS measurements, the DLS is characterized by a set of measured quantities, $\tan \gamma$ and I_d or $\Delta I'$ and $\Delta I''$. $\tan \gamma$ is the tangent of

the phase angle between the DLS intensity and strain. $\Delta I'$ and $\Delta I''$ are in-phase and out-of-phase part of the DLS intensity. These experimental variables are related to the kind of response of structures in polymer films to the applied dynamic strain.

A simple detection of these experimental variables by observing Lissajous figures of the variation of the DLS intensity and the dynamic strain is not, in general, possible because of the reasons already mentioned. Therefore the detection has been carried out by using a signal averaging technique in which the DLS signals have been averaged over a number of periods of vibrations at particular phase intervals. The experimental variables are then calculated as shown in later from these averaged DLS signals. Such a technique of synchronous detection of DLS signals with respect to the phase angle of strain is designed to be carried out by using an external trigger signal with the same frequency and phase relation to the dynamic strain.

The trigger signal is produced by a liner variable differential transformer (LVDT) (Model PC-210 gauge head and model CAS-2500 carrier amplifier demodulator power supply, Schaevitz Engineering, Pennsauken, N. J.) and a helical cam. The helical cam is attached to a shaft connected to one of the eccentric cams so that it rotates with same frequency as the sample vibration and has a definite phase relationship to the phase of vibration. The LVDT (L) and the helical cam (H) are seen in Fig. III-5. Fig. III-10 shows details of the helical cam. The diameter of the cam linearly increases with rotation. The cam is made under a computer-control and has a precision of about 0.1% in its

linear increment and 0.15 inch of maximum displacement. The output of the LVDT is, therefore, a saw-tooth type signal as shown in Fig. III-11 (signal C) and fed to the trigger gate of the integrator (see Fig. III-9).

The gate controlling circuit is composed of 1) a slope threshold controller, 2) an input Schmitt trigger circuit, 3) a gate pulse shaper and 4) a field effect transistor as shown in Fig. III-9. The threshold voltage determines a point at which a triggering occurs in the input Schmitt circuit, so that it determines a phase interval of gate-on and -off. The gate signal after the input Schmitt circuit is shown in Fig. III-11 (signal G) where the gate-on and -off time are equal in this particular case.

The gate signal is now used to operate the field effect transistor which makes the operational amplifier of the integrator turn on and off synchronously with the phase of the strain. In this way, one can get an averaged DLS signal for a given phase interval of strain. A part of the gate signal is used to determine the time interval over which the DLS signals are averaged by an electronic counter (Hewlett Packard, model 5216A). An additional electronic device is needed for this purpose in between the gate signal of the integrator and the counter. The circuit for this electronic device is shown in Fig. III-12.

Fig. III-11 shows an example of a relationship between the strain, trigger and gate signals. The top figure shows the trigger signal (C) synchronized with zero phase of the strain signal (S). In the middle figure, the gate signal (G) is adjusted such that it makes the field

effect transistor on for a half period of vibration. The bottom figure shows a relationship between strain and gate signal in which the DLS signal is averaged for a phase interval of strain from 0 to π over many periods of vibration.

An adjustment of the starting phase of signal averaging with respect to the phase of strain can be achieved by rotating a helical cam around the shaft leading to an eccentric cam as shown in Fig. III-13. In this manner the gate signal can be generated at any phase and phase interval of strain.

Finally a few comments may be added about the electronic system. As mentioned already the cancellation of the large baseline signal and its drift are carried out by matching and differentiating the two outputs of the detector and monitor tubes. The signal matching has been carried out by adjusting the supply voltage for the monitor PM tube. By this process the baseline stability of the DLS signals is improved very effectively compared with the system without having the differential process as in (b-3). However the stability is still not good enough when the electronic system is operated completely by D.C coupling (for both the differential amplifier and the integrator).

For this reason, the baseline drift is avoided by using A.C coupling for both the differential amplifier and the integrator when the DLS measurements are carried out at fixed frequency. The loss of gain and the phase shift between input and output of the electronics itself are then calibrated to obtain genuine DLS results. Obviously this method may be applicable only when the frequency of vibration is high (at least higher than 1 Hz). When the frequency of vibration is lowered,

there is too much loss of gain and phase shift so that the method is not usable. In such a case an alternative method has been adopted by using D.C coupling for both the preamplifier and the integrator. In this case the baseline drift is avoided by putting an external blocking capacitor of about 500 microfard (Mf) to the input of the integrator. The blocking capacitor is used to cut off a component of baseline drift which occurs with a rate lower than that characteristic of the capacitor and input impedance of the integrator. The drift occurring with higher rate may be easily averaged out through signal averaging process. A relatively large size of the capacitor is chosen to carry out the measurements at low frequency end (about 0.1 Hz when a 500 Mf blocking capacitor is used and a small correction made for the loss of gain and the phase shift).

For measurements in a wider range of frequencies, from about 10 Hz to any lower frequencies, it is necessary to use the electronic system with complete D.C couplings, which in turn requires some means to depress and/or to avoid the baseline drift. In order to depress the drift, one has to improve the factors which are responsible to the drift as discussed before. In our case the drift of electronics itself like the differential preamplifier and the integrator seems to be very small and the drift of the baseline seems to arise mainly from factors i) and ii) discussed on page 101. (According to these factors the incident and static scattered beam intensity has fluctuations of few percent.)

There may be two processes in order to avoid the drift problem.

The one way may involve an improvement of the cancellation process of the drift. In the electronics discussed in Fig. III-1, the cancellation may not be perfect, because the supply voltages for the two PM tubes are not identical and therefore the two outputs are not completely equivalent in noise and drift. Therefore an improvement may be made by using the same supply voltage for the two PM tubes and matching the two outputs electronically or optically or a combinations of them.

The second approach to avoid the drift problem which seems to be most effective for our case may be made by simultaneous averaging the DLS signals for different phase intervals of the strain using several integrators. Using this technique the drift may be cancelled out.

Actually in the condition when the dynamic strain is small enough (order of 1%) so that the DLS is varying sinusoidally, the characteristics of the DLS are obtained by averaging the intensity at three different phases of strain for which three integrators are required for the simultaneous signal averaging.

b-3) An electronic system which has been used for preliminary experiments

In the electronic system the output of the detector PM tube is fed to a D.C preamplifier whose circuit diagram is shown in Fig. III-14. The output of the preamplifier is fed to the integrator. The maximum preamplification is about a factor of 100 and the maximum input is about 15 volt. The rest of the mechanisms are similar to those of the electronic system discussed before. For the measurement at a fixed higher frequency, A.C coupling is used for the integrator and at lower frequencies D.C coupling is used with an input blocking capacitor.

The system was not satisfactory except when the DLS signals are relatively big because of the drift problem and a satisfactory amplification of the DLS signals was not possible by this system.

II-4. Variation of Frequency and Temperature

The frequency is varied by a combination of pulleys of various diameters connected to a driving motor with fixed speed rotation. A diagram of various combinations of the pulleys is shown in Fig. III-15 and the frequencies associated with the combinations are also shown in the figure. The frequencies are measured by an oscilloscope.

The DLS is also measured as a function of temperature of the sample vibration. The temperature is controlled by blowing dried air or nitrogen gas whose temperature is precontrolled in a temperature controlling chamber into a small temperature enclosure surrounding the sample area. A diagram of the chamber for temperature control is shown in Fig. III-16. Dried air is blown into the chamber in which two toaster heating elements are placed. The air passes slowly through many small holes of the elements. Two filaments are connected to a switch where the elements are connected in parallel (H-position) or series (L-position) or only a single element (M-position) is used. The temperature of the air in the chamber is controlled by a temperature controller (proportional null 1300 series with a sensor, type E157-2762, Cole-Parmer Instrument Co., Chicago, Illinois) which is designed to control the temperature from -100°F to 500°F with an accuracy $\pm 0.5^{\circ}\text{C}$. Compressed air is blown into the chamber in the case of temperature elevation, while cooled nitrogen gas is blown into the chamber in the

case of temperature lowering. A picture for the temperature controlling chamber is seen in Fig. III-4(b) (TC). The precontrolled air or nitrogen gas is then blown through the temperature enclosure whose diagram is shown in Fig. III-17. The air flow is diffused by a few layers of fine mesh. Also a small copper sheet is used in the vicinity of the entrance of the air flow in order to avoid a direct flow of the air to the sample specimen. The temperature in the vicinity of the sample is measured by a thermocouple and is controlled within a variation of few degrees centigrade. The temperature enclosure is seen in Figs. III-4(a) and 4(b) in which an upper cover for the enclosure is removed.

C H A P T E R III

PRINCIPLE OF THE DLS MEASUREMENTS
AND SOME PRELIMINARY RESULTSIII-1. Principle of the Measurements

In this section, the principle of experimental evaluation of the DLS signals will be discussed based upon the signal averaging technique.

If the applied dynamic strain (ϵ_d) is small enough, the DLS intensity (I_d) may respond linearly and their relation may be given by

$$\epsilon = \epsilon_s + \epsilon_d \sin \phi$$

$$I = I_s + I_d \sin(\phi + \gamma)$$

$$\phi = \omega t \tag{1}$$

where ϵ and I are the total strain and the scattered intensity, while ϵ_s and I_s are the static strain and the static scattered intensity. The static strain is imposed on the sample in order to prevent the sample from slackening. ω is an angular frequency of the sample vibration. γ is a phase difference between the dynamic strain and the DLS intensity and is defined here as an angle of the phase lead of the DLS intensity with respect to the dynamic strain.

An averaged DLS signal for a phase interval of strain between $(\phi - \delta)$ and $(\phi + \delta)$ defined as I_ϕ is given by

$$I_\phi = \int_{\phi-\delta}^{\phi+\delta} I d\phi / 2\delta \tag{2}$$

It should be noted here that the integrator which has been used here is an analog integrator and the averaged intensity obtained is a time-averaged intensity. As shown in eq. (1), I is characterized by three variables and therefore at least three averaged DLS intensities at different phases of the strain are required to evaluate those variables.

Experimentally this has been done by obtaining the averaged intensities at $\phi = \phi_0$, $\phi_0 + \pi/2$ and $\phi_0 + \pi$. These averaged intensities are defined as I_{ϕ_0} , $I_{\phi_0+\pi/2}$ and $I_{\phi_0+\pi}$, respectively. The change of the starting phases of the signal averaging is done by rotating the helical cam by 90° increment as already discussed in previous section. ϕ_0 is set closely to zero of the strain phase. Three averaged intensities are given by

$$I_{\phi_0} = I_s + \kappa_1 I_d \sin(\phi_0 + \gamma)$$

$$I_{\phi_0+\pi/2} = I_s + \kappa_1 I_d \cos(\phi_0 + \gamma)$$

$$I_{\phi_0+\pi} = I_s - \kappa_1 I_d \sin(\phi_0 + \gamma)$$

and

$$\kappa_1 = (\sin \delta) / \delta \quad (3)$$

In the case of the signal averaging over a half period of the vibration, δ is $\pi/2$ radian, so that $\kappa_1 = 2/\pi$. In case of δ being very small, κ_1 is almost 1. In this study, δ is set small enough so that κ_1 is 1 within 1% by changing the gate threshold voltage in the integrator as already discussed in the previous section. δ is calculated from the

time period for one cycle of vibration and the time period for the gate being opened which are measured by the electronic counter. The time period for one cycle of vibration is obtained by summing the gate-open time and the gate-off time. The gate-off time is measured from the time displaced on the electronic counter when the polarity of the threshold voltage is reversed. From eq. (3) one can estimate I_d and γ if ϕ_0 is known.

ϕ_0 is measured by using a standard signal which is synchronized with the phase of strain and has the same frequency as the strain. To make the standard signal two metal pieces are clamped to sample jaws of the deformation apparatus. One metal piece is just a flat rectangular sheet, while the other has a rectangular slit in its center. The sample clamps are adjusted such that a slit made out of the two sheets by overlapping each other comes in the middle of incident beam area. If the two clamps are vibrated, then the size of the slit made by two sheets varies sinusoidally in phase with the dynamic strain and with the same frequency of dynamic strain. Consequently the transmitted beam intensity through the slit can be used as a standard signal. One can change the amplitude of the standard signal by changing the width of the slit in one of the sheet. One can also change the height of the baseline on which the dynamic part of the standard signal is superimposed. The width and area of the slits are adjusted in such a manner that the standard signal is comparable to the actual DLS signals. In this case obviously γ is zero, so that

$$\begin{aligned}
I_{\phi_o}^o &= I_s^o + \kappa_1 I_d^o \sin \phi_o \\
I_{\phi_o + \pi/2}^o &= I_s^o + \kappa_1 I_d^o \cos \phi_o \\
I_{\phi_o + \pi}^o &= I_s^o - \kappa_1 I_d^o \sin \phi_o
\end{aligned} \tag{4}$$

where the superscript o denotes the quantities related to the standard signal. From eq. (4) ϕ_o is obtained and used for eq. (3) to obtain the DLS quantities.

As discussed in the previous section, when the baseline drift for the DLS signal is rather big, it may be useful to use A.C coupling for both the differential amplifier and the integrator, or to use an input blocking capacitor for the integrator by operating both electronics in D.C coupling in order to avoid serious errors on the averaged intensity due to an unstable baseline. However in this case one has to correct the intensity for the frequency dependence of the electronics. In this case eqns. (1), (3) and (4) must be modified as follows;

$$I = I_s + I_d \sin (\phi + \gamma + \gamma_e) \tag{5}$$

and therefore

$$\begin{aligned}
I_{\phi_o} &= I_s + \kappa_1 \kappa_2 I_d \sin (\phi_o' + \gamma) \\
I_{\phi_o + \pi/2} &= I_s + \kappa_1 \kappa_2 I_d \cos (\phi_o' + \gamma) \\
I_{\phi_o + \pi} &= I_s - \kappa_1 \kappa_2 I_d \sin (\phi_o' + \gamma)
\end{aligned} \tag{6}$$

where

$$\kappa_2 = (I_d)_{ob} / I_d$$

$$\phi_o' = \phi_o + \gamma_e \quad (7)$$

and

$$I_{\phi_o}^o = I_s^o + \kappa_1 \kappa_2 I_d^o \sin \phi_o'$$

$$I_{\phi_o + \pi/2}^o = I_s^o + \kappa_1 \kappa_2 I_d^o \cos \phi_o'$$

$$I_{\phi_o + \pi}^o = I_s^o - \kappa_1 \kappa_2 I_d^o \sin \phi_o' \quad (8)$$

where γ_e is a phase shift between the input and output of the electronics and κ_2 is a loss of gain due to the electronics. κ_2 is defined as a ratio of a magnitude of the DLS signal with loss of gain to that of the true DLS signal without the loss of gain. An apparatus constant ϕ_o' is obtained from eq. (8) by measuring $I_{\phi_o}^o$, $I_{\phi_o + \pi/2}^o$ and $I_{\phi_o + \pi}^o$ for the standard signal. From eqns. (6) to (8), the corrected DLS quantities are obtained and given by

$$\Delta I' = \left[(\Delta I')_{ob} \cos \phi_o' + (\Delta I'')_{ob} \sin \phi_o' \right] / \kappa_1 \kappa_2$$

$$\Delta I'' = \left[(\Delta I'')_{ob} \cos \phi_o' - (\Delta I')_{ob} \sin \phi_o' \right] / \kappa_1 \kappa_2$$

and

$$\tan \gamma = \Delta I'' / \Delta I' \quad (9)$$

where $\Delta I'$ and $\Delta I''$ are the corrected in-phase and out-of-phase part of the DLS intensities defined by

$$\Delta I' = I_d \cos \gamma$$

$$\Delta I'' = I_d \sin \gamma \quad (10)$$

$(\Delta I')_{ob}$ and $(\Delta I'')_{ob}$ are observed uncorrected in-phase and out-of-phase part of the DLS intensities which are obtained from the experimental quantities I_{ϕ_o} , $I_{\phi_o + \pi/2}$ and $I_{\phi_o + \pi}$ as follows;

$$(\Delta I')_{ob} = I_{\phi_o} - I_s = \kappa_1 \kappa_2 I_d \sin (\phi_o' + \gamma)$$

$$(\Delta I'')_{ob} = I_{\phi_o + \pi/2} - I_s = \kappa_1 \kappa_2 \cos (\phi_o' + \gamma)$$

and

$$I_s = (I_{\phi_o} + I_{\phi_o + \pi}) / 2 \quad (11)$$

Three different types of measurements are proposed in order to separate relative contributions of density and orientation heterogeneities; one designated as $I_{||}(\Omega)$ where the intensity is measured under conditions of $\psi = \psi_1 = \psi_2 = \Omega$ and one designated as $I_{\perp}(\Omega)$ where $\Omega = \psi = \psi_1 = \psi_2 - 90^\circ$ and one designated as $I_{+}(\Omega)$ where $\Omega = \psi = \psi_1 = \psi_2 - 90^\circ$. In any cases the stretching direction is set parallel to one of the polarization direction of the polarizer and analyzer in order to minimize an effect of birefringence on light scattering¹¹. These components of scattered intensity may be associated with H_V , V_V and H_H scattered intensity defined in photographic systems by following relations;

$$\begin{aligned}
I_{||}(\Omega) &= I_{VV}(\mu = 90^\circ - \Omega) \\
I_{\equiv}(\Omega) &= I_{HH}(\mu = 90^\circ - \Omega) \\
I_{+}(\Omega) &= I_{HV}(\mu = 90^\circ - \Omega)
\end{aligned}
\tag{12}$$

The corresponding intensities in the case of the DLS measurements are defined by $\Delta I_{||}'(\Omega)$, $\Delta I_{\equiv}'(\Omega)$ and $\Delta I_{+}'(\Omega)$ for the real part of the DLS and $\Delta I_{||}''(\Omega)$, $\Delta I_{\equiv}''(\Omega)$ and $\Delta I_{+}''(\Omega)$ for the imaginary part.

III-2. Some Preliminary Results

Some preliminary experiments have been carried out for medium density polyethylene (MDPE) with molecular weight^{a)} 33000 (\overline{M}_w), degree of branching^{b)} 1.3 CH₃/100 C, density^{c)} 0.937 g/cm³ (Sumikasen, Sumitomo Chemical Co. Ltd., Japan)*. Pellets of MDPE are melted at 160°C for about 10 minutes and then pressed by a laboratory press and naturally cooled down to room temperature in between the hotplates by turning off the switch. The time spent for the process of natural cooling to room temperature is about 6 hours. In this way MDPE films with thickness about 3 to 5 mil were carefully prepared from two points of view. (1) The films must have fairly clean surface to avoid surface scattering, especially for the case of DLS measurements under parallel polarization

* a) Calculated from intrinsic viscosity in xylene solution at 75°C by using the Harris equation. (I. Harris, J. Polymer Sci., 8, 353 (1952)).

b) Determined from infrared spectroscopy at 1376 and 1368 cm⁻¹ at melt.

c) Measured by floatation method in mixture of benzene and carbon tetrachloride at 25.0°C.

conditions. In case of static measurement, the surface scattering may be avoided by sandwiching the sample in between glass slides and using an immersion fluid whose refractive index is close to that of the sample. However in case of DLS measurements this may not easily be done. As a second point, (2) the sample must have uniform thickness in order to achieve a uniform deformation throughout the sample specimen. This may be especially necessary when the DLS is measured as a function of temperature.

Fig. III-18(b) shows an angular distribution of the scattering intensity with respect to scattering angle θ for undeformed MDPE under $I_+(\psi = 45^\circ)$. The scattering angles θ indicated in the figure are those in air and the scattering angle in the film is obtained by dividing θ by the refractive index of the sample (close to 1.5). The scattering angle at which the scattering intensity becomes maximum (θ_{\max}) is about 2.25° and the size of the spherulites calculated from a scattering equation³ is about 9.5 microns in radius. As seen from the figure, the intensity distribution is symmetrical around $\theta = 0^\circ$ indicating a fairly good optical arrangement of the apparatus in the θ direction. In Fig. III-18(a) ψ dependences of I_+ intensity at $\theta = \theta_{\max}$ and $\theta = 7^\circ$ are shown. The intensity is a maximum at odd multiples of $\psi = 45^\circ$ and a minimum at $\psi = 0^\circ$ and 90° as usually found in the case of scattering typical for spherulitic structures. As seen from the figure the intensity distribution is symmetry around $\psi = 0^\circ$ indicating again a fairly good optical arrangement of the apparatus in the ψ direction, too.

The preliminary DLS measurements have been made for the MDPE

sample stretched 8.2% statically and 0.85% dynamically. The thickness of the sample specimen is 4.3 mil. In the electronic system, the integrator and the preamplifier are operated by A.C coupling so that the baseline drift is not serious in this case. The frequency of the vibration is 2.9 Hz and the measurements have been made at room temperature.

Fig. III-19(a) shows the direct outputs from the detector (upper signal) for I_+ ($\Omega = 0^\circ$, $\theta = 7^\circ$) and the monitor (lower signal) PM tubes which are matched to each other in voltage and are 180° out of phase. Since in this study, the mercury vapor lamp is fired by A.C power (60 Hz), the two output signals have 120 Hz frequency. As seen from the figure, the upper signal corresponding to the total DLS intensity (I in eq. (1)) has wiggling on the bottom which arises from the fact that the scattered intensity is varying sinusoidally due to the sample vibration. In all oscilloscope pictures, one division in the scale corresponds to 2 volts and the sensitivity of the integrator is kept constant (one volt) when it is used. Fig. III-19(b) shows again the detector (upper) and the monitor (lower) signals obtained by using a lower sweep rate of the oscilloscope. The broad white line on the lower signal is associated with the static scattering intensity, while that on the upper signal is associated with the static scattered intensity plus the DLS signal which appears as a wiggling on the bottom. From the figure it may be seen that the DLS signal is quite small (about 1%) compared with the baseline signal corresponding to the static scattering intensity.

The matched signals are now differentiated by the differential preamplifier and further amplified and averaged by the integrator. In Fig. III-19(c), the lower signal is that after the differential preamplifier. The detector and monitor outputs shown in Fig. III-19(a) and III-19(b) are added at the same sensitivity. The signal arises from an offset of the null point due to the variation of the scattered intensity to the applied strain. The lower signal corresponding to the DLS signal is then fed to the integrator where the signal is amplified and averaged. In this case the signal was averaged simply by RC filtration with a time constant of 0.1 second. The DLS signal after the integrator is shown in the upper part of Fig. III-19(c). It may be seen that the signal is sinusoidally varying with a frequency of the sample vibration (2.9 Hz).

The differential output itself is quite small as shown in Fig. III-19(c) so that it can be amplified satisfactorily without having the problem of power saturation. The corresponding signals after further amplification of the signals in Fig. III-19(c) are shown in Fig. III-19(d) where the lower one is again observed after the differential amplifier and the upper one is observed after the integrator. The noisiness of the lower signal may arise from the lack of complete cancellation of the baseline signal and its noise. The imperfectness of the cancellation process may not affect the final DLS data so long as it is not large enough to involve the power saturation problem and so long as it does not involve extra instability of the zero line for the

DLS signals. As seen in the upper signal of Fig. III-19(d), the noisiness can be removed relatively easily by even a simple RC filtration process. In actual DLS measurements, the signal averaging technique is applied to the final signal and the signal is averaged synchronously with the phase of strain over many periods of vibrations as discussed before. Consequently the final DLS signal may be improved much more in noise and stability than the signal shown in Fig. III-19(d).

The DLS for I_+ ($\Omega = 0$, $\theta = 7^\circ$) arises from internal heterogeneities of the spherulites in terms of orientation²³ and anisotropy as discussed in Part II and shown briefly in the next chapter. Therefore the DLS signal shown in Fig. III-19 results mostly from the response of the internal heterogeneities to the applied dynamic strain.

In Figs. III-20(a) and (b), the DLS signal for I_+ at $\Omega = 0^\circ$, $\psi = 45^\circ$ and $\theta = 0^\circ$ is shown. Figs. III-20(a) and (b) correspond to Figs. III-19(b) and (d), respectively. The signal in this case corresponds to the dynamic birefringence signal⁴¹. The sinusoidal modulation of the signal is quite large and clean compared with that of Fig. III-19, and consequently one may detect the dynamic behavior simply by analyzing the lissajous figures between the signal and the dynamic strain. Since the original signal is quite big, 600 volts D.C is supplied for the detector PM tube in this case. Throughout most of the light scattering experiments, 920 volts D.C is supplied for the detector PM tube. From a comparison of Figs. III-19(d) and (b) with Figs. III-20(a) and (b), it turns out that for this particular case the DLS signal shown in Fig. III-19 is smaller than the signal in Figs. III-20(a) and (b) by factor

of about 250.

In fig. III-20(c), the corresponding figures to that in Fig. III-19(d) is shown for I_+ at $\psi = 45^\circ$, $\Omega = 0^\circ$ and $\theta = 7^\circ$. This is a case where a considerable effect of birefringence may be expected on the DLS signals while in case of Fig. III-19, the effect may be very small³³. From a comparison of Fig. III-19(d) with Fig. III-20(c), it may be seen that the DLS signal is much bigger in Fig. III-20(c) than in Fig. III-19(d) by 30% because of the birefringence effect.

The effect of birefringence on light scattering patterns may be seen in Fig. III-21, where the MDPE sample is stretched by 20%, and the scattering patterns are taken keeping the polarization of polarizer and analyzer $\pm 45^\circ$ with respect to vertical direction. The stretching direction (Ω) is changed from vertical ($\Omega = 0^\circ$) to horizontal ($\Omega = 90^\circ$). At $\Omega = 0^\circ$, the effect may be maximum and as a consequence the scattering pattern is diffused and distorted. With increasing Ω , the effect may become smaller, which leads to clear-cut four leaves clover patterns characteristic of those for deformed spherulites under a minimum birefringence effect. The effect seems to be minimized at $\Omega = 45^\circ$ where the stretching direction is parallel to one of the polarization direction of the polarizer and analyzer.

The DLS signals at $\theta = \theta_{\max}$ for $I_+(\Omega = 50^\circ)$ and $I_{||}(\Omega = 0^\circ)$ are shown in Figs. III-22(a) and (b), respectively, while that at $\theta = 7^\circ$ for $I_{||}(\Omega = 0^\circ)$ is shown in Fig. III-22(c). Ratios of maximum DLS signals at $\theta = \theta_{\max}$ to that at $\theta = 7^\circ$ for I_+ and $I_{||}$ intensity are about 2.5 and 5, respectively, which seems, however, to be considerable smaller

than the value expected for perfect spherulites. The fact may then suggest an important contribution of internal heterogeneities both in density and orientation to the DLS intensities. The DLS signal for $I_{||}(\Omega = 0^\circ, \theta = \theta_{\max})$ is bigger than $I_{+}(\Omega = 50^\circ, \theta = \theta_{\max})$ by a factor of 4. A bigger DLS intensity is associated with $I_{||}$ polarization. In the next chapters more quantitative DLS studies for $I_{||}$, $I_{=}$ and I_{+} polarization conditions shall be discussed as a function of θ and Ω as well as the temperature of vibration.

C H A P T E R IV

ANGULAR DEPENDENCE OF THE DLS

In this chapter we shall discuss the dynamic light scattering (DLS) behavior as a function of the scattering angle (θ) and the stretching direction of the sample (Ω) for the medium density polyethylene (MDPE) whose characteristics were described in the previous chapter (Chapter III). The DLS experiments have been made at a fixed frequency (2.9 Hz) and at room temperature for three types of polarization conditions, $I_+(\Omega)$, $I_=(\Omega)$ and $I_{||}(\Omega)$ which were defined in the previous chapter.

IV-1. Introduction

The idea for studying the angular dependence of the DLS arises from the reciprocal relationship between the scattering phenomena and the scattering entities^{52,53}. From this principle one may predict that the DLS at small scattering angles arises principally from a response of a large structure contour to the applied strain, while that at large scattering angles from a relative motions of small structures separated by shorter distance than the size of the larger structure. In case of the MDPE, the large structure is associated with the spherulitic structure and the DLS at small scattering angles may therefore depend upon (i) variation of the average spherulite shape, (ii) variation of an average distribution of scattering material which may be closely associated with variation of lamellae distribution and deformation, and (iii) variation of an average reorientation of optic axes within

lamellae to the applied strain.

On the other hand the small structures may be associated with crystallites or crystalline blocks constituting the lamellar structure so that the DLS at high scattering angles may be related to the relative motion of these within the spherulite. By measuring the DLS as a function of the scattering angle one may separate the response of the average spherulitic contour from that of the internal structures within the spherulite.

The motion of structures within the spherulite may produce variations in two types of fluctuations, those of density and orientation. The separation of the fluctuations may be achieved by comparing the DLS obtained for $I_{||}$, $I_{=}$ and I_{+} . The DLS for I_{+} arises essentially from the variation of the orientation fluctuations which is associated with the variation of the internal reorientation processes of optic axes. On the other hand the DLS for $I_{=}$ and $I_{||}$ depends both upon the variation of the density fluctuations as well as orientation fluctuations. It is obvious that if the DLS arises essentially from the variation of density fluctuations, then the DLS for $I_{=}$ and $I_{||}$ must be similar because the density fluctuations is optically isotropic in its nature and should be independent of polarization directions. Consequently the differences of the DLS under these two different parallel polarization conditions depend upon the relative contribution of the two types of fluctuations and therefore the two measurements may be used to separate the two contribution in addition to the other separation method which involves a comparison of the DLS intensities between I_{+} and either $I_{||}$

or I_{\perp} polarization condition.

The density fluctuations may be associated with (i) a difference of the refractive index between the spherulite and its surrounding medium³ and (ii) mutual packing of the crystalline lamellae and amorphous regions within the spherulite. The first factor may be significant at very small scattering angles corresponding to the central part of V_V and H_H scattering patterns and may become less important with increasing the scattering angle. On the other hand the second factor may be much more important at usual scattering angles than the first. The DLS behavior related to the density fluctuations may provide us an interesting information about the relative motion of crystalline lamellae and/or crystalline blocks constituting the lamellae (i. e., separation of the lamellae and the crystalline blocks).

The reciprocity principle may also be applied, at least qualitatively, to Ω dependence of the DLS. In the photographic coordinate system the principle may be stated in such a way that the DLS at equatorial ($\mu = 90^\circ$) region of the scattering pattern is primarily associated with the response of structure in the polar region of the spherulite, while the DLS at meridional ($\mu = 0^\circ$) region is associated with the response of structure in the equatorial part of the spherulite. In the photometric coordinate system, $\mu = 0^\circ$ and 90° are replaced by $\Omega = 90^\circ$ and 0° , respectively. Consequently one may study the angular dependence of the spherulite deformation in terms of both density and orientation by measuring the DLS for I_+ , I_{\perp} and $I_{||}$ as a function of Ω .

IV-2. Some Static Experimental Results

The static scattering experiments were carried out to elucidate some of the morphological features of the sample. In Fig. III-23, H_V and V_V scattering patterns are shown for the undeformed MDPE. The patterns suggest a presence of a well developed spherulitic structure. The size of the spherulite can be estimated by finding θ_{\max} at which the H_V scattering has maximum intensity³.

In Fig. III-24(a), I_+ intensity distribution is shown for $\psi = 0^\circ$ and 45° for the undeformed MDPE. The scattering angle θ is referred to the θ in air here and hereafter. The sine of the scattering angle in the sample (θ^*) can be obtained by dividing $\sin \theta$ by the refractive index of the medium (about 1.5). At sufficiently small angles, the sine of the angles may be approximated by the angles themselves. The corrections⁴² for the reflection of the scattered beam at the sample-air interface and for the secondary scattering were not made throughout this study. According to the correction theory by Stein and Keane⁴² it may be easily seen that the correction factors for the reflection and the secondary scattering are independent of the scattering angles when the scattering angles are small less than 10° . Therefore these two factors do not affect the angular dependence of the scattering intensity at the small scattering angles. From the experimental intensity distribution for $I_+(\psi = 45^\circ)$ one finds θ_{\max} is 2.20° , from which the size of the spherulite is calculated by using the equation³,

$$\frac{4\pi}{\lambda} R \sin \frac{\theta^*_{\max}}{2} = 4.1 \quad (1)$$

where λ is wavelength of the light in the medium (0.364μ) and θ_{\max}^* is the scattering angle of maximum intensity in the sample. R is the radius of the spherulite which was 9.5μ for the sample.

The theoretical curve is based upon the perfect spherulite model by Stein and Rhodes³ and is matched to the experimental curve for $I_+(\psi = 45^\circ)$ at the peak. From a comparison between the experimental and theoretical curve it may be seen that the deviations from the theory are observed in each side of the peak for $I_+(\psi = 45^\circ)$ and at any scattering angles for $I_+(\psi = 0^\circ)$. It should be noted that the theoretical intensity for $I_+(\psi = 0^\circ)$ is always zero for the perfect spherulite³. The deviations are especially prominent at high scattering angles and at any scattering angles for $\psi = 0^\circ$, indicating the scattering may arise almost from the internal heterogeneities under these conditions.

In Fig. III-24(b), the experimental intensity distribution of $[I_+(\psi = 45^\circ) - I_+(\psi = 0^\circ)]$ is plotted against θ and compared with the theoretical intensity distribution of $I_+(\psi = 45^\circ)$. The treatment is based upon the composite model proposed by KVP²¹ which is described in Part I. According to this approach, the scattering from the spherulite is given by weighted average of the scattering from perfect spherulite (I_S) and random orientation fluctuations (I_R). Therefore the total I_+ intensity is given by

$$I_+ = \phi_R I_R + \phi_S I_S \quad (2)$$

where ϕ_R and ϕ_S are the fraction of each component. And

$$I_+(\psi = 45^\circ) = \phi_R I_R(\psi = 45^\circ) + \phi_S I_S(\psi = 45^\circ)$$

$$I_+(\psi = 0^\circ) = \phi_R I_R(\psi = 0^\circ) \quad (3)$$

As already discussed in Part I, the random orientation fluctuations gives rise to the intensity distribution which is cylindrically symmetry around the incident beam axis, so that

$$I_R(\psi = 45^\circ) = I_R(\psi = 0^\circ) \quad (4)$$

Therefore

$$I_+(\psi = 45^\circ) - I_+(\psi = 0^\circ) = \phi_S I_S(\psi = 45^\circ) \quad (5)$$

The intensity distribution of $[I_+(\psi = 45^\circ) - I_+(\psi = 0^\circ)]$ should be proportional to the scattering from the perfect spherulite term. As shown in Fig. III-24(b), the experimental intensity distribution deviates, slightly from the theoretical one at θ less than θ'_{\max} and the deviation is much greater at θ greater than θ'_{\max} . θ'_{\max} is defined as the scattering angle at which $[I_+(\psi = 45^\circ) - I_+(\psi = 0^\circ)]$ becomes maximum (about 2.5°). The deviation may arise from the following factors;

- (i) The internal fluctuations may not be random but non-random in their nature.
- (ii) The assumption given by eq. (2) may be oversimplification in a sense that the two types of scattering are assumed to be incoherent to each other. In actual system the disorders are built in the spherulite and therefore the two components are coherent to each other. Consequently an additional term related to a cross corre-

lation between the two components must be added in eq. (2) and the additional term may take into account the greater ψ dependence found in the experimental result.

In this regard the disordered spherulite theory discussed in Part II may be more general than the KVP approach. In this general approach the extra intensity at high scattering angles may be uniquely related to the correlation distance of the disorder. However it should be noted that in the theory the disorder is treated separately for the case of angular and radial disorder simply for mathematical simplification, which may imply implicitly that the treatment assumes quite strong non-randomness of the disorder. In actual systems the disorder may have an intermediate non-randomness between the two extreme cases of random disorder and one-dimensional disorder.

In Fig. III-25, the ψ dependence of $I_{||}$ intensity is shown at $\theta = \theta_{\max}$ and $\theta = 7^\circ$. It is seen from the figure that the ratio of $I_{||}(\theta = \theta_{\max})$ to $I_{||}(\theta = 7^\circ)$ is about 10, while that of $I_+(\theta = \theta_{\max})$ to $I_+(\theta = 7^\circ)$ is shown to be about 6 in Fig. III-24(a). These ratios shall be compared with those obtained for the DLS in next section.

The scattering patterns for the samples stretched by 10% and 20% are shown in Fig. III-26 for H_V and in Fig. III-27 for V_V and H_H . The stretching direction (SD) and polarization direction of the polarizer (P) and the analyzer (A) are shown in these figures. Upon stretching the sample, the H_V patterns is elongated toward equator ($\mu = 90^\circ$), suggesting the deformation of the spherulite from a sphere to an ellipsoid. In more detail it may be seen that the patterns become more

diffuse and that the intensity build up is pronounced along the $\mu = 0^\circ$ and 90° direction. This fact may suggest increased internal disorders in orientation and anisotropy which may result from the internal rearrangement of the structure within the deformed spherulite. Qualitatively the disorder may be greater in the equatorial part of the spherulite than in the polar part as pointed out in Part II.

The V_V and H_H scattering patterns also become more diffuse with increasing stretching, which may be related to the increased internal disorder in terms of both density and orientation. Another pronounced change may be seen in the central part of the V_V and H_H patterns. The intensity remarkably increases in the central region, which may suggest that the refractive index difference between the spherulite and its surrounding medium increases with increasing elongation. It may be seen from a comparison of the V_V and H_H pattern that the scattering pattern in the central part is almost independent of the polarization condition. The fact may suggest that the central part of the patterns arises essentially from the density heterogeneities occurring over a large distance comparable with the size of the spherulite. On the other hand, outside the central region the V_V and H_H patterns are quite different from each other, indicating the static scattering primarily depends upon the orientation fluctuations in this region.

IV-3. Ω Dependence of the DLS at Small Scattering Angle

The DLS measurements were carried out as a function of Ω at $\theta = \theta_{\max}$

for the same MDPE sample. The sample was elongated statically by 7.1% and dynamically by 0.9%. The measurements were carried out at constant frequency (2.9 Hz) and at room temperature. The same sample specimen was used for the whole measurements. The specimen was mechanically conditioned for about two hours to achieve stationary deformation. The thickness of the specimen (designated by t) was 4.3 mil.

In Fig. III-28, the Ω dependence of the DLS for $I_+(\theta = \theta_{\max})$ is shown. The real part of the DLS, $\Delta I'_+$, changes from a small positive value to a large negative value with a minimum at $\Omega = 50^\circ$ by changing Ω from 0° to 90° , while the imaginary part, $\Delta I''_+$, changes from a negative value to a positive value by changing Ω from 0° to 90° . The "scattering loss tangent", $\tan \gamma$, passes through infinite value at about $\Omega = 20^\circ$ where the real part $\Delta I'_+$ becomes zero but the imaginary part $\Delta I''_+$ has definitely non-zero value. The negative $\tan \gamma$ indicates that the DLS intensity is lagging to the dynamic strain. The angular dependence of the DLS may be primarily associated with the variation of spherulite shape from sphere to ellipsoid. The variation of the shape may occur in phase with the applied strain as shown in the earlier work on photographic dynamic light scattering study⁴⁴. If this is true, then the loss component of the DLS may suggest that the internal rearrangement of optic axes within the spherulite must occur out of phase with the applied strain. The internal reorientation processes may affect, more or less, the angular dependence of the DLS. In Chapter VI of this part, it will be shown that two internal reorientation processes, a tilting process occurring primarily in the polar part of the spherulite

and a twisting process in the equatorial part, appreciably affect the angular dependence of the DLS and are associated with the loss component of the DLS.

The origin of the DLS intensity at $\Omega = 0^\circ$ and 90° is not zero. The non-zero intensity may arise from the variation of the spherulite disorder. One may consider here two types of disorder, i) internal disorder and ii) disorder in shape such as truncation³⁹ of the spherulite. The response of these two types of disorder to the applied strain can produce non-zero value for DLS at $\Omega = 0^\circ$ and 90° . On the basis of photographic DLS result one may predict that the disorders of the second type may not be accompanied by the large loss component as shown in the data and that the loss component may result from the disorder of the first type. Consequently the disorder of the first type may make a greater contribution on the DLS at $\Omega = 0^\circ$ and 90° than that of the second type.

The azimuthal angular dependences of the DLS are shown in Fig. III-29(a) for $I_{\perp}(\theta = \theta_{\max})$ at 27°C and (b) for $I_{\parallel}(\theta = \theta_{\max})$ at 28°C . In case of the DLS for I_{\perp} , the real part is negative at small Ω and positive at large Ω , which corresponds to the intensity of the H_H pattern being decreased in the equatorial region ($\mu = 90^\circ$) and increased in the meridional region ($\mu = 0^\circ$) with increasing strain by a small amount. The angular dependence of $\Delta I_{\perp}'$, $\Delta I_{\perp}''$ and $\tan \gamma$ are associated with the variation of (i) spherulite shape and (ii) the internal reorientation of optic axes as well as (iii) the variation of density distribution of the scattering materials. The third factor affects the DLS for I_{\parallel} and I_{\perp} .

but does not appreciably affect that for I_+ . It is related to the separation of the lamellae and the crystalline blocks as discussed already.

In case of the DLS for $I_{||}$, the angular dependence of $\Delta I_{||}'$ shows an opposite tendency to that of $\Delta I_{\perp}'$, which corresponds to the intensity of V_V pattern being increased in the equatorial region and decreased in the meridional region upon increasing the strain. The angular dependence of $\tan \gamma$ for $I_{||}$ and I_{\perp} is fairly similar at large Ω but quite different at small Ω .

If the total DLS intensity (ΔI_t^*) under parallel polarizers is given by weighted average of the intensity due to the density variation (ΔI_d^*) and that of the orientation variation (ΔI_o^*), then

$$\Delta I_t^* = X_d \Delta I_d^* + X_o \Delta I_o^* \quad (6)$$

where X_o and X_d are the weight fraction of each component. If the imaginary part of ΔI_d^* and ΔI_o^* are not large then, the loss tangent of the total DLS ($\tan \gamma$) is given by

$$\tan \gamma \approx X_d \tan \gamma_d + X_o \tan \gamma_o \quad (7)$$

where $\tan \gamma_d$ and $\tan \gamma_o$ are the loss tangent of the density and orientation term, respectively. The term associated with X_d is optically isotropic in nature and is independent of the polarization conditions, while the term associated with X_o is optically anisotropic and dependent upon the polarization conditions.

The observation that $\tan \gamma$ at large Ω is almost independent of the polarization condition suggests that the DLS at large Ω may essentially arise from the variation of the density term. In more detail, one may see that $|\tan \gamma|$ for I_{\perp} is greater than that for I_{\parallel} by approximately 0.1 for the DLS at large Ω . The difference may be due to the minor contribution of the internal reorientation process on the DLS. In the DLS for I_{\parallel} at $\Omega = 90^\circ$, the applied field of the incident beam is parallel to the orientation of optic axes, while in the DLS for I_{\perp} at $\Omega = 90^\circ$, the field is perpendicular to the orientation of optic axes. Therefore the contribution of the orientation term may be greater in the DLS for I_{\parallel} than in the DLS for I_{\perp} . From the experimental evidence and the theoretical consideration it is proposed that (i) the deformation of structures in the equatorial part of the spherulite involves a time dependent process which occurs with rather large phase lag to the applied strain and that (ii) the variation of the density in the equatorial part may occur with a larger phase lag than that of the internal reorientation.

On the other hand, the fact that $\tan \gamma$ at small Ω is quite dependent upon the polarization condition may suggest that there is a significant contribution of the orientation term on the DLS coming principally from the polar part of the spherulite. The difference of $\tan \gamma$ for the two polarization conditions may be interpreted as the difference of the orientation contributions. In the polar part of the spherulite the variation of the orientation may occur principally by the chain tilting process. If this is the case and if the tilting process is not too

extensive, (which may be legitimate for small static and dynamic strain), then the variation of the tilting process may involve a greater variation of the induced dipole moment for the $I_{||}$ case than for the I_{\perp} case, suggesting that the DLS for $I_{||}$ may be more sensitive to the orientation variation than that for I_{\perp} . This tendency may also be seen in temperature dependence of the DLS at $\Omega = 0^\circ$ in Chapter V of this part. In any case $\tan \gamma$ is much smaller at small Ω than at large Ω , indicating that less optical loss mechanism is involved in the deformation of the spherulite in the polar part.

IV-4. Dependence of the DLS at High Scattering Angle

In this section the angular dependence of the DLS shall be discussed at high scattering angle ($\theta = 7^\circ$) where the scattering arises mostly from the internal heterogeneities which are shown to be non-random in terms of orientation in Chapter IV-2 of this part. The variation of the internal heterogeneities due to the applied dynamic strain may be characterized by the variation of (i) the magnitude and (ii) the correlation distance of the heterogeneities which may result from the relative motion of structures separated at a shorter distance than the spherulite size.

The experimental results shall be qualitatively interpreted on the basis of the reciprocity principle of the scattering phenomena to its objects and compared with the previous results obtained at small scattering angle.

The angular dependence of the DLS for $I_{+}(\theta = 7^\circ)$ is shown in Fig. III-30. The real part is positive at small Ω and negative at large Ω ,

which corresponds to the intensity of H_V pattern being increased at the equator ($\mu = 90^\circ$) and decreased at the meridian ($\mu = 0^\circ$). The loss tangent of the DLS, $\tan \gamma$, is very small and negative at small Ω and is large and negative at large Ω . On the basis of reciprocity it may be qualitatively proposed again that the variation of orientation fluctuations in the equatorial part of the spherulite occurs with large phase difference to the applied strain and is associated with a time-dependent process, while that in the polar part occurs almost in phase with the strain and is independent of time. From a morphological point of view the variation of the orientation fluctuations is indirectly related to the fluctuations of some sort of internal reorientation processes, one suitable example of which may be the tilting process occurring in the polar part and the twisting or rotation process of lamellae around their crystallographic b-axis in the equatorial part of the spherulite.

The DLS for $I_+(\theta = 7^\circ)$ at $\Omega = 0^\circ$ and 90° show quite large intensity compared with the DLS at other Ω and are larger than that for $I_+(\theta = \theta_{\max})$ at $\Omega = 0^\circ$ and 90° by a factor of about 2, indicating that the DLS at high scattering angles arises mostly from the variation of the internal heterogeneities with the applied strain. It may be also worthwhile to point out the fact that a ratio of maximum intensity for the DLS at $\theta = \theta_{\max}$ to that at $\theta = 7^\circ$ (about 1.6) is much smaller than the ratio for the static scattering intensity for undeformed sample (about 6 as shown in Fig. III-24(a)). The fact may then suggest that scattering intensity associated with internal heterogeneities has much greater "scattering-strain coefficient" (defined by the gradient of the scatter-

ing intensity vs strain) than that associated with the average spherulitic contour.

The angular dependence of the DLS is shown in Fig. III-31(a) for $I_{\perp}(\theta = 7^\circ)$ and (b) for $I_{\parallel}(\theta = 7^\circ)$. $\Delta I_{\perp}'$ is always positive and large at $\Omega = 0^\circ$ corresponding to the intensity of the H_H pattern being increased as a whole with increasing elongation, while $\Delta I_{\parallel}'$ is positive at small Ω and negative at large Ω corresponding to the intensity of V_V pattern being increased at the equator and decreased at the meridian. The ratio of maximum intensity at $\theta = \theta_{\max}$ to that at $\theta = 7^\circ$ for the DLS is about 1.5 for I_{\perp} and about 2.5 for I_{\parallel} , while the ratio for the undeformed sample is about 10 as shown in Fig. III-25. Again as in the case of the DLS for $I_{+}(\theta = 7^\circ)$, the DLS for I_{\perp} and I_{\parallel} at $\theta = 7^\circ$ has much greater intensity than that expected from the static light scattering, suggesting that the scattering may arise almost from the internal density and orientation heterogeneities at $\theta = 7^\circ$ and that the scattering-strain coefficient is much greater at $\theta = 7^\circ$ than at $\theta = \theta_{\max}$.

The angular dependence of $\tan \gamma$ for $I_{\perp}(\theta = 7^\circ)$ and $I_{\parallel}(\theta = 7^\circ)$ are similar to each other at large Ω and somewhat different at small Ω , indicating again that the density fluctuations may be major contribution to the DLS in the equatorial part of the spherulite and that the contribution of the orientation fluctuations is significant in the polar part. In any case $\tan \gamma$ is appreciably large at large Ω and quite small at small Ω , indicating again that a significant loss mechanism is associated with the motion of the structures in the equatorial part of the

spherulite and that the motion of structures may occur almost in phase with strain in the polar part.

In more detail, at large Ω , $|\tan \gamma|$ is large for $I_{\perp}(\theta = 7^\circ)$ than for $I_{\parallel}(\theta = 7^\circ)$ by about 0.1 as found for the DLS at $\theta = \theta_{\max}$, which may indicate again that the variation of the density fluctuations is associated with a process having greater time dependence and which occurs in greater phase lag with the applied strain than that of orientation fluctuations in the equatorial part of the spherulite.

IV-5. Some Conclusions of the Study on the Angular Dependence of the DLS

In the previous sections, IV-3 and IV-4, the experimental results for the angular dependence of the DLS have been qualitatively interpreted on the basis of the reciprocity principle of the scattering phenomena. It may be proposed on the basis of such qualitative interpretation that:

- (i) The DLS at high scattering angle ($\theta = 7^\circ$) may arise essentially from the variation of internal orientation and density heterogeneities, while that at small scattering angles may arise essentially from the variation of the average spherulitic contour in terms of shape, orientation of optic axes and distribution of scattering materials.
- (ii) The variation of the average spherulitic contour may not occur always in phase with strain. This may be due to the fact that the internal rearrangement of structures in terms of density and orientation may not occur in phase with strain, although the variation of spherulite shape may occur essentially in phase with

strain as demonstrated from the previous photographic DLS experiments⁴⁴.

- (iii) The time dependence of such internal rearrangement of structures within the deformed spherulite may be quite angularly dependent. The deformation of the spherulite in the equatorial part may occur with a rather large phase lag with the strain and be associated with a time-dependent process, while that in the polar part may occur almost in phase with the strain and be associated with an almost time-independent process. The deformation of the spherulite may produce a variation of both density and orientation heterogeneities. In terms of a morphological point of view the variation of the density heterogeneities may be related to the separation of the lamellae and the crystalline blocks constituting the lamellar structure, and the variation of the orientation heterogeneities may be related to the twisting or rotation of the lamellae around their crystal b-axes in the equatorial part of the spherulite and tilting of the optic axes (or c-axes) around their crystal a-axes in the polar part. The details of the mechanisms shall be discussed in Chapter VII of this part.
- (iv) In the equatorial part of the spherulite, the variation of the density heterogeneities may occur with a greater phase lag to the applied strain and may be associated with a greater time-dependent process than that of the orientation heterogeneities. The prediction that the larger loss mechanism is related to the density variation is consistent with the previous results obtained

by LeGrand et. al.⁴³ under stress relaxation experiments which were briefly discussed in Chapter I of this part.

- (vi) The relaxation time involves in the rearrangement of the structures in large scale may not be the same as that in short scale.

C H A P T E R V

TEMPERATURE DEPENDENCE OF THE DLS

In this chapter the temperature dependence of the DLS shall be discussed to confirm the previous results obtained and predictions made from the study of the angular dependence. The dynamic mechanical properties shall be discussed briefly for purposes of characterization of the sample.

V-1. Dynamic Mechanical Properties of the Sample

The dynamic mechanical experiment was carried out for the same sample as a function of temperature and frequency by using the vibron viscoelastometer (Toyo Measuring Instrument Co., Ltd., Japan). The results are shown in Fig. III-32(a) for the mechanical loss tangent, $\tan \delta$, and in Fig. III-32(b) for the real (E') and imaginary part (E'') of the complex dynamic modulus.

As shown in the figure, the temperature dependence of E'' and $\tan \delta$ are rather broad and do not show clearly the mechanical loss peaks related to the motion of chain molecules or some structure units in the crystalline (α -peak) and amorphous regions (β -peak). By looking at the data in detail it may be seen, however, that β mechanical loss peak is shown around -10°C at 110 Hz and that α mechanical loss peak is shown around 40°C at 3.5 Hz and around 60°C to 70°C at 110 Hz. The temperature dependence of E'' at 11 Hz is not shown in the figure but is almost the same as that at 110 Hz except in the temperature region from 10°C to 60°C in which the intensity of mechanical absorption is

quite dependent upon frequency. E'' at 11 Hz in that temperature region lies in between E'' at 110 Hz and 3.5 Hz. In this temperature region there may be a tendency to shift the peak toward the higher temperature side with increasing frequency. It is also seen that the intensity of the mechanical absorption is decreased with increasing frequency. On the other hand at temperatures above approximately 70°C, E'' hardly shifts with the change of frequency. The fact may suggest that there are two relaxation mechanisms which are quite different in their activation energies. It is impossible, however, in this case to apply the time-temperature superposition in order to obtain the activation energies for the two relaxation processes, since the intensity of absorption varies with frequency.

In general it has been proposed⁴⁸⁻⁵¹ that the α loss mechanism is composed at least two components, the lower temperature mechanism (α_1) being associated with inter-lamellar slip and the higher temperature mechanism (α_2) being associated with molecular motion within the crystalline lattice. Although the presence of α_1 and α_2 loss mechanisms cannot be clearly seen for this particular sample, it may be still conceivable to expect the presence of these two α loss mechanisms.

V-2. Temperature Dependence of the DLS

The temperature dependence of the DLS has been studied for the same sample (MDPE) at a fixed frequency (2.9 Hz) under three different conditions, I_+ , $I_{||}$ and I_{\perp} in order to separate the contribution of density and orientation fluctuations to the DLS. The measurements were carried out for $\Omega = 0^\circ$ and 90° at the high scattering angle where the

DLS arises essentially from the variation of the internal heterogeneities in terms of density and orientation. From the comparison of the DLS at $\Omega = 0^\circ$ with that at $\Omega = 90^\circ$, it may be qualitatively possible to study the angular dependence of the spherulite deformation as a function of temperature. The measurements for a given θ and Ω were carried out during the heating cycle for the same sample. The specimen was mechanically conditioned for at least one hour at the room temperature and for about 20 minutes at each temperature of measurement.

The temperature dependence of the DLS is shown in Fig. III-33(a) for $I_+(\theta = 7^\circ)$ at $\Omega = 90^\circ$ and (b) for $I_+(\theta = 7^\circ)$ at $\Omega = 0^\circ$. From the figure it may be seen that the DLS at $\Omega = 90^\circ$ is accompanied by a much greater phase lag with respect to the applied strain than that at $\Omega = 0^\circ$, and that the temperature dependence of $\tan \gamma$ is greater at $\Omega = 90^\circ$ than at $\Omega = 0^\circ$. In more detail, $|\tan \gamma|$ at $\Omega = 90^\circ$ increases slightly and reaches to a maximum at about 40°C with increasing temperature from 10°C to 70°C . Upon further increase of temperature, $|\tan \gamma|$ decreases rapidly toward 0. On the other hand $\tan \gamma$ at $\Omega = 0^\circ$ changes gradually from a small negative value to small positive value with increasing temperature from 20°C to about 60°C and stays constant with further increase of temperature. From the figure it is suggested that the variation of the orientation heterogeneities in the equatorial part of the spherulite is accompanied by a bigger phase lag with respect to the applied strain for the measured temperature range than that in the polar part of the spherulite and that the loss tangent shows much greater temperature dependence for the deformation of the spherulite

in the equatorial part than in the polar part.

The temperature dependences of the DLS under parallel polarization conditions are shown in Fig. III-34(a) for $I_{||}(\theta = 5^\circ)$ at $\Omega = 90^\circ$ and (b) for $I_{||}(\theta = 7^\circ)$ at $\Omega = 0^\circ$, and in Fig. III-35(a) for $I_{\perp}(\theta = 5^\circ)$ at $\Omega = 90^\circ$ and (b) $I_{\perp}(\theta = 7^\circ)$ at $\Omega = 0^\circ$. The DLS for I_{\perp} and $I_{||}$ at $\Omega = 90^\circ$ were measured at $\theta = 5^\circ$ instead of $\theta = 7^\circ$, because the DLS signals at $\theta = 5^\circ$ were accompanied the noise less than those at $\theta = 7^\circ$. As shown in Fig. III-24, the DLS at $\theta = 5^\circ$ still arises primarily from the variation of internal heterogeneities rather than the variation of the average spherulitic contour. Therefore the DLS at $\theta = 5^\circ$ may arise from the same origins as the DLS at $\theta = 7^\circ$.

From the figures it may be seen again that the DLS for both I_{\perp} and $I_{||}$ at $\Omega = 90^\circ$ are accompanied by much greater phase lag to the applied strain than those at $\Omega = 0^\circ$. $|\tan \gamma|$ for $I_{||}$ and I_{\perp} at $\Omega = 90^\circ$ show a similar tendency that they show a maximum value at about 30°C and then decrease monotonically with further increase of temperature. $|\tan \gamma|$ for $I_{||}$ and I_{\perp} at $\Omega = 0^\circ$ show also a similar tendency in that they increase by a small amount with increasing temperature from 20°C to about 60°C and then stay constant with further increase of temperature. The tendency is also similar to that for I_+ at $\Omega = 0^\circ$. The temperature dependence of $\Delta I_{||}'$ at $\Omega = 0^\circ$ and 90° are quite similar to those of $\Delta I_+'$ at $\Omega = 0^\circ$ and 90° , having a maximum intensity at about 50°C for $|\Delta I_{||}'|$ and $|\Delta I_+'|$ at $\Omega = 90^\circ$; and at about 80°C for $\Delta I_{||}'$ and $\Delta I_+'$ at $\Omega = 0^\circ$. On the other hand the temperature dependence of $\Delta I_{\perp}'$ is somewhat different from those for $\Delta I_+'$ and $\Delta I_{||}'$ and increases

monotonically with increasing the temperature.

The differences in the temperature dependence of the DLS under different polarization conditions may arise from the difference of the relative contribution of the density and orientation fluctuations. The experimental observations are consistent with the previous predictions based upon the study on the angular dependence of the DLS at room temperature that the contribution of the orientation fluctuations is greater on the DLS for $I_{||}$ than for I_{\perp} and that the DLS for $I_{||}$ is associated with the variation of both density and orientation heterogeneities, while the DLS for I_{\perp} may arise mostly from the variation of density heterogeneities.

From the comparison of $\tan \gamma$ at $\Omega = 0^\circ$ and 90° for I_{+} , $I_{||}$ and I_{\perp} it may be proposed again that the variation of structures in terms of the density and orientation heterogeneities is accompanied by much greater loss component in the equatorial part of the spherulite than in the polar part. From the comparison of the DLS for I_{+} with that for I_{\perp} at $\Omega = 90^\circ$, it is proposed that in the equatorial part of the spherulite the variation of the density heterogeneities occurs with a larger phase lag with respect to the applied strain than that of the orientation heterogeneities and that the variation of the density heterogeneities has a much greater temperature dependence than that of the orientation heterogeneities. The variation of the density heterogeneities increases and becomes easier with increasing temperature. It may be also seen that the difference of $\tan \gamma$ between the DLS associated with the variation of the orientation and density heterogeneities decreases with

increasing the temperature, from which it is proposed that the difference of the hindrance opposing the variation of the density and orientation heterogeneities becomes smaller with increasing temperature.

By comparing the DLS for I_+ , $I_{||}$ and I_{\perp} at $\Omega = 0^\circ$, it may be seen that the DLS for $I_{||}$ is primarily related to the variation of orientational heterogeneities, while the DLS for I_{\perp} depends upon the variation of density heterogeneities as well as those of orientational heterogeneities. The experimental observation may be consistent with the previous predictions based upon the study on the angular dependence that the DLS for $I_{||}$ is more sensitive to the variation of orientation heterogeneities than that for I_{\perp} at $\Omega = 0^\circ$.

In addition to those observations discussed above, there are the following interesting observations whose detailed interpretations shall not be made here but left to future work.

- (i) The change of $\tan \gamma$ at $\Omega = 0^\circ$ for I_+ , $I_{||}$ and I_{\perp} levels off at about 50°C to 60°C . The change must be associated with the α_1 or/and α_2 mechanical loss processes.
- (ii) In connection with factor (i), $\tan \gamma$ at $\Omega = 0^\circ$ for I_+ , $I_{||}$ and I_{\perp} is positive in some cases, suggesting that the DLS is apparently leading the applied strain in phase. It should be noted, however, that the absolute value of $\tan \gamma$ is quite small and may involve some uncertainty in experimental evaluation.
- (iii) $\tan \gamma$ for I_+ , $I_{||}$ and I_{\perp} at $\Omega = 90^\circ$ reaches a maximum value at about 30°C to 40°C . This temperature is apparently correlated to the temperature at which the α_1 mechanical loss peak was

observed at 3.5 Hz.

- (iv) $\tan \gamma$ for I_+ at $\Omega = 90^\circ$ decreases quite rapidly above 70°C , while $\tan \gamma$ values for $I_=$ and $I_{||}$ decrease gradually. The difference of $\tan \gamma$ associated with the variation of orientation and density heterogeneities becomes minimum at about 70°C . Again the changes shown in (iii) and (iv) must be associated with the α_1 and/or α_2 mechanical loss processes.

In Chapter VII of this part, we shall interpret the tendencies of these changes in relation to other type of optical studies as well as dynamic mechanical studies.

C H A P T E R VI

A THEORETICAL STUDY ON THE DYNAMIC LIGHT SCATTERING
ARISING FROM THE DEFORMATION OF SPHERULITES

The dynamic light scattering (DLS) intensity has been calculated for cross polarization condition as a function of the scattering angle (θ) and the stretching direction (Ω) based upon the spherulite deformation models of (i) Samuels, and (ii) van Aartsen and Stein. The dependence of the DLS on Ω is discussed in terms of internal reorientation processes of crystals, i. e., (i) the tilting and (ii) twisting motions occurring within the deformed spherulites which are introduced as time-dependent process and is compared with the previous experimental results described in Chapter IV of this part.

VI-1. Introduction

The theories for light scattering from deformed spherulites have been developed for both two-dimensional^{6,54} and three-dimensional^{4,5} spherulites for a variety of deformation models. It may be worthwhile to apply all these theories to the case of dynamic light scattering. In this work, however, we shall restrict ourselves to the three-dimensional cases only for the purpose of comparing the theories with the previous experimental data obtained for a system having three dimensional spherulites.

The first model to be considered is that proposed by Samuels⁴ for the scattering by an anisotropic ellipsoid, which is an extension of the Roess and Schull⁵⁵ approach to the scattering due to an isotropic

ellipsoid. In this approach, the original equations for the H_V (eq. (1)) and V_V scattering of Stein and Rhodes³ for an undeformed spherulite (treated as an optically anisotropic sphere) are extended to a deformed spherulite (anisotropic ellipsoid) simply by changing the shape factor U in eq. (2) into U^* in eq. (3) and using it instead of U in eq. (1).

For H_V scattering,

$$I_{H_V} = AV_0^2 \left(\frac{3}{U}\right)^2 \frac{1}{\cos^2 \theta + \sin^2 \theta \sin^2 \mu} [(\alpha_r - \alpha_t) \cos^2 \frac{\theta}{2} \sin \mu \cos \mu \\ (4 \sin U - U \cos U - 3 \text{Si } U)]^2 \quad (1)$$

$$U = \frac{4\pi R_0}{\lambda'} \sin \frac{\theta}{2} \quad (2)$$

$$U^* = \frac{4\pi R_0}{\lambda'} \lambda_s^{-1/2} \sin \frac{\theta}{2} [1 + (\lambda_s^3 - 1) \cos^2 \frac{\theta}{2} \cos^2 \mu]^{1/2} \quad (3)$$

where V_0 and R_0 are the volume and the radius of the spherulite in the undeformed state, respectively. α_t and α_r are the polarizabilities of the spherulite along the tangential and radial direction. λ' is the wavelength of light in the medium and λ_s is the extension ratio of the uniaxially deformed spherulite along the stretching direction. It is assumed here that the deformation of the spherulite occurs under constant volume. θ and μ are the scattering and azimuthal angles as defined in Fig. III-36.

Although this approach can take into account in a semi-empirical manner shape of the spherulite upon deformation, it ignores any internal reorientation processes of optic axes of the optically anisotropic

scattering elements occurring within the deformed spherulite. The optic axes remain perpendicular to the radii of the spherulite through the deformation process.

The other model to be considered in the Model I of van Aartsen and Stein⁵ which requires an affine transformation for the scattering power distribution upon deforming the spherulite such that

$$\begin{aligned} N'(\alpha', r', \Omega') (r')^2 \sin \alpha' d\alpha' dr' d\Omega' \\ = N(\alpha, r, \Omega) r^2 \sin \alpha d\alpha dr d\Omega \end{aligned} \quad (4)$$

where

$$\cos \Omega' = \lambda_1 P^{-1/2} \cos \Omega$$

$$\sin \Omega' = \lambda_2 P^{-1/2} \sin \Omega$$

$$\cos \alpha' = \lambda_3 \phi^{-1/2} \cos \alpha$$

$$\sin \alpha' = P^{1/2} \phi^{-1/2} \sin \alpha$$

$$\phi = [P \sin^2 \alpha + \lambda_3^2 \cos^2 \alpha]$$

and

$$P = \lambda_2^2 \sin^2 \Omega + \lambda_1^2 \cos^2 \Omega \quad (5)$$

α' , Ω' and r' are defined in Fig. III-37 and refer to the deformed state, whereas unprimed quantities refer to the undeformed state. N' and N are the amounts of scattering material per unit volume at a given position within the spherulites. λ_1 , λ_2 and λ_3 are the extension ratios of the spherulites along the x, y and z directions. For the case of uniaxial stretching at constant volume

$$\lambda_1^2 = \lambda_2^2 = 1/\lambda_3$$

and

$$N'(\alpha', r', \Omega') = N = \text{constant}$$

From this, the scattering field strengths for V_V , H_H and H_V polarization conditions are given by

$$\begin{aligned} E_{||} = & K(\alpha_1 - \alpha_2) \left[\cos^2 \psi \int_0^{U^*} \int_0^\pi F_1 \sin \alpha \cos(q \sin \delta \cos \alpha) \right. \\ & J_0(q \cos \delta \sin \alpha) q^2 d\alpha dq + \sin^2 \psi \int_0^{U^*} \int_0^\pi \\ & (\cos^2 \beta' + \sin^2 \beta' \cos^2 \omega') \sin \alpha \cos(q \sin \delta \cos \alpha) \\ & J_0(q \cos \delta \sin \alpha) q^2 d\alpha dq - \sin^2 \psi \int_0^{U^*} \int_0^\pi F_2 \sin \alpha \\ & \cos(q \sin \delta \cos \alpha) \frac{J_1(q \cos \delta \sin \alpha)}{q \cos \delta \sin \alpha} q^2 d\alpha dq \\ & + \sin^2 \psi \int_0^{U^*} \int_0^\pi F_3 \sin \alpha \sin(q \sin \delta \cos \alpha) J_1(q \cos \delta \sin \alpha) \\ & \left. q^2 d\alpha dq \right] + K(\alpha_2 - \alpha_s) \int_0^{U^*} \int_0^\pi \sin \alpha \cos(q \sin \delta \cos \alpha) \\ & J_0(q \cos \delta \sin \alpha) q^2 d\alpha dq \end{aligned} \quad (6)$$

From the eq. (6), E_{V_V} and E_{H_H} are given by

$$E_{V_V} = E_{||} \text{ for } \psi = 0^\circ \quad (7a)$$

$$E_{H_H} = E_{||} \text{ for } \psi = 90^\circ \quad (7b)$$

and

$$E_{H_V} = K(\alpha_1 - \alpha_2) \int_0^{U^*} \int_0^\pi F_3 \sin \alpha \sin(q \sin \delta \cos \alpha) J_1(q \cos \delta \sin \alpha) q^2 d\alpha dq \quad (8)$$

The factor K is given by

$$K = CNE_0 \cdot 2\pi R_0^3 / (U^*)^3 \quad (9)$$

where CNE_0 is a proportional constant. U^* , F_1 , F_2 and F_3 are given by

$$U^* = \frac{4\pi}{\lambda'} R_0 \sin \frac{\theta}{2} [\lambda_2^2 \sin^2 \frac{\theta}{2} + \cos^2 \frac{\theta}{2} (\lambda_2^2 \sin^2 \mu + \lambda_3^2 \cos^2 \mu)]^{1/2} \quad (10)$$

$$F_1 = (\cos^2 \beta' - \sin^2 \beta' \cos^2 \omega') \cos^2 \alpha' + \sin^2 \beta' \cos^2 \omega' - 2 \sin \beta' \cos \beta' \cos \omega' \sin \alpha' \cos \alpha' \quad (11)$$

$$F_2 = -F_1 + \cos^2 \beta_1' + \sin^2 \beta_1' (\cos^2 \omega' - \sin^2 \omega') \quad (12)$$

$$F_3 = (\cos^2 \beta' - \sin^2 \beta' \cos^2 \omega') \sin \alpha' \cos \alpha' + \sin \beta' \cos \beta' \cos \omega' (\cos^2 \alpha' - \sin^2 \alpha') \quad (13)$$

and δ is defined as

$$\sin \delta = \lambda_3 \cos \frac{\theta}{2} \cos \mu [\lambda_2^2 \sin^2 \frac{\theta}{2} + \cos^2 \frac{\theta}{2} (\lambda_2^2 \sin^2 \mu + \lambda_3^2 \cos^2 \mu)]^{-1/2} \quad (14)$$

α_1 and α_2 are the polarizabilities along and perpendicular to the optic axes of uniaxially anisotropic scattering elements, respectively, and α_s is the polarizability of the medium surrounding the spherulites. The angles β' and ω' are the tilting and twisting angles of the optic axes with respect to the radii of the spherulites in the deformed state and are defined in Fig. III-37. In general, β' and ω' are not constant throughout the spherulite but depend on location within the deformed spherulite. The angular dependences of β' and ω' are assumed to have the functional forms assumed by van Aartsen and Stein⁵, where optic axis tilting process is assumed to predominate at small α' (i. e. in the polar region of the deformed spherulite) while the optic axis twisting process is assumed greatest near $\alpha' = 90^\circ$ (i. e. in the equatorial region).

$$\beta' = \beta_0 \exp [-K (\lambda_3^2 - \lambda_2^2) \cos^2 \alpha'] \quad (15)$$

$$g(\omega') = 2\langle \cos^2 \omega' \rangle_{av} - 1 = 1 - \exp [-\eta (\lambda_3^2 - \lambda_2^2) \sin^2 \alpha'] \quad (16)$$

Because of the inclusion of these two relationships the model does take into account the effects of internal reorientation processes as well as the change of spherulite shape.

Both of the theories considered are based upon models of perfect spherulites in which the effects of internal heterogeneities are ignored. In real systems, however, additional scattering arises from internal heterogeneities⁵⁴ of density and anisotropy as well as orientation as discussed mainly in Part II and in Chapter IV of Part III. The effect of such internal heterogeneities is especially important for scattering at $\Omega = 0^\circ$ and 90° where perfect spherulitic scattering is zero, and at very small and high scattering angles. Therefore computations based upon models of perfect spherulites would not be expected to predict well the experimental behavior for those particular regions.

VI-2. Application to the DLS

The theories have been applied to the DLS in which the variation of the light scattering from sample subjected to sinusoidal strain is considered.

In the Samuels' model, the scattered intensity is a unique function of λ_3 (eq. (3)) and the DLS intensity for H_V ($\Delta I_{H_V}^*$), for example, is given by

$$\Delta I_{H_V}^* = I_{H_V}(\lambda_s + \Delta \lambda_s^*) - I_{H_V}(\lambda_s)$$

where λ_s and $\Delta \lambda_s^*$ are static and dynamic extension ratios of the spherulites, respectively. The asterisk (*) in the superscript refers to complex quantity. The equation is valid only when $|\Delta \lambda_s^*|$ is small enough to give a liner relation between scattering intensity and extension ratio. Experimental results indicate that this will be so for dynamic strain amplitude up to at least about 1% for the MDPE

sample. In these studies $\Delta\lambda_s^*$ was assumed to be in phase with the applied strain, although, in general, a phase lag may exist. This assumption appears to be verified by its experimental predictions⁴⁴, indicating a very rapid response of change of spherulite shape from sphere to ellipsoid in the case of polyethylene spherulites.

Experimental results of dynamic light scattering, dynamic birefringence⁴¹, and dynamic x-ray diffraction⁴⁵ demonstrate that response of molecular orientation in amorphous and crystalline region occurs out of phase with the applied strain. The fact may be empirically introduced into our model by allowing two types of strain to occur, the first is related to the change of distribution of scattering materials within the deformed spherulites, and the second to the internal reorientation processes involving changes in β' and $g(\omega')$. The former strain is designated λ_s and is related to λ_1 , λ_2 and λ_3 in eqns. (5), (10) and (14), the latter strain is designated λ_ℓ and is related to λ_2 and λ_3 in eqns. (15) and (16). λ_s and λ_ℓ in the case of a dynamic strain are assumed to be given by

$$\begin{aligned}\lambda_s^d &= \lambda_s + \Delta\lambda_s e^{i\omega t} \\ \lambda_\ell^d &= \lambda_\ell + \Delta\lambda_\ell e^{i(\omega t + \gamma_\ell)} = \lambda_\ell + (\Delta\lambda_\ell)^* e^{i\omega t}\end{aligned}\quad (17)$$

where λ_s^d and λ_ℓ^d are the total dynamic extension ratios. λ_s and λ_ℓ are the static and $\Delta\lambda_s$ and $\Delta\lambda_\ell$ the dynamic extension ratios. γ_ℓ is a phase difference between λ_ℓ^d and λ_s^d . As the simplest case it is assumed that λ_s and $\Delta\lambda_s$ are equivalent to λ_ℓ and $\Delta\lambda_\ell$, respectively and

that both λ_s^d and λ_s^ℓ undergo constant volume deformation. It is also assumed that λ_ℓ and $(\Delta\lambda_\ell)^*$ for the tilting (β) and twisting ($g(\omega')$) processes are equivalent to each other except a case to study an effect of irreversibility of the tilting process.

Consequently the DLS intensity is in general, a complex quantity and is given by, for example in case of H_V scattering,

$$\begin{aligned}\Delta I_{H_V}^* &= I_{H_V}(\lambda_s + \Delta\lambda_s, \lambda_\ell + \Delta\lambda_\ell e^{i\gamma_\ell}) - I_{H_V}(\lambda_s, \lambda_\ell) \\ &= \Delta I_{H_V}' + i \Delta I_{H_V}''\end{aligned}\tag{18}$$

and

$$[\tan \gamma]_{H_V} = \Delta I_{H_V}'' / \Delta I_{H_V}'\tag{19}$$

where primed and double primed quantities are the in-phase and out-of-phase component of the DLS, and $\tan \gamma$ is the loss tangent of the DLS intensity relative to λ_s^d . $\Delta I_{V_V}^*$ and $\Delta I_{H_H}^*$ are also given in the same manner and these are numerically calculated by using eqns. (7a), (7b) and (8).

In order to compare theory and experiment, it is useful to rewrite the equations in terms of the photometric system shown in Fig. I-1. This can be done by using the following relationship between the photographic and photometric notations as already discussed in section III-1 of Part III.

$$\Delta I_{+}'(\Omega) = \Delta I_{H_V}'(\mu = 90^\circ - \Omega), \text{ and } \Delta I_{+}''(\Omega) = \Delta I_{H_V}''(\mu = 90^\circ - \Omega)$$

$$\Delta I_{||}'(\Omega) = \Delta I_{V_V}'(\mu = 90^\circ - \Omega), \text{ and } \Delta I_{||}''(\Omega) = \Delta I_{V_V}''(\mu = 90^\circ - \Omega)$$

$$\Delta I_{==}'(\Omega) = \Delta I_{H_H}'(\mu = 90^\circ - \Omega), \text{ and } \Delta I_{==}''(\Omega) = \Delta I_{H_H}''(\mu = 90^\circ - \Omega)$$

(20)

VI-3. Results of Numerical Calculations and Comparison with the Experimental Results

Numerical calculations of the DLS theory were made for I_{+} . The results shall be compared with the experimental results discussed in Chapter IV and V of the Part III.

(a) Samuels' model

Numerical calculations have been carried out using the CDC 3600 computer of the University of Massachusetts Research Computing Center for $\lambda' = 0.364 \mu$. An arbitrarily chosen value of $AV_0^2(\alpha_t - \alpha_r)^2$ of 10^5 was used. The Ω dependence of the DLS has been calculated for values of U of 4.0 and 12.63. These are equivalent to $\theta = 1.5^\circ$ and 4.67° in the sample, or 2.25° and 7° in air if $R_0 = 9 \mu$. The values of θ used hereafter refer to the scattering angle in air.

The Ω dependences of the DLS at $\theta = 2.25^\circ$ and 7° are shown in Fig. III-38(a). At $\theta = 2.25^\circ$, $\Delta I_{+}'$ is negative for all Ω , indicating a decrease of the scattered intensity for a small increase of the stretching ratio for all Ω . However, at $\theta = 7^\circ$, $\Delta I_{+}'$ is small and positive at small values of Ω , and large and negative at large Ω , reflecting the shift of μ_{\max} (the angle μ at which there is a maximum scattering intensity at a given scattering angle and elongation) toward

higher values of μ at high scattering angles. It is seen that the predicted values of ΔI_+ at $\Omega = 0^\circ$ and 90° are zero, which results from the assumption of a perfect spherulite model. The observed intensity changes at these values of Ω result from the background intensity associated with internal spherulite disorder. Experimental results differ also from the theory in Fig. III-38(a) in that ΔI_+ is found to change sign with increasing Ω , being positive at small Ω and negative at large Ω .

In Fig. III-38(b) is shown the θ dependence of the DLS for various values of μ . The values of ΔI_+ are predicted to decrease with increasing θ much more rapidly than is experimentally observed. The fact again suggests that the DLS at high scattering angles arises mainly from a response of the internal heterogeneities to the applied strain in the real system, and that the heterogeneities give rise to additional scattering at large θ and at $\Omega = 0^\circ$ and 90° . The maxima and minima predicted for the DLS at high scattering angles in Fig. III-38(b) may be due to the variation of the scattering intensity in the higher order maximum region.

While the Samuels' model has the virtue of simplicity and is quite useful for predicting the qualitative changes in the scattering patterns with elongation, it does not appear adequate for describing the more subtle changes in the DLS experiments. Consequently, the other model, the van Aartsen-Stein model, has been used for further computations and discussions.

b) van Aartsen-Stein model

Fig. III-39 shows the angular dependence of twisting ($g(\omega')$) and tilting (β') factors calculated for $\lambda_\ell = 1.09$ for various values of the parameters K and η using the empirical equations (15) and (16). As discussed previously it is seen that the effect of twisting is greatest in the equatorial region and zero in the polar regions of the spherulite, and that the effect of tilting is greatest in the polar regions and zero in the equatorial region. For a given angular position (α'), the effect of tilting and twisting increases with an increase of the local strain (λ_ℓ) and with an increase of the adjustable compliance parameters η and K .

The effects of the tilting and twisting processes are shown in Fig. III-40 on the Ω dependences of $\Delta I_+'$ and $\Delta I_+''$ at $\theta = 2.25^\circ$ for $\lambda_s = \lambda_\ell = 1.09$, $\Delta\lambda_s = \Delta\lambda_\ell = 0.01$, and $\gamma_\ell = \pi/32$ for both β' and ω' . (The positive $\tan \gamma_\ell$ of order of 0.1 corresponds to the local strain which leads the applied strain in phase if the applied strain is assumed to be indentical to the spherulitic strain (λ_s and $\Delta\lambda_s$).) The case where $\eta = K = 0$ is the case where no internal reorientation processes can take place. In such a case, $\Delta I_+'$ depends uniquely upon the change of spherulite shape and, as a consequence, $\Delta I_+'$ is positive at small Ω and negative at large Ω , corresponding to the intensity of the H_V patterns increasing at the equator ($\mu = 90^\circ$) and decreasing in the meridional ($\mu = 0^\circ$) region. It is obvious from the assumption made that $\Delta I_+'' = \tan \gamma = 0$ is in this case. The prediction for the case of $\eta = K = 0$ is somewhat different from that based upon the Samuels' model.

This arises from the difference in the distribution of scattering material within the deformed spherulite between the two models. The model of van Aartsen-Stein assumes the affine transformation for the distribution of scattering materials as shown in eqns. (4) and (5), while in the semi-empirical approach of Samuels the change of the distribution upon stretching may obey some sort of non-affine transformation process. From the figure it is seen that the tilting and twisting processes give rise to opposing effects on the DLS, twisting tends to increase $\Delta I_+'$ and $\Delta I_+''$ and to shift the peak towards higher values of Ω whereas tilting tends to make them more negative and to shift the peak toward smaller values of Ω .

The Ω dependence of $\tan \gamma$ (Fig. III-41) is such that the tilting process causes a large phase difference at small Ω , and the twisting process gives rise to a similar effect at large Ω . This would seem reasonable as the variation of the tilting and twisting motion to the applied strain occur most effectively in the polar and equatorial part of the spherulite, respectively. It is found that $\Delta I_+'$ and $\Delta I_+''$ are again zero at $\Omega = 0^\circ$ and 90° because the model cannot take into account the variation of the background scattering intensity due to the effect of the applied dynamic strain on the internal heterogeneities.

The effect of the magnitude of dynamic strain may be inferred from Fig. III-42 where the Ω dependences of $\Delta I_+'$ and $\Delta I_+''$ are shown for $\Delta \lambda_s = \Delta \lambda_\ell = 0.005$, all other parameters being unchanged from the data given in Figs. III-40 and 41. By comparing Fig. III-42 with Fig. III-40, it may be seen that the Ω dependences have similar tendencies but that

the magnitudes of $\Delta I_+'$ and $\Delta I_+''$ are half as large as before. This suggests that the equations behave in a linear manner leading to a proportionality between the DLS and strain when the dynamic strain is small.

Fig. III-43 shows the Ω dependences of $\Delta I_+'$ and $\Delta I_+''$ under the same conditions as the data shown in Fig. III-42 except that the static strain ($\lambda_s = \lambda_\ell$) has been decreased from 9% to 6%. By comparing Fig. III-42 and Fig. III-43, it is apparent that the DLS depends upon static strain, i. e. on the original structure upon which the dynamic strain is superimposed, even though the tendencies are not much affected. Increasing the static strain from 6 to 9% causes $\Delta I_+'$ and $\Delta I_+''$ to increase in a negative sense, the effect being much more appreciable for the tilting process. In this calculation it is assumed that both the static and dynamic strains are reversible and that the crystal reorientations resulting from both are given by eqns. (15) and (16). It is found experimentally that if one stretches polyethylene beyond a few percent the recovery of length is not complete on releasing the stress⁵⁶. It would appear to be quite possible that the orientation change accompanying such an irreversible deformation may differ from the simple behavior described by eqns. (15) and (16).

The DLS at high scattering angle is illustrated in Fig. III-44 where the predicted Ω dependences of $\Delta I_+'$ and $\Delta I_+''$ at $\theta = 7^\circ$ are shown. The effects of the tilting and twisting processes on $\Delta I_+'$ and $\Delta I_+''$ at small Ω are similar to those observed for $\theta = 2.25^\circ$. The ratio of the maximum DLS intensity at $\theta = 2.25^\circ$ to that at $\theta = 7^\circ$ is much higher

than that observed experimentally, and the DLS intensity is zero at $\Omega = 0^\circ$ and 90° . This is again a consequence of the presence of internal heterogeneities, the variation of which has a greater effect on the DLS intensity at high scattering angles. Thus the predicted dynamic intensity changes occurring at $\theta = 7^\circ$ really represent only a small part of the total intensity change, so that a comparison of the predictions of the theory with experiments at these θ and Ω is not too meaningful.

In Fig. III-45 the effect of reversibility of the tilting process on the DLS at $\theta = 2.25^\circ$ is illustrated. Here it is assumed that $\lambda_s = \lambda_\ell = 1.09$ for both tilting and twisting processes and that $\Delta\lambda_\ell = 0$ for tilting and 0.01 for twisting. This is the case in which only the tilting process is irreversible, and gives rise to positive values of $\Delta I_+'$ and $\Delta I_+''$ and to a large $\tan \gamma$ at $\Omega = 90^\circ$. The tendencies are quite similar to the case where only a twisting process exists without any tilting process. A comparison with the theory with the previous experimental results suggests that both tilting and twisting processes must occur reversibly.

The values of γ_ℓ chosen may also affect the DLS, and an illustration of this may be seen in Fig. III-46 where $\theta = 2.25^\circ$ for the case of $\lambda_s = \lambda_\ell = 1.09$ and $\Delta\lambda_s = \Delta\lambda_\ell = 0.01$ for both tilting and twisting. It is apparent from the figure that doubling γ_ℓ gives rise to doubled values of $\tan \gamma$ and $\Delta I_+''$. It is also worth noticing that if the sign of γ_ℓ is changed, then the signs of $\tan \gamma_\ell$ and $\Delta I_+''$ are also changed, but the sign of $\Delta I_+'$ remains the same.

So far the Ω dependences of the DLS for I_+ have been discussed for the case where either K or η is zero as the simplest case to elucidate effects of the internal reorientation processes on the DLS. By comparing the theoretical and experimental results, it is proposed that reversible variations for both tilting and twisting must occur simultaneously to the applied strain. In Fig. III-47, the effect of a combination of tilting and twisting motions on the DLS is shown for a constant values of $K = 0.6$ and various values of the parameter η , all at $\theta = 2.25^\circ$. Here γ_ℓ is again $\pi/32$. $\lambda_s = \lambda_\ell = 1.09$ and $\Delta\lambda_s = \Delta\lambda_\ell = 0.01$ for both processes. Both $\Delta I_+'$ and $\Delta I_+''$ increase positively with increasing degree of twisting, and $|\tan \gamma|$ at $\Omega = 90^\circ$ also increases with increasing degree of twisting. The general tendencies are quite similar to those described for data in Figs. III-40, 41 and 42, except that now both components of ΔI_+^* are of much greater magnitude simply because the reversible components of structural response are greater in this case. From a comparison of the result with the previous experimental result, the values of K and η of 0.6 and 0.5 respectively seem to fit rather well to the experimental result, indicating both tilting and twisting motions must occur equally well to the applied dynamic strain at room temperature. It should be also noted that the best fit of the theory to the experiment requires positive value of γ_ℓ . In another words it is necessary to assume the local strain leads the applied strain in phase.

The DLS under parallel polarization conditions depends upon density fluctuations which appear in the last term of eq. (6) as well as upon orientation fluctuations. Consequently an additional parameter

$(\alpha_2 - \alpha_s)$ is required in this case. From the previous experimental evidences $(\alpha_2 - \alpha_s)$ may be dependent of α' (i. e. the angular location within the spherulites) and the local strain related to this term may have out-of-phase component with respect to the applied strain. Theories of the DLS for $I_{||}$ and I_{\perp} are now under investigation by using the same model described in this chapter and a new model⁹⁴ based upon a non affine deformation concept.

An interpretation on the positive γ_l for the local strain shall be made in terms of a simple mechanical model in Chapter VII of this part.

C H A P T E R VII

RELATIONSHIP TO OTHER OPTICAL
AND DYNAMIC MECHANICAL STUDY

In this chapter the results of dynamic light scattering (DLS) studies shall be discussed in relation to the results obtained by other types of static and dynamic optical studies such as small angle x-ray scattering, wide angle x-ray diffraction and birefringence as well as dynamic mechanical spectra.

We shall try to qualitatively correlate the tendencies shown by these studies. However at this moment, quantitative discussions are very difficult because of two principal reasons; (1) The quantitative study of the DLS has just been started, so that at this stage, experimental and theoretical evidence must be cumulated in order to further elucidate the deformation mechanism and time-dependent response of internal structures of the spherulite. Secondly, (2) each study has not been made for the same sample with the same molecular weight, degree of branching and thermal history. The morphology (including size and perfection of lamellae and spherulites etc.) and deformation mechanism of spherulites are believed to appreciably depend upon these factors. Consequently in order to make quantitative correlation of the various physical properties it is desirable to study them for the same sample under the same conditions.

VII-1. Relationship to Static X-ray Study

In Chapter IV of this part, it has been suggested that the time-dependence of the spherulite deformation is angularly dependent with respect to the stretching axis where (1) internal rearrangements of structure in the equatorial part of the spherulite lags with applied strain in phase and be associated with time-dependent viscoelastic processes, while (2) the rearrangements in the polar part occur almost in-phase with the applied strain and are associated with less time-dependent processes. The inhomogeneities of the response of the internal structure to the bulk strain has been studied in terms of the response of both density and orientation fluctuations. It has been suggested that (3) in the equatorial part of the spherulite, the response of density fluctuations may occur with greater phase lag with the bulk strain than that of orientation fluctuations, while (4) in the polar part both type of fluctuations may occur relatively in phase with the applied strain.

The change in density and orientation fluctuations must be correlated with the results of small angle x-ray scattering (SAXS) and with those of orientation studies by wide angle x-ray diffraction, respectively.

Relationship to Small Angle X-ray Scattering

The variation of density fluctuations which is sensitive to the scattering at high scattering angles principally arises from motion or/and deformation of lamellae and interlamellar regions within the spherulite. Such deformation may also cause changes in density

fluctuations correlated over a short distance characteristic to small angle x-ray scattering. Thus a component of the light scattering arising from density fluctuations is correlated with the small angle x-ray scattering. The variation of the density fluctuations observed in the equatorial part of the spherulite is related to the change of small angle x-ray scattering at the meridian. The earlier small angle x-ray studies^{12,13,78} have shown that the meridional small angle x-ray maximum first shifts very slightly to smaller angle and then gradually disappears with increasing stretching. This fact suggests that the lamellae are first separated, and then irregularly deformed and bent with increasing stretching, so that the regularity of interlamellar spacing is lost.

Similarly the variation of the density fluctuations in the polar part of the spherulite is related to the change of small angle x-ray scattering at the equator. The equatorial small angle x-ray scattering has been shown^{12,13,78} to shift to larger angles as a consequence of slight compression of lamellae or interlamellar spacing. The lamellae may eventually slip over each other¹³ which may promote rotation of the crystal c- and a-axes around the b-axis.

The observation that the meridional small angle x-ray maximum is diffused more rapidly than the equatorial maximum and soon disappears with increasing stretching suggests that irregularity of interlamellar spacing tends to become greater in the equatorial part of the spherulites than in the polar part with increasing stretching. This fact may be consistent with the previous DLS predictions that the contribution

of density fluctuations to the DLS is greater in the equatorial part of the spherulites than in the polar part where orientation fluctuations are supposed to predominate. Other evidence for greater density fluctuations in the equatorial part of the spherulites than in the polar part comes from observations with the polarizing microscope⁹.

The change of long spacing in initial stage of stretching has been shown⁸¹ to depend upon stretching temperature and initial long period, i. e. thermal history of the sample.

In this work the time-dependent response of density fluctuations to the bulk strain has been studied by qualitative separation of the density contribution from orientation contribution to the DLS. It is obvious that an application of small angle x-ray scattering to the dynamic studies (although not feasible at this moment) does provide more directly information about the time-dependent response of the density fluctuations than the light scattering method. Such a study is believed to be of great value to further confirm the deformation mechanism of spherulites as well as the previous DLS results.

Relationship to Wide Angle X-ray Orientation Study

The variation of the orientation fluctuations with applied strain is related to the mobility of the motion of individual crystallites and amorphous chains. As seen in Part I and II, this is composed of three types of variations; (1) variation in average degree of orientation of optic axes of the scattering elements, (2) variation of correlation distance in orientation of the optic axes, and (3) magnitude of the orientation fluctuations. These variations cannot be independent of

each other but must be closely interrelated in the spherulitic systems. This may be so because each crystallite must move, more or less, as a member of a lamella, the motion of which, in turn, correlates with other lamellae through tie chains, which may be considered as part of the amorphous structure. Therefore the interrelation between these effects may depend upon the fine structure of the spherulite, the degree of stretching, the stretching temperature as well as the rate of stretching.

Consequently the change of orientation fluctuations may be closely correlated with the change of orientation of crystallites as studied by wide angle x-ray diffraction, although these two observations are somewhat different from each other as discussed above.

As shown in the previous chapter, the response of the orientation fluctuations to the bulk strain is quite different in the polar and equatorial part of the spherulite. This observation is believed to be associated with different orientation mechanisms of crystallites in different parts of the spherulite as proposed from the studies by microbeam x-ray, polarizing microscope, electron microscope⁶⁴ and conventional (macrobeam) x-ray^{11,58,60,64,65}. The orientation behavior of the crystallographic, a-, b- and c-axes, of polyethylene films^{11,58,61,65,82} has been shown to change with increasing uniaxial stretching in such a way that (i) crystal c-axis tends to orient parallel, while crystal b- and a-axes tend to orient perpendicular to the stretching direction and that (ii) the crystal a- and c-axes orient preferentially over the crystal b-axis.

As well born out from electron microscopic study the spherulites are radiating aggregates of crystals. In the case of polyethylene, the crystal b-axis is oriented in the radial direction (extension direction of a lamella)⁶² of the spherulites, while the a- and c-axes are oriented perpendicular to the radius and rotate, more or less, in a helicoidal fashion about the radius⁶³. If such spherulites are uniaxially stretched, they may be initially deformed more or less homogeneously into ellipsoids. Accompanying this shape change, lamellae tend to orient toward the stretching axis, so that the lamellae (i. e. crystal b-axis) tend to orient parallel to stretching direction. However such positive orientation for the crystal b-axis has hardly been observed for 'statically drawn polyethylene films'.^{*} The fact that crystal a-, b- and c-axis orientations do change in such a fashion of (i) and (ii) as stated above, instead of positive b-axis orientation is believed to occur as a consequence of the ease of internal reorientation processes of crystallites within the deformed spherulites.

The internal reorientation mechanism has been proposed to be different in different parts of the spherulites^{11,58,64,65,82}. The process is summarized in a manner similar to that by Hay and Keller⁶⁴ as follows;

(1) Internal Reorientation Processes in the Polar Part of the Spherulite.

This is composed of following processes;

* However the positive b-axis orientation is seen in case of dynamic x-ray diffraction and dynamic birefringence for annealed polyethylene films at lower temperature (see ref. (90) and (91)).

- (1a) rotation of crystals as a whole around the crystal a-axis⁶⁴.
- (1b) plastic deformation of crystals themselves by [001] (010) slip^{11,64,66}.
- (1c) crystal transtion from folded crystals (b-axis paralled to the radius of spherulites) to fibrillar crystals (c-axis parallel to the radius)⁶⁵⁻⁶⁸.

All these processes cause rotation of crystals around the crystal a-axis and tend to make c-axis orientation positive.

(2) Internal Reorientation Processes in the Equatorial Part of Spherulite.

This is composed of following processes,

- (2a) rotation (twist and detwist) of lamellae around crystal b-axis^{11,64}.
- (2b) interlamellar slip with lamellar interfaces as slip planes by shearing force^{64,69-71}.
- (2c) intralamellar slip involving [001] (100) slip by shearing force^{11,64}.

All of these processes cause rotation of crystals around the crystal b-axis and tend to make c-axis orientation positive.

(3) Internal Reorientation Processes in the Section of 45° Direction.

The reorientation processes are very complicated and involve both rotation around the crystal a- and b-axis.

All of these mechanisms cause, reversibly or irreversibly, positive orientation of the crystal c-axis. The previous static orientation behavior of the crystal axes has been interpreted by the combination of these mechanisms. In the treatment of Stein et. al.^{60,65}

the factors, (1c) and (2a), and in the treatment of Kawai et. al.^{11,82}, the factors, (1b) and (2a) are taken into account.

The previous results of the DLS arising from the internal orientation fluctuations and the dynamic x-ray are associated with the reversibility of these various modes of motion with respect to the applied strain. In this work, the mobility of the reversible components has been shown to be quite different in the equatorial and polar parts of the spherulites by means of light scattering.

VII-2. Relationship to Dynamic X-ray Study and Dynamic Mechanical Properties

The dynamic x-ray diffraction technique⁷²⁻⁷⁵ has been developed for the purpose of studying the mobility of crystal orientation. From the variation of diffracted intensity (related to specific crystallographic planes) of polyethylene film subjected to sinusoidal tensile strain, dynamic orientation compliances for crystal a-, b- and c-axes (C_a^* , C_b^* and C_c^*) have been analyzed⁸⁰. These compliances are given by

$$C_i^* = (\partial f_i / \partial \epsilon) = C_i' + i C_i''$$

$$C_i' = |C_i| \cos \chi_i$$

$$C_i'' = - |C_i| \sin \chi_i$$

where C_i^* is complex dynamic orientation compliance of i-th crystal axis, and C_i' and C_i'' are the real and imaginary part of the C_i^* . f_i is the second moment orientation function defined by

$$f_i = [3\langle \cos^2 \alpha_i \rangle_{av} - 1] / 2$$

The orientation functions for crystal a-, b- and c-axes are designated as f_a , f_b and f_c . α_i is the angle that the i-th crystal axis makes with respect to the stretching direction. χ_i is the angle related to the loss tangent ($\tan \chi_i$) of the crystal orientation with respect to the bulk strain,

$$\tan \chi_i = -C_i'' / C_i'$$

The dynamic compliance C_i^* is related to the mobility of the reversible components of the various internal reorientation processes of crystals which, in turn, may be a principal contribution to changes in the internal orientation fluctuations in the DLS. As discussed before, it should be noted, however, that the response of orientation fluctuations and crystal orientations are not necessarily the same.

Now among the various kinds of internal crystal reorientation processes in the polar part of the spherulites, the only reversible process may be the process of (1a) in the previous section. One may consider a crystal block as a unit of the reversible motion. The lamellae may be composed of numbers of such crystallographically coherent blocks which are connected to each other by structures with less perfect lattice fit^{13,85-89}. The lamellae may be deformed more easily at the boundaries of the blocks than inside the blocks. The blocks may slip over each other and rotate as a whole around the crystal a-axis. In the polar part of the spherulite, lamellae tend to be

compressed and eventually slip, which may favor the rotation of the blocks as a whole. Bending of the lamellae may also cause the reversible rotation of crystals around their a-axes.

The process of (1b) may be irreversible and may become important with increasing temperature, especially above the disordering temperature (T_d) where the expansion coefficient of the crystal a-axis changes^{4,22,23}.

In the equatorial part of the spherulite, the processes of (2a) and (2b) may be reversible, while the process (2c) may be irreversible and be activated at elevated temperature, especially above T_d .

The effect of temperature upon the orientation functions of the crystal a-, b- and c-axes (f_a , f_b and f_c) was studied by Kawai et. al.⁵⁸ for low and high density polyethylene films slowly cooled from melts. The results showed that with increasing temperature from room temperature to temperatures above T_d , the magnitudes of f_a and f_c decreased by nearly the same amount, while that of f_b slightly increased for both polyethylene films at an initial stage of stretching (elongation percent less than about 30%). This fact is interpreted in such a way that with increasing the stretching temperature above T_d , the crystal rotation around the crystal b-axis by the reversible processes of (2a) and (2b) is depressed by the onset of the irreversible process of (2c), while the crystal rotation around the crystal a-axis is promoted by the irreversible process of (1b).

The temperature dependence of C_i^* has been studied for low density polyethylene slowly cooled from melt^{79,89}.

It has been shown from the study that (i) C_c' and C_a' are positive and negative, respectively as in the case of static f_c and f_a (i. e. $f_c > 0$, $f_a < 0$) and that (ii) magnitude of C_c' and C_a' increases with increasing temperature near T_d and then decreases with a further increase of temperature above T_d . Compared with C_c' and C_a' , C_b' has been shown to be very small negative and almost constant with respect to temperature.

The tendency can be generally interpreted in terms of competing effects of the reversible processes, i. e. (1a), (2a) and (2b) and the irreversible processes, i. e. (1b) and (2c). With increasing temperature, mobility of the former modes of motion increases because of the decreasing viscosity for the interlamellar slip (2b), rotation (2a) and the slip in between the crystal blocks (1a). With a further increase of temperature above T_d , these reversible motions are partially or entirely replaced and absorbed by irreversible motions of (1b) and (2c). As a consequence, C_c' and $-C_a'$ increase with increasing temperature at the lower temperature side of T_d and decrease with a further increase of temperature above T_d . C_b' becomes small and negative as a consequence of a compensation of negative C_b' due to the internal reorientation processes (1a) and (1b) by the reversible lamellar orientation process which tends to make C_b' positive. Thus the constancy of C_b' with respect to temperature may be kept by the ballance of the opposing effects.

In relation to the changes of C_i^* , the DLS intensity for I_+ at high scattering angles (which arises from the internal orientation fluctuations) changes with temperature (see Fig. III-33).

The changes may be qualitatively interpreted as follows;

1) In the DLS for I_+ at $\Omega = 0^\circ$ (corresponding to variation of the fluctuations in the polar part of the spherulite), ΔI_+ increases with increasing temperature up to about 80°C partially due to the increasing mobility of the rotation of the crystals around their a-axis, (1a) or/and due to the increasing variation of the orientation correlation distance related to the process of (1a). The loss tangent is very small, suggesting that the process is fairly elastic in nature, especially at higher temperature above about 50°C . With a further increase of temperature, ΔI_+ tends to decrease, which may arise from the effect of the irreversible plastic deformation of (1b).

2) In the DLS for I_+ at $\Omega = 90^\circ$ (corresponding to variation of the fluctuations in the equatorial part of the spherulite), the magnitude of ΔI_+ again increases with increasing temperature and decreases with a further increase of temperature above about 70°C . Again the tendency may be qualitatively interpreted in terms of two opposing effects; reversible (2a) and (2b) processes, and irreversible (2c) processes. The loss tangent at temperature below 70°C shows big phase lag, suggesting that the processes (2a) and (2b) are encountered a viscoelastic opposing effect. Above 70°C , the loss tangent tends to rapidly decrease. This may be due to the fact that the crystallites tend to move as members of a smaller subgroup rather than a larger subgroup of a lamella or a lamella as a whole as in the case at lower temperature. At higher temperature the viscosity of the surrounding may be decreased considerably and the motion of the subgroups may be subjected to less

viscoelastic opposing force than for the mode of motion at lower temperature.

It may be apparent that the various internal reorientation processes studied by dynamic x-ray, birefringence and light scattering are essentially related to the dynamic mechanical α loss processes. The motions of (1a), (2a) and (2b) are associated with α_1 , the lower temperature loss mechanism, while (1b) and (2c) are associated with α_2 , the higher temperature loss process. It should be noted, however, that the process observed by the rheo-optical studies are, more or less, modified from the dynamic mechanical α process by the fact that static and dynamic strain imposed on the rheo-optical studies are quite large compared with the dynamic mechanical study.

In the discussions of the preceeding sections, we qualitatively discussed the DLS results and the results of static and dynamic x-ray measurements in terms of the reversible and irreversible components. However the details of the relative contribution of each mode of motion may depend upon properties of polyethylene samples, thermal history, degree of branching, molecular weight and so on as well as conditions of stretching.

Finally it should be again noted that the DLS depends upon both crystal and amorphous orientation, since orientation of optic axes of the scattering elements depends upon both components. However, at this moment, the contribution of each component to the total DLS is not known. This problem is left to future work, and may be solved by combining the results of DLS with those of dynamic birefringence and

dynamic x-ray diffraction techniques.

VII-3. A Simple Mechanical Model Treatment for Rheo-Optical Properties

In this section we shall discuss the DLS results at small and high scattering angles in terms of a simple mechanical model which is adopted by Iwayanagi^{49,83} et. al. in order to explain dynamic mechanical properties of crystalline polymers.

Iwayanagi et. al. have represented the mechanical properties in terms of a six-parameter model as shown in Fig. III-48. The Voigt element α represents the retarded viscoelastic response of crystalline lamellae while element β represents the viscoelastic deformation of the interlamellae amorphous material. These elements are associated with moduli E_α and E_β , viscosities η_α and η_β and retardation times $\tau_\alpha = \eta_\alpha/E_\alpha$ and $\tau_\beta = \eta_\beta/E_\beta$. The isolated spring with modulus E_I represents the instantaneous elastic deformation of both the crystalline lamellae and the interlamellar amorphous material while the isolated dashpot with viscosity η_a represents the viscous flow of the interlamellar material. Although Iwayanagi formulated the equations in terms of shear moduli ϵ_i , we have substituted these by tensile moduli since our experiment is carried out in tension.

An application of the six-parameter Voigt model to the description of the rheo-optical behavior has been proposed by Stein et. al.⁸⁰ in order to describe time-dependent crystal orientation behaviors (C_a' , C_b' and C_c') of polyethylene films. We shall adopt here the same principle in order to describe the DLS results. Although the phenomenological

description of the rheo-optical behavior in terms of the six-parameter Voigt model is less general and rigorous compared with that in terms of generalized Maxwell model^{80,84}, it is easier to interrelate the simplified model to molecular processes. The application of the simplified model may be of great value to elucidate qualitatively the nature of the response of structures to the applied strain.

On the basis of the Iwayanagi's model, stress σ and strain ϵ are given by

$$\sigma = \sigma_I = \sigma_\alpha = \sigma_\beta = \sigma_a = \sigma_o e^{i\omega t} \quad (1)$$

$$\epsilon = \sum_j \epsilon_j = \epsilon_I + \epsilon_\alpha + \epsilon_\beta + \epsilon_a \quad (2)$$

where σ_j and ϵ_j are the components of stress and strain related to the j -th viscoelastic mechanism and ϵ_j are given by

$$\epsilon_I = (1/E_I) \sigma_o e^{i\omega t} \quad (3)$$

$$\epsilon_\alpha = \frac{1 - i\omega\tau_\alpha}{E(1 + \omega^2\tau_\alpha^2)} \sigma_o e^{i\omega t} \quad (4)$$

$$\epsilon_\beta = \frac{1 - i\omega\tau_\beta}{E(1 + \omega^2\tau_\beta^2)} \sigma_o e^{i\omega t} \quad (5)$$

$$\epsilon_a = - (i/\omega\eta_a) \sigma_o e^{i\omega t} \quad (6)$$

In the treatment of the orientation compliance, C_i^* by Stein et. al., the total orientation function of i -th crystallographic axis of polyethylene was assumed to be given by

$$f_i = \sum_j f_{ij} = L_{iI} \epsilon_I + L_{i\alpha} \epsilon_\alpha + L_{i\beta} \epsilon_\beta + M_{ia} \epsilon_a \quad (7)$$

where the coefficients L_{ij} and M_{ia} are those associated with strength of contribution of each viscoelastic mechanism to the total orientation function. They discussed variation of the orientation-stress coefficient, $C_{si}^* = (\partial f_i / \partial \sigma)^*$, and the orientation-strain coefficient, $C_i^* = (\partial f_i / \partial \epsilon)^*$ as a function of frequency, temperature and thermal history of the sample in terms of relative contribution of the respective viscoelastic mechanisms.

Instead of the orientation function, we apply here eq. (7) to the internal reorientation processes, i. e., 1) the tilting process related to β' and 2) the rotation process related to g which have been defined in Chapter VI of this part in order to explain theoretically the DLS at small scattering angle.

$$g(\omega') = 2\langle \cos^2 \omega' \rangle_{av} - 1 = 1 - \exp\left[-\eta\left(\lambda_\ell^2 - \frac{1}{\lambda_\ell}\right) \sin^2 \alpha'\right] \quad (8)$$

$$\beta' = \beta_0 \exp\left[-K\left(\lambda_\ell^2 - \frac{1}{\lambda_\ell}\right) \cos^2 \alpha'\right] \quad (9)$$

On the basis of the simplified mechanical model, both g and β' processes are represented by the single mechanical model and given by a formular in eq. (7). For example,

$$g = L_{gI} \epsilon_I + L_{g\alpha} \epsilon_\alpha + L_{g\beta} \epsilon_\beta + M_{ga} \epsilon_a \quad (10)$$

where as before, L_{gi} and M_{ga} are the coefficients associated with relative contribution of the respective viscoelastic mechanism to the rotation

factor g .

It has been shown in Chapter VI of this part that the local strain associated with the β' and g processes leads in phase to the applied strain. The phase relation of the local and applied strain shall be qualitatively discussed here in this section in terms of this simple model.

Now rotational compliance designated by C_g^* is given by

$$C_g^* \equiv (\partial g / \partial \epsilon)^* = (\partial g / \partial \lambda_\ell) (\partial \lambda_\ell / \partial \epsilon)^* \quad (11)$$

where ϵ is the applied strain and λ_ℓ is the local strain. The asterisks designate complex quantities. From eq. (11) the phase relationship between ϵ and λ_ℓ is obviously equivalent to that between ϵ and g .

From eqns. (4), (5), (6) and (10), the rotation-stress coefficient C_{sg}^* is given by

$$C_{sg}^* \equiv (\partial g / \partial \sigma)^* = C_{sg}' - i C_{sg}'' \quad (12)$$

where

$$C_{sg}' = \frac{L_{gI}}{E_I} + \frac{L_{g\alpha}}{E_\alpha (1 + \omega^2 \tau_\alpha^2)} + \frac{L_{g\beta}}{E_\beta (1 + \omega^2 \tau_\beta^2)} \quad (13)$$

and

$$C_{sg}'' = \frac{\omega \tau_\alpha L_{g\alpha}}{E_\alpha (1 + \omega^2 \tau_\alpha^2)} + \frac{\omega \tau_\beta L_{g\beta}}{E_\beta (1 + \omega^2 \tau_\beta^2)} + \frac{M_{ga}}{\omega \eta_a} \quad (14)$$

The loss tangent of the rotational motion with respect to the applied stress is given by

$$\tan \gamma_{sg} = C_{sg}'' / C_{sg}' \quad (15)$$

$\tan \gamma_{sg}$ should be physically positive in this definition, since the rotational motion cannot lead the applied stress in phase.

The rotational compliance is similarly given by

$$C_g^* = (\partial g / \partial \epsilon)^* = \frac{(\partial g / \partial \sigma)^*}{(\partial \epsilon / \partial \sigma)^*} = C_{sg}^* / J^* = C_g' + i C_g'' \quad (16)$$

where

$$C_g' = [C_{sg}' J' + C_{sg}'' J''] / [(J')^2 + (J'')^2] \quad (17)$$

$$C_g'' = [C_{sg}' J'' - C_{sg}'' J'] / [(J')^2 + (J'')^2] \quad (18)$$

where C_{sg}' and C_{sg}'' are given by eqns. (13) and (14). J^* is dynamic mechanical compliance and is given by

$$J^* = J' - i J'' \quad (19)$$

where

$$J' = \frac{1}{E_I} + \frac{1}{E_\alpha (1 + \omega^2 \tau_\alpha^2)} + \frac{1}{E_\beta (1 + \omega^2 \tau_\beta^2)} \quad (20)$$

$$J'' = \frac{1}{\omega \eta_a} + \frac{\omega \tau_\alpha}{E_\alpha (1 + \omega^2 \tau_\alpha^2)} + \frac{\omega \tau_\beta}{E_\beta (1 + \omega^2 \tau_\beta^2)} \quad (21)$$

Now the loss tangent of the rotational compliance is given by

$$\begin{aligned} \tan \gamma_g &= C_g'' / C_g' = (C_{sg}' J'' - C_{sg}'' J') / (C_{sg}' J' + C_{sg}'' J'') \\ &= (\tan \delta - \tan \gamma_{sg}) / (1 + \tan \gamma_{sg} \tan \delta) \end{aligned} \quad (22)$$

where $\tan \delta$ is the mechanical loss tangent and is positive. Consequently sign of $\tan \gamma_g$ depends upon the relative magnitude of $\tan \delta$ and $\tan \gamma_{sg}$. In another words, the phase relationship between the local strain, λ_l and the applied strain, ϵ is determined by the relative magnitude of $\tan \delta$ and $\tan \gamma_{sg}$. If $\tan \delta$ is greater than $\tan \gamma_{sg}$, then the local strain for the rotational motion leads the applied strain in phase.

Suppose that the frequency of the DLS experiment (3Hz) is such that $\tau_\beta \ll (1/\omega_1) \ll \tau_\alpha$ for the medium density polyethylene at room temperature, that is, the frequency is low enough for the β process to occur but not low enough for the α process (related to the motion of crystal itself) and for viscous flow to occur, then $\tan \delta$ and $\tan \gamma_{sg}$ are given by

$$\tan \delta = \frac{\omega_1 \tau_\beta}{E_\beta} / \left(\frac{1}{E_I} + \frac{1}{E_\beta} \right) \quad (23)$$

$$\tan \gamma_{sg} = L_{g\beta} \frac{\omega_1 \tau_\beta}{E_\beta} / \left(\frac{L_{gI}}{E_I} + \frac{L_{g\beta}}{E_\beta} \right) \quad (24)$$

Thus

$$\tan \gamma_g \sim (\tan \delta - \tan \gamma_{sg}) \sim \frac{1}{\frac{1}{E_I} + \frac{1}{E_\beta}} - \frac{1}{\frac{L_{gI}}{L_{g\beta}} \frac{1}{E_I} + \frac{1}{E_\beta}} \quad (25)$$

Consequently in such a condition as described above

$$\begin{aligned} \tan \gamma_g &> 0 & \text{if} & \quad L_{gI} / L_{g\beta} > 1 \\ \tan \gamma_g &< 0 & \text{if} & \quad L_{gI} / L_{g\beta} < 1 \end{aligned} \quad (26)$$

Therefore the local strain of the rotational motion leads (lags) the applied strain in phase if the elastic contribution (L_{gI}) is greater (less) than the contribution of the viscoelastic mechanism ($L_{g\beta}$). It is easily seen that the same conclusion is also reached for a frequency or temperature of $(1/\omega_2) \approx \tau_\beta \ll \tau_\alpha$.

At lower frequency or higher temperature where the α process is activated, i. e., $\omega_3 \tau_\beta \ll \omega_3 \tau_\alpha \approx 1$,

$$\begin{aligned} \tan \gamma_g &\sim (\tan \delta - \tan \gamma_{sg}) \\ &= \frac{(1/\omega\eta_a) + (1/2E_\alpha)}{(1/E_I) + (1/2E_\alpha) + (1/E_\beta)} - \frac{(M_{ga}/\omega\eta_a) + (L_{g\alpha}/2E_\alpha)}{(L_{gI}/E_I) + (L_{g\alpha}/2E_\alpha) + (L_{g\beta}/E_\beta)} \end{aligned} \quad (27)$$

where the viscous flow is included in this equation. Thus in this case the phase relation is determined by the relative magnitude of L_{gI} , $L_{g\alpha}$, $L_{g\beta}$ and M_{ga} as well as by the viscoelastic constants.

The local strain was observed to lead the applied strain in phase in the DLS at small scattering angles. In terms of this model, this observation shows that the rotational motion is primarily controlled by the elastic mechanism related to L_{gI} rather than the viscoelastic mechanism related to $L_{g\beta}$. The elastic mechanism may result from the instantaneous rotation of the lamellae around their crystal b-axes accompanied by the instantaneous change of the spherulite shape⁴⁴ to the applied stress.

On the other hand the DLS for I_+ at large Ω and at high scattering angle have been shown to lag the applied strain in phase as shown in

Chapter IV and V of this part. This observation has been interpreted as indicating that the variation of internal orientation fluctuations in the equatorial part of the spherulite lags the applied strain in phase. As discussed in the previous section of this chapter this variation of the internal orientation fluctuations is, in principle, related to motion of crystals around their b-axes which is correlated over a shorter distance than the spherulite radius. Therefore the experimental evidence may be interpreted as showing that the rotational motion is primarily controlled by the viscoelastic mechanism rather than the elastic mechanism (i. e. $L_{gI}/L_{g\beta} < 1$), when larger angle scattering arising from correlations over distances smaller than the radius of the spherulite is studied. The viscoelastic mechanism may arise from an interaction of motion of one lamella over the other through slip or rotation processes. The DLS at small scattering angle arises from the motion of structure correlated over distances comparable with spherulite sizes, so that it is insensitive to such viscoelastic mechanisms.

From the same argument, the DLS behavior at small Ω and at high scattering angle may be qualitatively interpreted such that the viscoelastic contribution to the tilting process related to the factor of β' ($L_{\beta',\beta}$) is comparable to or even less than the elastic contribution ($L_{\beta',I}$). The model can be also applied to the dynamic orientation behavior of crystals. The phase relationship between the crystal orientation and the applied strain is again determined by the relative contribution of the elastic and viscoelastic mechanism.

It should be noted here that the mechanical model adopted here is

an oversimplification in two major points as pointed out by Stein et. al.⁸⁰ as well as in the previous section of this chapter. (1) Each process has been associated with a single retardation time. Instead, each process should really be described in terms of a distribution of retardation times. (2) The model implies a homogeneous stress model in which the stress on the crystalline and amorphous regions is the same. This may be reasonable for the equatorial part of the spherulite where the stress is perpendicular to the lamellar axis and crystalline and amorphous regions are mechanically in series with each other and may be subjected to the same stress. However a homogeneous strain model may be more reasonable for the polar part of the spherulite where the stress is parallel to the lamellar axis and crystalline and amorphous regions may be subjected to the same strain. In this regard and in regard to the different orientation mechanism in the polar and equatorial part as discussed in the previous section of this chapter, it is more reasonable to establish a model which is able to take into account the difference of the response in the polar and equatorial part of the spherulite.

P A R T IV

FUTURE WORK

Theoretical

1. Effect of non-affine deformation of the spherulites.

In Chapter VI of Part III, the result of dynamic light scattering (DLS) at small scattering angle has been treated in terms of affine spherulite deformation model. The model may be an oversimplification in that the deformation of structure within the spherulites may not necessarily occur affinely, even though the changes in the external dimensions of the spherulite are proportional to the changes in the external dimensions of the sample in the initial stage of elongations^{44,92}. The non-affiness of the internal deformation of the spherulites is especially prominent in the case where they are deformed in their equatorial part more easily than in their polar part^{8,93}. In such a case, (1) the degree of volume increase is angularly dependent and is large in the equatorial part of the spherulite, and (2) the local strain for internal reorientation of optic axes of the scattering element, λ_ℓ (see Chapter VI of Part III) is no longer constant throughout the spherulite but is angularly dependent.

In order to take into account the effect of non-affine deformation on the light scattering, one has to modify the previous equations in Chapter VI of Part III. For example as the simplest case⁹⁴

$$\lambda_{3s} \lambda_{2s}^2 = 1 + \xi (\lambda_{3s}^2 - 1) \sin^2 \alpha' \quad (1)$$

and

$$\lambda_{3\ell} \lambda_{2\ell}^2 = 1 + \xi (\lambda_{3\ell}^2 - 1) \sin^2 \alpha' \quad (2)$$

where λ_{3s} and λ_{2s} are the spherulitic strain parallel and perpendicular to the stretching direction, and $\lambda_{3\ell}$ and $\lambda_{2\ell}$ are the local strain parallel and perpendicular to the stretching direction. ξ is a parameter describing the non-affineness and characterizing the degree of volume increase which is a function of α' and is maximum at $\alpha' = 90^\circ$. When $\xi = 0$, the equations reduce to the previous affine deformation model with constant volume. As before the first and simplest case to be considered is where $\lambda_{3\ell} = \lambda_{3s} = \lambda$. λ may be again a complex number resulting from time-dependent reorganization of structure within the spherulite.

The same spherulite deformation model can be also applied to evaluate static and dynamic birefringence⁹⁵ and crystal orientation for spherulitic polymers, the study of which is very important for characterization of the deformation mechanism of spherulites as well as for further checking the proposed model.

2. Quantitative interpretations of the dynamic light scattering at high scattering angles.

In Chapter IV and V of Part III, the Ω dependence and the temperature dependence of the DLS at high scattering angles are qualitatively interpreted on the basis of the reciprocity principle of light scattering. It has been shown that static and dynamic light scattering at the high scattering angles arise mostly from internal density and orientation fluctuations.

Although this analysis is not rigorously correct and only applied as a first approximation to the case of polyethylene as discussed in Chapter IV of Part III, it appears to be of great value to analyze the data in terms of the two-phase model proposed by Keijzers, van Aartsen and Prins¹⁸. The two phase model can be extended to oriented systems. For the scattering from the spherulitic component the deformed spherulite scattering calculated by van Aartsen and Stein⁵, and for the scattering from random component the random orientation fluctuation theory calculated by Stein and Hotta²⁷ can be used.

According to this model, the total DLS intensity for I_+ scattering, for example, is given by

$$\Delta I_+^* = \phi_s \Delta I_{+,s}^* + \phi_R \Delta I_{+,R}^* \quad (3)$$

where ϕ_s and ϕ_R again the fractional contributions of the spherulitic and random orientation fluctuations to the total DLS where these fractions are assumed to be independent of dynamic strain. The asterisk designates a complex number resulting from the component of the DLS out-of-phase to the bulk strain. From the angular dissymmetry²⁶ of the DLS for I_+ polarization with respect to scattering angles θ_1 and θ_2 at $\mu = 0^\circ$ and 90° (or $\psi = \Omega = 0^\circ$ and 90°), one can evaluate the response of orientation correlation distances parallel (c) and perpendicular (a) to stretching direction. This is done for the assumption of a Gaussian correlation function for the internal orientation fluctuations given by

$$f(r) = [3\langle \cos^2 \theta_{ij} \rangle_r - 1]/2 = \exp \left\{ -[(z/c)^2 + (y/a)^2 + (x/a)^2] \right\} \quad (4)$$

The evaluated responses of c and a with respect to the bulk strain manifest time-dependent response of internal orientation fluctuations. It should be noted that the time-dependent responses of c and a thus obtained are the averaged responses over all angular positions within the spherulite. Actually the response is probably different in the polar and equatorial parts of the spherulite so that one cannot easily resolved the response of the structures into the contributions from these parts.

One might also evaluate the time-dependent response of the orientation of optic axes by separating the contribution of the spherulite term from the random part and then analyzing the Ω dependence of the random term. Also the variation of the internal density fluctuation may be analyzed by separating the contribution of density fluctuations from orientation fluctuations and then analyzing the density fluctuations. Again the evaluated response of the density fluctuations are the average of those from the equatorial and polar parts of the spherulites.

Other possibilities for theoretical interpretation of the DLS at high scattering angles might involve further elaboration and application of the theories of non-random orientation fluctuations discussed in Part I and disordered spherulite discussed in Part II. Although these theories are more general than the two-phase model, the application of them to the DLS would compound complexity and may not be

feasible at this moment.

Experimental

1. Instrumentation

The DLS apparatus constructed for this work was satisfactory and yielded significant data to elucidate the deformation mechanism of polyethylene spherulites. However from the discussions in Chapter II of Part III, it would be apparent that one needs further improvements of the apparatus, especially for stabilization of the small DLS signals in order to extend the study to that of frequency dependence. These improvements will also be required to extend the technique to systems with low scattering power found in non-spherulitic crystalline or non-crystalline polymers as well as in spherulitic polymers. This will also be required for polymers with less reversible deformability such as high density polyethylene having high degree of crystallinity. For the latter systems one must decrease dynamic strain, which again requires the stabilization of the small DLS signals.

Some possibilities for further refinements of the apparatus have been already pointed out in Chapter II of Part III.

2. Frequency dependence of the DLS

In this work the DLS experiments have been carried out at a constant frequency (2.9 Hz), because of the problem on stability of the baseline signal of the DLS. However the DLS for I_{\parallel} and I_{\perp} at $\theta = \theta_{\max}$ are fairly big and are accompanied by less noise as compared with the DLS for I_{+} . Consequently the frequency dependence for the DLS under these conditions may be studied with a satisfactory accuracy.

It is our feeling that the frequency dependence of the DLS for I_+ and $I_{||}$ at small and high scattering angles may be also studied without great difficulties by the aid of two additional integrators as discussed in Chapter II of Part III.

The study of the frequency dependence of the DLS serves to confirm further the previously proposed mechanism of spherulite deformation and elucidate the nature of the deformation through the process of time-temperature superposition.

3. Static strain dependence of the DLS

The DLS is also expected to depend upon static strain upon which the dynamic strain is superimposed. By studying the static strain dependence, one may study the effect of the original structure upon which the dynamic strain is applied on the mobility of structure elements.

4. Effect of morphology on optical and mechanical properties.

4-1. Study of low and medium density polyethylene with different thermal histories

In this work the DLS behavior has been studied for medium density polyethylene (MDPE) slowly cooled from the melt. Since the deformation mechanism of polyethylene depends upon the thermal history of the sample, it is interesting to carry out the DLS experiments for various thermal histories.

Recently dynamic x-ray diffraction, dynamic birefringence and dynamic mechanical properties have been investigated for two kinds of low density polyethylene with different thermal histories^{90,91} i. e.,

one obtained by quenching molten polyethylene into dry ice-ethanol temperature (Q sample) and the other obtained by annealing the Q sample at 95°C for 1 hour. The dynamic mechanical properties and the change of H_V scattering patterns upon deformation of these samples are shown in Figs. IV-1 and IV-2.

From a comparison of Fig. III-32 with Fig. IV-1, it is seen that the temperature dependences of E'' and $\tan \delta$ of the MDPE sample studied in this work are fairly different from those for Q and H samples. A difference in deformation behavior of spherulitic superstructure as a whole between these Q and H samples and the MDPE is seen by comparing Figs. III-23 and III-26 with Fig. IV-2. From the comparison, it is seen that (1) average sizes of the spherulites for the Q and H samples (about 2 μ radius) are quite different from those of the MDPE sample (9.5 μ radius), and that (2) the change of the patterns is also different between the low density polyethylene samples (Q and H) and the MDPE sample. The difference can be seen in that for the Q and H samples, four leaf clover type H_V patterns with a clear dark cross along $\mu = 0^\circ$ and 90° are maintained up to a high elongation percent. In the MDPE sample however, the patterns become diffuse with an increase of elongation. Simultaneously with this change, the dark cross becomes diffuse and tends to disappear. The difference is believed to arise from a difference in the deformation of the superstructure as a whole. It is also expected intuitively that the response of internal structures to the bulk strain would be different for the Q and H samples and the MDPE sample. In this regard the dynamic x-ray and dynamic birefringence studies for the

MDPE sample would be interesting.

On the other hand the H_V patterns for Q and H samples are similar, suggesting that in this case there is not a significant difference in the deformation of spherulite as a whole between the two samples. However as shown by the study of dynamic x-ray diffraction⁹⁰, there is a significant difference in the dynamics of crystal orientation between these two samples, suggesting that the mobility of crystallites and/or lamellar within the spherulite are quite different in these two samples. The difference of the dynamic orientation mechanism may also cause a subtle difference in the static and dynamic light scattering intensity distribution with respect to Ω . In this regard light scattering studies for these two sample would be very interesting.

4-2. Ring scattering

Another interesting application of the static and dynamic light scattering is for the study of ringed spherulites^{63,96-99}. The wide angle light scattering intensity maximum arising from the periodicity of the helicoidal twisting of the lamellae was first observed by Stein and Rhodes³. Moore et. al.¹⁰⁰⁻¹⁰² extended the study to the deformed ringed spherulite and photographically investigated the change of the ring scattering upon deforming high density polyethylene at room temperature. They showed that the ring spacing increased in the polar part of the spherulite and decreased in the equatorial part in the initial stage of stretching. The change of ring spacing is believed to be related to the detailed deformation mechanism of the polar and equatorial

part of the spherulite such as discussed in Chapter VII of Part III.

In this regard it would be of great value to study this as a function of temperature and time-scale of experiment in relation to the α mechanical loss mechanism of polyethylene. The reversibility of deformation in the polar and equatorial part of the spherulites manifested by the reversibility of the change of the ring spacings upon stretching and releasing the sample can be studied as a function of temperature more precisely by the photometric method. Such studies may provide an additional information on the α relaxation mechanism of polyethylene.

B I B L I O G R A P H Y

1. R. S. Stein, P. F. Erhardt, S. B. Clough and G. Adams, Appl. Phys., 37, 3980 (1966).
2. R. S. Stein, P. F. Erhardt, J. J. van Aartsen, S. B. Clough and M. B. Rhodes, J. Polymer Sci., PtC, No. 18, 1 (1966).
3. R. S. Stein and M. B. Rhodes, J. Appl. Phys., 31, 1873 (1960).
4. R. J. Samuels, J. Polymer Sci., PtC, No.,13, 37 (1966).
5. J. J. van Aartsen and R. S. Stein, paper submitted for publication.
6. S. Clough, J. J. van Aartsen and R. S. Stein, J. Appl. Phys., 36, 3072 (1965)
7. M. B. Rhodes and R. S. Stein, J. Polymer Sci., A2, 7, 1539 (1969).
8. I. L. Hay and A. Keller, Kolloid-Z. U. Z. Polymere, 204, 43 (1965).
9. H. D. Keith and F. J. Padden, Jr., J. Polymer Sci., 41, 525 (1959).
10. K. Kobayashi and T. Nagasawa, paper presented before the U. S. - Japan Joint Seminar in Polymer Physics, Kyoto, 1965.
11. T. Oda, S. Nomura and H. Kawai, J. Polymer Sci., A3, 1993 (1965).
12. H. Hendus, cited on p. 428 in "Polymer Single Crystals" by P. H. Geil, New York, 1963.
13. A. Peterlin, Kolloid-Z. U. Z. Polymere, 233, 857 (1969).
14. A. Keller, J. Polymer Sci., 17, 351 (1955).
15. R. Yang, Ph. D. thesis, University of Massachusetts, Amherst, Mass., (1968).
16. R. S. Stein and P. R. Wilson, J. Appl. Phys., 33, 1914 (1962).
17. R. S. Stein, P. F. Erhardt, S. B. Clough and G. Adams, J. Appl. Phys., 37, 3980 (1966).

18. A. E. M. Keijzers, J. J. van Aartsen and W. Prins, J. Appl. Phys., 36, 2874 (1965).
19. R. S. Stein and M. B. Rhodes, J. Appl. Phys., 31, 1873 (1960).
20. M. B. Rhodes and R. S. Stein, J. Polymer Sci., in press.
21. A. E. M. Keijzers, J. J. van Aartsen and W. Prins, J. Am. Chem. Soc., 90, 3107 (1968).
22. R. S. Stein, P. R. Wilson and S. N. Stidham, J. Appl. Phys., 34, 46 (1963).
23. R. S. Stein and W. Chu, J. Polymer Sci., A2, 8, 1137 (1970).
24. M. B. Rhodes and R. S. Stein, J. Polymer Sci., 62, S84 (1962).
25. G. C. Adams and R. S. Stein, J. Polymer Sci., A2, 6, 31 (1968).
26. F. H. Norris and R. S. Stein, J. Polymer Sci., 27, 87 (1958).
27. R. S. Stein and T. Hotta, J. Appl. Phys., 35, 2237 (1964).
28. W. Yau and R. S. Stein, J. Polymer Sci., A2, 6, 1 (1968).
29. S. N. Stidham and R. S. Stein, J. Polymer Sci., A2, 4, 89 (1966).
30. R. S. Stein, P. F. Erhardt and W. Chu, J. Polymer Sci., A2, 7, 271 (1969).
31. D. G. LeGrand, J. Polymer Sci., 7, 279 (1969).
32. W. Chu and R. S. Stein, J. Polymer Sci., A2, in press.
33. M. Motegi, M. Moritani and H. Kawai, J. Polymer Sci., A2, in press.
34. R. S. Stein, J. J. Keane, F. H. Norris, F. A. Bettelheim, and P. R. Wilson, Ann. N. Y. Acad. Sci., 83, Art. I, 37 (1959).
35. W. Chu, Ph. D. thesis, University of Massachusetts, Amherst, Mass., 1969.

36. M. Motegi, T. Oda, M. Moritani and H. Kawai, *Polymer Journal* (Japan), 1, 209 (1970).
37. P. H. Geil, "Polymer Single Crystals", Interscience, New York, 1963, Chapter IV.
38. C. Picot and R. S. Stein, M. Motegi and H. Kawai, paper submitted for publication.
39. C. Picot and R. S. Stein, paper submitted for publication.
40. R. S. Stein, P. R. Wilson and S. N. Stidham, *J. Appl. Phys.*, 34, 46 (1963).
41. R. Yamada and R. S. Stein, *J. Appl. Phys.*, 36, 3005 (1965).
42. R. S. Stein and J. J. Keane, *J. Polymer Sci.*, 17, 21 (1955).
43. D. G. LeGrand and W. R. Haaf, *J. Polymer Sci.*, C5, 153 (1963).
44. P. F. Erhardt and R. S. Stein, *J. Appl. Polymer Sci.*, Applied Polymer Symposia, High Speed Testing, Vol. VI, The Rheology of Solids, 5, 113 (1967).
45. T. Kawaguchi, T. Ito, H. Kawai, D. A. Keedy and R. S. Stein, *Macromolecules*, 1, 126 (1968).
46. R. S. Stein, *Polymer Engineering and Sci.*, 9, 320 (1969).
47. D. G. LeGrand and P. F. Erhardt, *J. Appl. Phys.*, 34, 68 (1963).
48. H. Nakayasu, and M. Markovitz, D. J. Plazek, *Trans. Soc. Rheology*, 5, 261 (1961).
49. S. Iwayanagi, "Solid State Physics" (F. Seitz and D. Turnbull, Ed., Academic Press, New York, 1963) Vol. 14, PP. 458.
50. S. Manabe, A. Sakoda, A. Katada and M. Takayanagi, *J. Macromol. Sci.-Phys.*, B4(1), 161 (1970).
51. M. Takayanagi, and T. Matsuo, *J. Macromol. Sci.-Phys.*, B1(3), 407

(1967).

52. R. S. Stein, "Newer Method of Polymer Characterization", B. Ke, Ed., Interscience, New York, 1964, PP. 155-206.
53. A. Guinier, et. al., "Small Angle Scattering of X-rays", John Wiley and Sons, Incorporated, New York, 1955, Chapter 2.
54. R. S. Stein and T. Hashimoto, paper submitted for publication.
55. L. C. Roess and C. G. Schull, J. Appl. Phys., 18, 308 (1947).
56. P. F. Erhardt, K. Sasaguri and R. S. Stein, J. Polymer Sci., C5, 179 (1964).
57. H. Hendus, Kolloid-Z., 165, 32 (1959).
58. T. Oda, N. Sakaguchi and H. Kawai, J. Polymer Sci., C15, 223 (1966).
59. R. S. Stein and F. H. Norris, J. Polymer Sci., 21, 381 (1956).
60. K. Sasaguri, R. Yamada, and R. S. Stein, J. Appl. Phys., 35, 3188 (1964).
61. S. Hoshino, J. Powers, D. G. LeGrand, H. Kawai, and R. S. Stein, J. Polymer Sci., 58, 185 (1962).
62. A. Keller, J. Polymer Sci., 15, 31 (1955).
63. Y. Fujiwara, J. Appl. Polymer Sci., 4, 10 (1960).
64. I. L. Hay and A. Keller, Kolloid-Z. U. Z. Polymere, 204, 43 (1965).
65. K. Sasaguri, S. Hoshino, and R. S. Stein, J. Appl. Phys., 35, 47 (1964).
66. F. C. Frank, A. Keller and A. O'Connor, Phil. Mag., 3, 664 (1958).
67. P. H. Geil, "Polymer Single Crystal", Chap. 4 and 7, Interscience, New York (1963).

68. P. Ingram, and A. Peterlin, J. Polymer Sci., B2, 739 (1964).
69. A. Keller and S. Sawada, Macromol. Chem., 74, 190 (1964).
70. D.C. Bassett, F. C. Frank and A. Keller, Phil. Mag., 8, 1739 (1963).
71. I. L. Hay, T. Kawai, and A. Keller, International Symposium on Macromolecules Chemistry, Prague 1965. Preprint No. P325.
72. H. Kawai, T. Ito, D. A. Keedy and R. S. Stein, J. Polymer Sci., B2, 1075 (1964).
73. T. Ito, T. Oda, and H. Kawai, Repts., Prog. Polymer Phys., Japan, 11, 191 (1968).
74. T. Ito, T. Oda, H. Kawai, T. Kawaguchi, D. A. Keedy and R. S. Stein Rev. Sci. Inst., 39, No. 12, 1847 (1968).
75. T. Kawaguchi, T. Ito, H. Kawai, D. A. Keedy and R. S. Stein, Macromolecules, 1, 126 (1968).
76. M. Takayanagi, T. Aramaki, M. Yoshino and H. Hoashi, J. Polymer Sci., 46, 531 (1960).
77. K. Iohara, K. Imada and M. Takayanagi, "Thermal Expansion of Lattice Constants of Polyethylene Single Crystal" in press.
78. R. C. Crystal and D. Hansen, J. Polymer Sci., A2, 6, 981 (1968).
79. R. S. Stein, A. Tanaka, E. P. Chang and I. Kimura, ONR Tech. Rept. No. 111, 1968, University of Massachusetts, Amherst, Mass.
80. I. Kimura, A. Tanaka, E. P. Chang, B. Delf and R. S. Stein, unpublished paper.
81. P. Corneliussen and A. Peterlin, Makromol. Chem., 105, 193 (1967).
82. K. Fujino, H. Kawai, T. Oda and H. Maeda, Proc. 4th Intern. Congress on Rheology, Part 3, PP. 501, Interscience Publishers, New York (1963).

83. S. Iwayanagi and H. Nakane, "Role of the Lamellar Boundary in the Relaxation of Crystalline Polymers", in preparation.
84. R. S. Stein, S. Onogi and D. A. Keedy, J. Polymer Sci., 57, 801 (1962)
85. R. Hoseman, W. Wilke, and F. J. Balta Calleja, acta. cryst. 21, 118 (1966)
86. R. Hosemann, J. Polymer Sci., C20, 1 (1967).
87. V. F. Holland, J. Appl. Phys., 35, 3235 (1964).
88. P. H. Lindenmeyer, Textile Res. Journal, 34, 825 (1964).
89. P. H. Lindenmeyer, J. Polymer Sci., C15, 107 (1966).
90. A. Tanaka, Ph. D. thesis, University of Massachusetts, Amherst, Mass., (1970).
91. E. P. Chang, Ph. D. thesis, University of Massachusetts, Amherst, Mass., (1970).
92. R. S. Stein, Polymer Eng. and Sci., 8, 259 (1968).
93. K. Kobayashi and T. Nagasawa, J. Polymer Sci., C15, 163 (1967).
94. R. S. Stein, T. Hashimoto and P. J. Phillips, in preparation.
95. T. Hashimoto, P. J. Phillips and R. S. Stein, in preparation.
96. K. Kobayashi, "Kobunshi no Busei", (Ed. by Nakajima et. al.), Kagaku Dojin, Chapt. 11, PP. 216 (1962).
97. E. W. Fischer, J. Polymer Sci., 34, 721 (1959).
98. C. C. Price, J. Polymer Sci., 39, 101, 123 (1959).
99. A. Keller, J. Polymer Sci., 17, 291, 447 (1955).
100. R. S. Moore and C. Gieniewski, J. Appl. Phys., 36, 3022 (1965).

101. R. S. Moore, J. Polymer Sci., Pt. A, Vol. 3, 4093 (1965).
102. R. S. Moore and C. Gieniewski, J. Polymer Sci., C13, 55, 95 (1966).

C A P T I O N S F O R F I G U R E S

- I-1. The coordinate system for scattering experiment.
- I-2. The orientation correlation between optic axes of scattering elements.
- I-3. A calculated I_+ scattering pattern for $\beta_o = 90^\circ$.
- I-4. A calculated $I_{||}$ scattering pattern for $\beta_o = 0^\circ$.
- I-5. A calculated I_+ scattering pattern for $\beta_o = 45^\circ$.
- I-6. A calculated $I_{||}$ scattering pattern for $\beta_o = 45^\circ$.
- I-7. A calculated $I_{||}$ scattering pattern for an equal mixture of regions with $\beta_o = +45^\circ$ and -45° .
- I-8. The orientation of optic axes of scattering elements i and j separated by distance r in a uniaxially oriented film with the orientation direction Z' rotated through Ω away from vertical direction Z .
- I-9. A calculated I_+ scattering contour for an oriented film where $\beta_o = 90^\circ$ and $\sigma_o = \sigma = \rho_2 = 0$. $d_o = 2\mu$ and $d = 1\mu$ in this and the following figures.
- I-10. A calculated I_+ scattering contour for an oriented film where $\beta_o = 90^\circ$, $\sigma = \sigma_o = 0$ and $\rho_2 = 1/4$.
- I-11. A calculated scattering contour for an oriented film where $\beta_o = 90^\circ$, $\sigma = \sigma_o = 1/16$ and $\rho_2 = 1/4$.
- I-12. A calculated I_+ scattering contour for an oriented film where $\beta_o = 90^\circ$, $\sigma = \sigma_o = 1/16$ and $\rho_2 = 1/2$.
- I-13. A calculated I_+ scattering contour for an oriented film where $\beta_o = 0^\circ$, $\sigma = \sigma_o = 1/16$ and $\rho_2 = 1/2$.

- I-14. A calculated I_+ scattering contour for an oriented film where $\beta_o = 90^\circ$, $\sigma_o = 0$, $\sigma = 0.385$ and $\rho_2 = 1/2$.
- I-15. A calculated I_+ scattering contour for an oriented film where $\beta_o = 90^\circ$, $\sigma_o = 1/16$, $\rho_2 = 1/2$ and $\sigma = 0.385$.
- II-1. The coordinate of the scattering element in a two dimensional spherulite.
- II-2. The calculated variation of H_V scattered intensity with θ at $\mu = 45^\circ$ for 3μ spherulites having radial disorder with $a = 1.5\mu$ and $\lambda = 0.364\mu$, and various $\langle(\Delta(r_i))^2\rangle_{av}/\delta_o^2$.
- II-3. The calculated variation of H_V scattered intensity for the case of Fig. (II-2) for $a = 0.6 \mu$.
- II-4. The calculated variation of H_V scattered intensity for the case of Fig. (II-2) for $a = 0.1 \mu$.
- II-5. The calculated variation of H_V scattered intensity with θ at $\mu = 45^\circ$ for 3μ spherulites having angular disorder with $c = 0.7\pi$ radians and $\lambda = 0.364 \mu$ and various values of $\langle(\Delta(\alpha_i))^2\rangle_{av}/\delta_o^2$.
- II-6. The calculated variation of H_V scattered intensity for the case of Fig.(II-5) for $\langle(\Delta(\alpha_i))^2\rangle_{av}/\delta_o^2 = 5 \times 10^{-3}$ and $c = \pi$, 0.7π and 0.5π radians.
- II-7. Intensity contour diagrams for H_V scattering for a 3μ spherulite with angular disorder in the magnitude of the anisotropy characterized by angular correlation distance of 0.7π radians and $\langle(\Delta(\alpha_i))^2\rangle_{av}/\delta_o^2$ of (a) 0, (b) 0.005 and (c) 0.01. The

numbers on the contour lines refer to relative intensities enumerated in Table II-1.

- II-8. An H_V scattering pattern corresponding to an undeformed perfect two dimensional spherulite.
- II-9. The intensity contour diagram for an undeformed spherulite ($\lambda_s = 1.0$) for various values of the mean square orientation fluctuation parameter g_o equal to (a) 1.0, (b) 0.9, and (c) 0.7.
- II-10. The variation of scattered intensity with θ for an undeformed spherulite with $g_o = 0.9$ for azimuthal angles of $0^\circ(90^\circ)$, 45° and $30^\circ(60^\circ)$.
- II-11. The variation of $\langle \cos^2 2\Delta\beta_1 \rangle_{av}$ with α corresponding to $g_o = 1.0$ and $\sigma = 0, -0.1, -0.2, -0.3, -0.4, -0.5$ and for $g_o = 0.5$ with $\sigma = 1.0$.
- II-12. Scattering intensity contour diagrams of a deformed spherulite with $\lambda_s = 1.5$ and (a) $g_o = 0.8$ and $\sigma = 0.0$ (no angular dependence of fluctuation amplitude) and for $g_o = 1.0$ with angular dependence of fluctuation amplitude characterized by values of σ (b) 0.0, (c) -0.2, (d) -0.5 and (e) for $g_o = 0.5$ and $\sigma = 1.0$.
- II-13. The variation of scattering intensity with θ for a deformed spherulite ($\lambda_s = 1.5$) at azimuthal angle $\mu = 0^\circ$ for $g_o = 1.0$ and for curve 1 at $\sigma = 0.0$, 2 at $\sigma = -0.1$, 3 at $\sigma = -0.2$, 4 at $\sigma = -0.3$, 5 at $\sigma = -0.4$ and 6 at $\sigma = -0.5$.
- II-14. The variation of scattering intensity with θ for a deformed spherulite ($\lambda_s = 1.5$) at azimuthal angle $\mu = 90^\circ$ for $g_o = 1.0$

and the same values of σ as for Fig.II-13.

III-1. A block diagram of the dynamic light scattering (DLS) apparatus.

III-2. A schematic diagram of the light source part:

M; mercury vapor lamp, B; lamp housing, C; cooling pipe,
L1; lens ($f_1^* = 106$, $d_m^* = 52$), F; filter box(for neutral
density and monochromatic filters), L2; lens($f_1=114$, $d_m = 29$),
P; pinhole with $d_m = 1$, L3; lens ($f_1 = 82$, $d_m = 32$), G; partial-
ly reflecting slide glass, D; diaphragm and shutter, A; polarizer,
PM; monitor photomultiplier tube (RCA 1P21).

III-3. The correction factor for the partial polarization of the inci-
dent beam. $I_{||}^0$ is intensity of incident beam under parallel
polarizer and analyzer (arbitrary unit).

III-4a. A picture of a part of the DLS apparatus showing the light
source part (in the right half) and the deformation apparatus
(in the left half).

The light source part:

B; lamp housing, F; filter box for neutral density and mono-
chromatic filters, P; polarizer, PM; monitor PM tube.

The deformation apparatus:

D; worm gear for varying Ω , F; worm gear for varying the sample
tilting angle, ϕ . D1 and D2; disks on which the detector PM
tubes are set. T1 and T2; worm gear to vary θ . E; eccentric cam.
S; sample clamp, TE; temperature enclosure, A; analyzer.

* f_1 and d_m are the focus length and diameter of the lens in millimeter.

- III-4b. A picture of a part of the DLS apparatus showing the detector part and the deformation apparatus. The light source part is behind the deformation apparatus.
- TC; temperature controlling chamber, R; refrigerated PM tube chamber.
- III-5. A picture of a part of the DLS apparatus showing the deformation apparatus and a part of the light source part.
- L; LVDT, H; helical cam.
- III-6. The optical system to detect scattered beam.
- (a) The system which has been used in this study.
- (b) A conventional system.
- S; sample, A; analyzer, B; shutter, L; lens($f_l = 283$, $d_m = 27.6$), F; field stoppers, D; diaphragm, C; filter box, E; frosted glass, P; detector PM tube (RCA 1P21).
- III-7. The dynode string resistors for the PM tubes.
- III-8. The circuit diagram for the differential preamplifier. A point at which the output signal is taken in the preamplifier is shown in the diagram.
- III-9. A block diagram of a part of the integrator (CW-1 BOX CAR INTEGRATOR) which has been used in this study.
- III-10. A schematic diagram for the helical cam to produce the trigger signal.
- III-11. An example of the relationships among strain, trigger and gate signals.
- S; strain, C; trigger, G; gate signal.

- III-12. The electronic circuit which is used in between the integrator and the electronic counter to measure gate-on and -off time.
- III-13. The device to adjust the starting phase of the gate signal.
- III-14. The D.C preamplifier which has been used for the preliminary experiment.
- III-15. A diagram for various combinations of the pulleys to change frequency of vibration. A symbol R represents a reduction gear.
- III-16. A diagram of the chamber for temperature control:
A; toaster heating element with many small holes, B; sensor, C; heat insulator, D; air flow diffuser, E; entrance for air flow, F; exit for air flow, G; air flow stopper.
- III-17. A diagram for the temperature enclosure;
A; exit for air flow, B; air flow diffuser, C_1 ; front window for scattered ray, C_2 ; rear window for incident ray, D; sample clamp, E; entrance for air flow.
- III-18. I_+ scattering intensity distributions for undeformed medium density polyethylene (MDPE).
(a) ψ dependences at $\theta = \theta_{\max}$ and $\theta = 7^\circ$.
(b) θ dependence at $\psi = 45^\circ$.
- III-19. The DLS signals for $I_+(\Omega = 0^\circ, \theta = 7^\circ)$ for MDPE at room temperature. $\epsilon_s = 0.082$, $\epsilon_d = 0.0085$.
(a) output signals of the monitor (lower) and detector (upper) PM tubes after the differential preamplifier with sensitivity of 0.5 volt.

(b) same as (a) except that a lower sweep rate is used in (b) for the oscilloscope.

(c) the output of the differential preamplifier (lower) with the same DA^* ($=0.5$ volts) as in (a) and (b), and the output of the integrator (upper).

(d) same as (c) except that a higher DA ($= 50$ millivolts) is used in (d).

III-20. The DLS signals for $I_+(\Omega=0^\circ, \psi = 45^\circ, \theta = 0^\circ)$ and for $I_+(\psi = 45^\circ, \Omega = 0^\circ, \theta = 7^\circ)$.

(a) Output signals for the monitor (lower) and detector (upper) PM tubes for $I_+(\Omega = 0^\circ, \psi = 45^\circ, \theta = 0^\circ)$ after the differential preamplifier with $DA = 2$ volts.

(b) Output signals of the differential preamplifier (lower) and the integrator (upper) for $I_+(\Omega = 0^\circ, \psi = 45^\circ, \theta = 0^\circ)$. $DA = 1$ volt.

(c) Output signals of the differential preamplifier (lower) and the integrator for $I_+(\psi = 45^\circ, \Omega = 0^\circ, \theta = 7^\circ)$. $DA = 0.1$ volts.

III-21. The effect of birefringence on light scattering patterns for MDPE stretched by 20%. The stretching direction of sample (Ω) is changed from vertical ($\Omega = 0^\circ$) to horizontal ($\Omega = 90^\circ$) keeping the polarizer and analyzer axes $+45^\circ$ and -45° with respect

* DA is referred to the sensitivity of the differential preamplifier hereafter.

to the vertical direction.

- III-22. The DLS signals for (a) $I_+(\Omega = 50^\circ, \theta = \theta_{\max})$; (b) $I_{||}(\Omega = 0^\circ, \theta = \theta_{\max})$ and (c) $I_{||}(\Omega = 0^\circ, \theta = 7^\circ)$. The DA is 0.2 volts for (a), 0.5 volts for (b), and 0.1 volts for (c). In each figure the upper signal is after the integrator and the lower signal is after the differential preamplifier.
- III-23. H_V and V_V scattering patterns for the undeformed MDPE.
- III-24. θ dependences of I_+ scattered intensity for the undeformed MDPE.
 (a) θ dependences of theoretical and experimental $I_+(\psi = 45^\circ)$ and $I_+(\psi = 0^\circ)$.
 (b) θ dependences of theoretical $I_+(\psi = 45^\circ)$ and experimental $[I_+(\psi = 45^\circ) - I_+(\psi = 0^\circ)]$.
- III-25. ψ dependences of $I_{||}(\theta = \theta_{\max})$ and $I_{||}(\theta = 7^\circ)$ for the undeformed MDPE.
- III-26. H_V scattering patterns for MDPE stretched by 10 and 20%.
- III-27. V_V and H_H scattering patterns for MDPE stretched by 10 and 20%.
- III-28. Ω dependence of the DLS for $I_+(\theta = \theta_{\max})$ at 24°C . $\epsilon_d = 0.009$, $\epsilon_s = 0.071$ and $t = 4.3$ mil.
- III-29. Ω dependences of the DLS for (a) $I_=(\theta = \theta_{\max})$ at 27°C and (b) $I_{||}(\theta = \theta_{\max})$ at 28°C . $\epsilon_d = 0.009$, $\epsilon_s = 0.071$ and $t = 4.3$ mil.
- III-30. Ω dependence of the DLS for $I_+(\theta = 7^\circ)$ at 24°C . $\epsilon_d = 0.009$, $\epsilon_s = 0.079$ and $t = 4.2$ mil.
- III-31. Ω dependences of the DLS for (a) $I_=(\theta = 7^\circ)$ and (b) $I_{||}(\theta = 7^\circ)$ at 23°C . $\epsilon_d = 0.009$, $\epsilon_s = 0.070$ and $t = 3.8$ mil.

- III-32. Temperature dependence of dynamic mechanical properties.
- $\tan \delta$
 - E' and E''
- III-33. Temperature dependences of the DLS for I_+ at $\theta = 7^\circ$.
- at $\Omega = 90^\circ$, $\epsilon_d = 0.009$, $\epsilon_s = 0.072$ and $t = 4.7$ mil.
 - at $\Omega = 0^\circ$, $\epsilon_d = 0.009$, $\epsilon_s = 0.080$ and $t = 4.8$ mil.
- III-34. Temperature dependences of the DLS for $I_{||}$
- at $\Omega = 90^\circ$ and $\theta = 5^\circ$. $\epsilon_d = 0.009$, $\epsilon_s = 0.079$ and 0.077 , and $t = 4.7$ and 4.8 mil.
 - at $\Omega = 0^\circ$ and $\theta = 7^\circ$. $\epsilon_d = 0.009$, $\epsilon_s = 0.080$ and $t = 4.8$ mil.
- III-35. Temperature dependences of the DLS for $I_{=}$
- at $\Omega = 90^\circ$ and $\theta = 5^\circ$. $\epsilon_d = 0.009$, $\epsilon_s = 0.076$ and 0.074 , $t = 4.8$ and 4.7 mil.
 - at $\Omega = 0^\circ$ and $\theta = 7^\circ$. $\epsilon_d = 0.009$, $\epsilon_s = 0.080$ and $t = 5.1$ mil.
- III-36. The definition of the angles θ , μ and ψ .
- III-37. The definition of the angles, α' , Ω' , r' , β' and ω' .
- III-38. The DLS results based upon the Samuels' model.
- Ω dependences of ΔI_+ at $\theta = 2.25^\circ$ and 7° .
 - θ dependences of ΔI_+ at $\Omega = 30^\circ$, 45° , and 60° .
- λ_s and $\Delta\lambda_s$ are 1.09 and 0.01 , respectively.
- III-39. The angular dependences of the tilting (β') and twisting factor ($g(\omega')$) for various K and η at $\lambda_\ell = 1.09$.
- III-40. Ω dependences of the DLS for I_+ at $\theta = 2.25^\circ$ for various K and η . $\lambda_s = \lambda_\ell = 1.09$, $\Delta\lambda_s = \Delta\lambda_\ell = 0.01$ and $\gamma_\ell = \pi/32$.

(a) $\Delta I_+'.$

(b) $\Delta I_+''$

III-41. The Ω dependences of the DLS for I_+ at $\theta = 2.25^\circ$ for various values of η and K . The values of λ_s , λ_ℓ , $\Delta\lambda_s$, $\Delta\lambda_\ell$ and γ_ℓ are the same as those for Fig.III-40.

(a) $\tan \gamma$ for various values of K in the case of $\eta = 0$.

(b) $\tan \gamma$ for various values of η in the case of $K = 0$.

III-42. The effect of dynamic strain on $\Delta I_+'.$ and $\Delta I_+''$ at $\theta = 2.25^\circ$ for various values of η and K . $\lambda_s = \lambda_\ell = 1.09$, $\Delta\lambda_s = \Delta\lambda_\ell = 0.005$ and $\gamma_\ell = \pi/32$.

III-43. The effect of static strain on $\Delta I_+'.$ and $\Delta I_+''$ at $\theta = 2.25^\circ$ for various values of η and K . $\lambda_s = \lambda_\ell = 1.06$, $\Delta\lambda_s = \Delta\lambda_\ell = 0.005$ and $\gamma_\ell = \pi/32$.

III-44. The Ω dependences of $\Delta I_+'.$ and $\Delta I_+''$ at $\theta = 7^\circ$ for various values of η and K under the same conditions as Figs.III-40 and III-41.

(a) $\Delta I_+'.$

(b) $\Delta I_+''$

III-45. The effect of irreversibility of the tilting motion on the dependences of $\Delta I_+'.$ and $\Delta I_+''$ at $\theta = 2.25^\circ$. $\Delta\lambda_s = 0.01$ and $\lambda_s = \lambda_\ell = 1.09$ for both tilting and twisting processes. $\Delta\lambda_\ell = 0.01$ for twisting process but $\Delta\lambda_\ell = 0$ for tilting process.

(a) $\Delta I_+'.$

(b) $\Delta I_+''$

III-46. The effect of γ_ℓ on $\tan \gamma$ for I_+ at $\theta = 2.25^\circ$ under various η

and K. The solid line is for $\gamma_\ell = \pi/16$ and broken line for $\gamma_\ell = \pi/32$. $\lambda_s = \lambda_\ell = 1.09$ and $\Delta\lambda_s = \Delta\lambda_\ell = 0.01$.

III-47. The effect of a coupled tilting and twisting processes on the Ω dependences of the DLS for I_+ at $\theta = 2.25^\circ$ for various values of η and constant K ($= 0.6$). $\lambda_s = \lambda_\ell = 1.09$, $\Delta\lambda_s = \Delta\lambda_\ell = 0.01$ and $\gamma_\ell = \pi/32$.

(a) $\Delta I_+'.$

(b) $\Delta I_+''.$

(c) $\tan \gamma$

III-48. The Iwayanagi's six-parameter Voigt model for representing the mechanical and optical properties of polyethylene.

IV-1. The dynamic mechanical properties of low density polyethylene (data by A. Tanaka⁹⁰).

(a) Q-sample

(b) H-sample

IV-2. The change of H_V scattering patterns upon deforming the Q- and H-samples.

A-1. The relationship between ψ_1 and ψ_2 according to the new definition of \tilde{Q} vector.

A-2. The relationship between ψ_1 and ψ_2 according to the new definition of \tilde{O} vector.

A-3. The relationship between ψ_1 and ψ_2 according to the new definition of \tilde{O} vector.

A-4. The relationship between ψ_1 and ψ_2 according to the new definition of \tilde{O} vector.

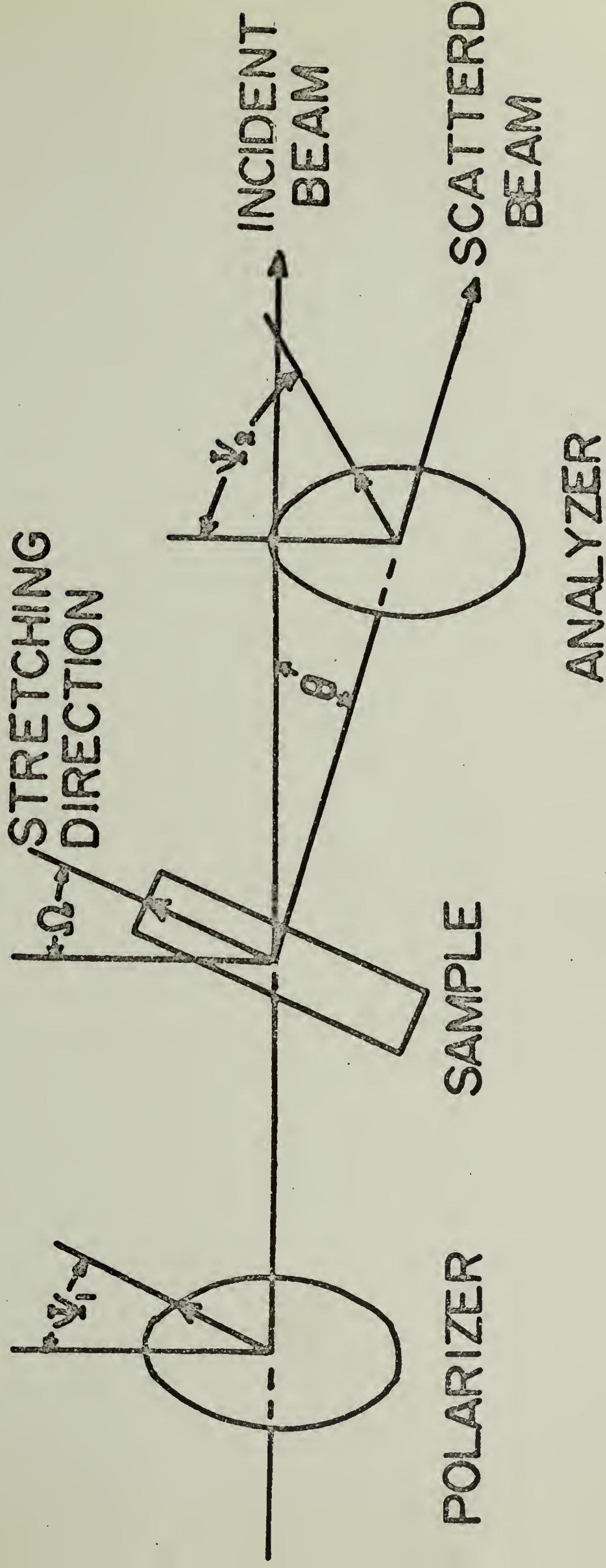


FIGURE I-1

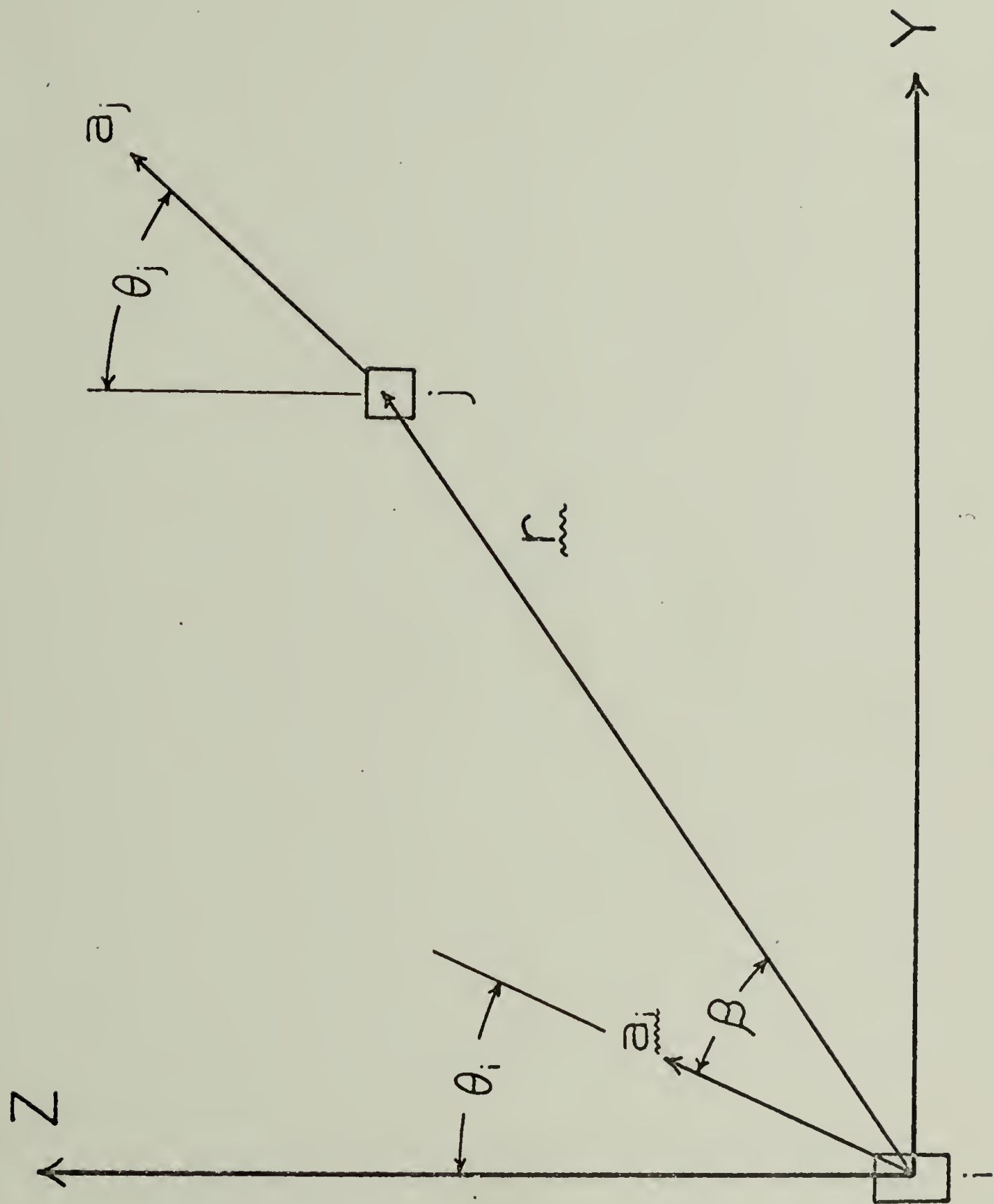
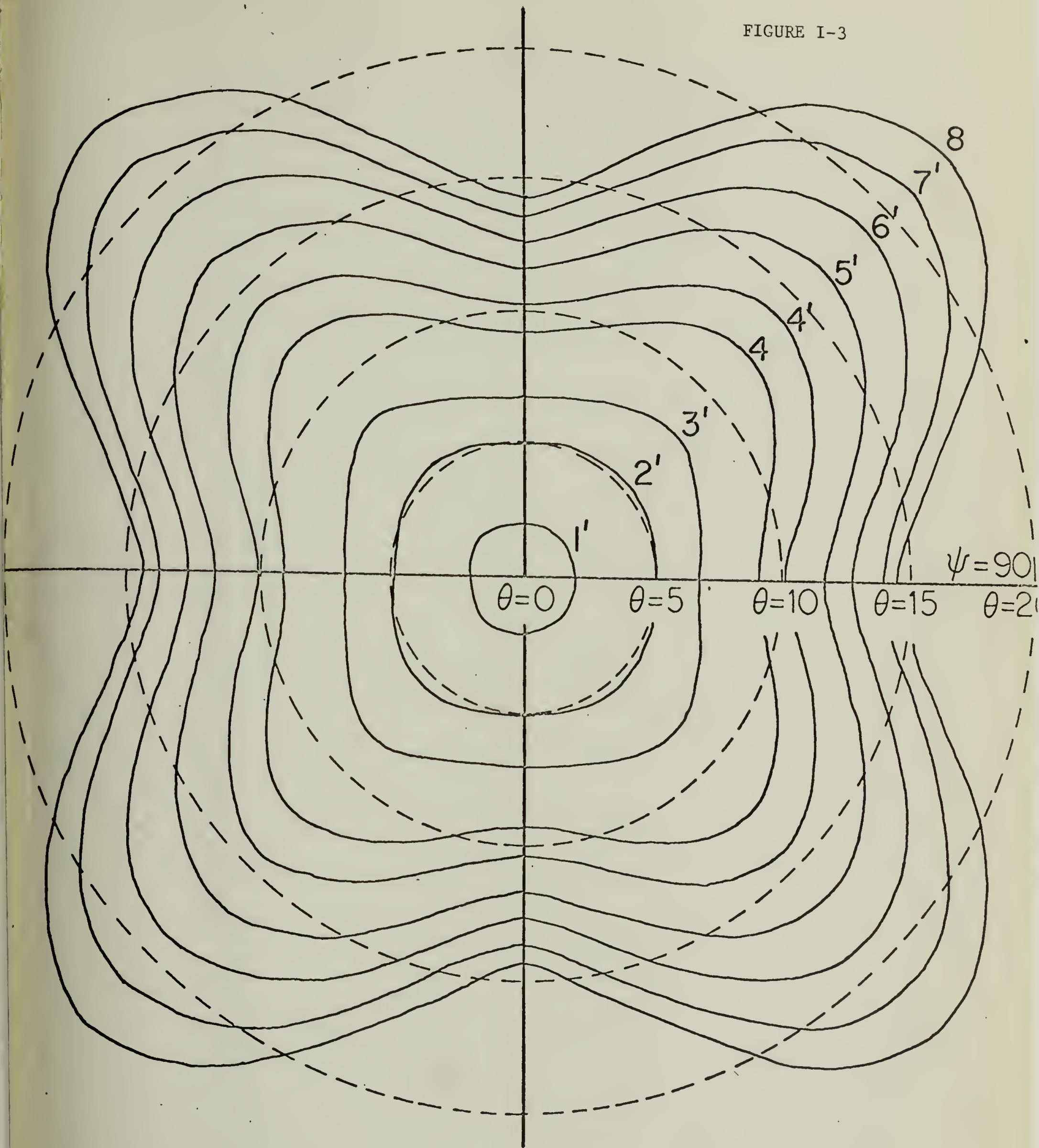


FIGURE I-2

$I_+(\beta_0 = 90)$

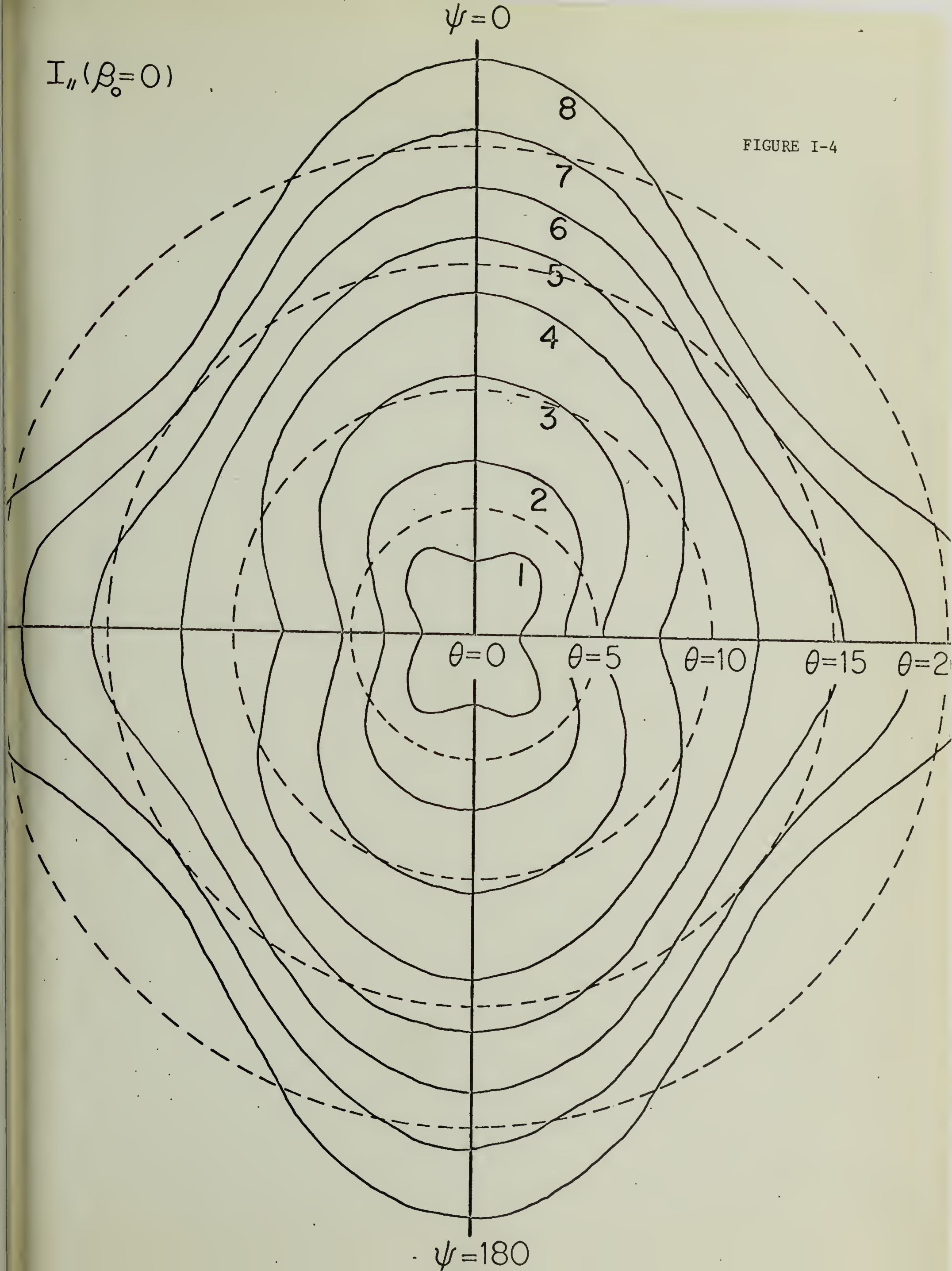
$\psi = 0$

FIGURE I-3



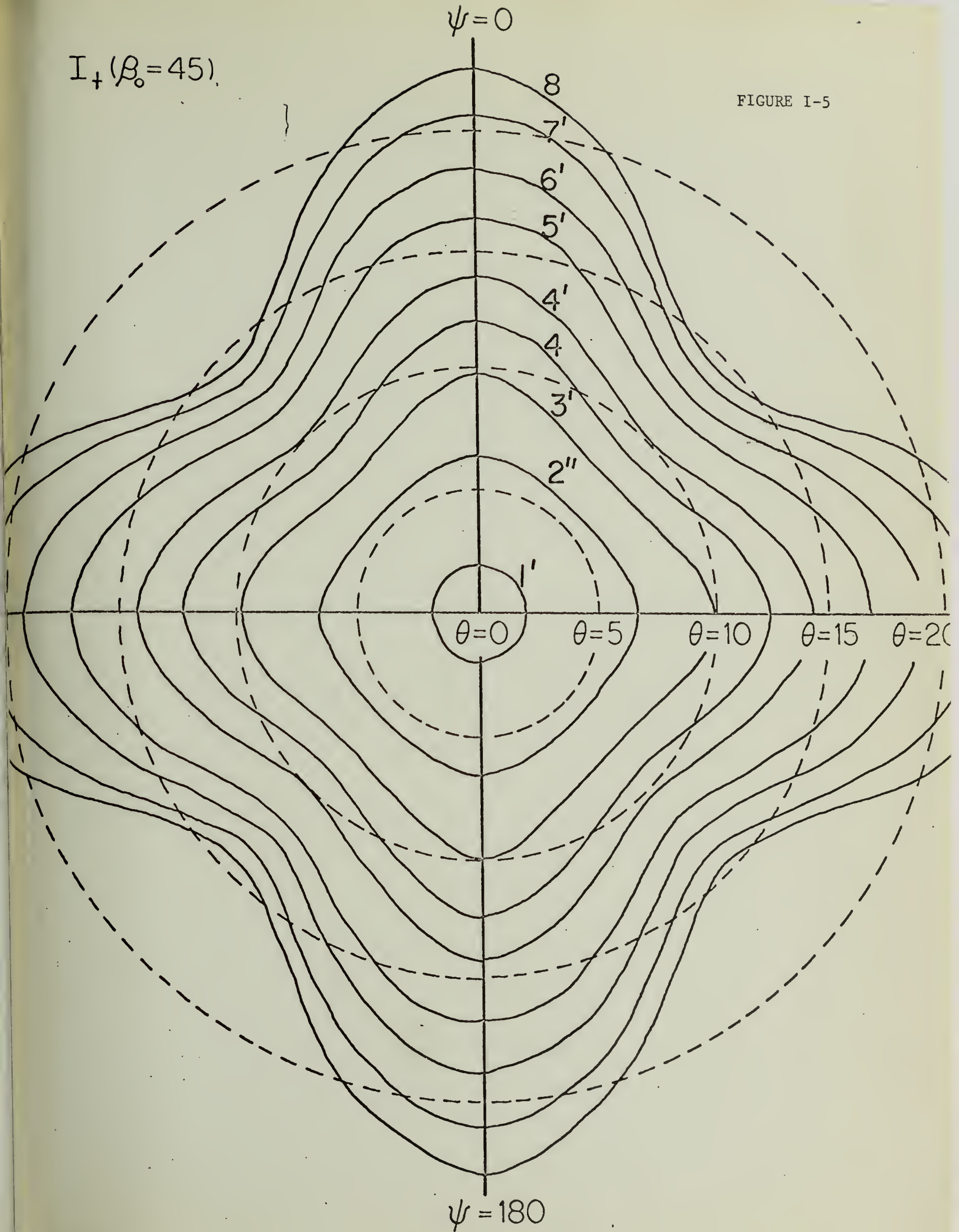
$I_{\parallel}(\beta_0=0)$

FIGURE I-4



$I_+(\beta_0=45)$

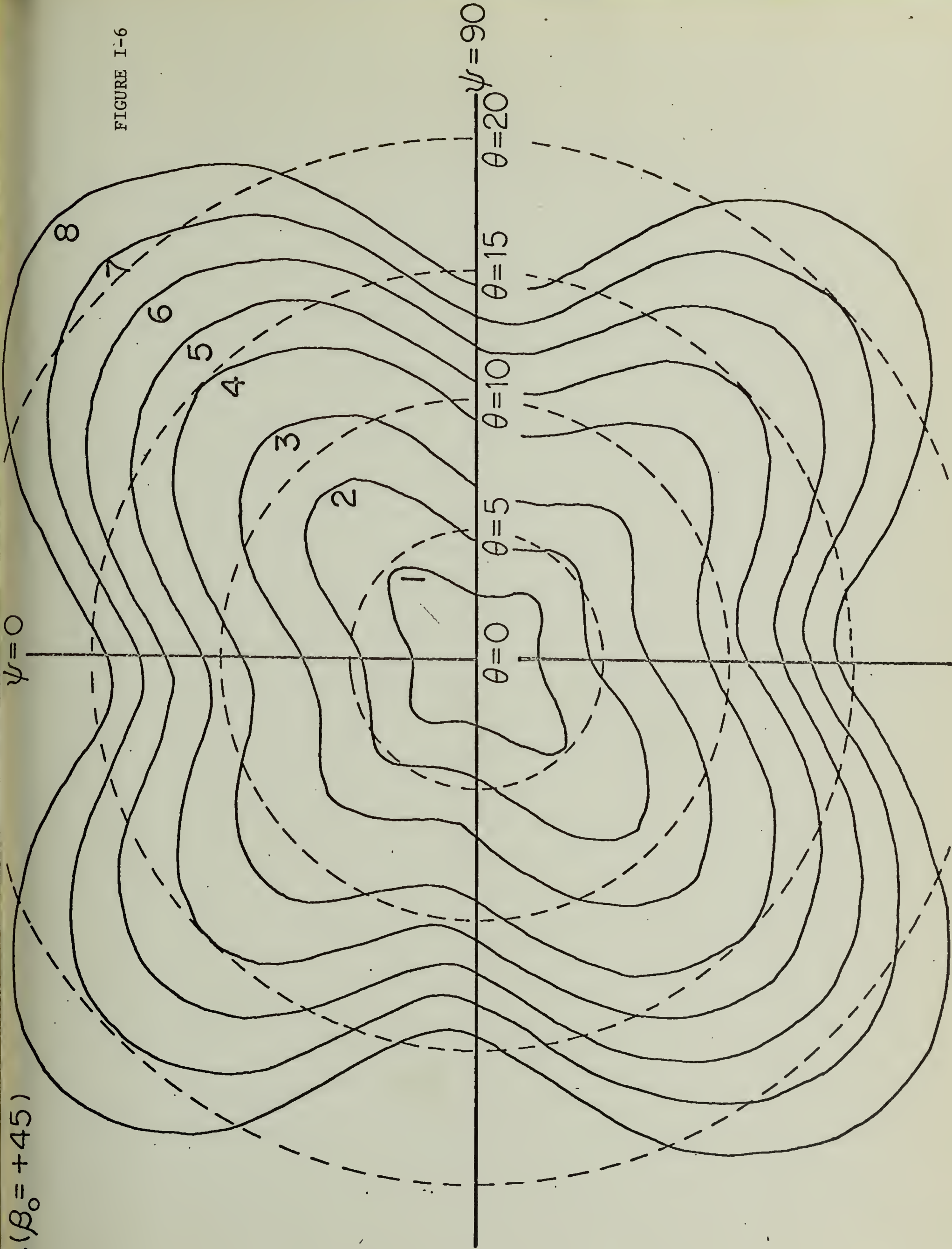
FIGURE I-5



$I_{\parallel}(\beta_0 = +45)$

$\psi = 0$

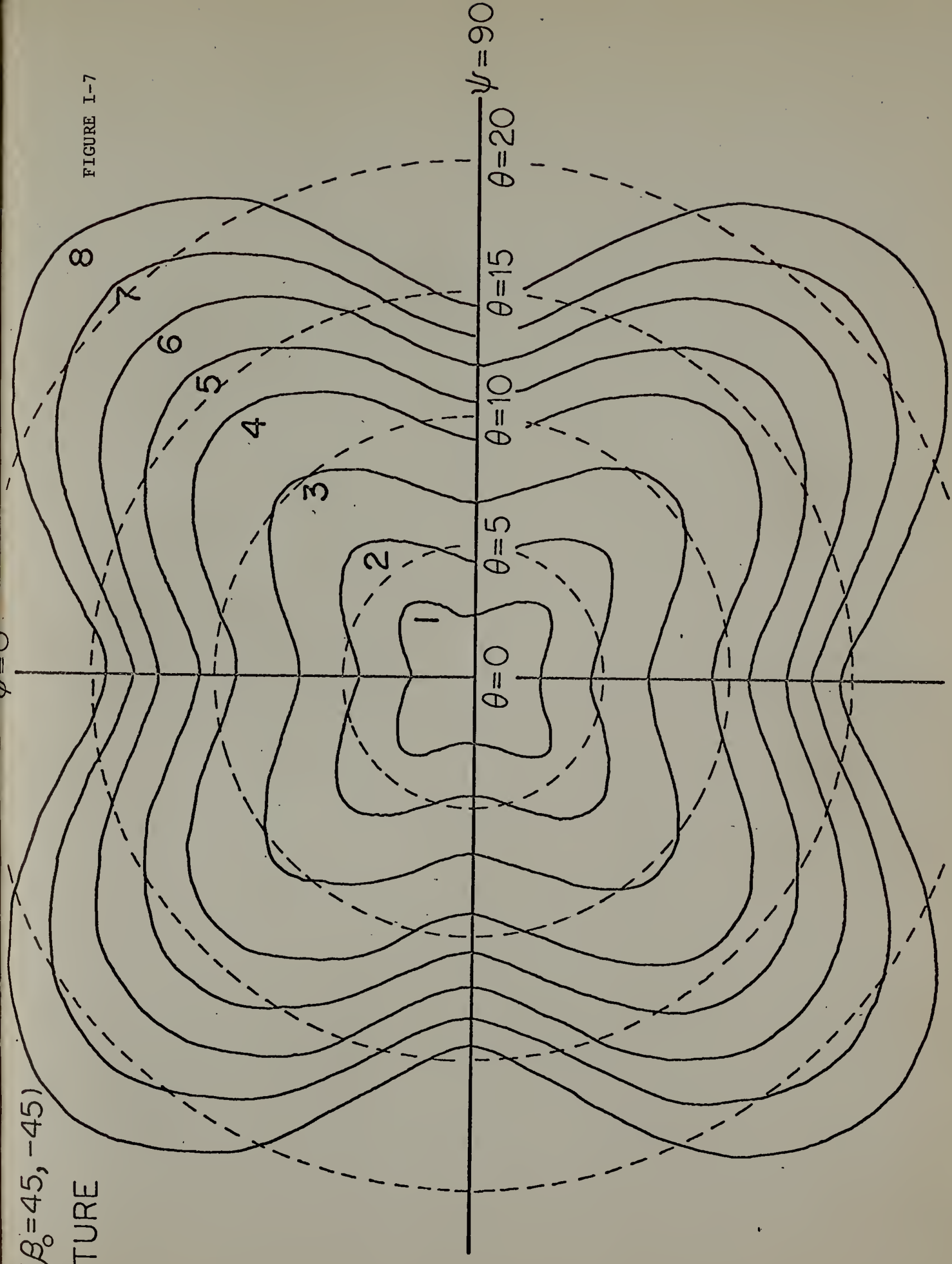
FIGURE 1-6



$I_{\parallel} (\beta_0 = 45, -45)$

MIXTURE

FIGURE 1-7



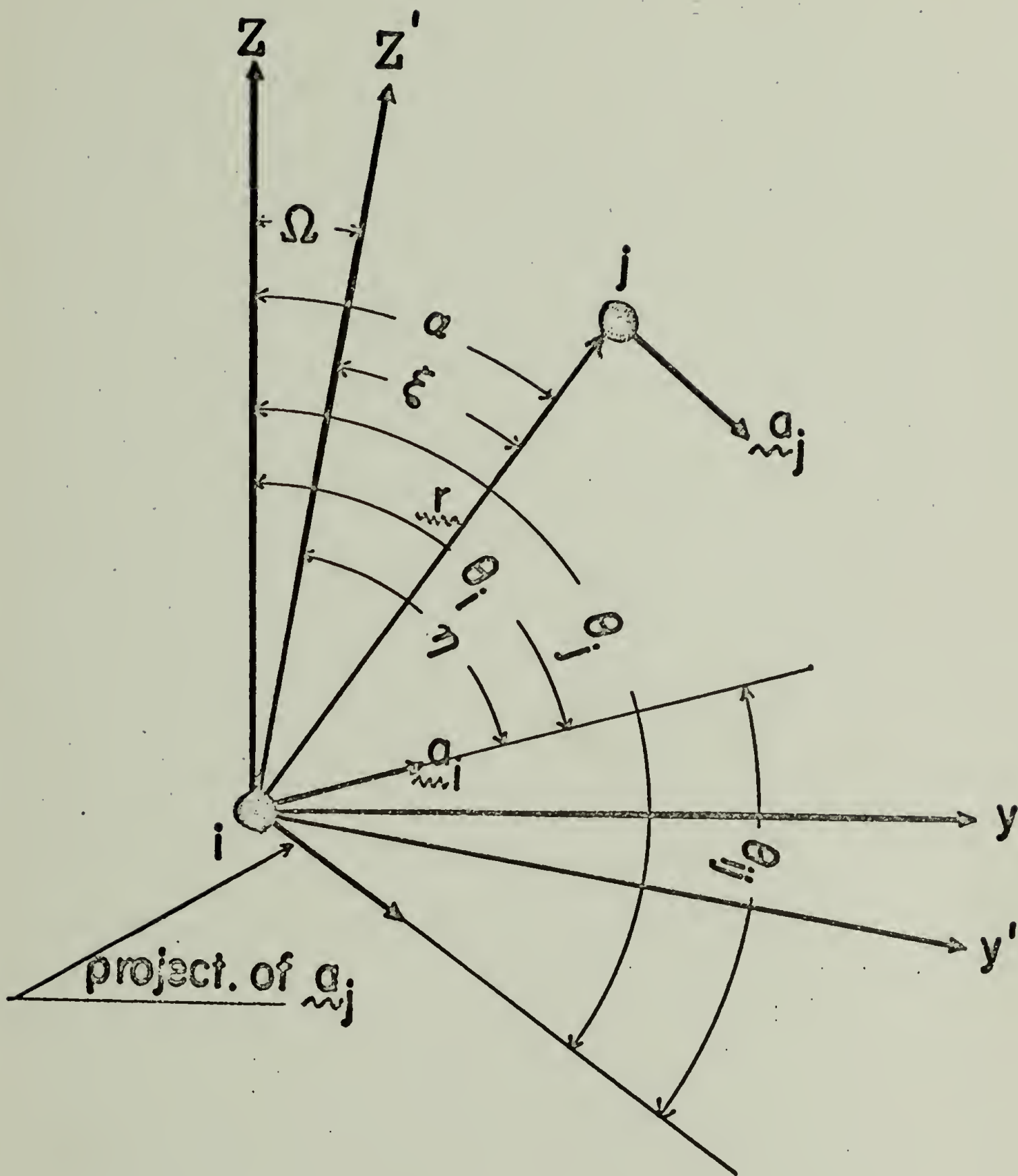


FIGURE I-8

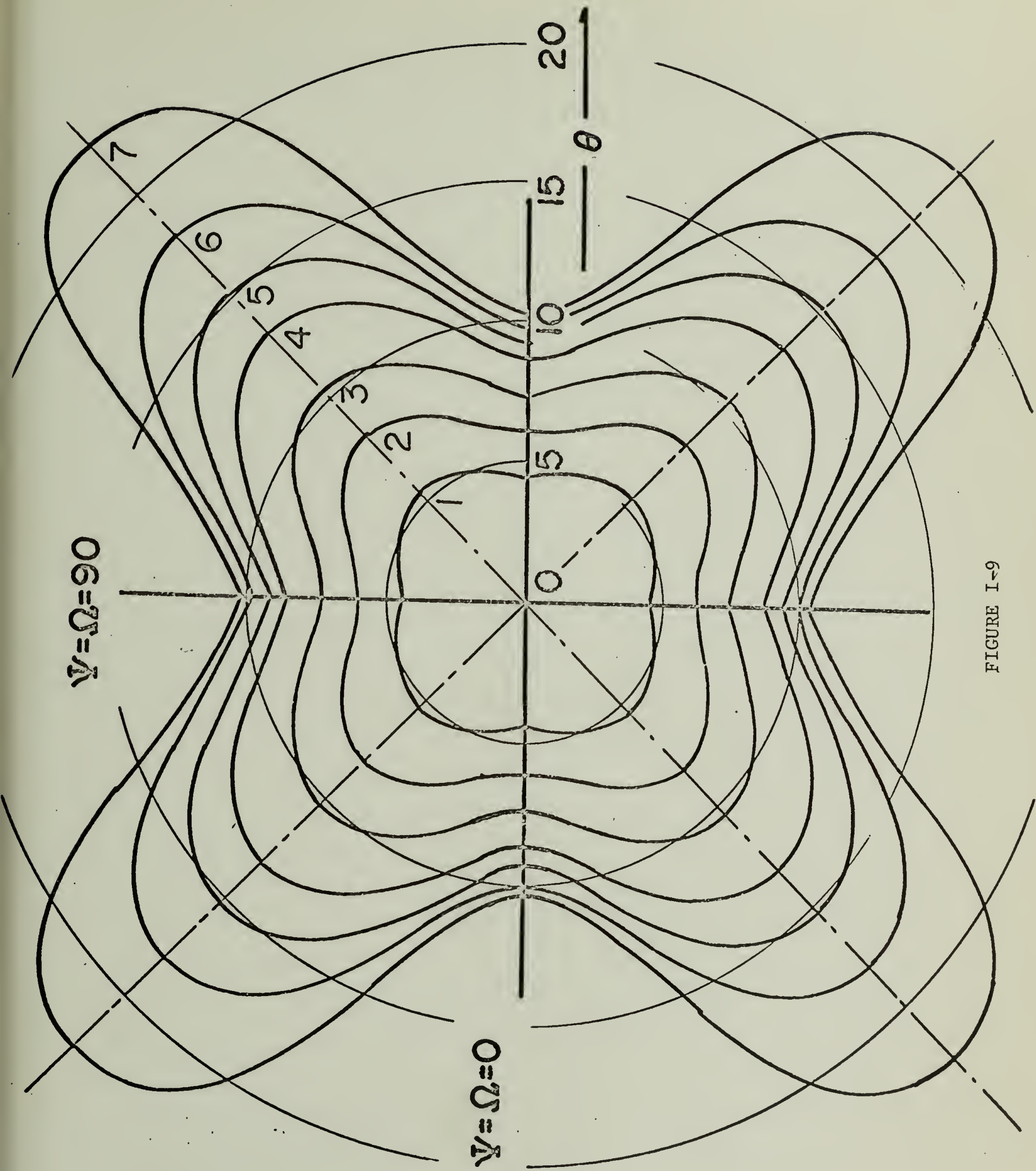


FIGURE 1-9

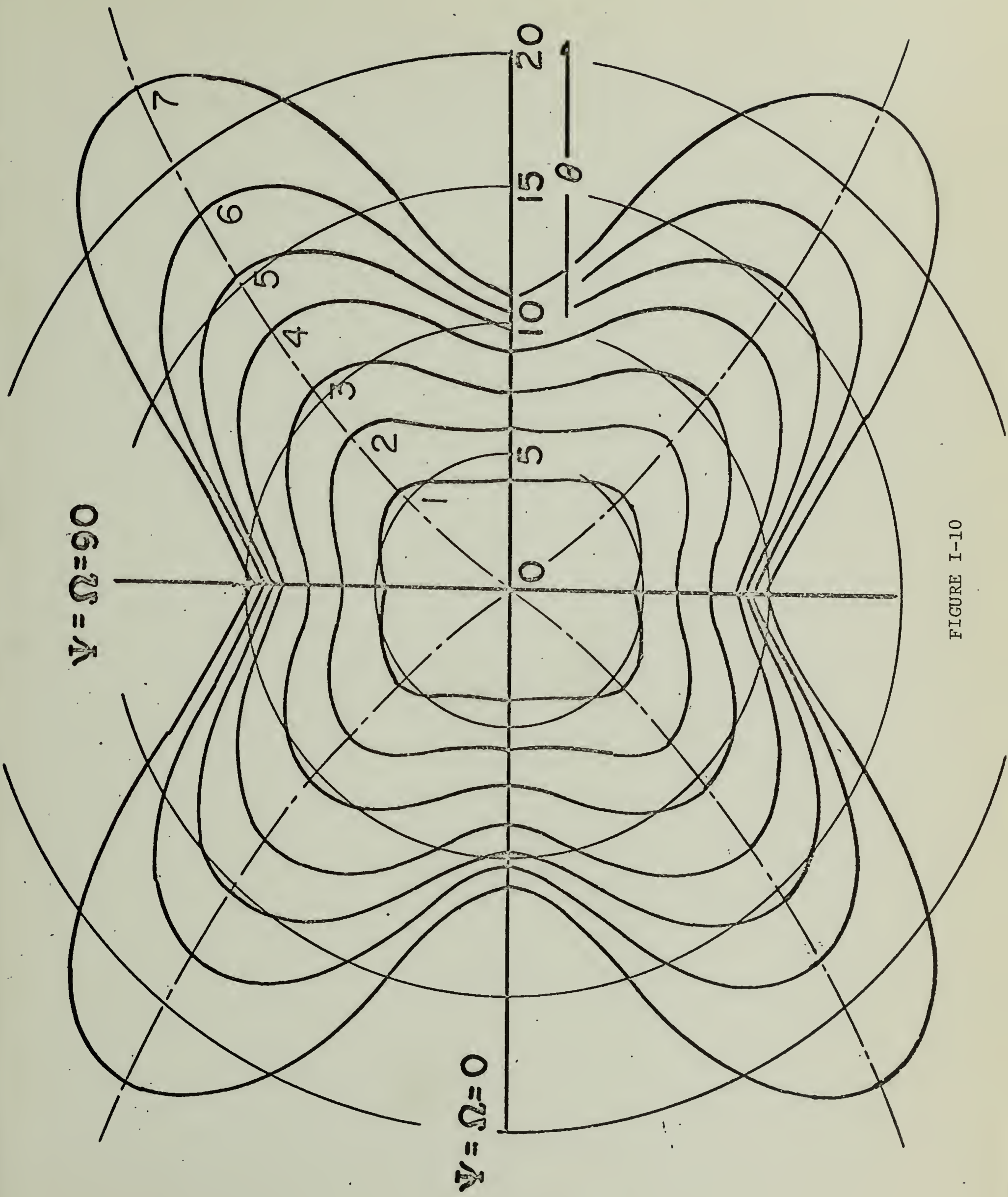


FIGURE I-10

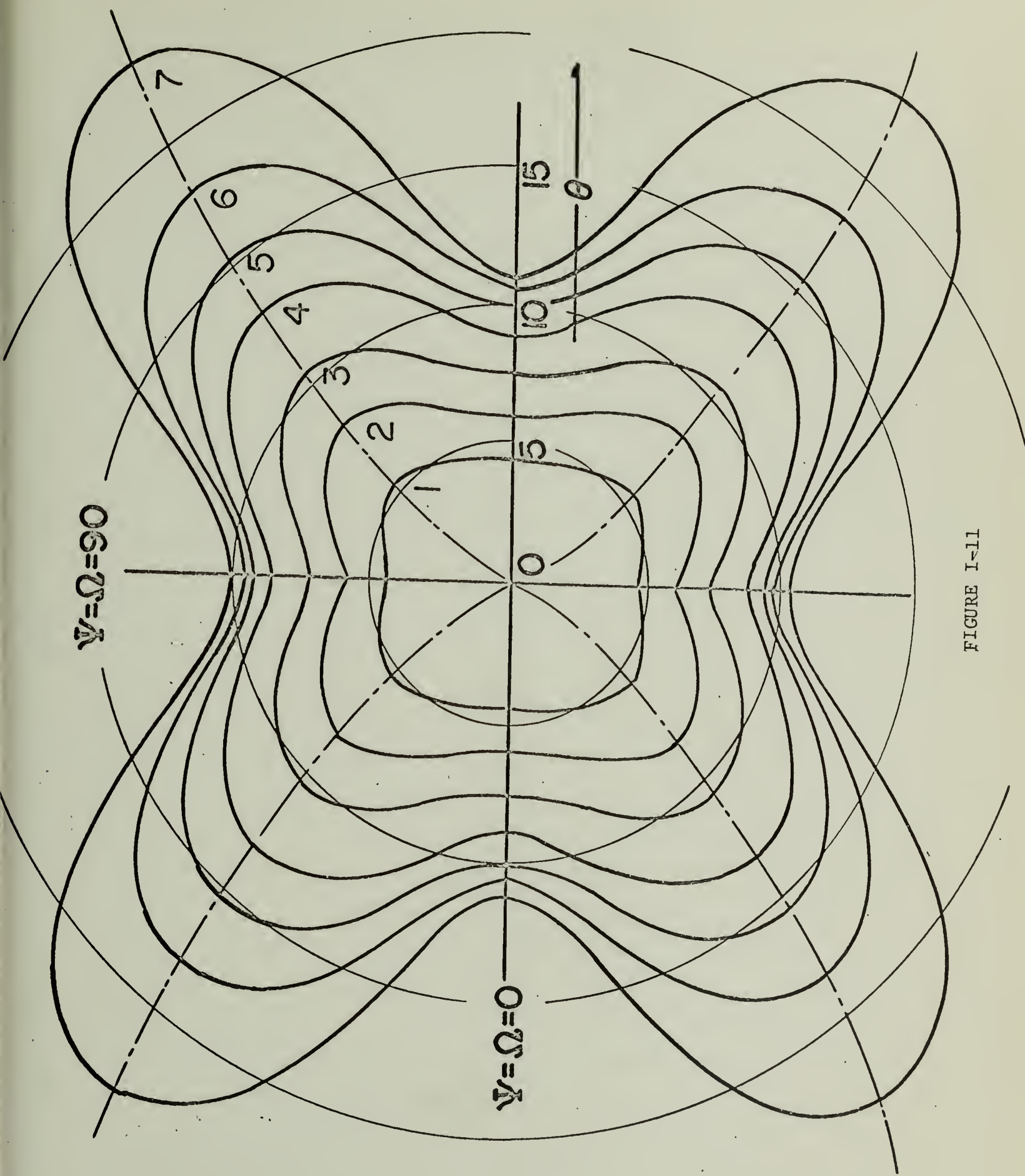


FIGURE I-11

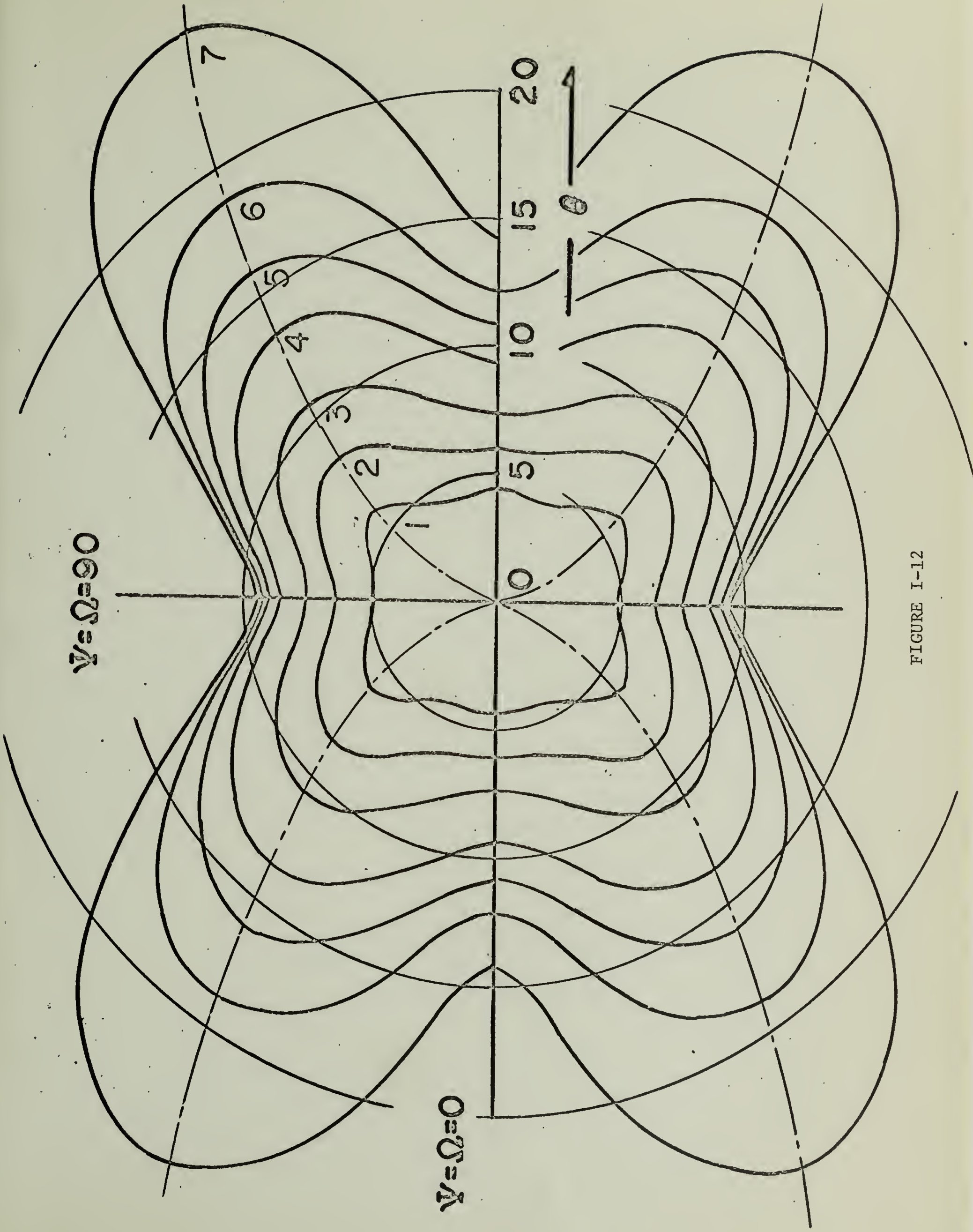


FIGURE I-12

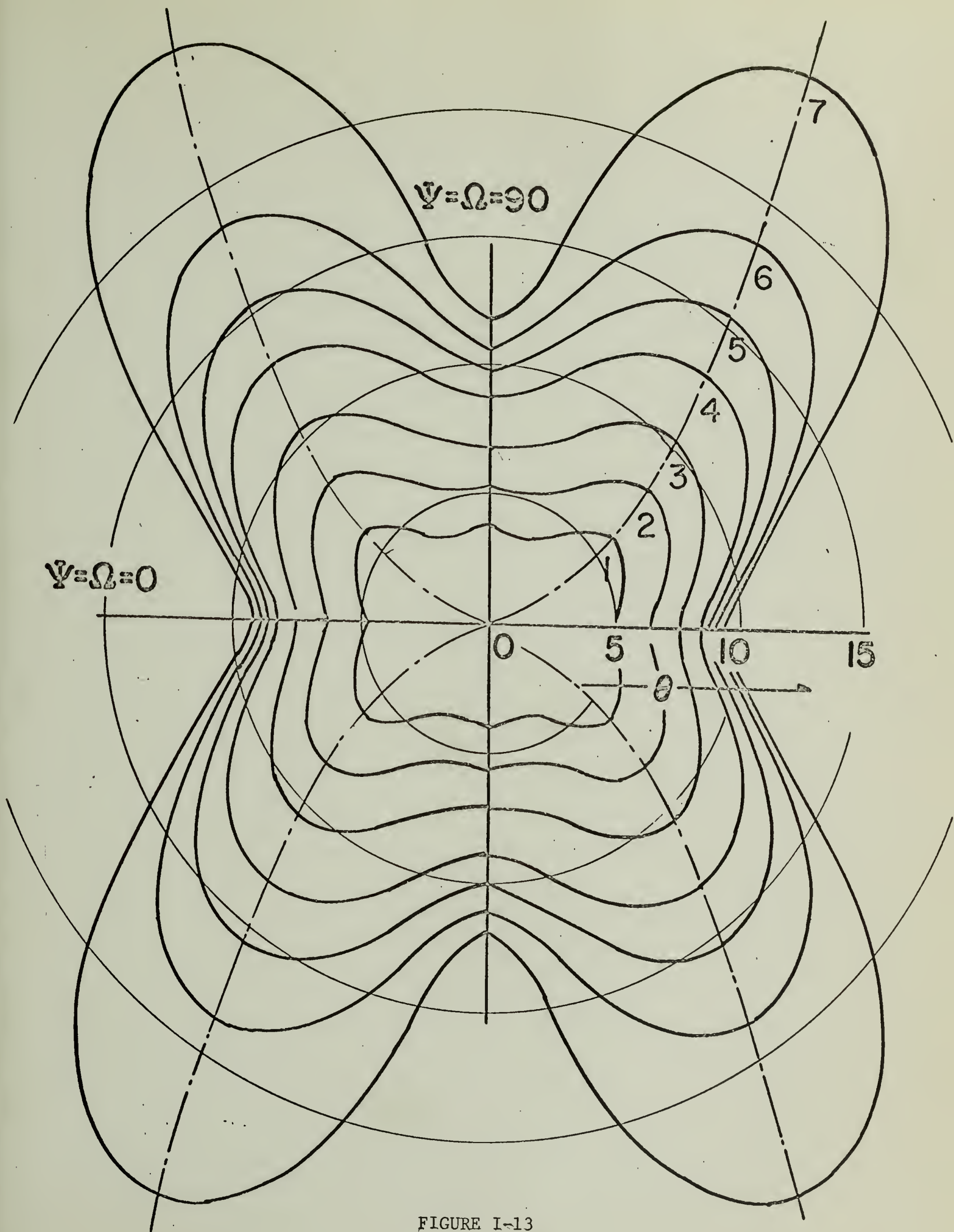


FIGURE I-13

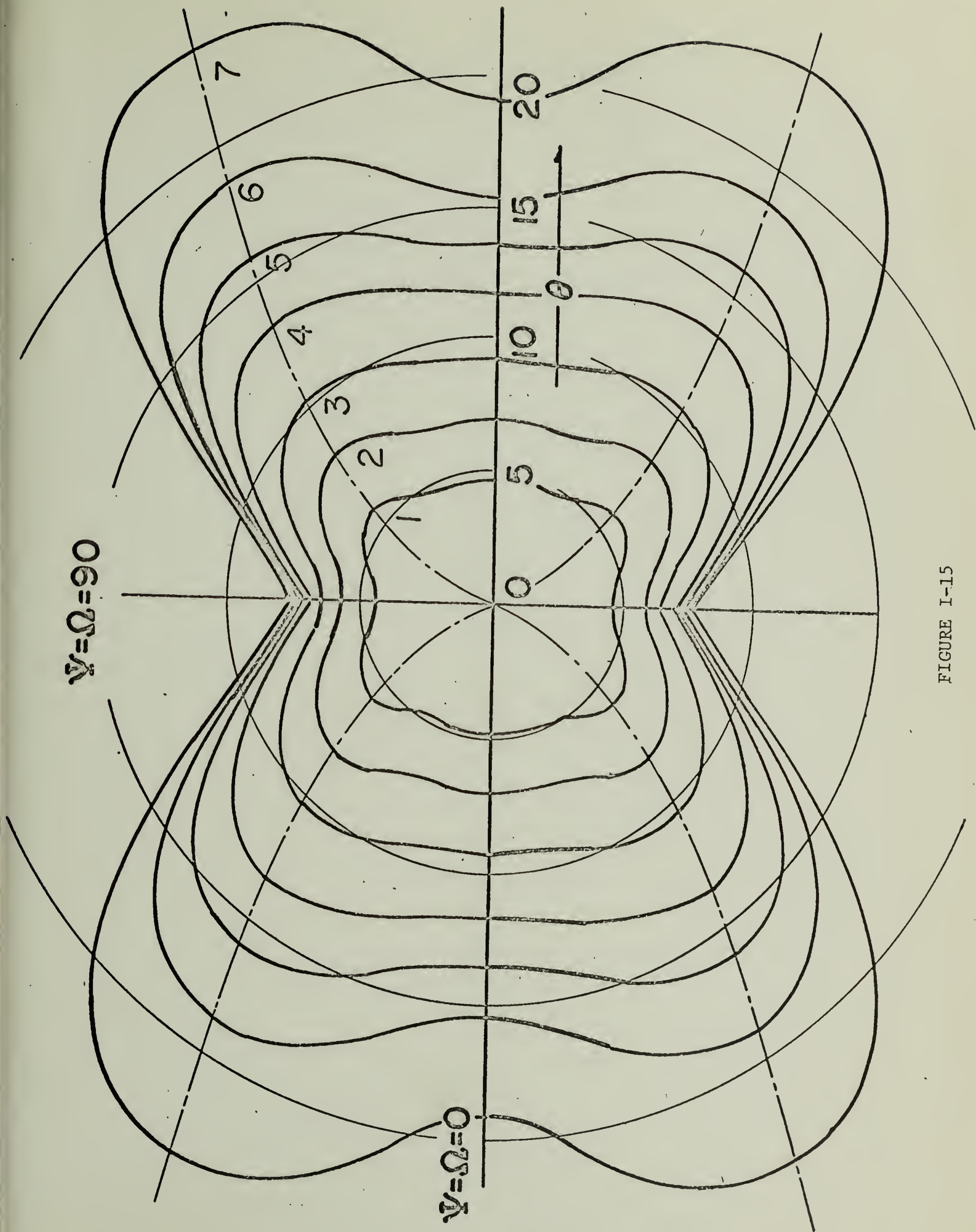


FIGURE I-15

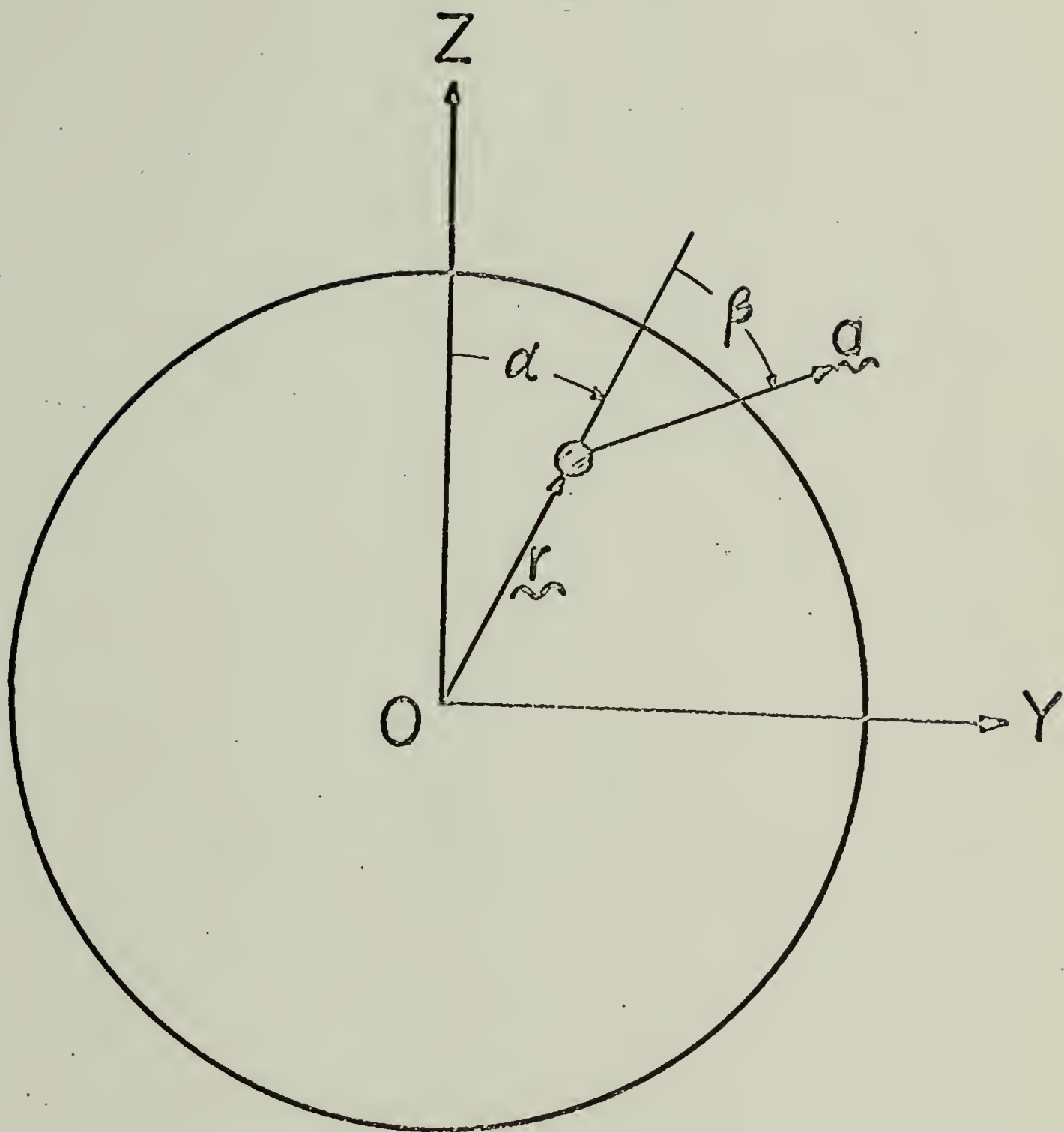


FIGURE II-1

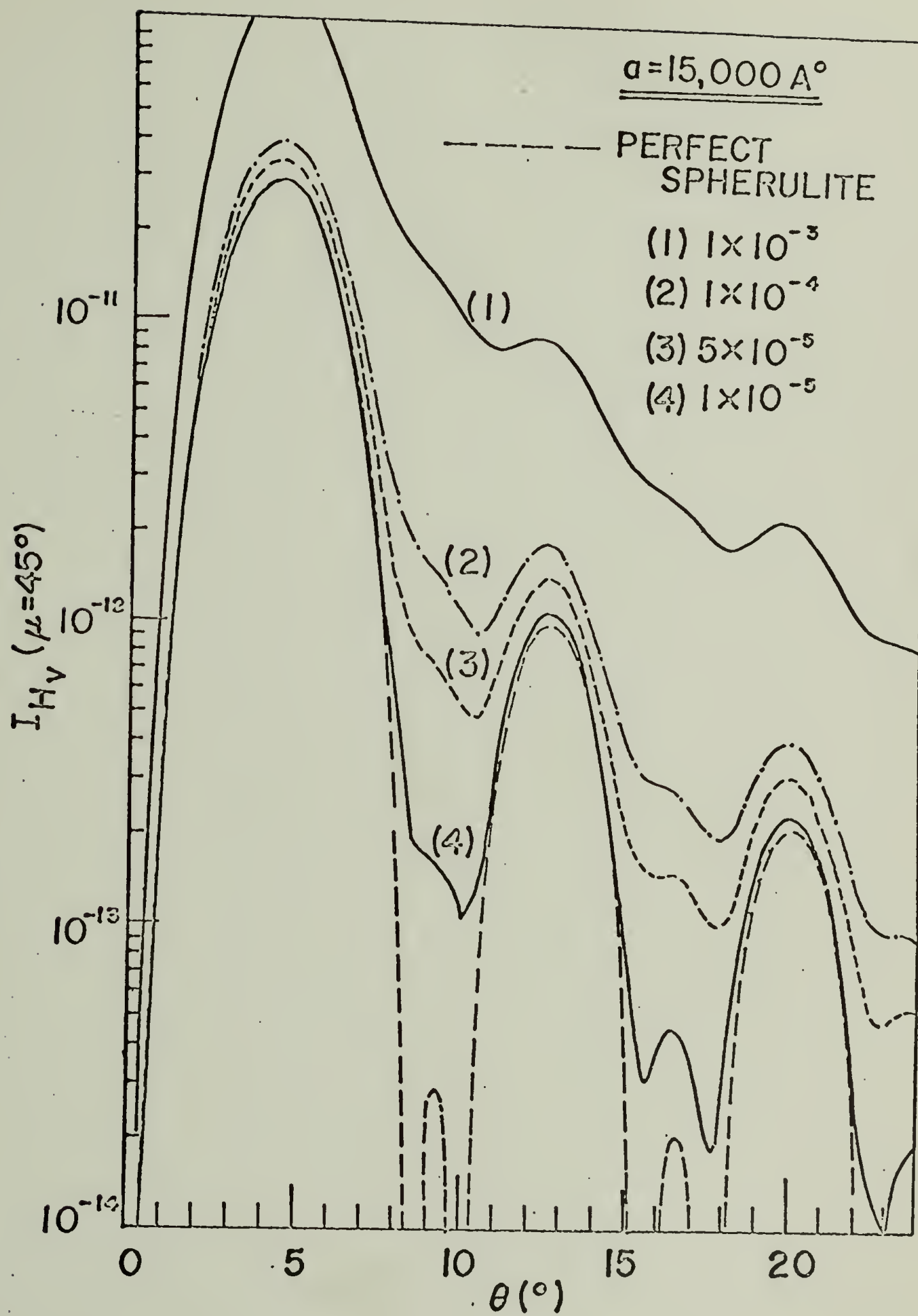


FIGURE II-2

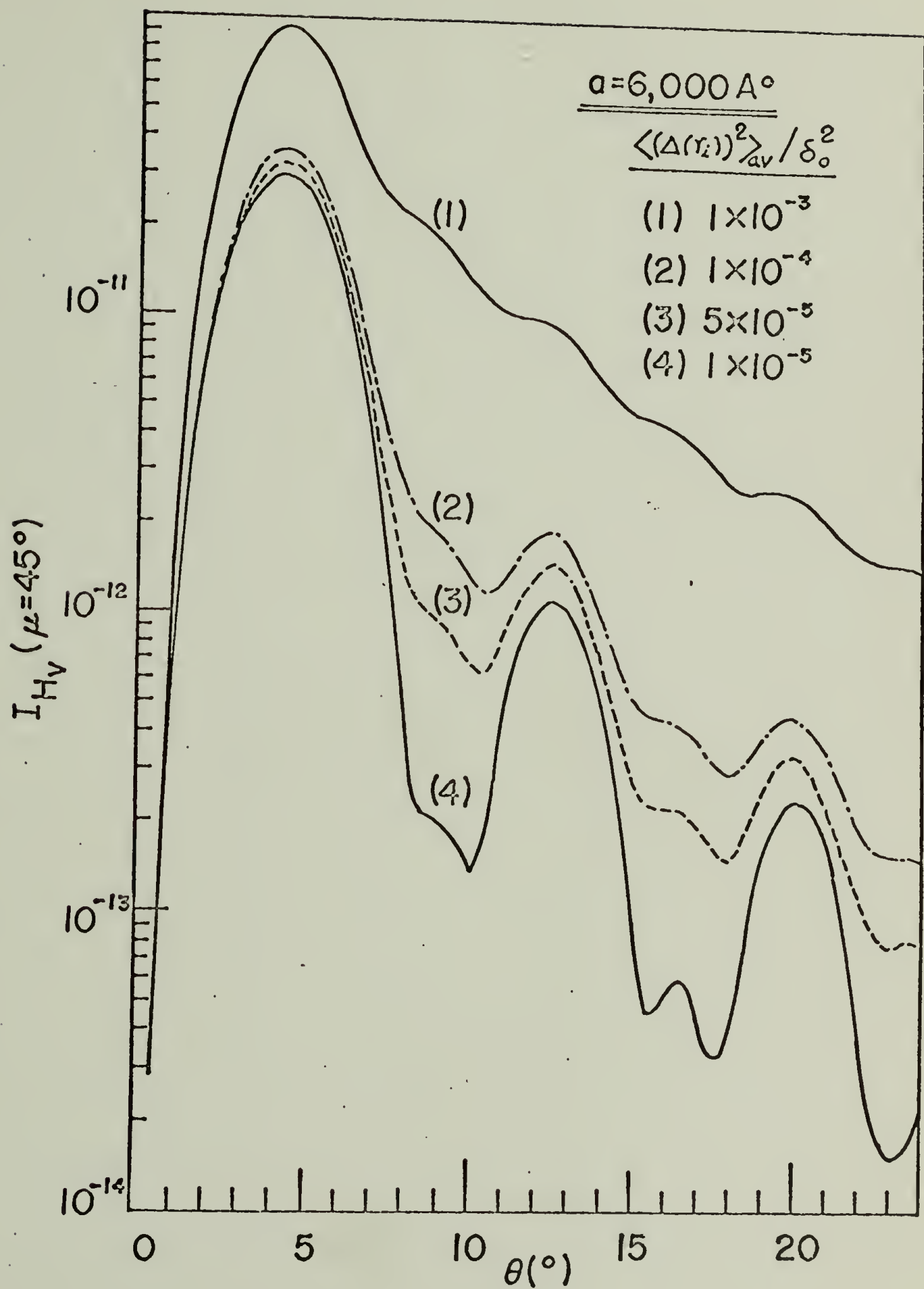


FIGURE II-3

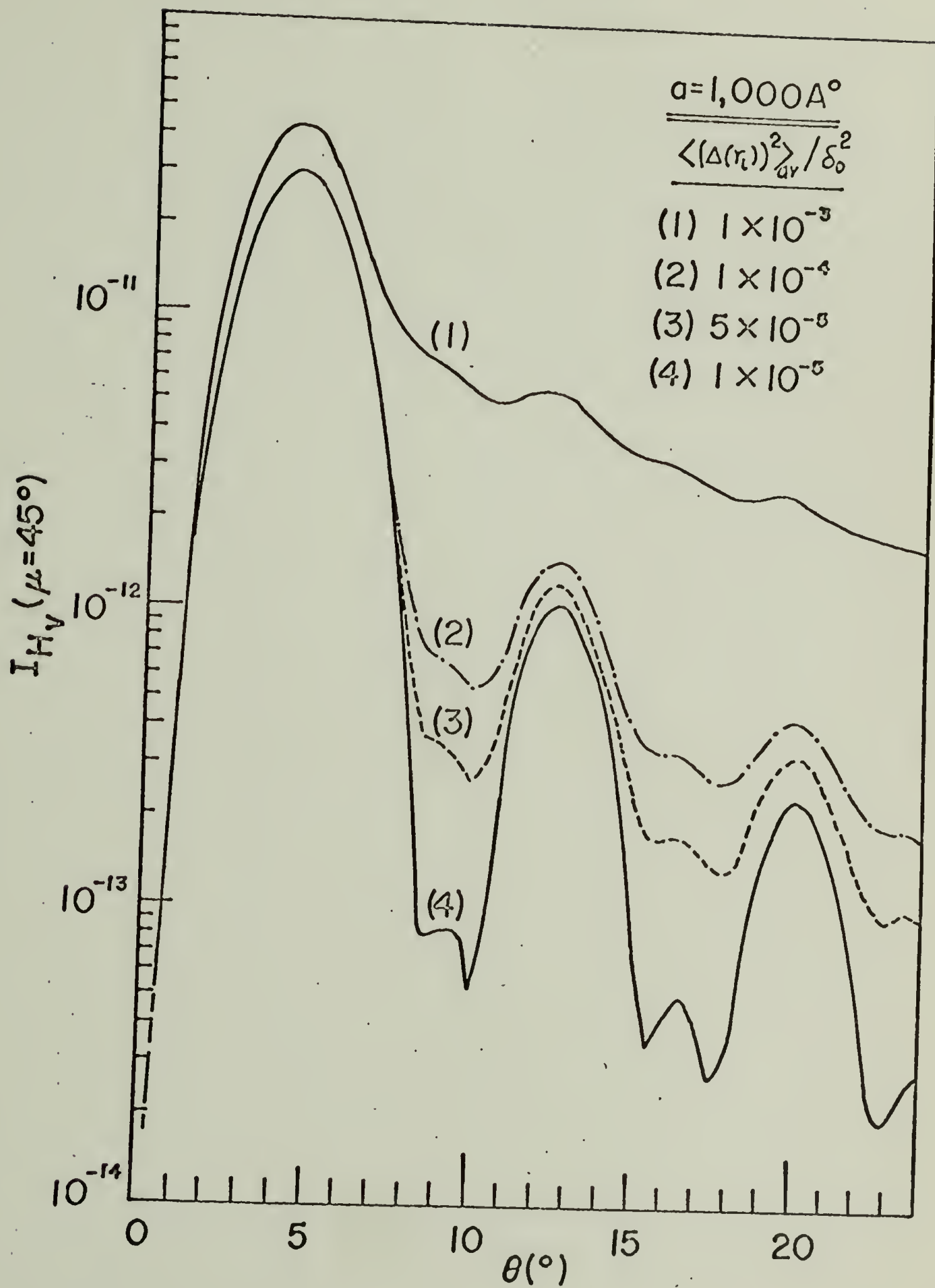


FIGURE II-4

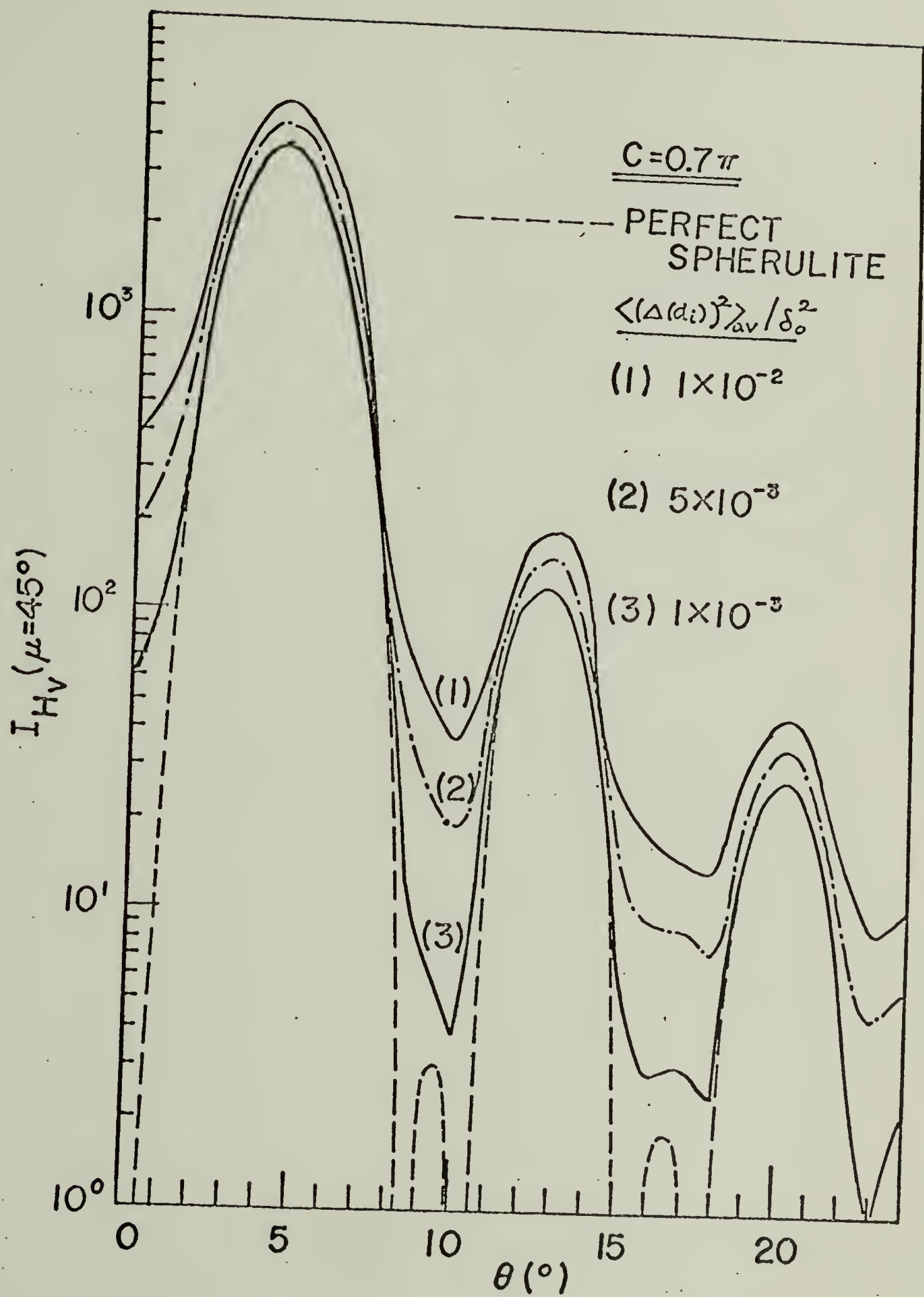


FIGURE II-5

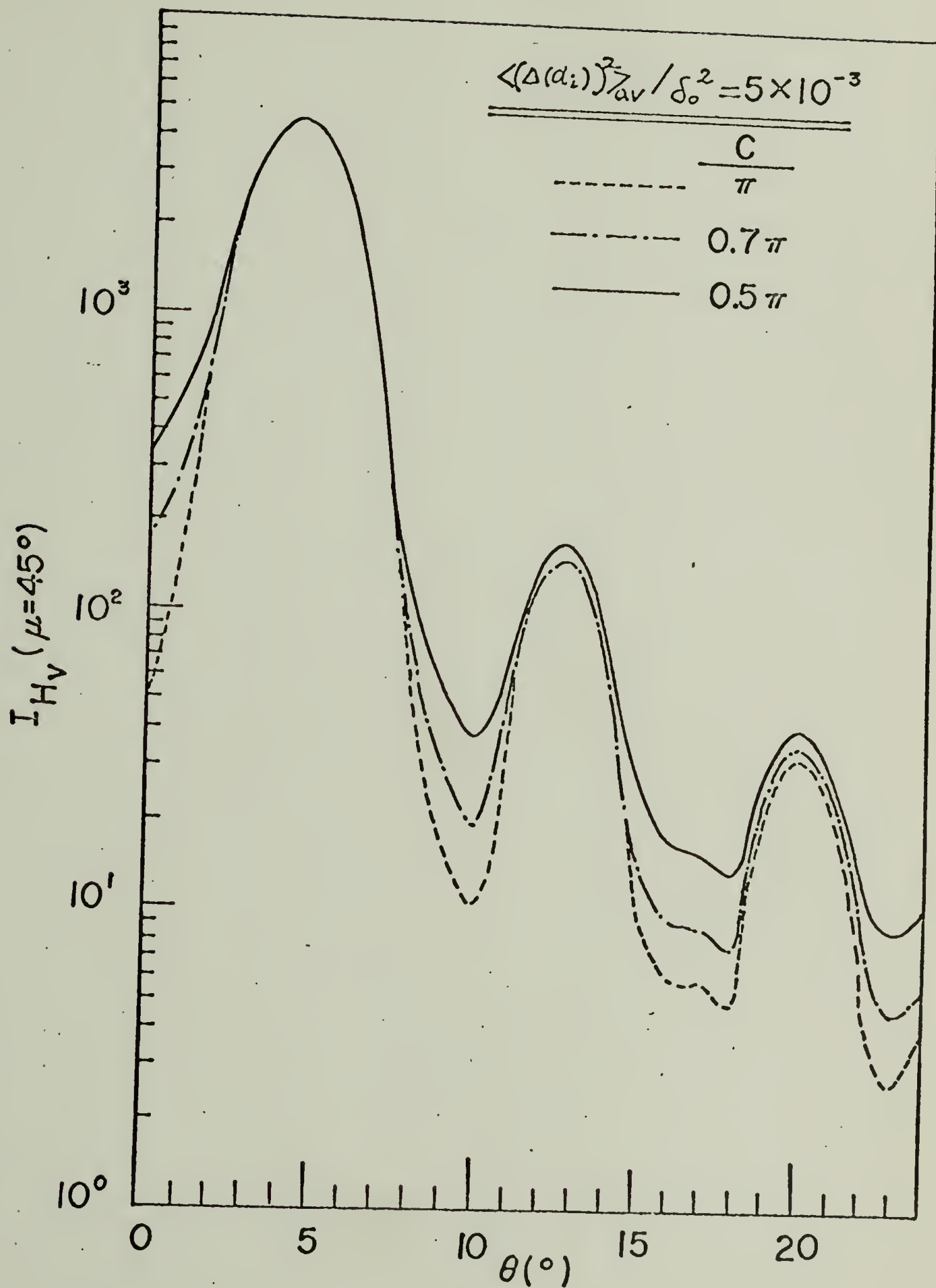


FIGURE II-6

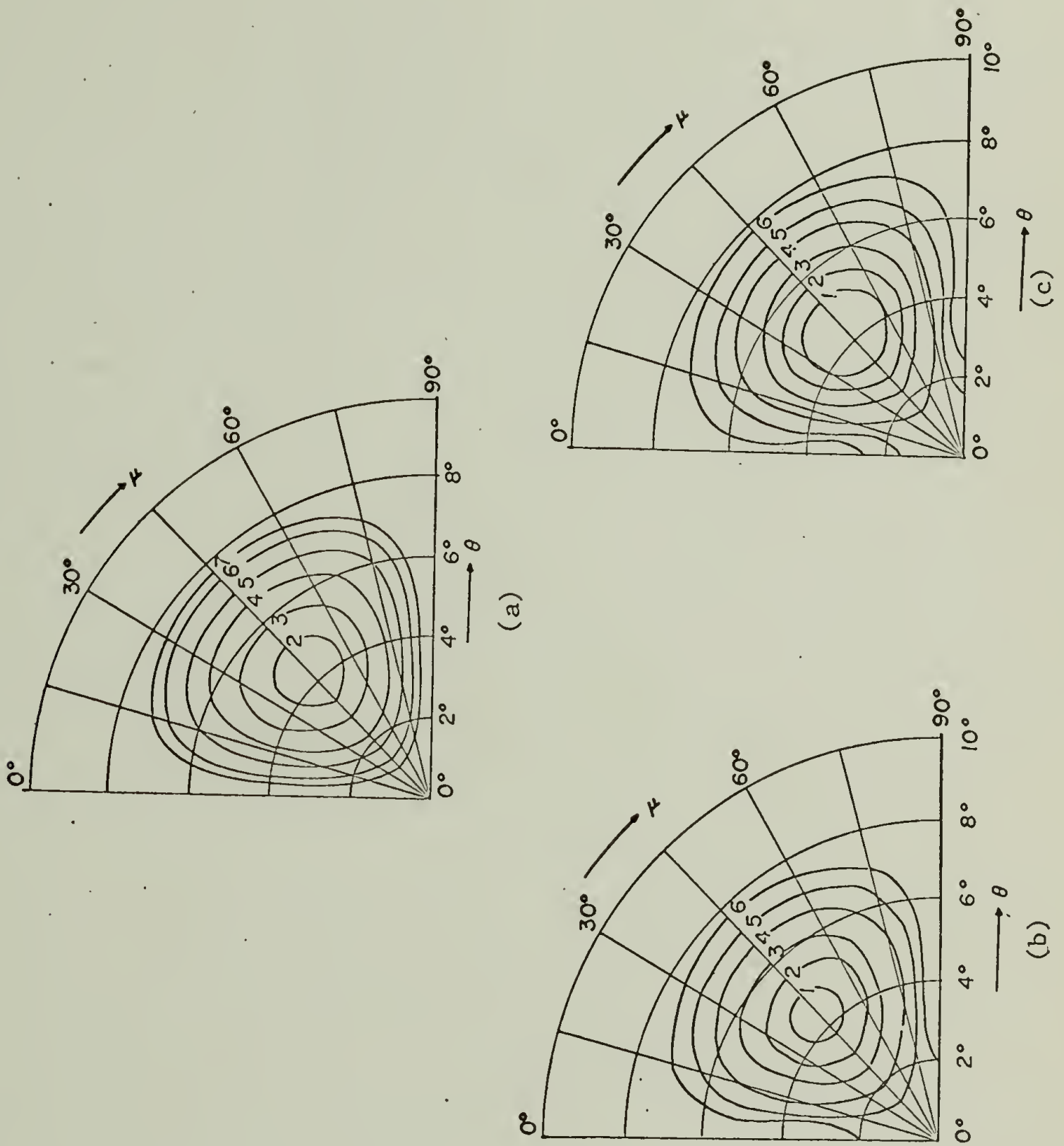
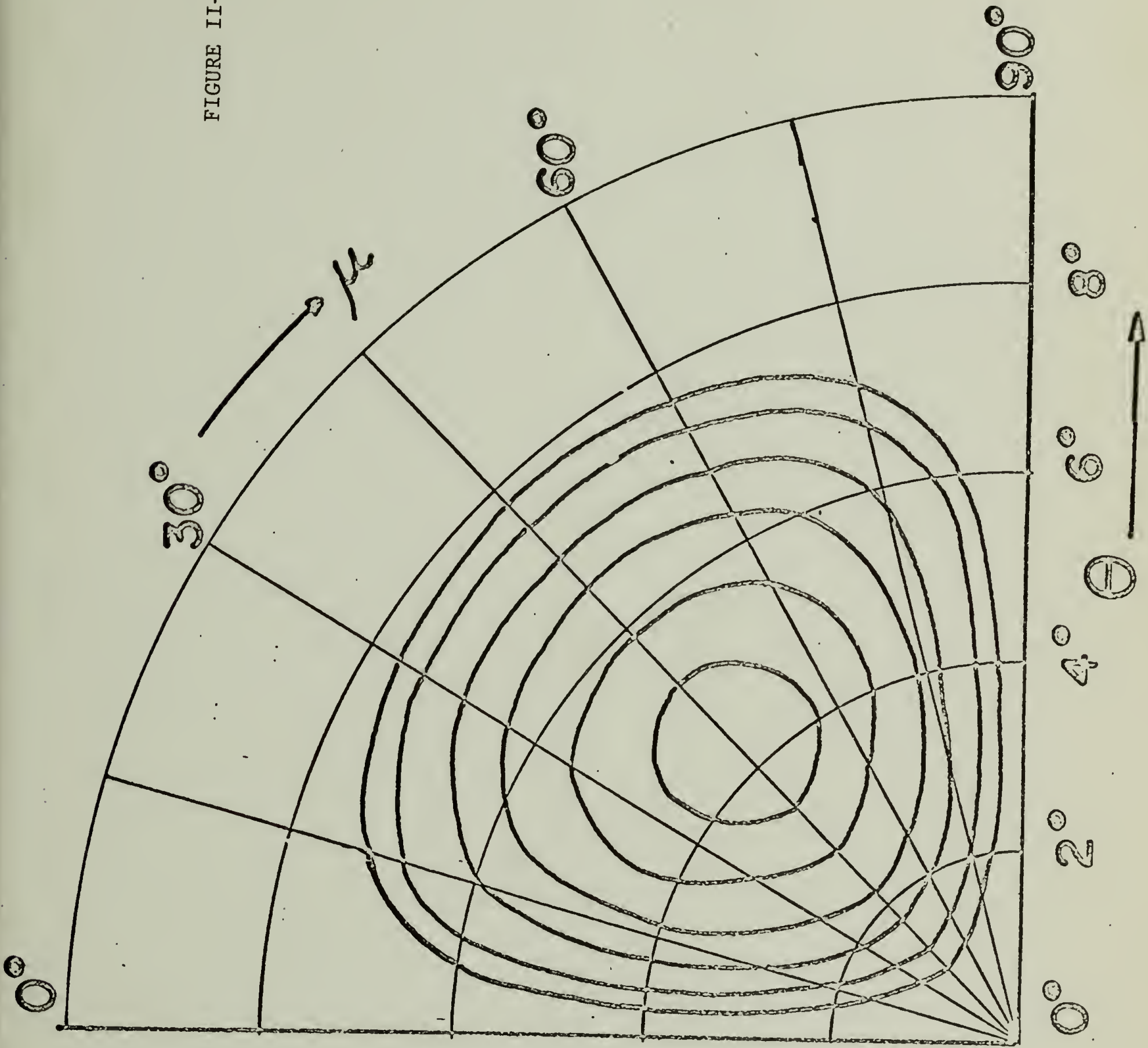


FIGURE II-7

FIGURE II-8



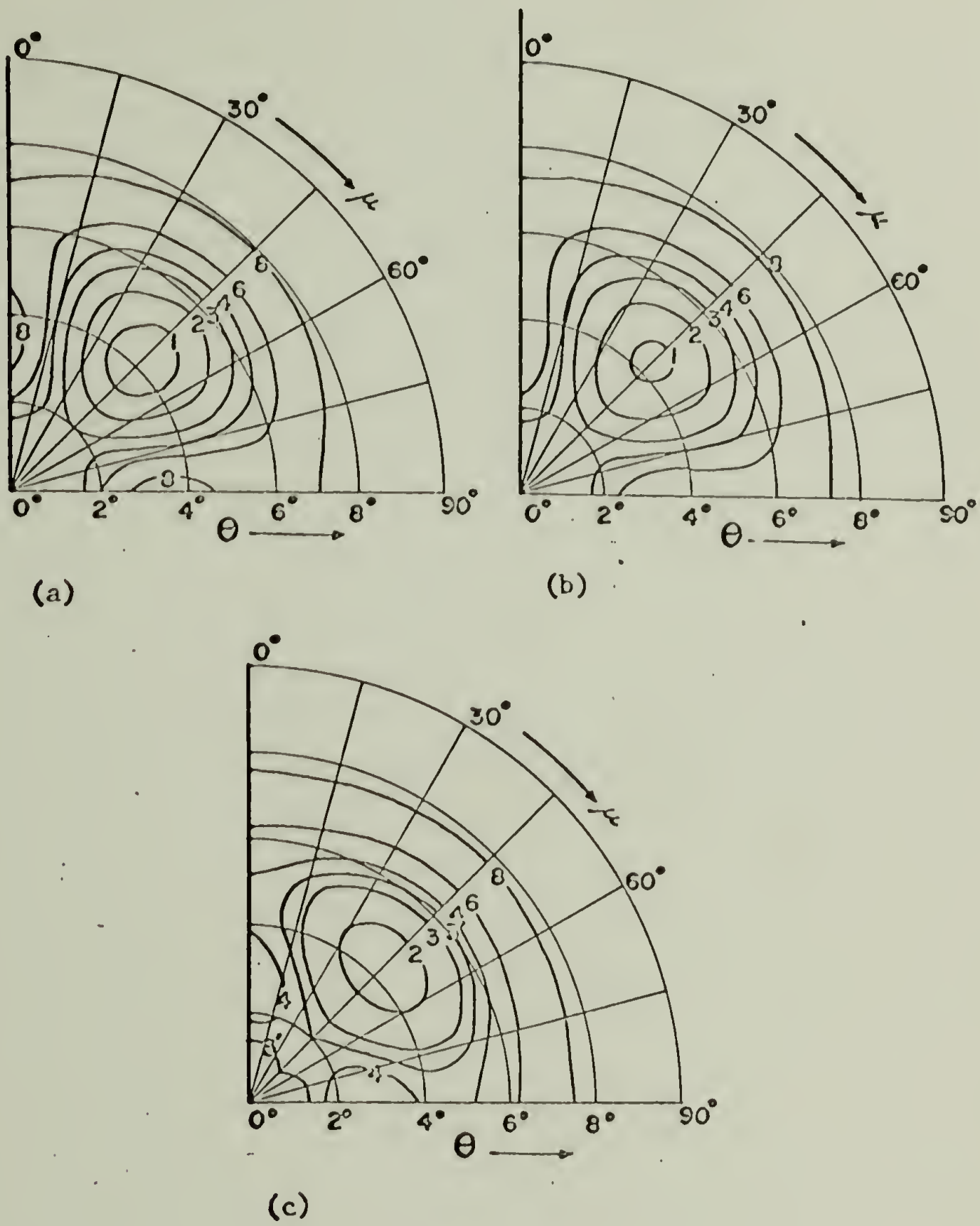


FIGURE II-9

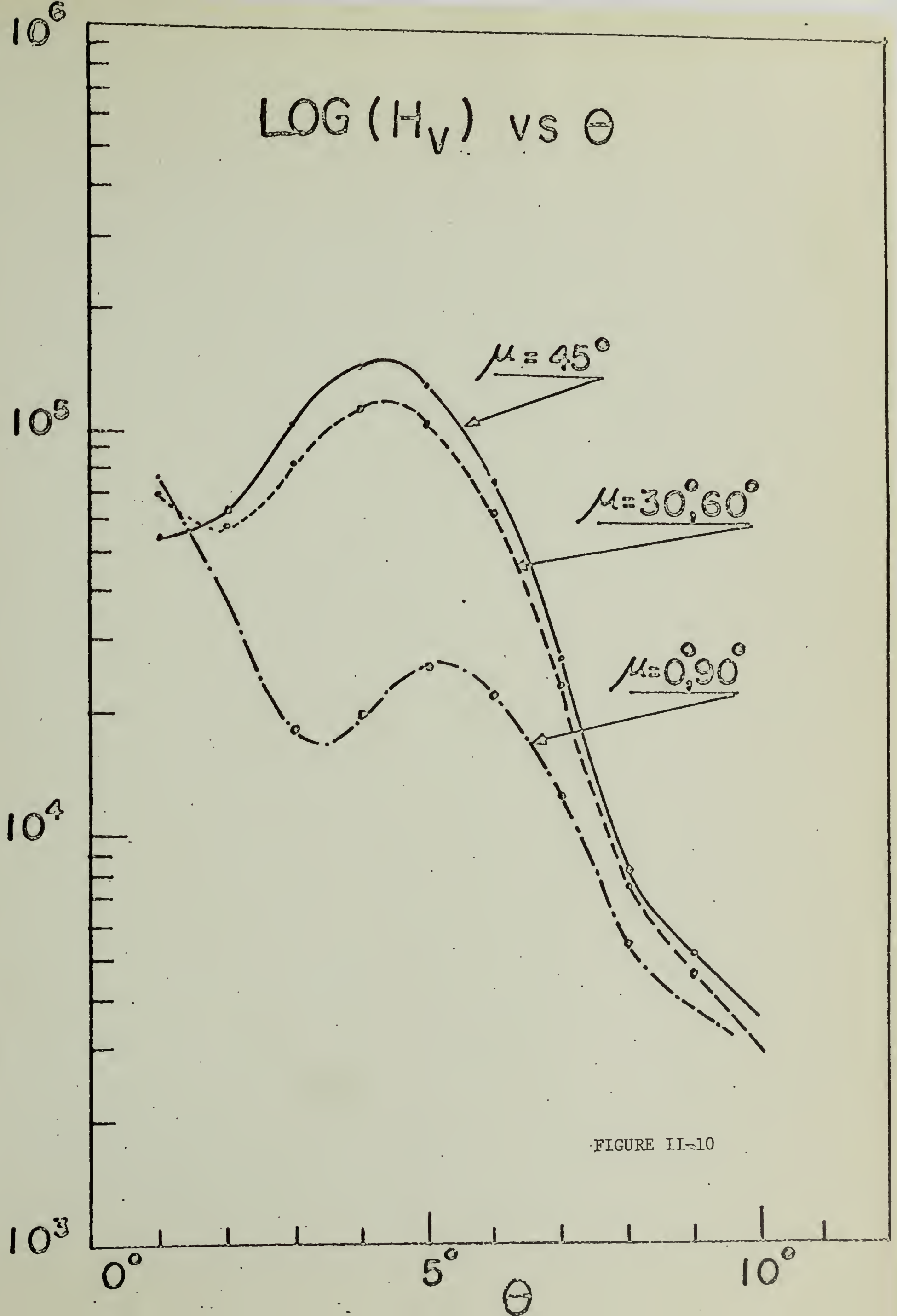


FIGURE II-10

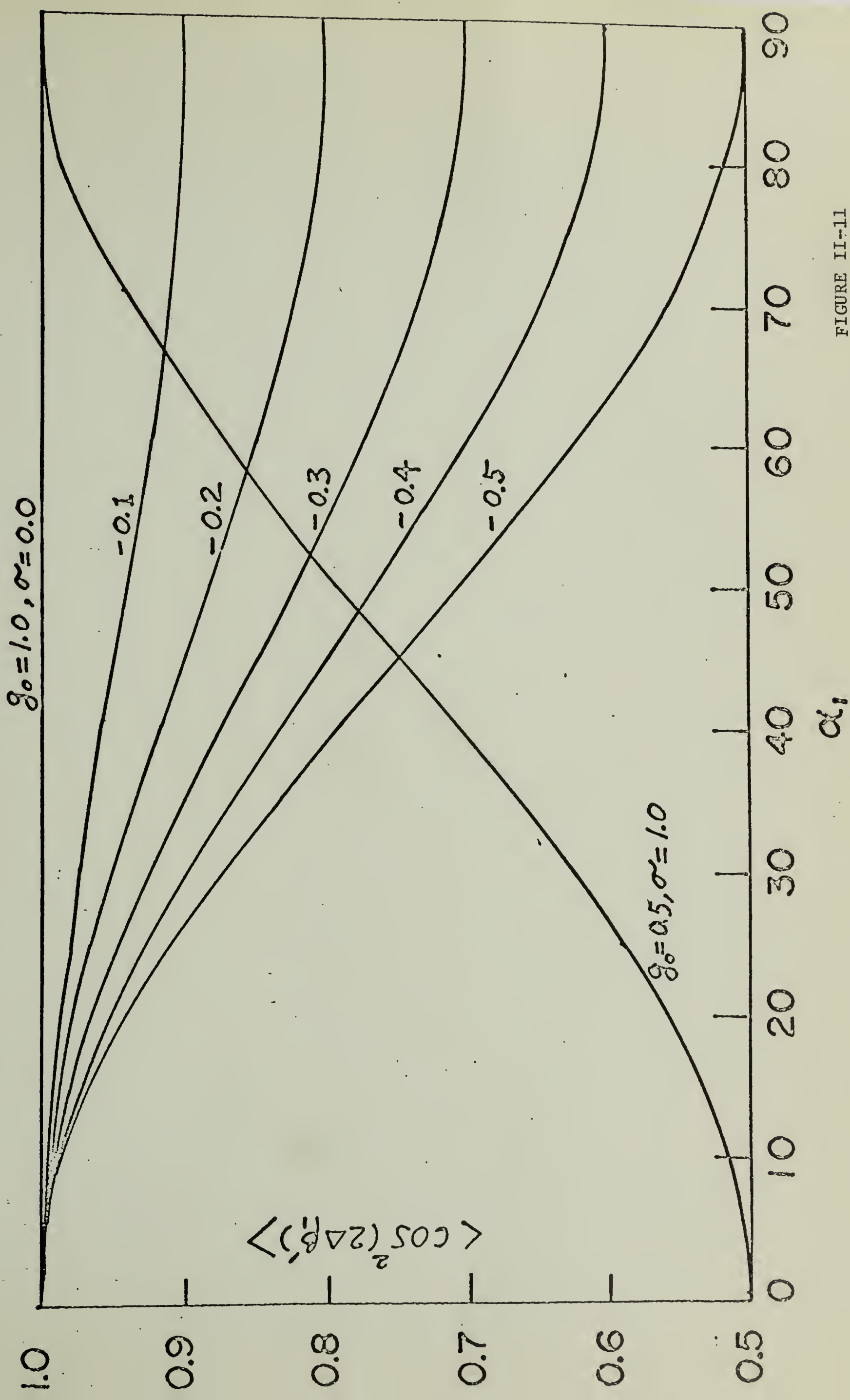
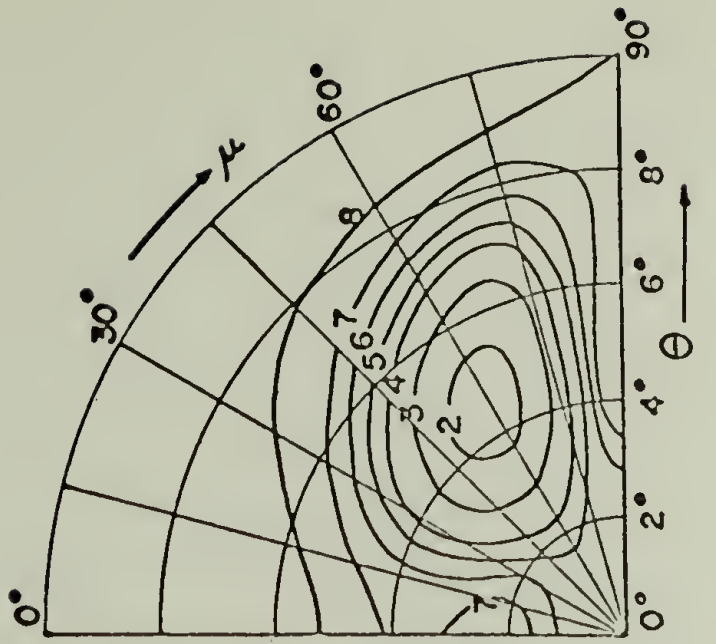
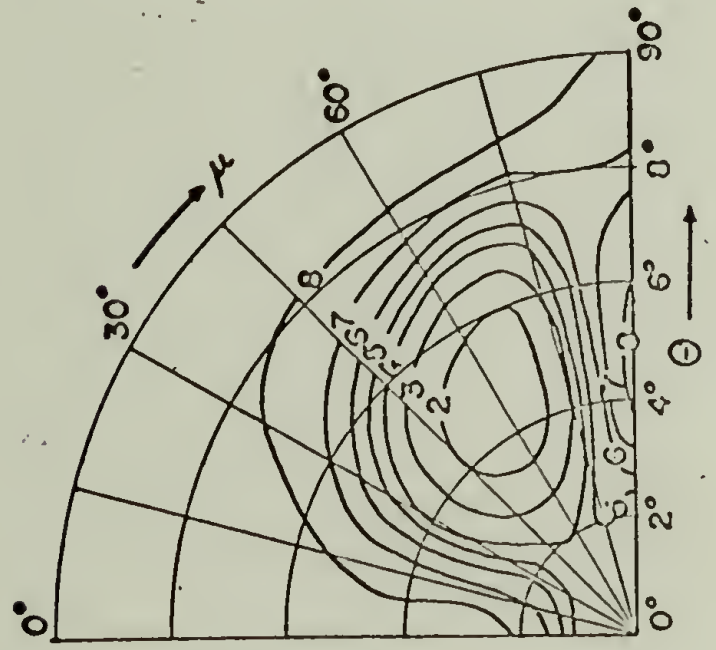
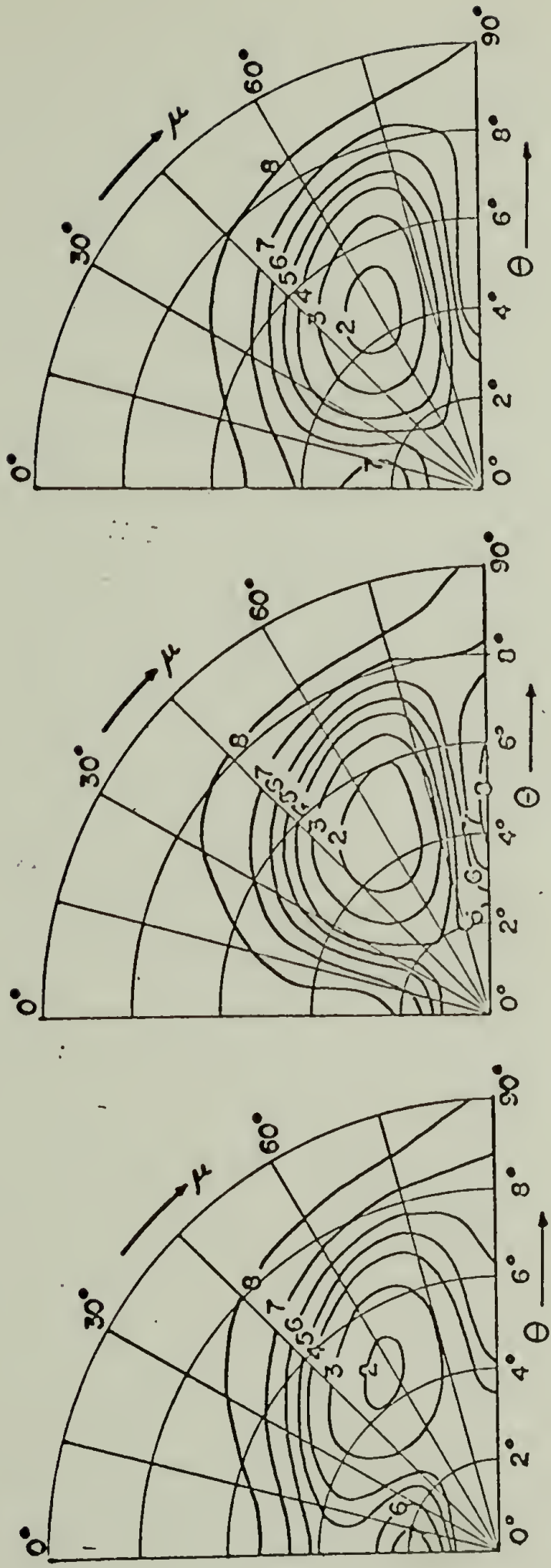
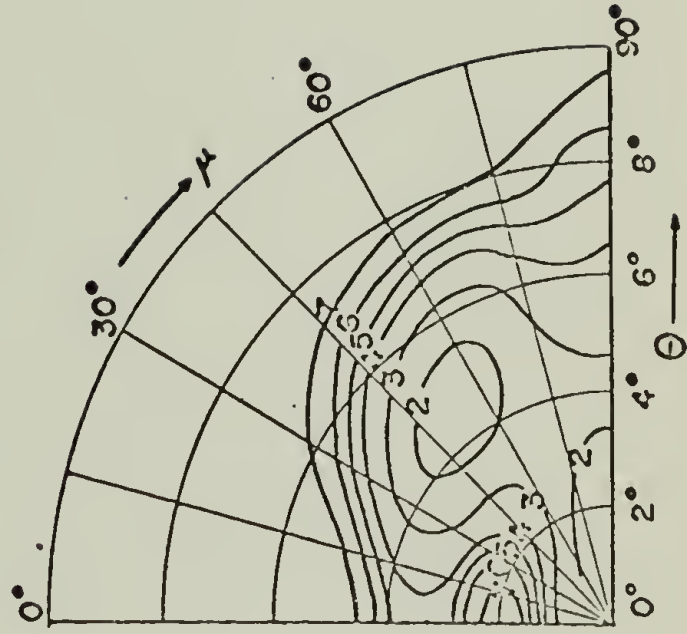
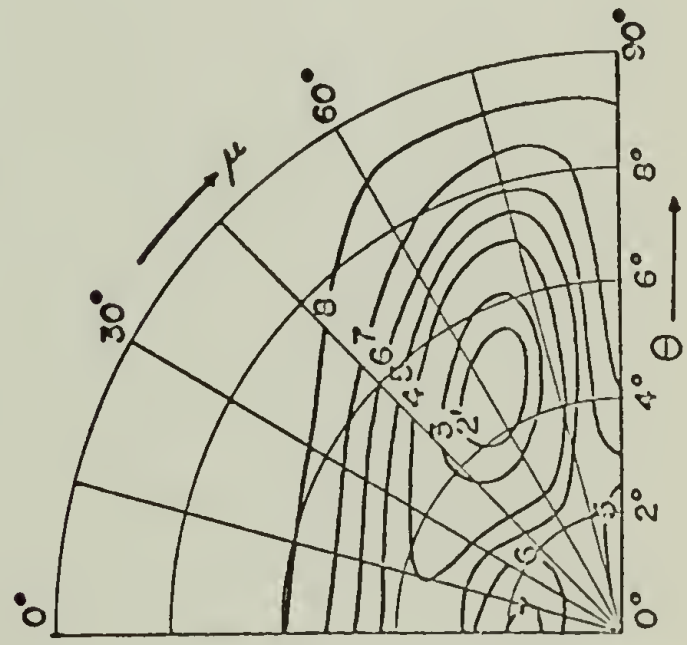


FIGURE II-11



(a)

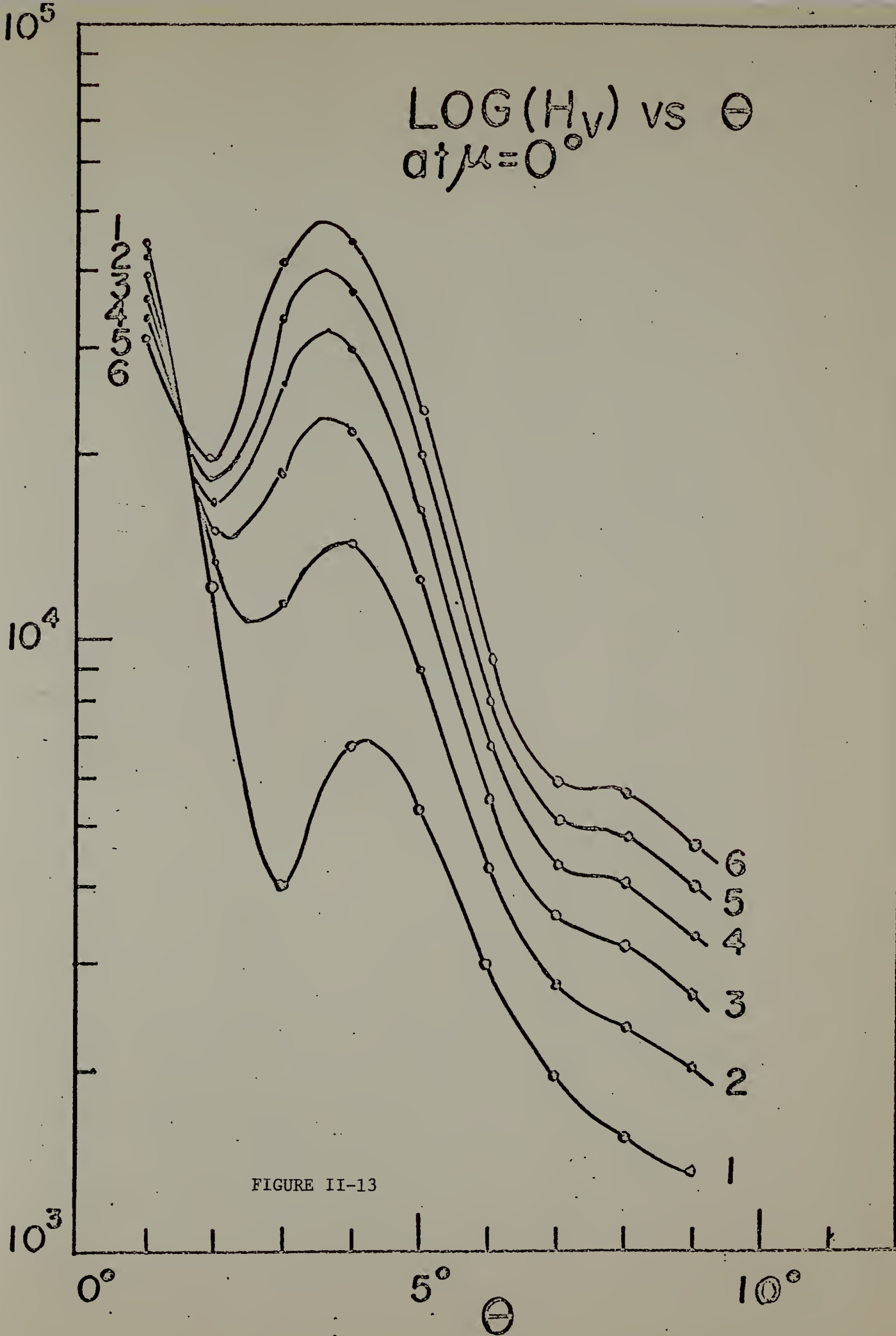
(c)

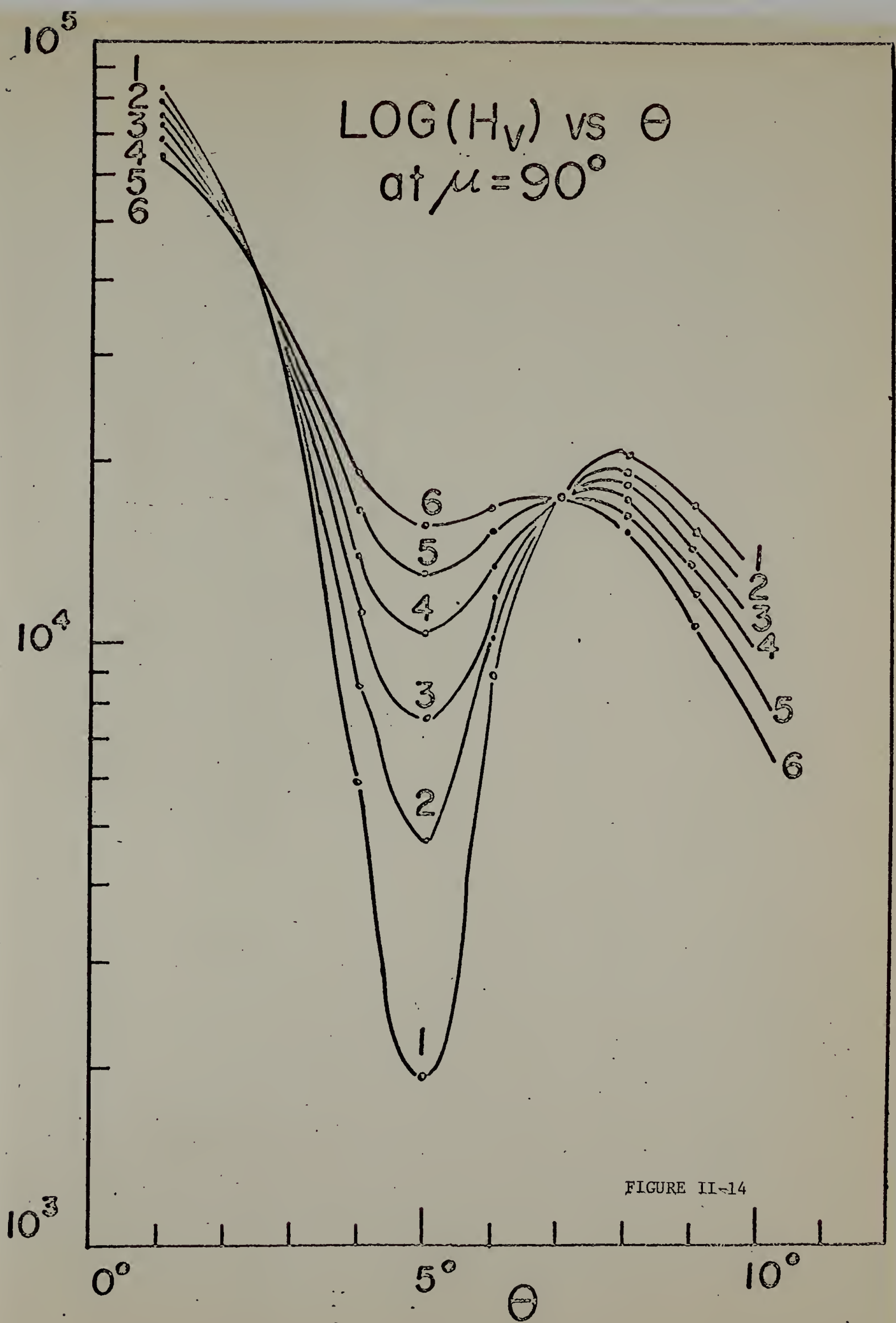


(d)

(e)

FIGURE II-12





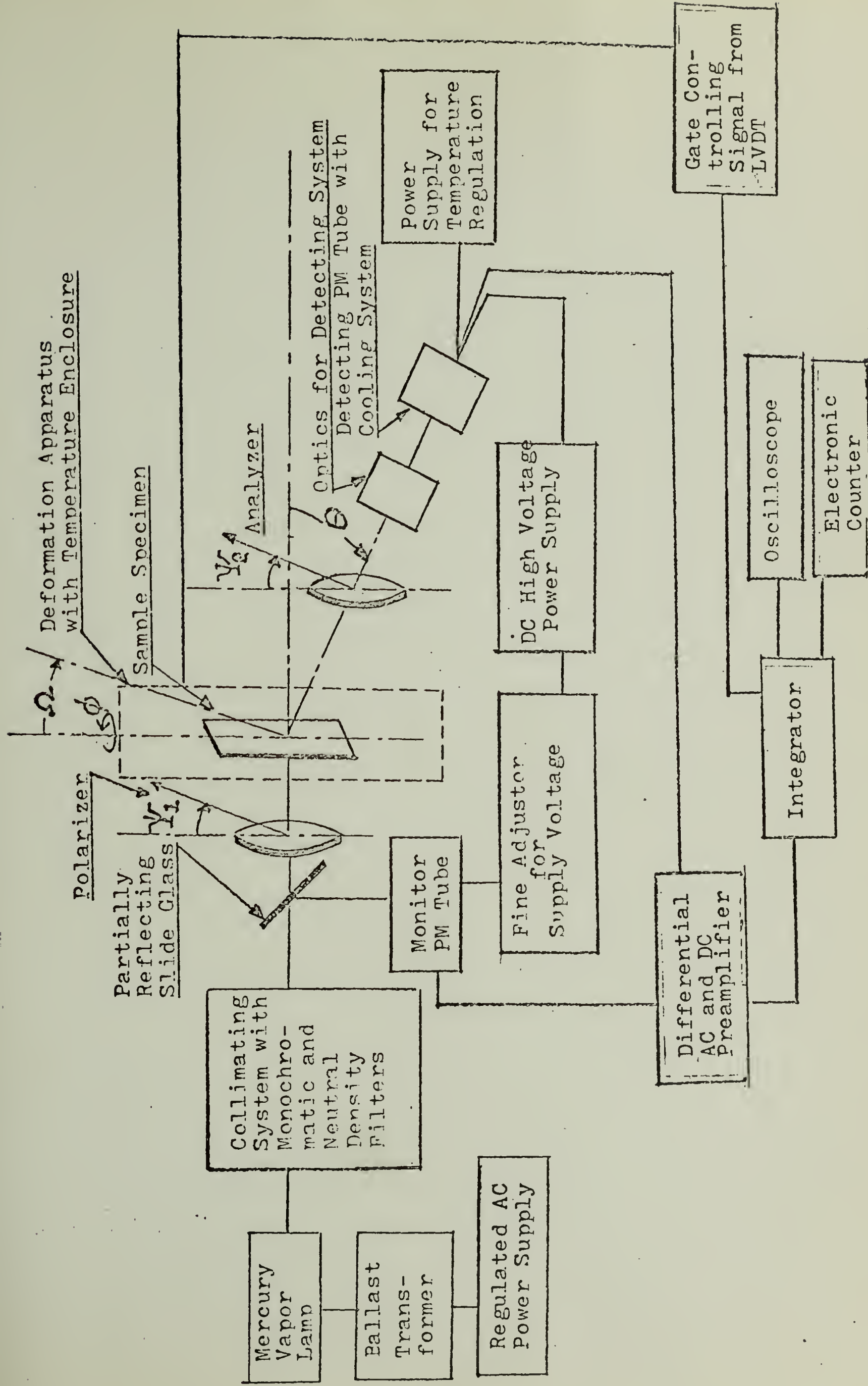
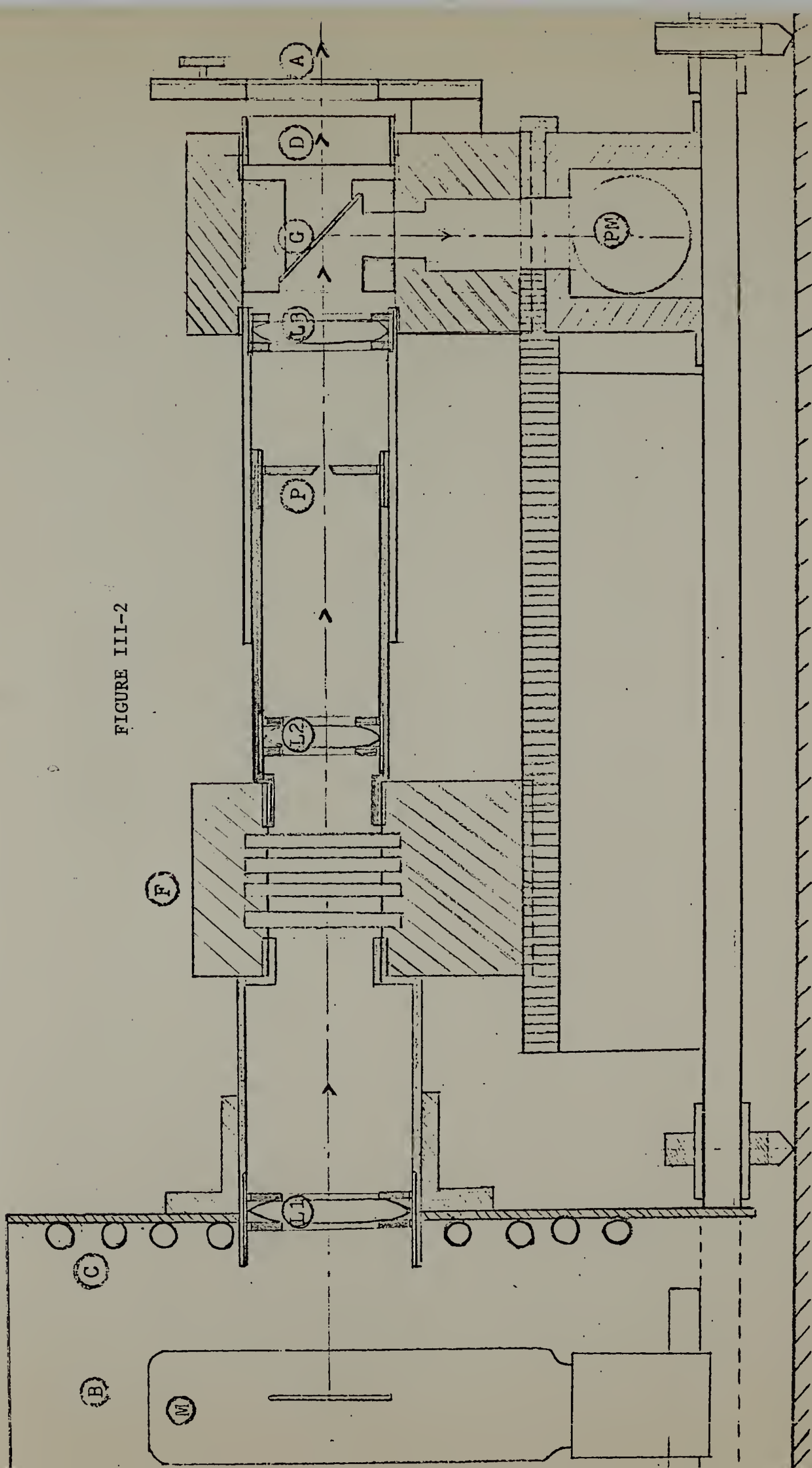


FIGURE III-1. A block diagram for the dynamic light scattering apparatus

FIGURE III-2



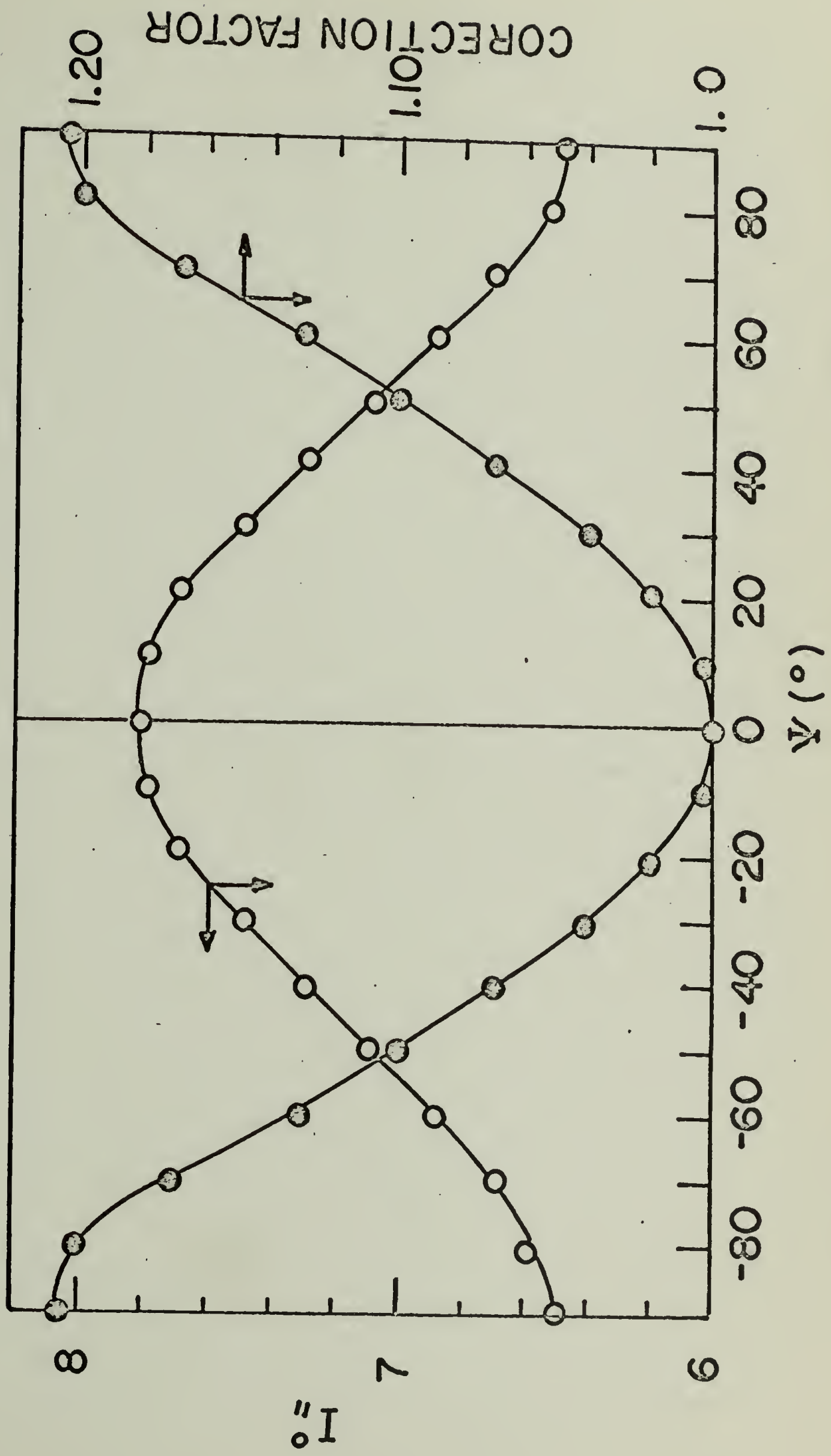


FIGURE III-3

FIGURE III-4(a)

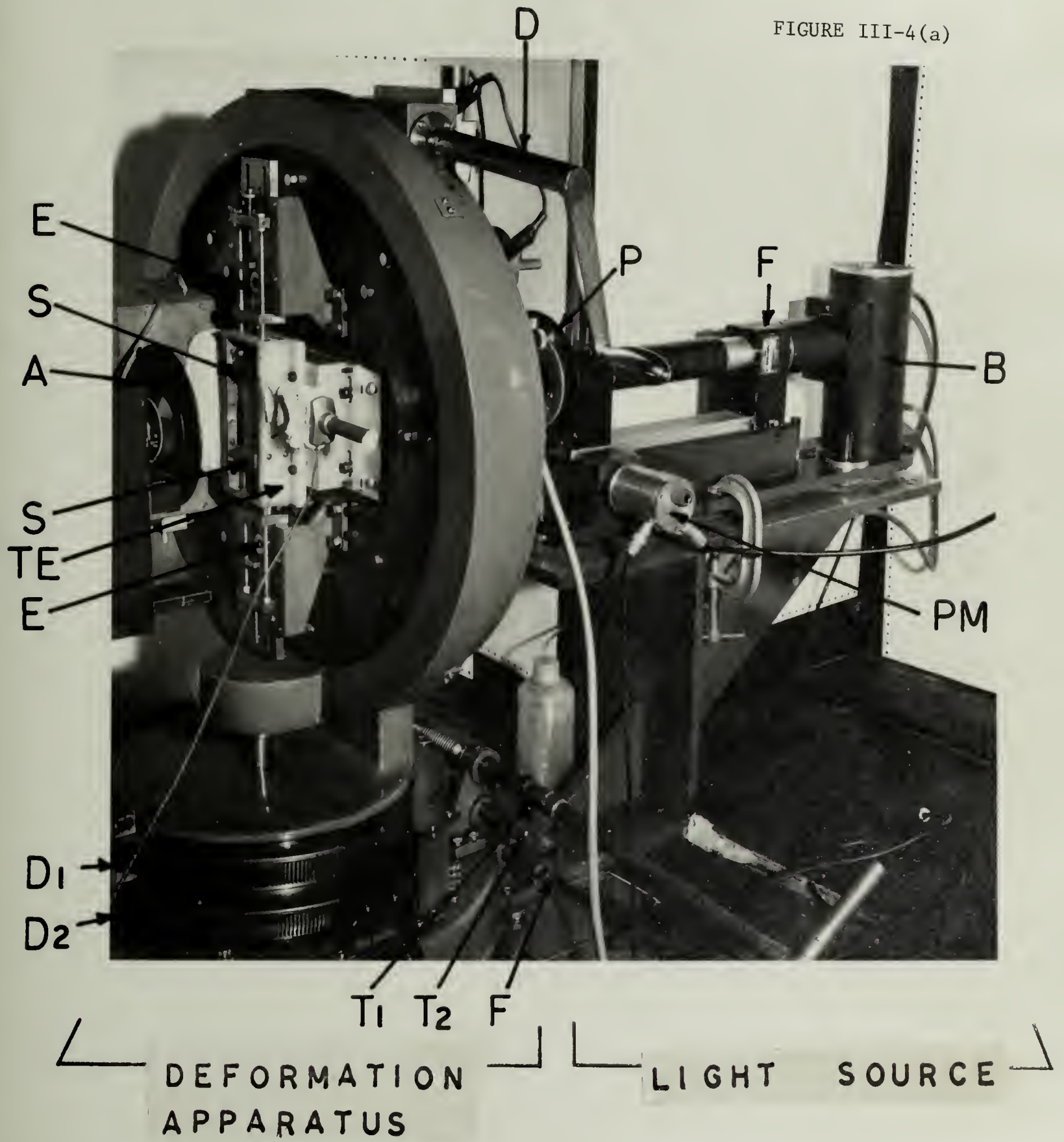
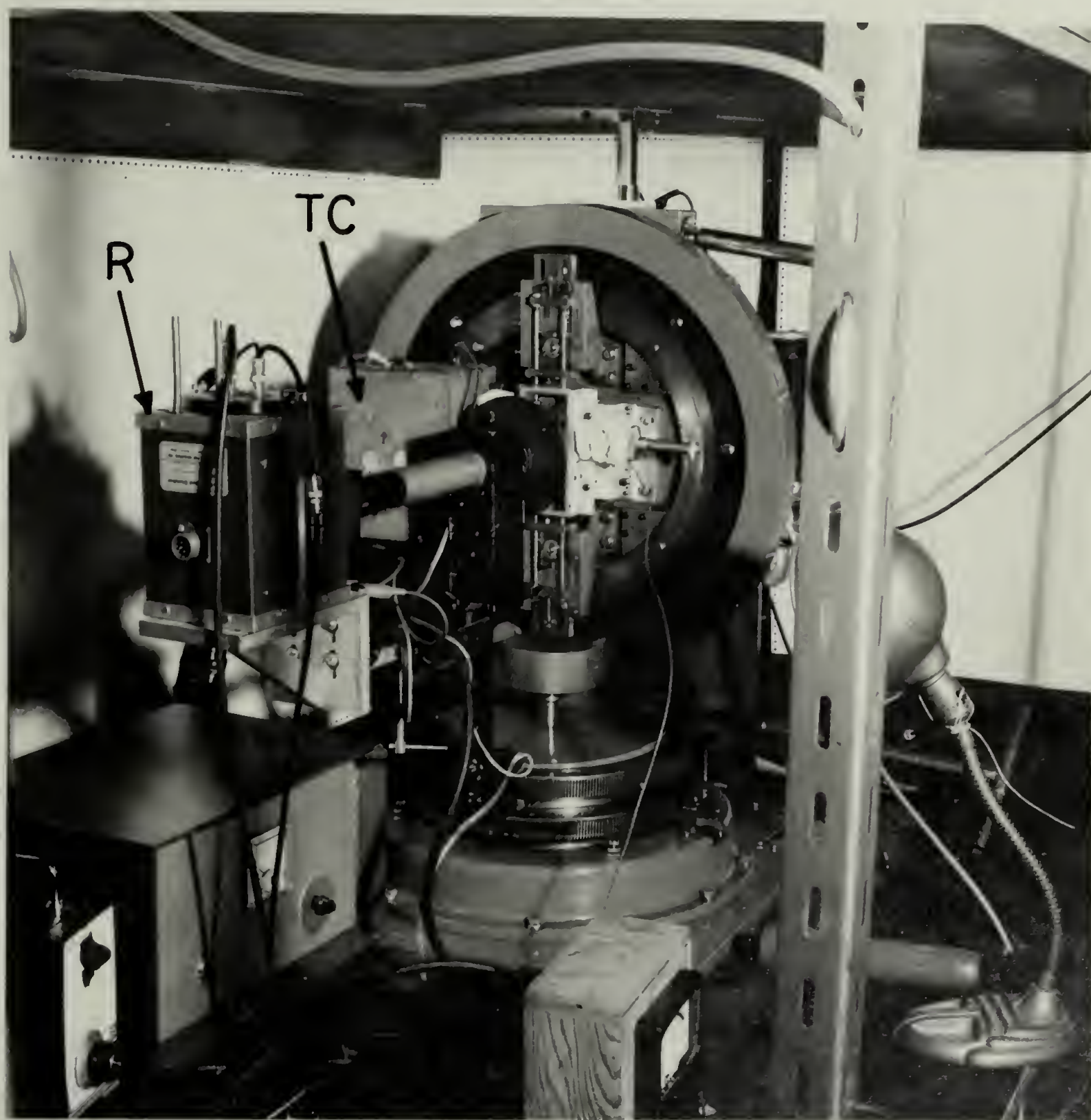
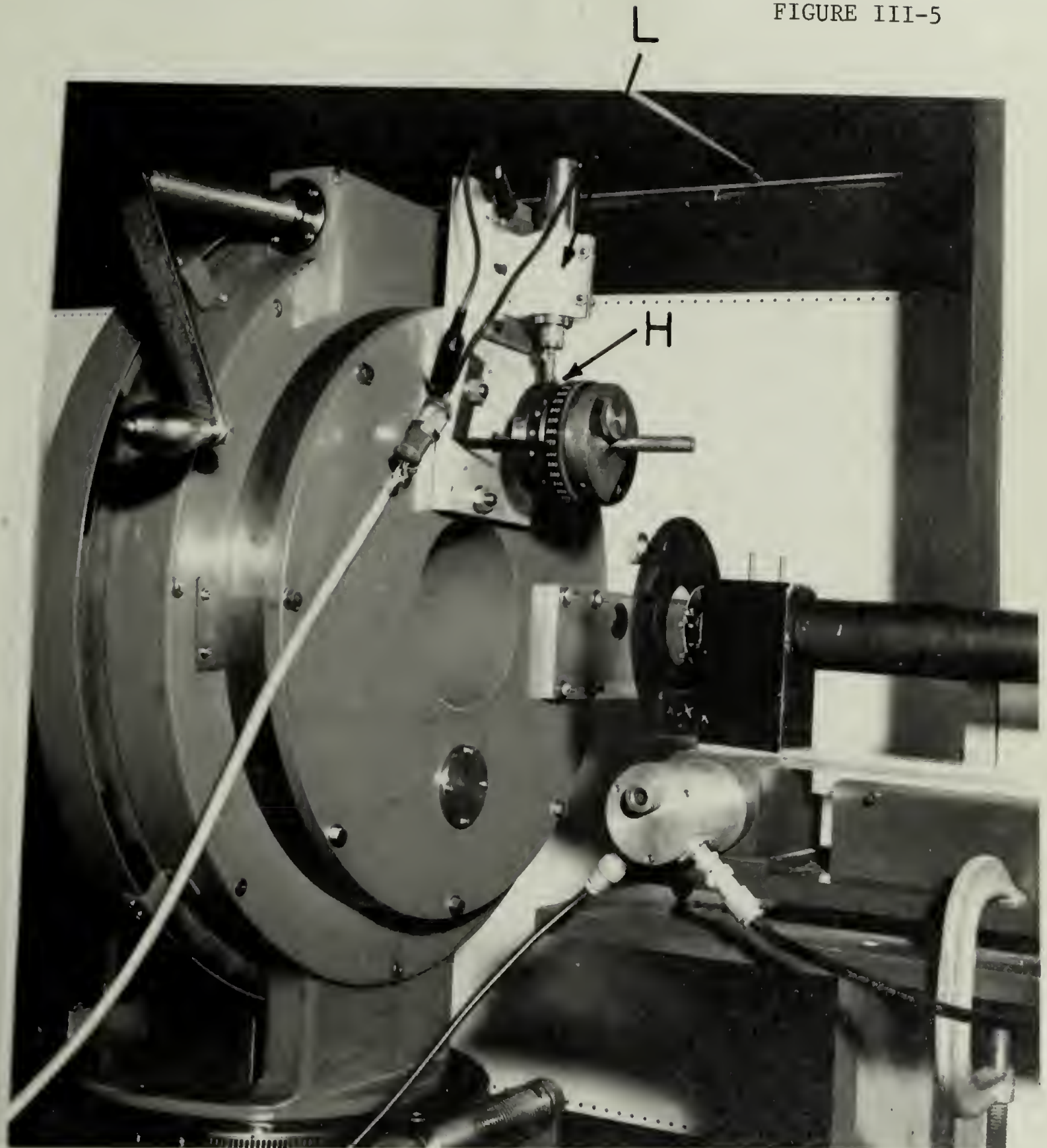


FIGURE III-4(b)



— DETECTOR SYSTEM —

FIGURE III-5



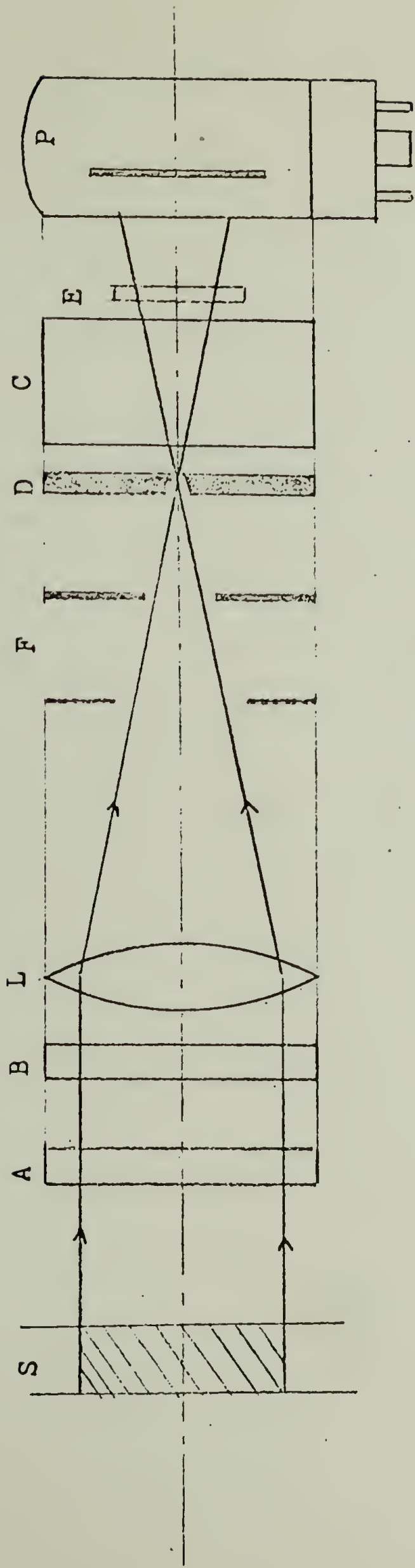


FIGURE III-6(a)

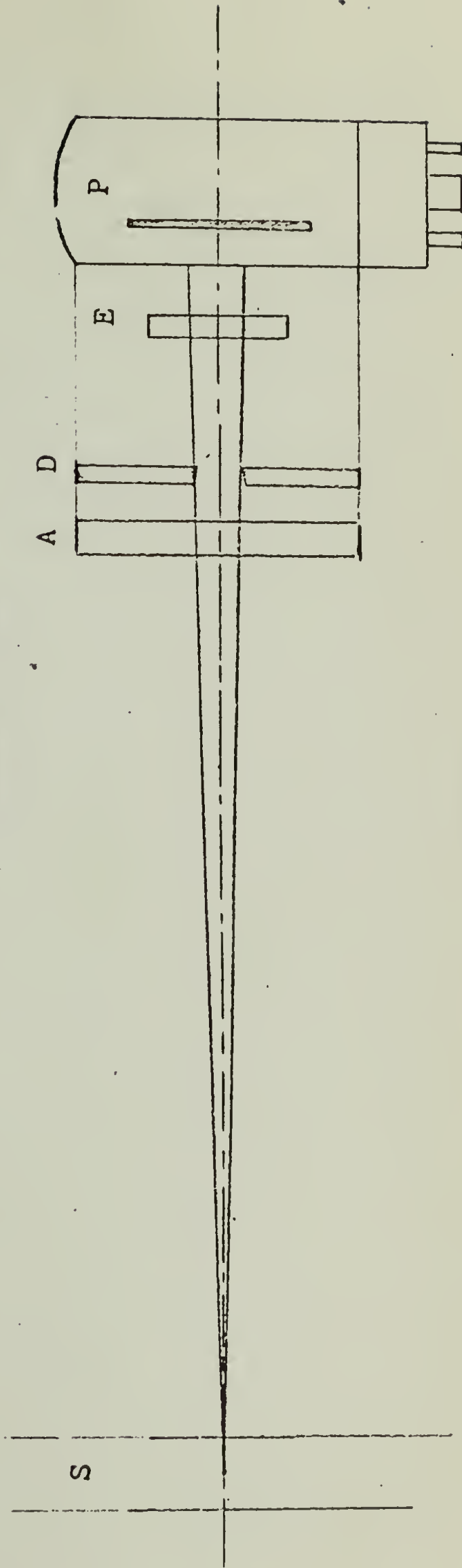


FIGURE III-6(b)

DC High Voltage

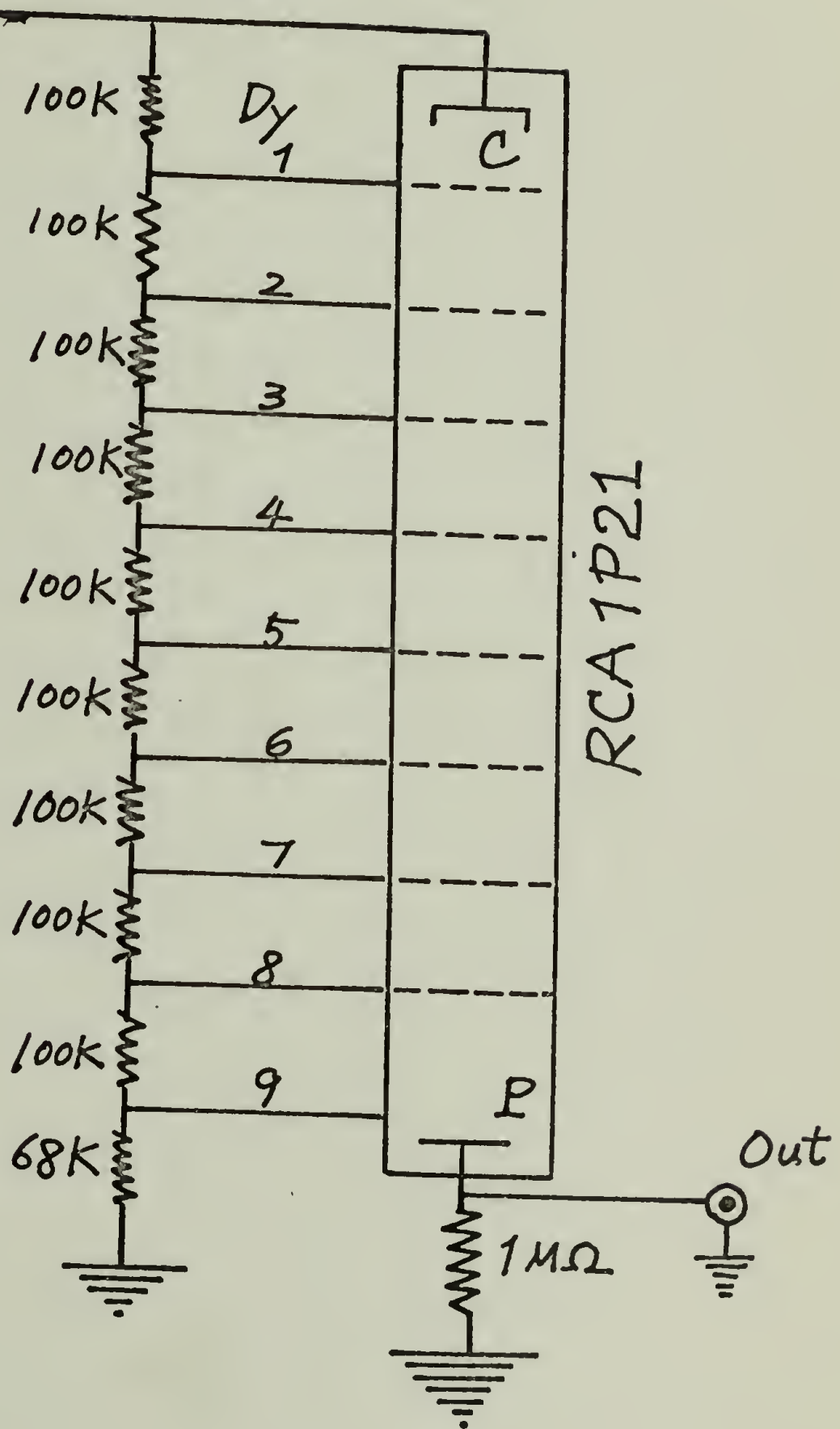


FIGURE III-7

SWITCH DETAIL

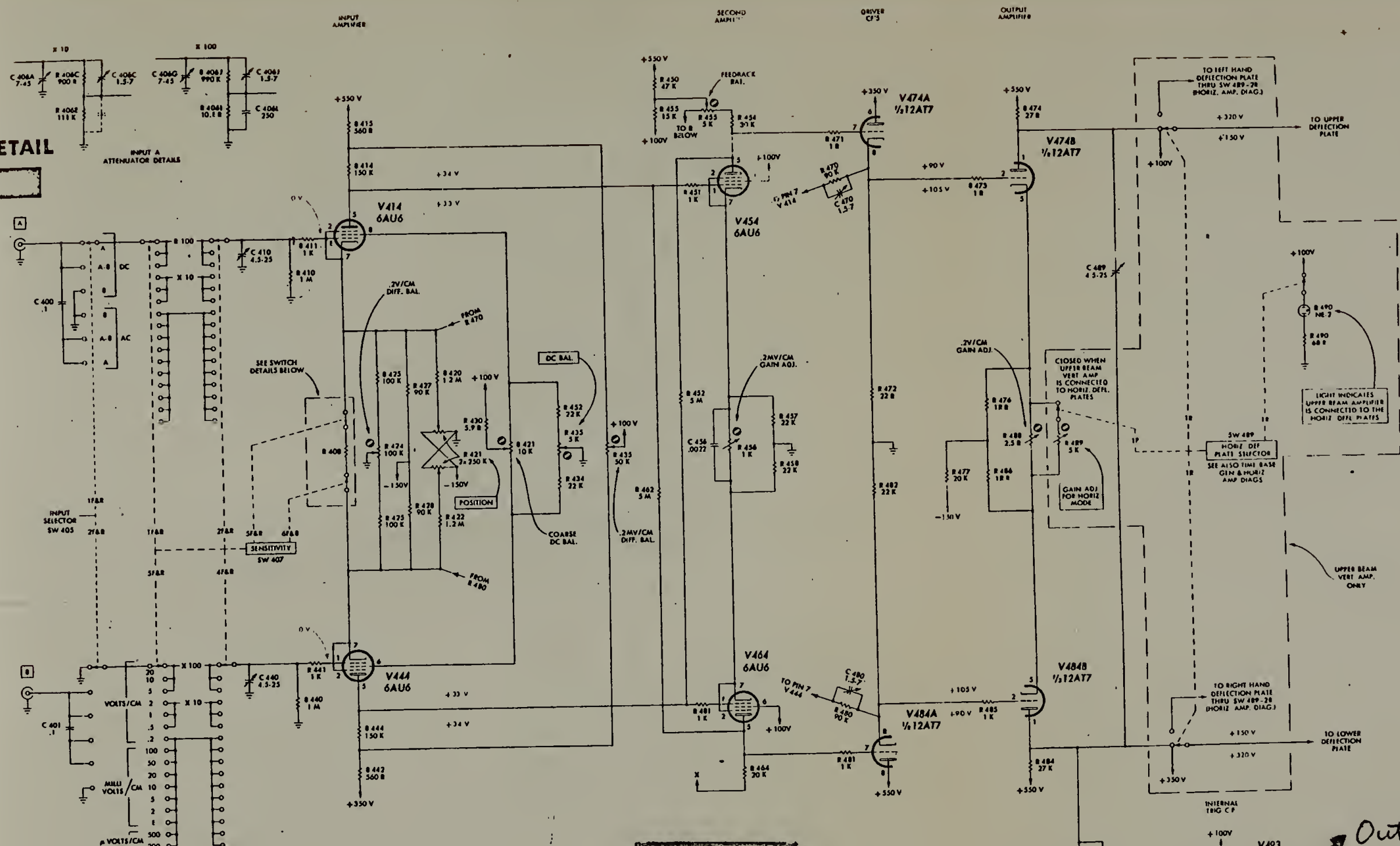
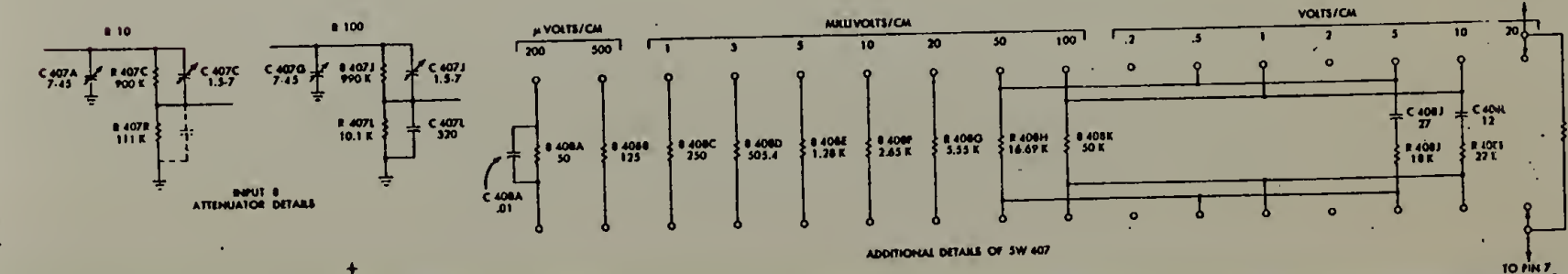
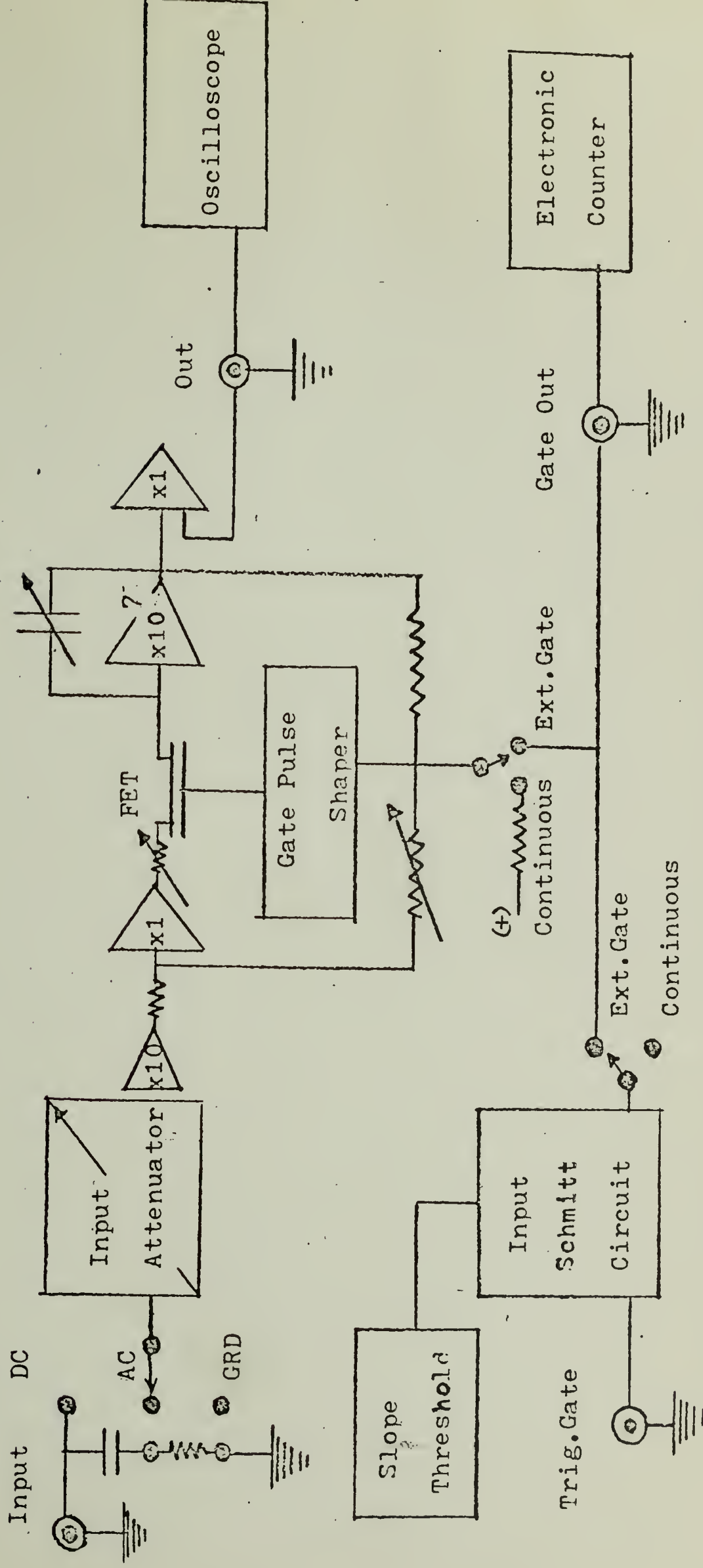


FIGURE III-8



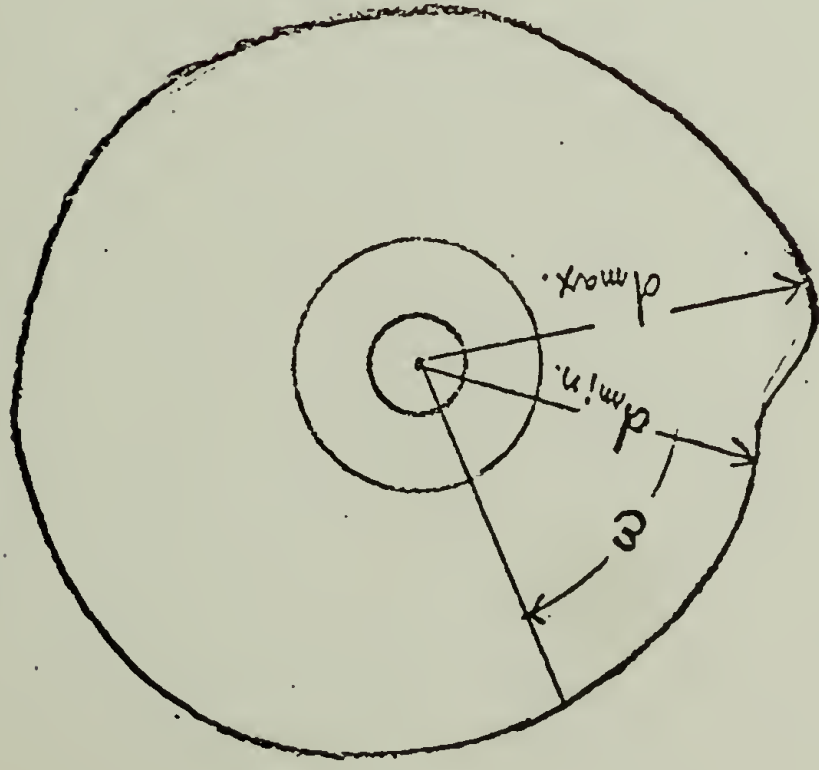
UPPER BEAM & LOWER BEAM VERTICAL AMPLIFIERS

FIGURE III-9

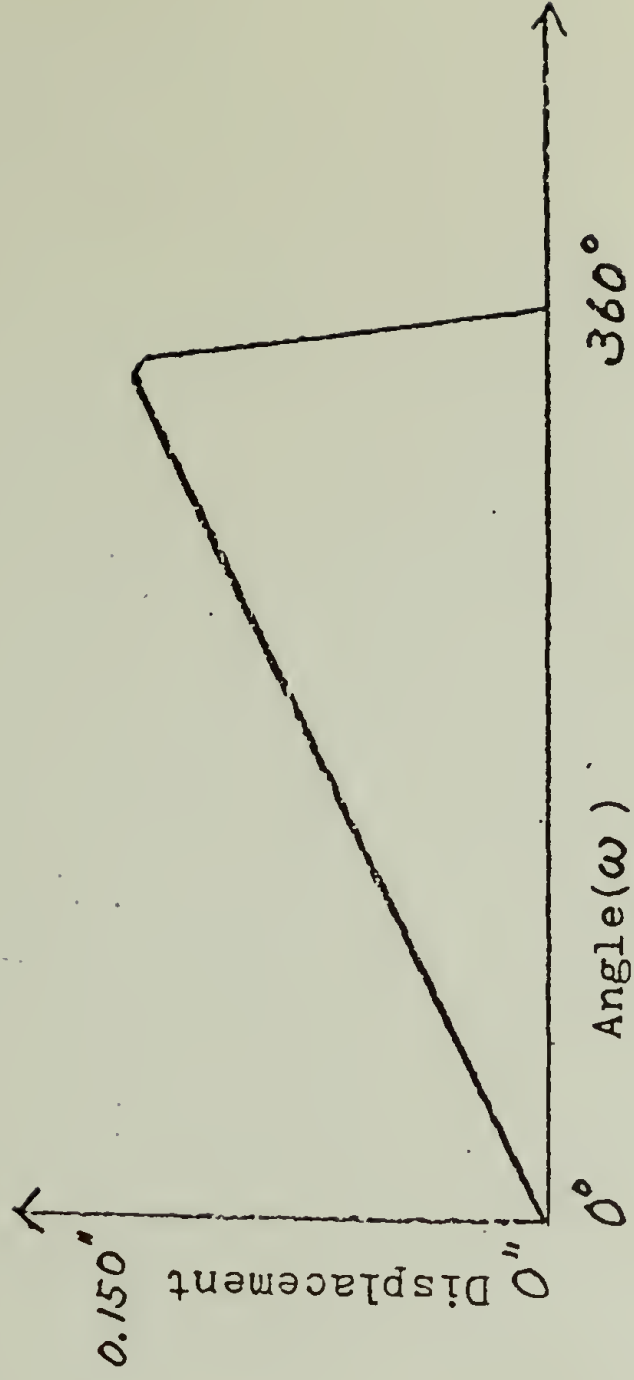


A block diagram of a part of the integrator (CW-1 BOX CAR) which has been used in this study.

Helical Cam



$$d_{min.} = 1.35", d_{max.} = 1.50"$$



Helical cam and its linear displacement

FIGURE III-10

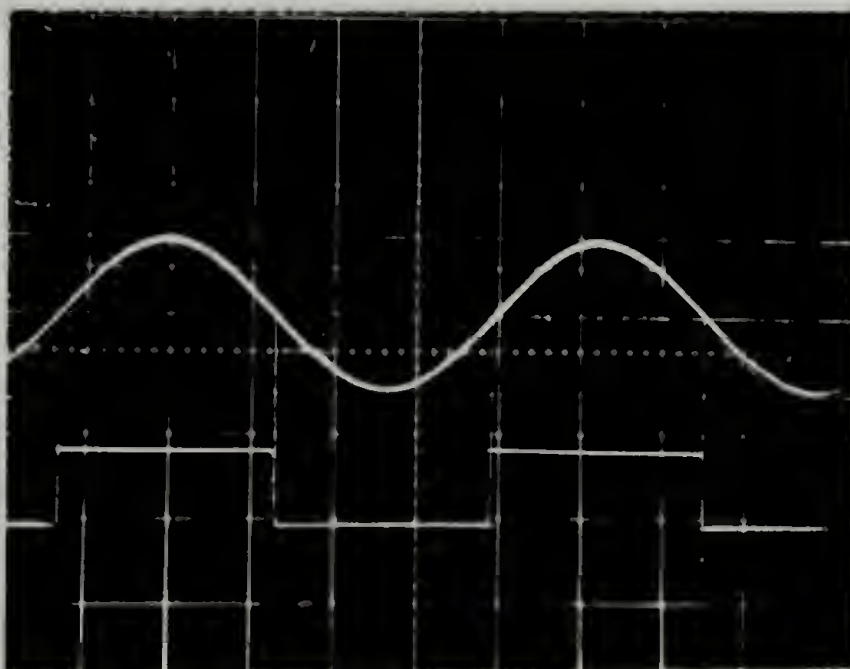
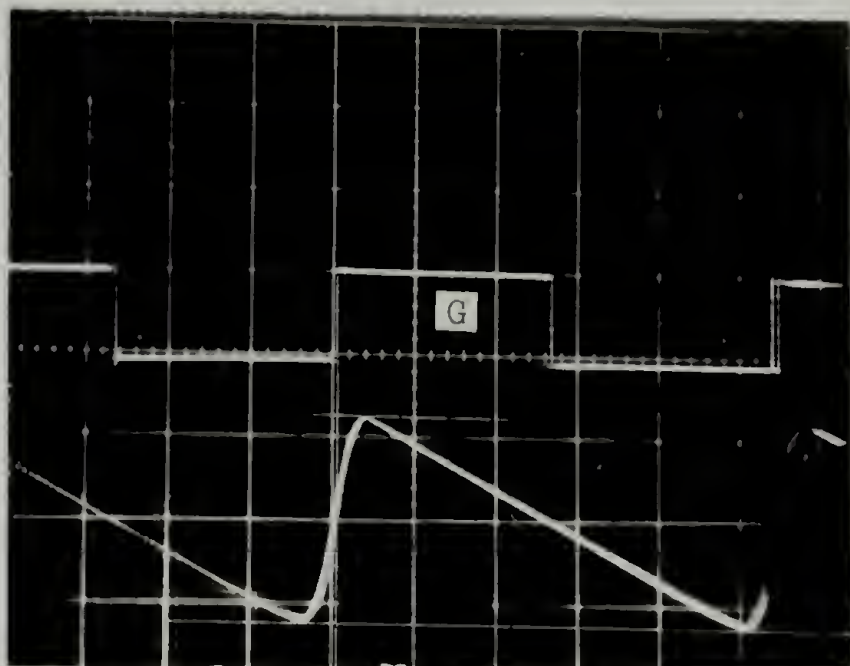
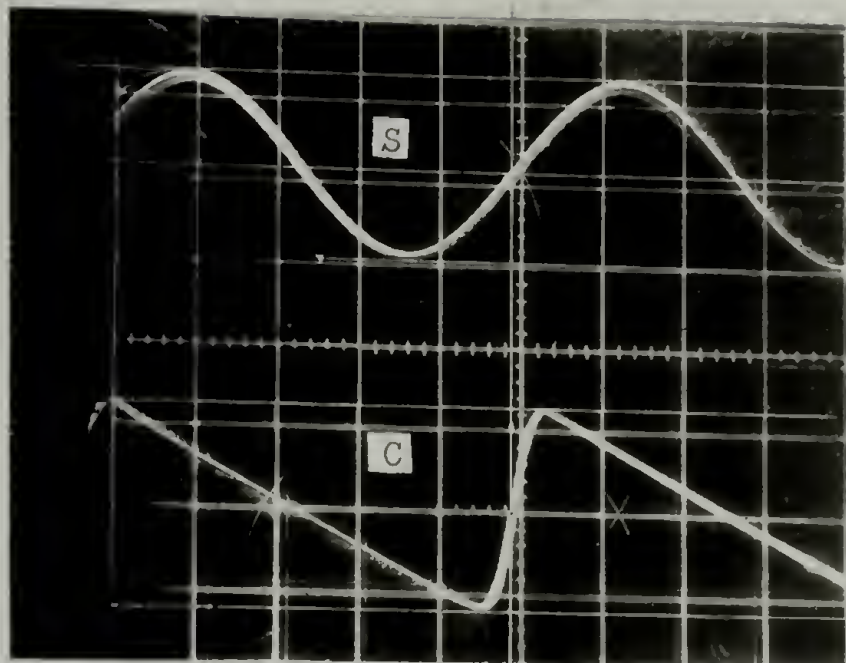


FIGURE III-11

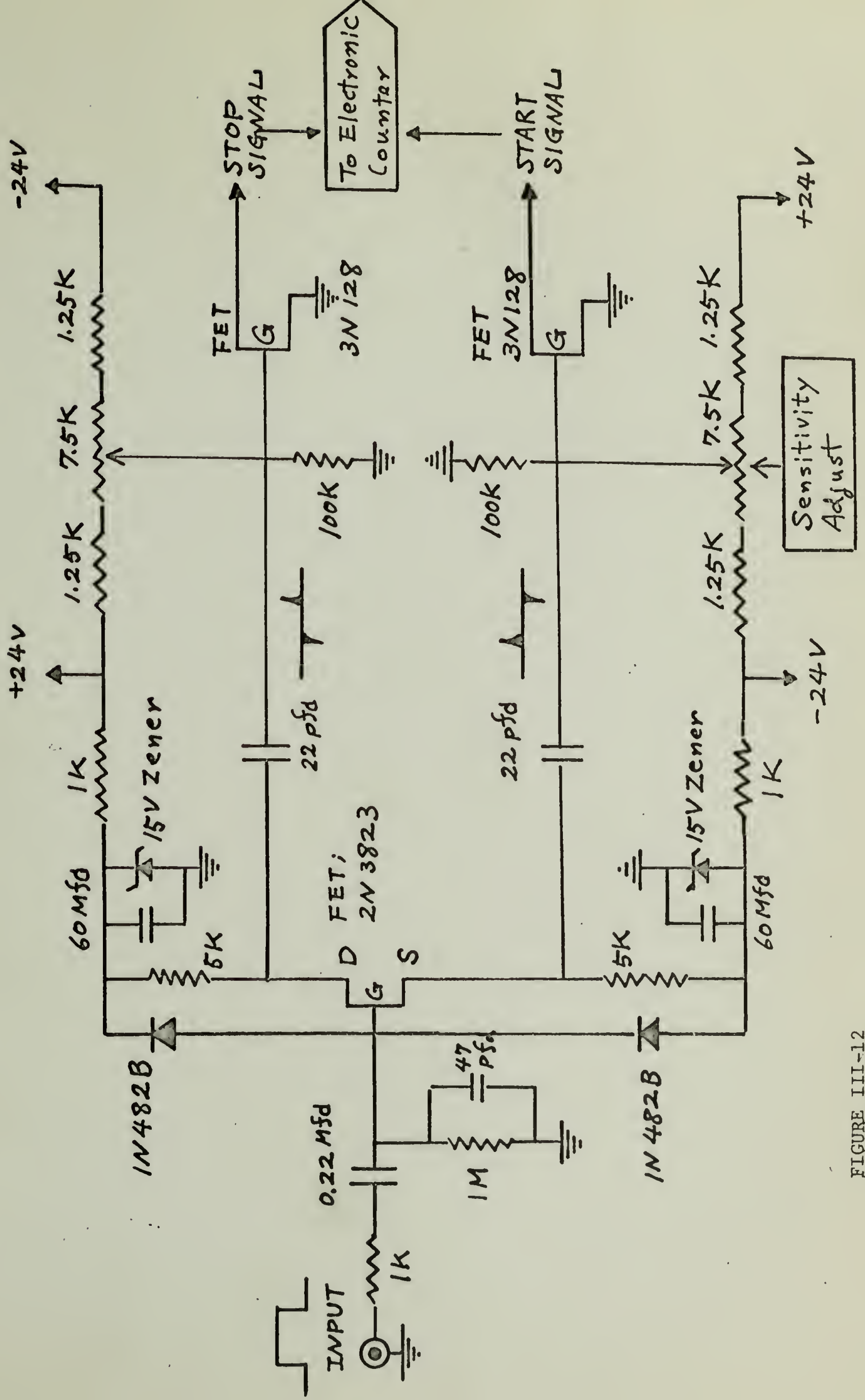


FIGURE III-12

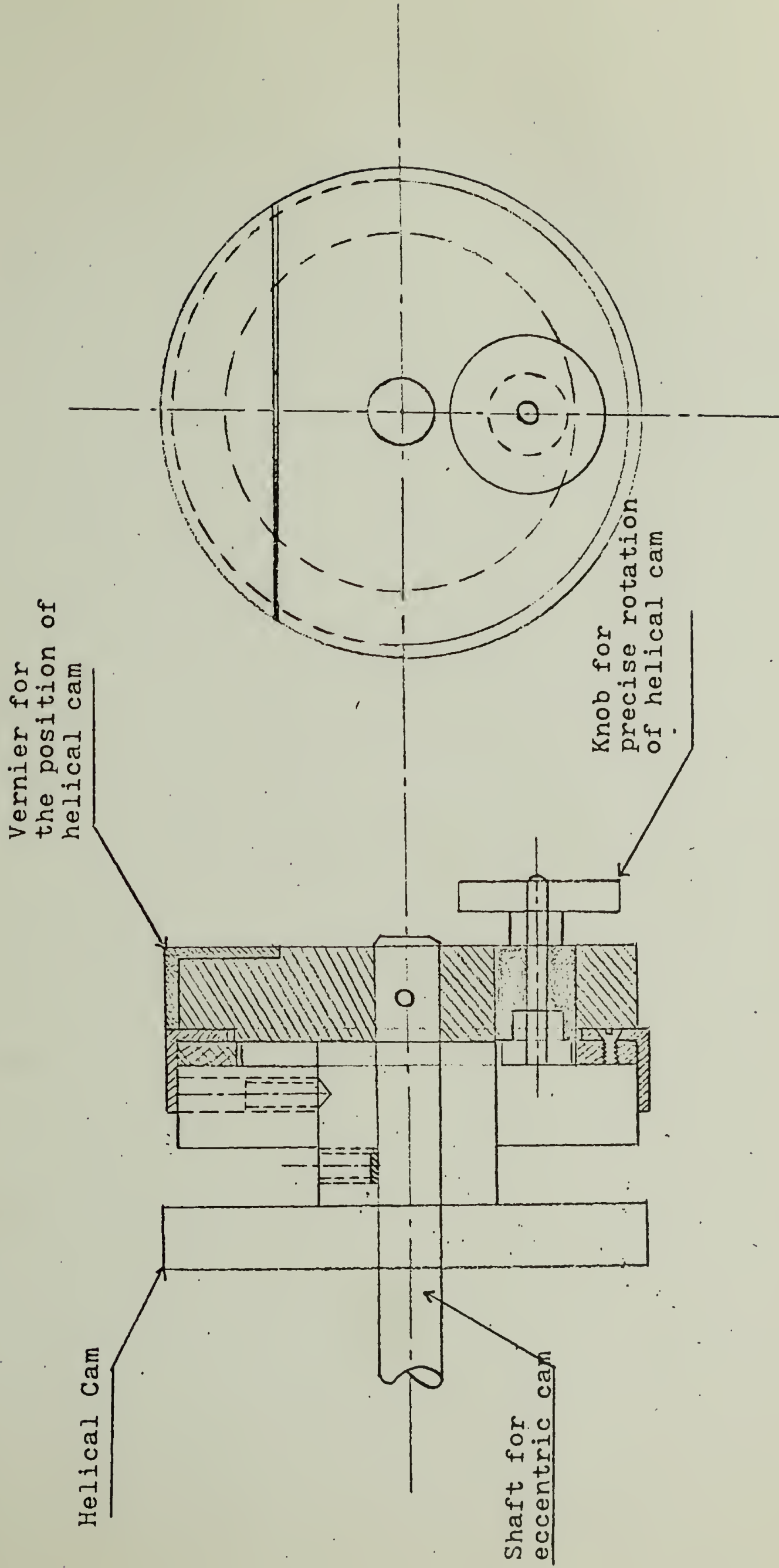


FIGURE III-13 Fine adjustment of orientation of helical cam with respect to that of eccentric cam

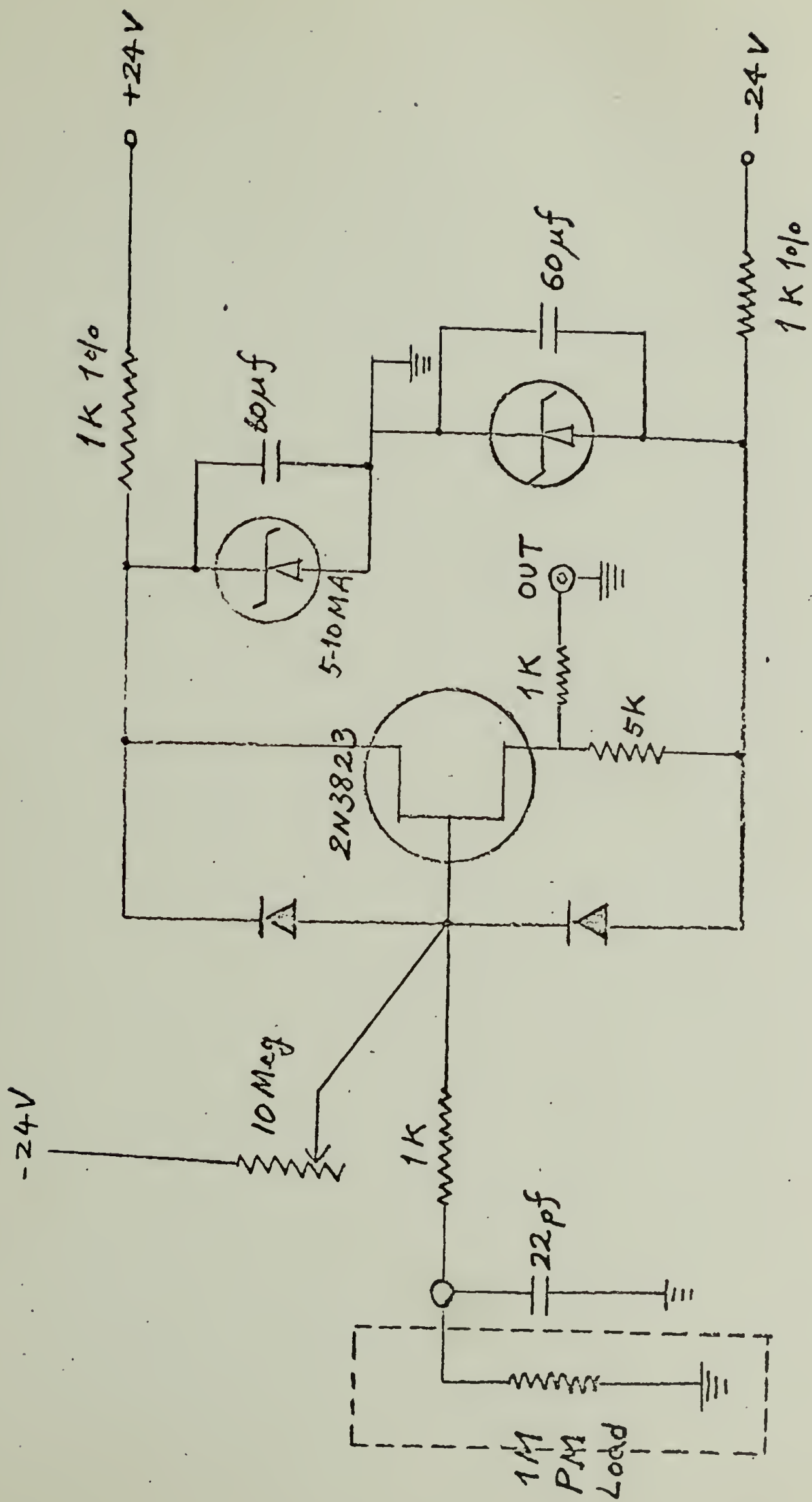
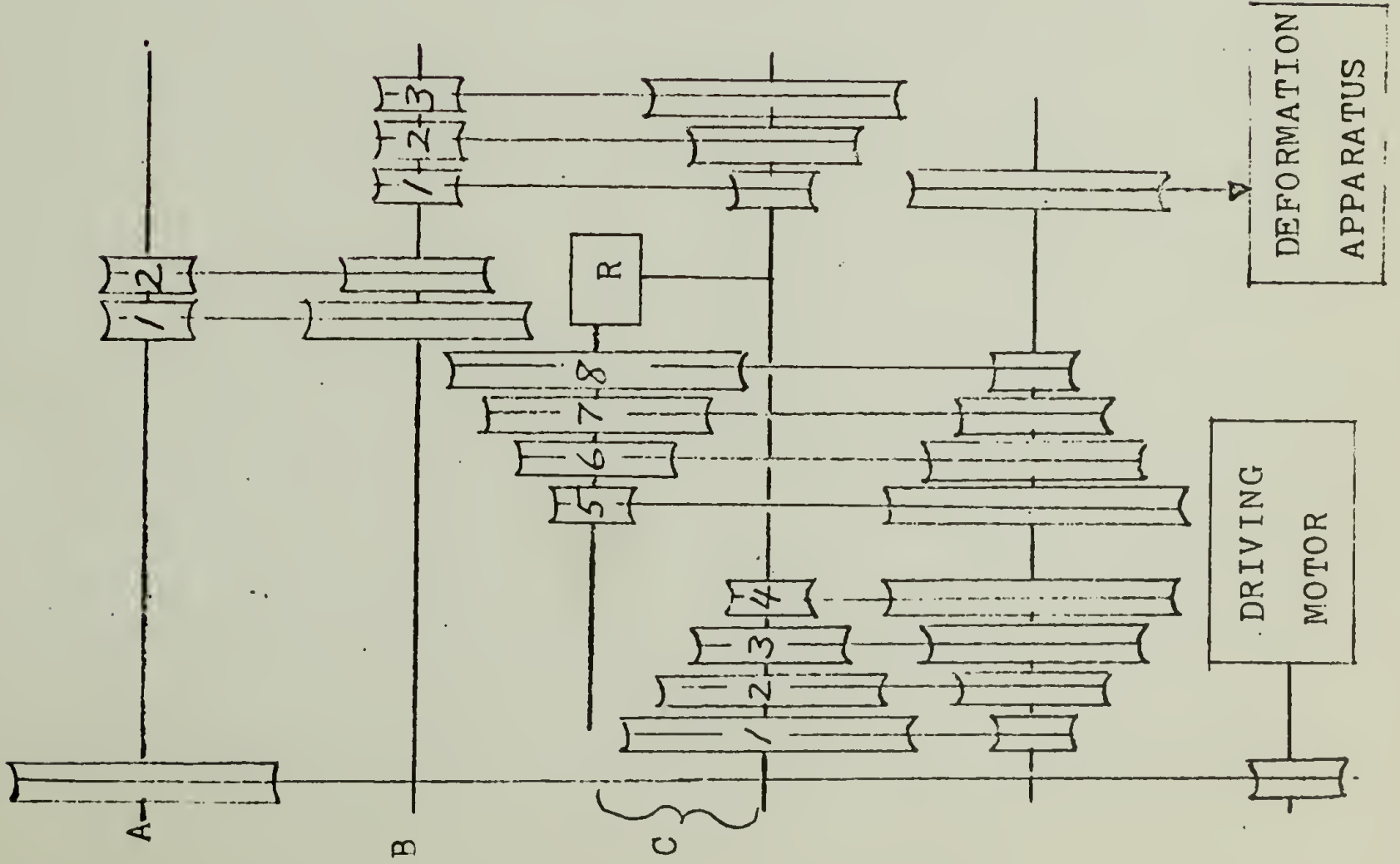


FIGURE III-14. Preamplifier



Various Combinations of Pulleys to Change the Frequency of Vibration

FREQUENCY (H _z)	COMBINATION OF PULLES			FREQUENCY (H _z)	COMBINATION OF PULLES		
	A	B	C		A	B	C
4.1	2	1	1	0.38	1	3	2
2.9	2	2	1	0.29	2	3	4
2.4	2	1	2	0.27	1	2	3
1.9	2	3	1	0.17	1	3	3
1.7	2	2	2	0.15	1	2	4
1.4	1	1	1	0.09	1	3	4
1.1	1	3	2	0.082	2	1	5
1.0	1	2	1	0.056	2	2	5
0.89	1	2	3	0.049	2	1	6
0.80	1	1	2	0.036	2	3	5
0.71	1	1	4	0.033	2	2	6
0.60	2	3	3	0.029	1	1	5
0.57	1	3	1	0.021	2	3	6
0.57	1	1	3	0.020	1	2	5
0.56	1	2	2	0.016	1	1	5
0.50	1	2	4	0.012	1	3	6
0.40	1	1	3	0.011	1	2	6
				0.087	1	3	6

FIGURE III-15

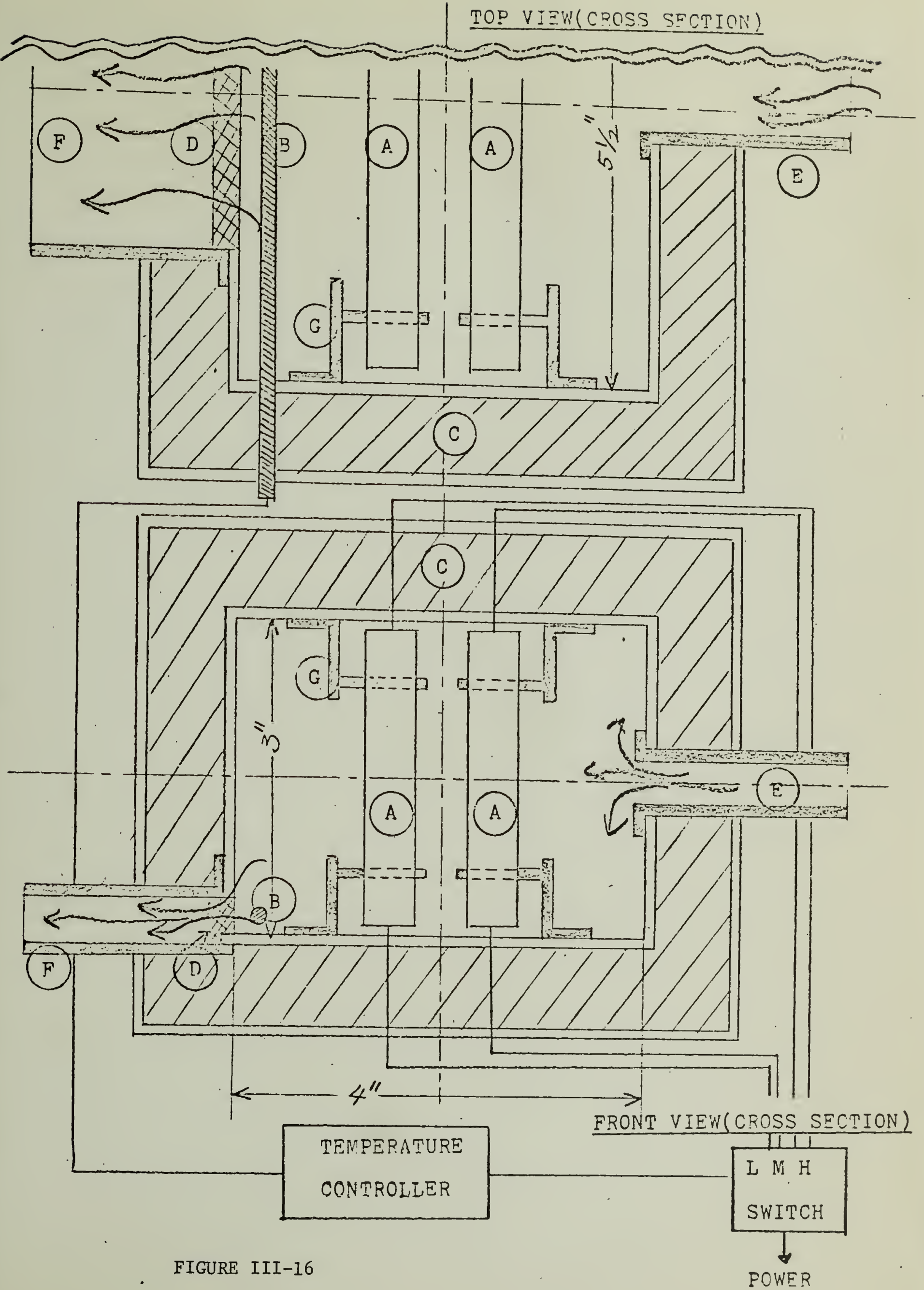
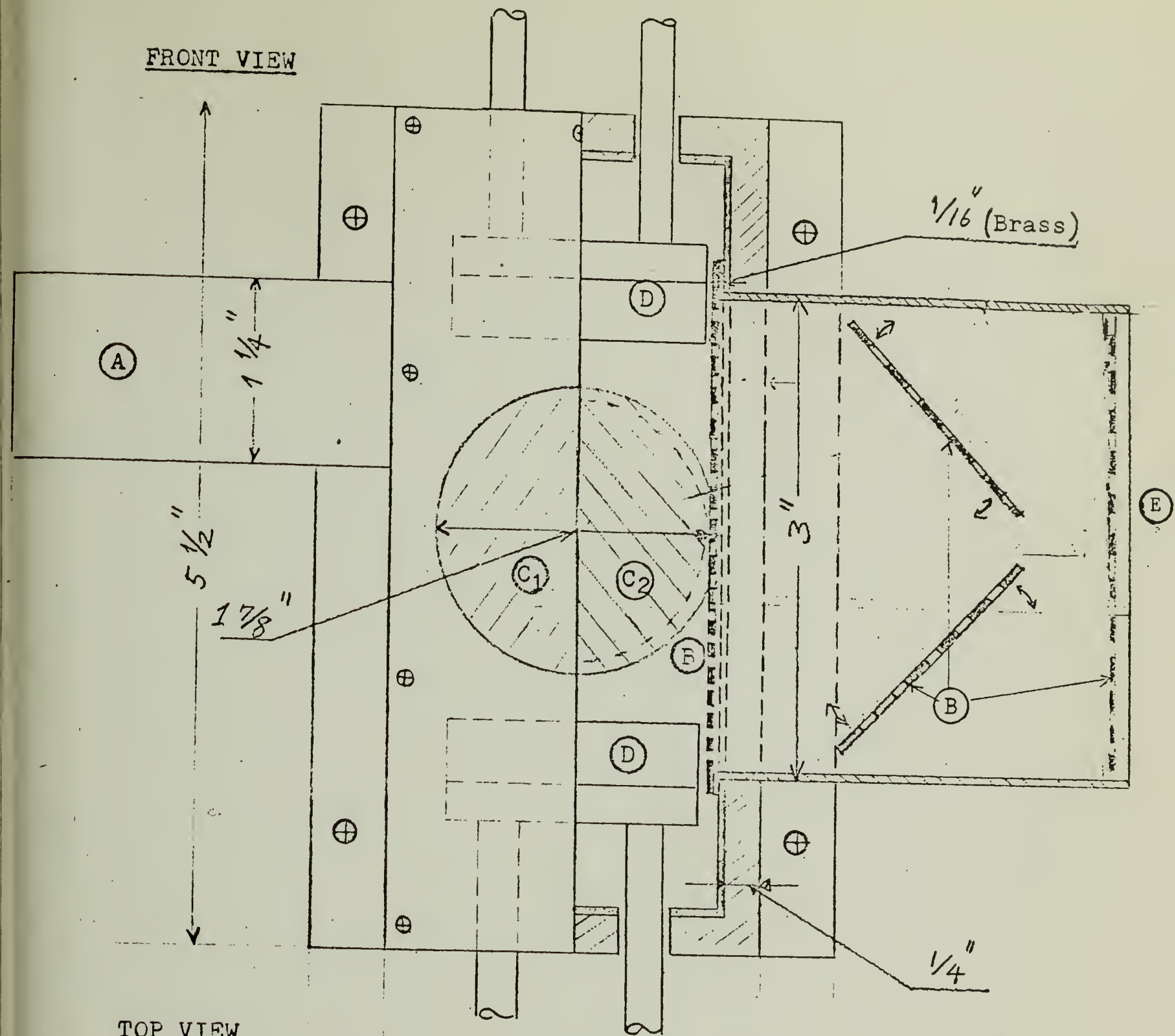


FIGURE III-16

FRONT VIEW



TOP VIEW

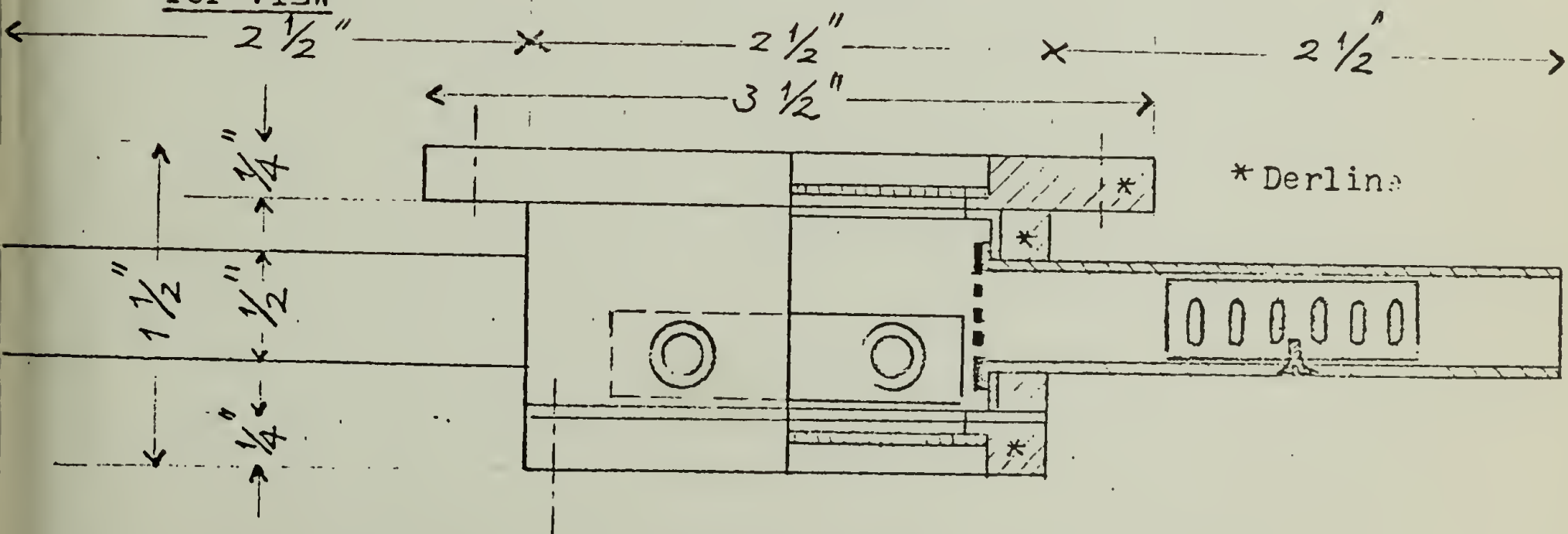


FIGURE III-17. An outline of temperature enclosure

Fig. III-18(a)

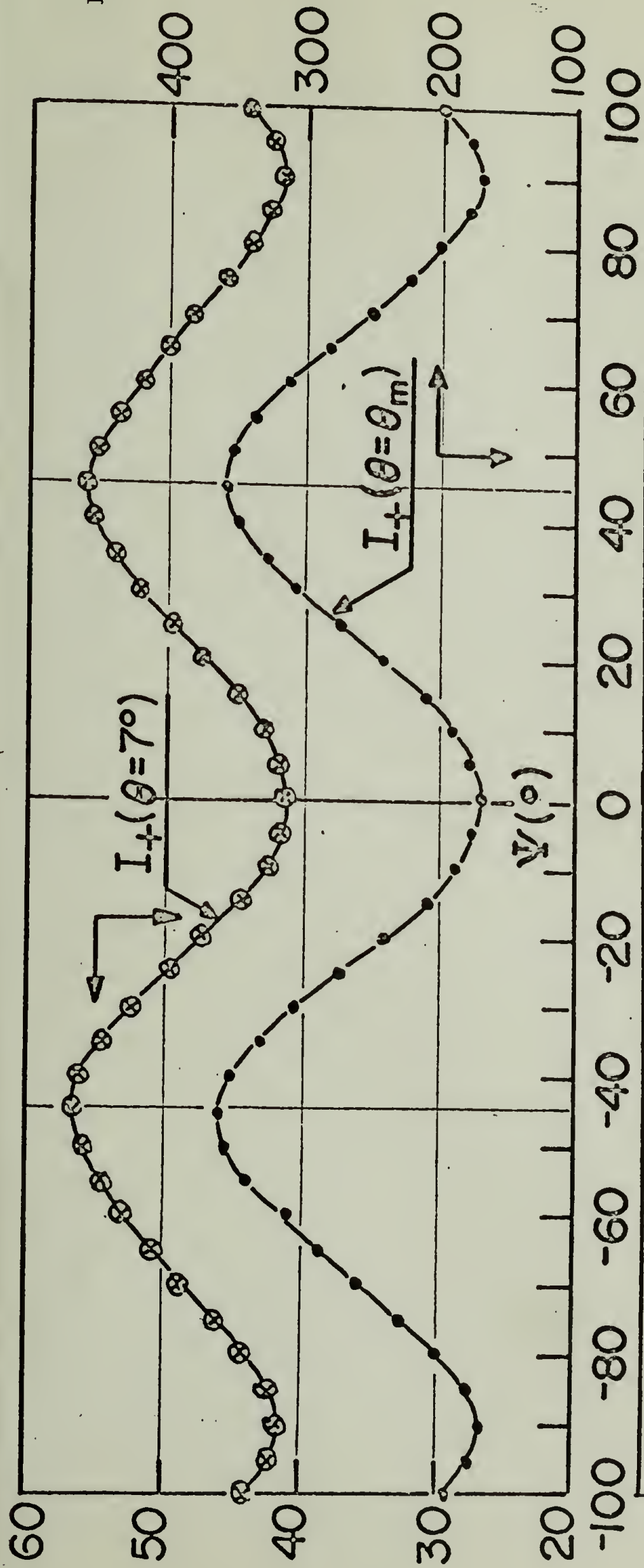
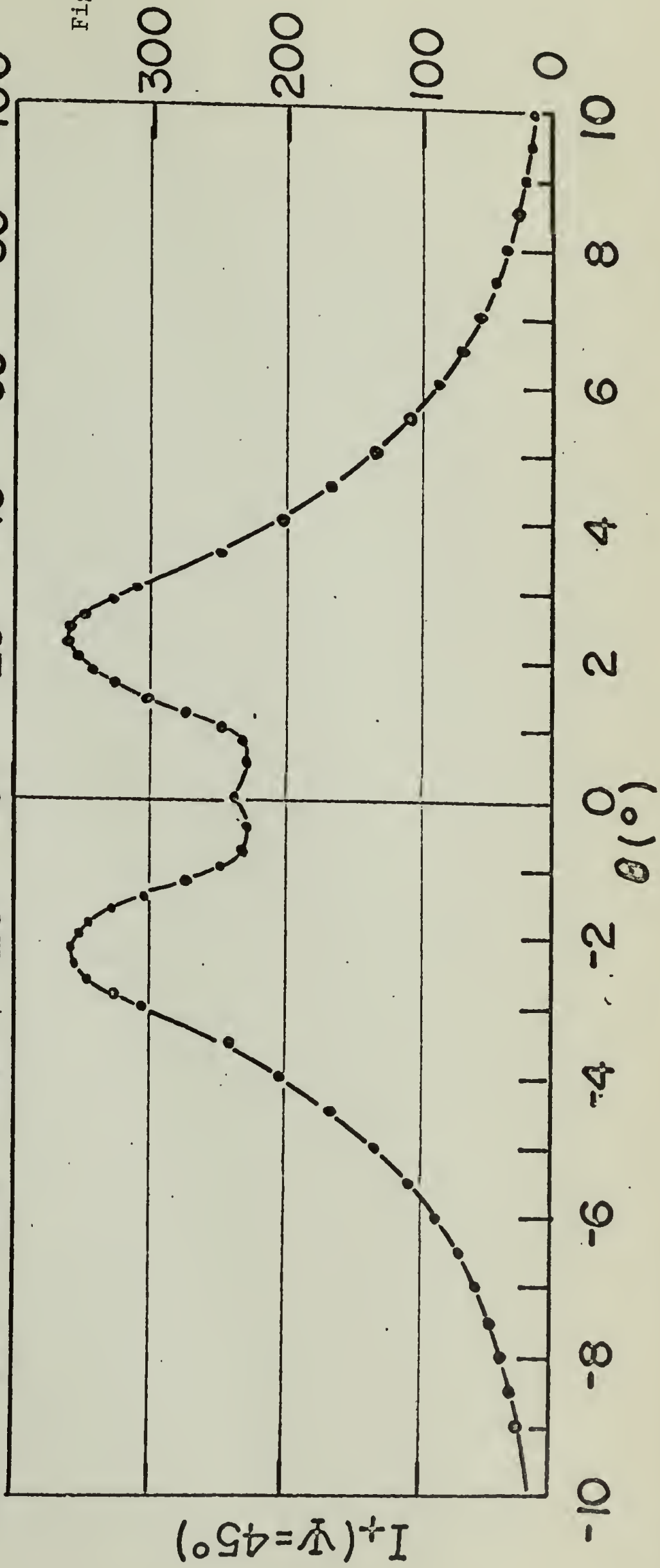
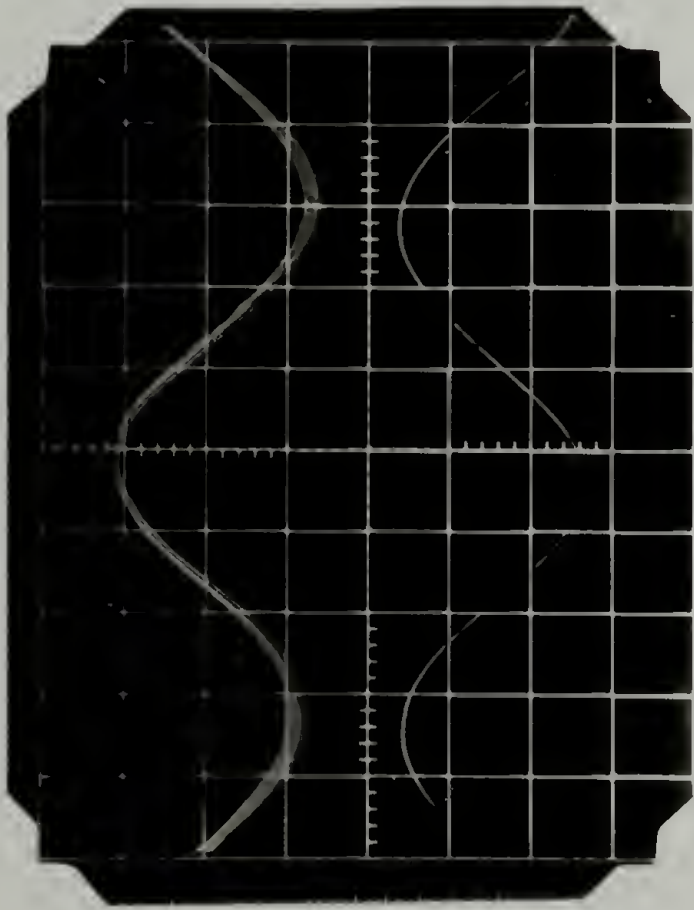
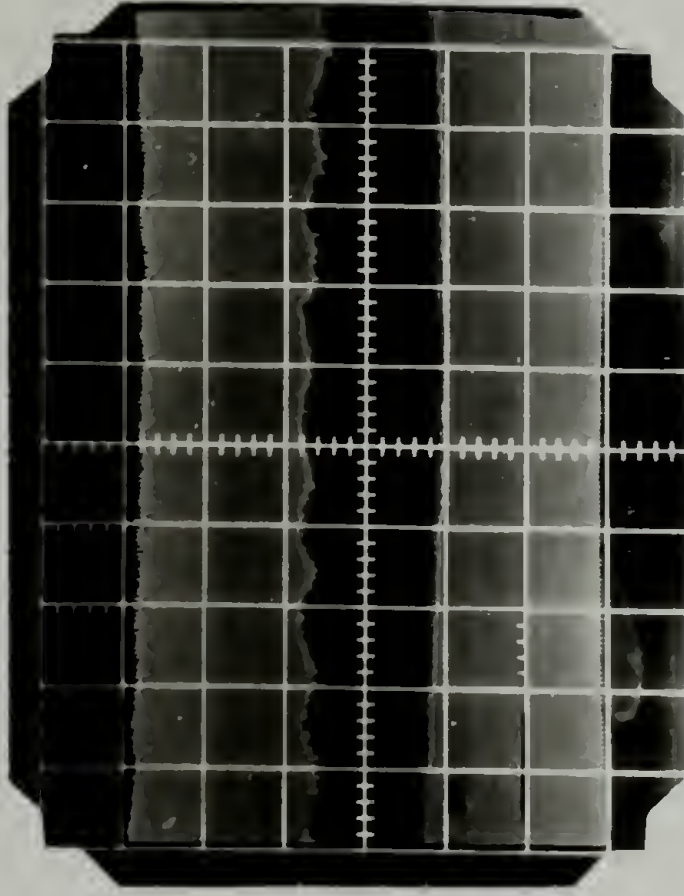


Fig. III-18(b)

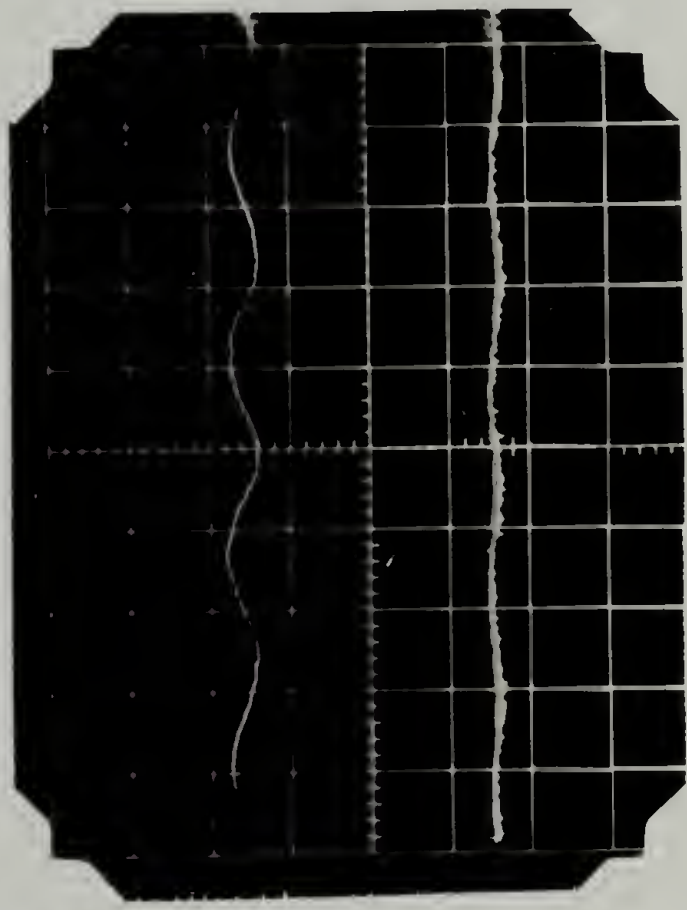




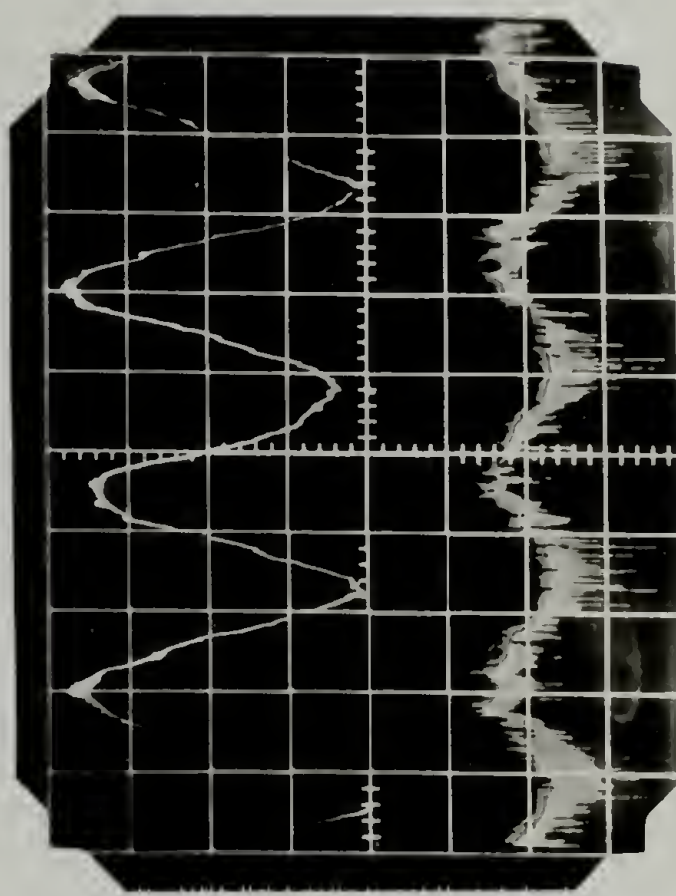
(a)



(b)

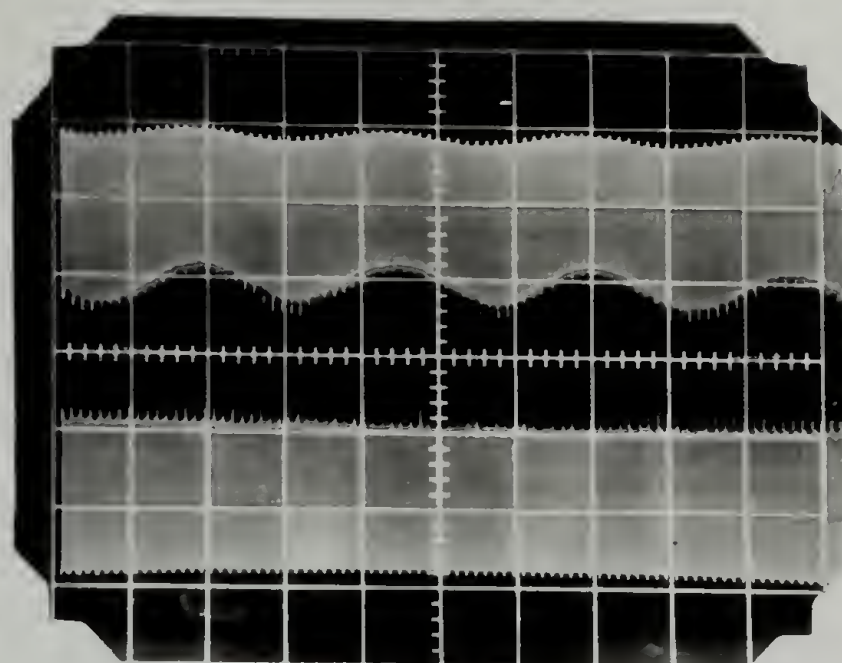


(c)

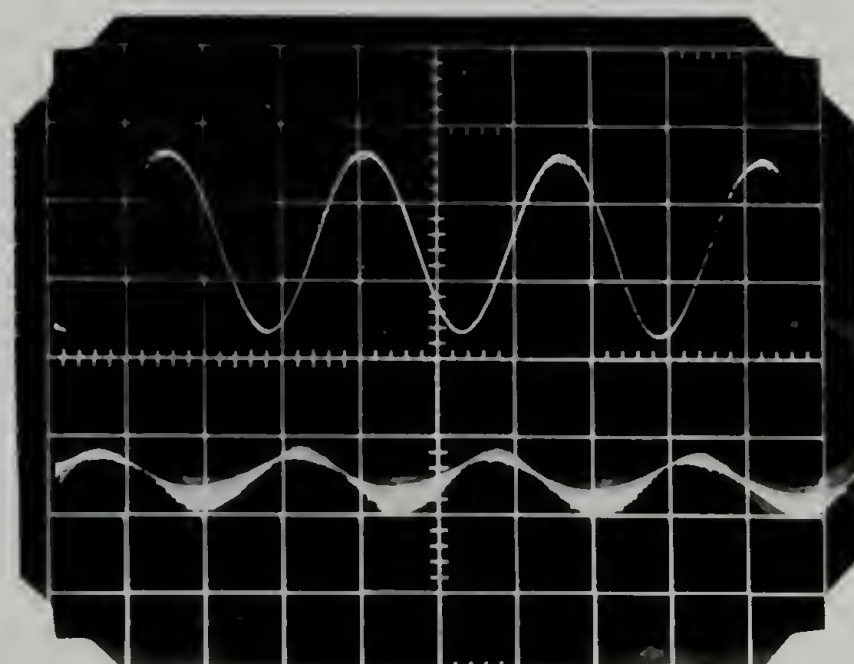


(d)

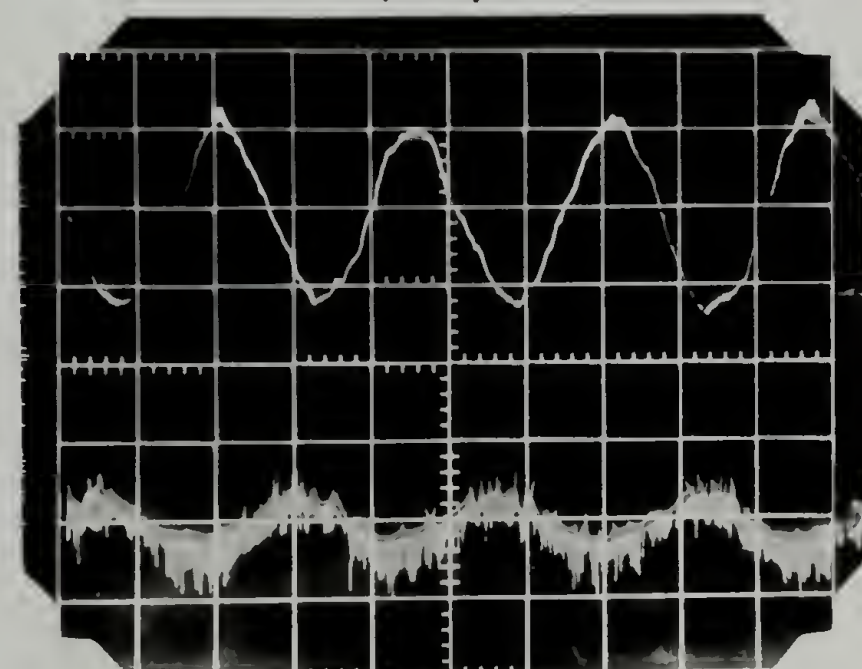
FIGURE III-19



(a)

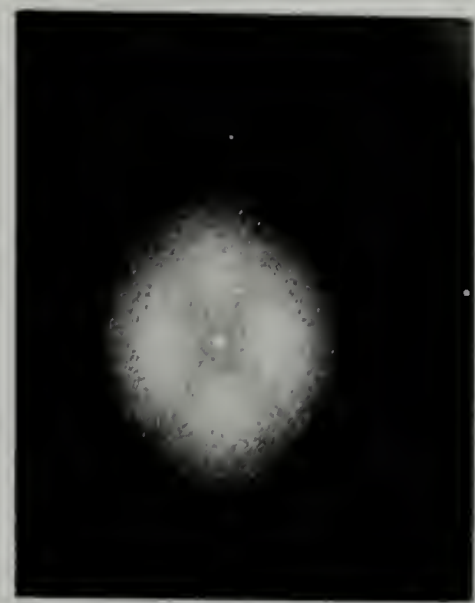


(b)



(c)

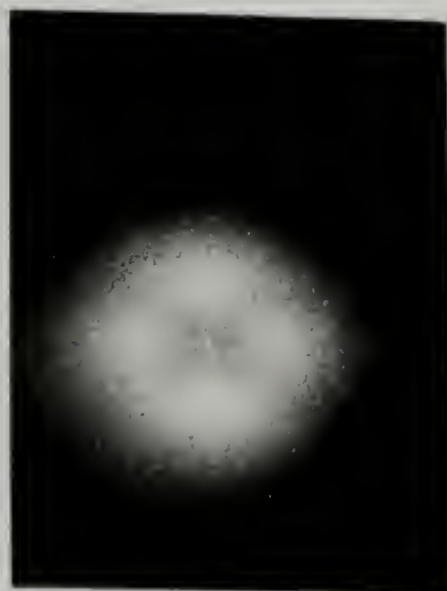
FIGURE III-20



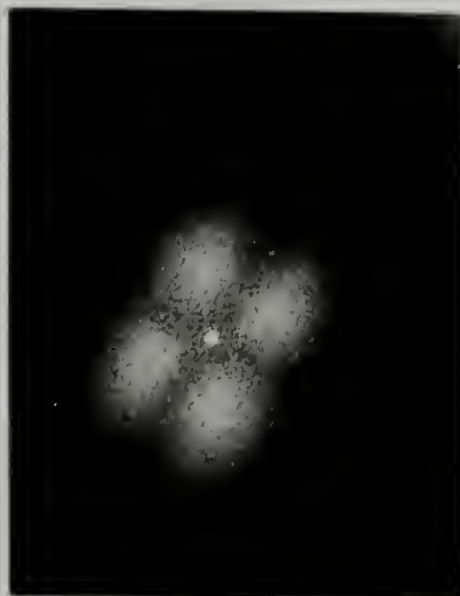
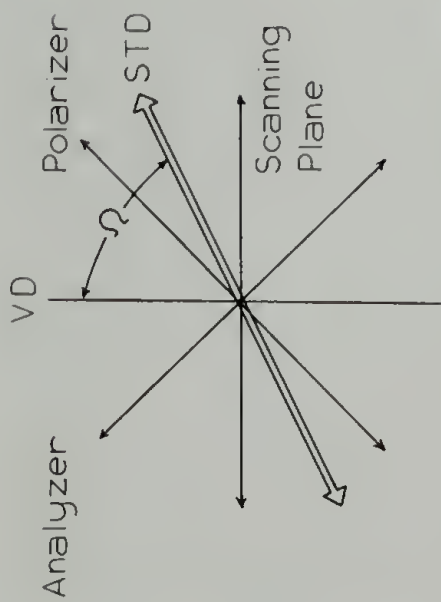
$\Omega = 0$



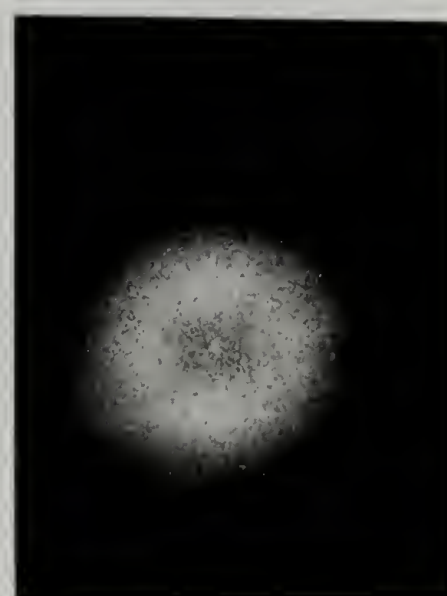
$\Omega = 45$



$\Omega = 90$



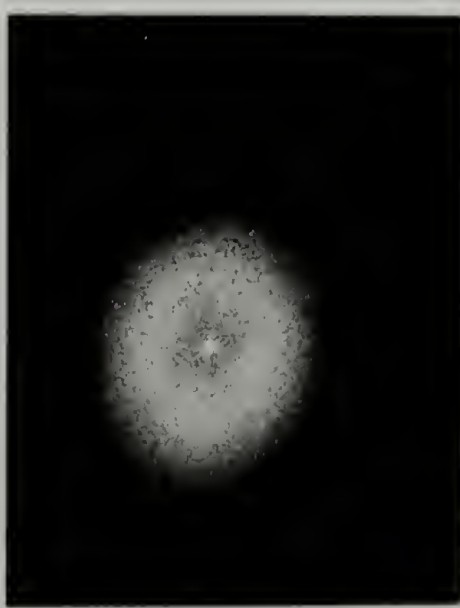
$\Omega = 30$



$\Omega = 75$



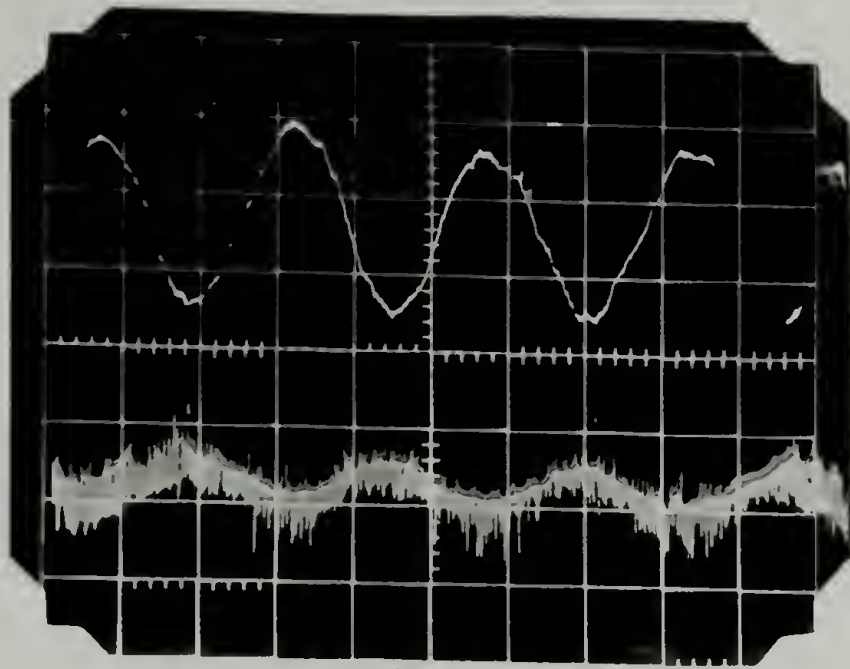
UNDEFORMED



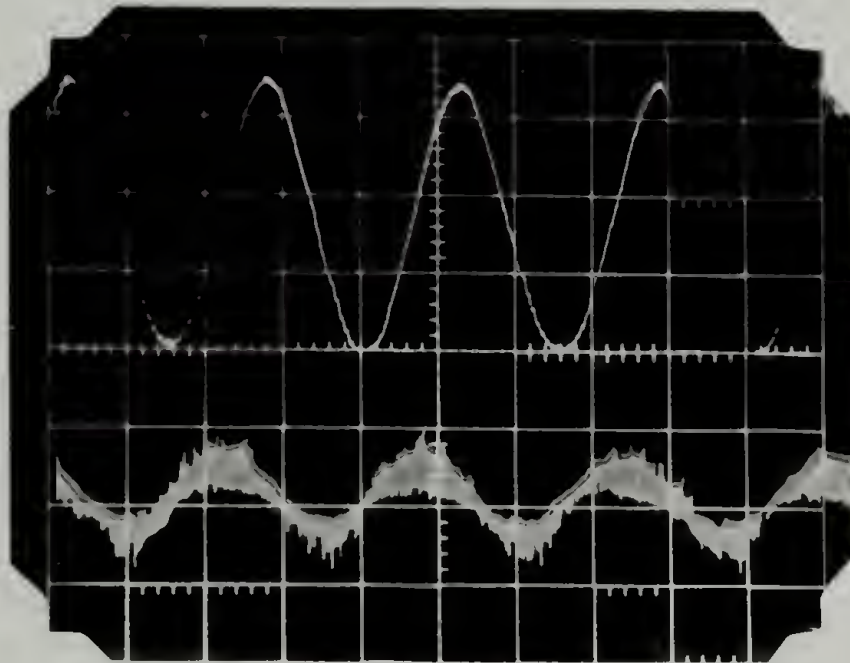
$\Omega = 15$



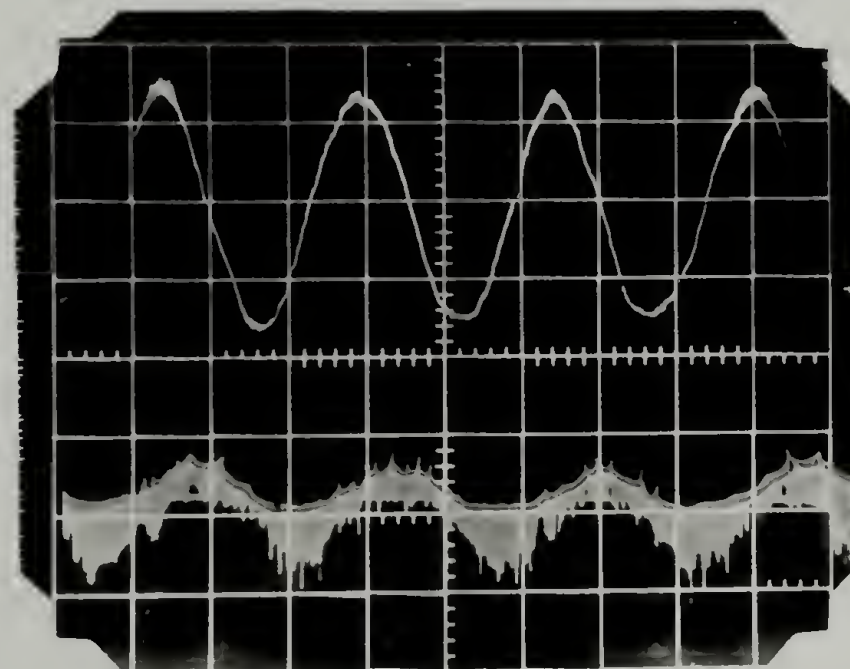
$\Omega = 60$



(a)

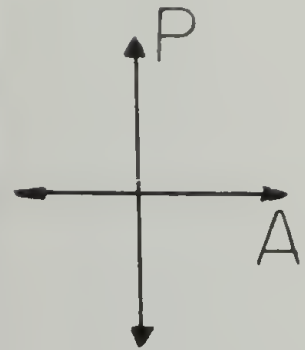
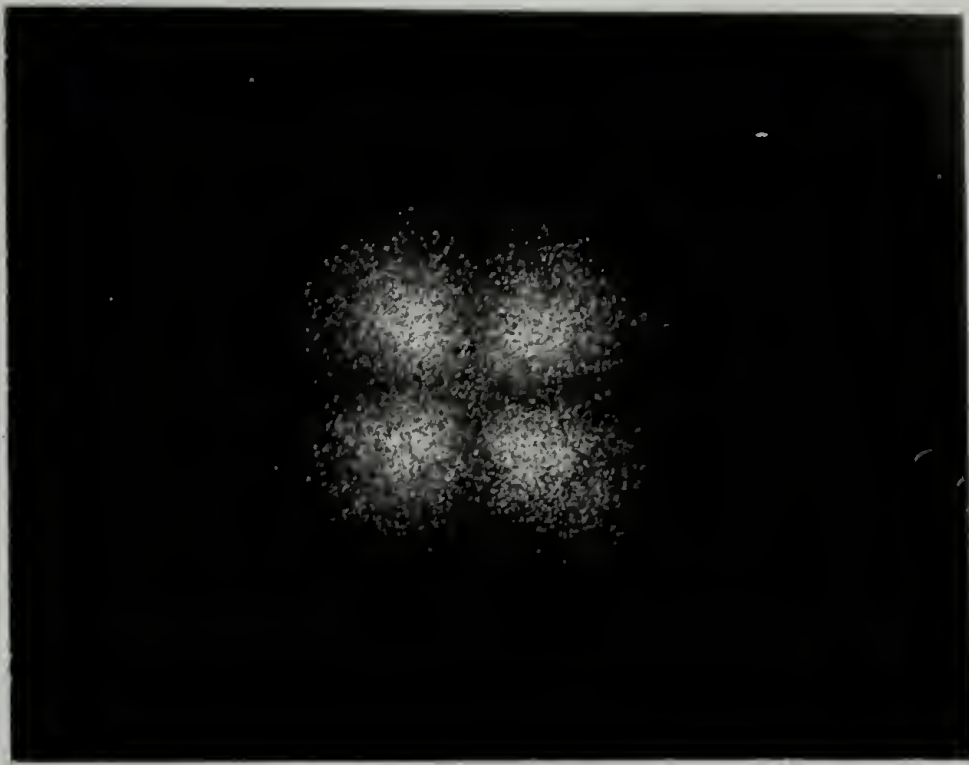


(b)

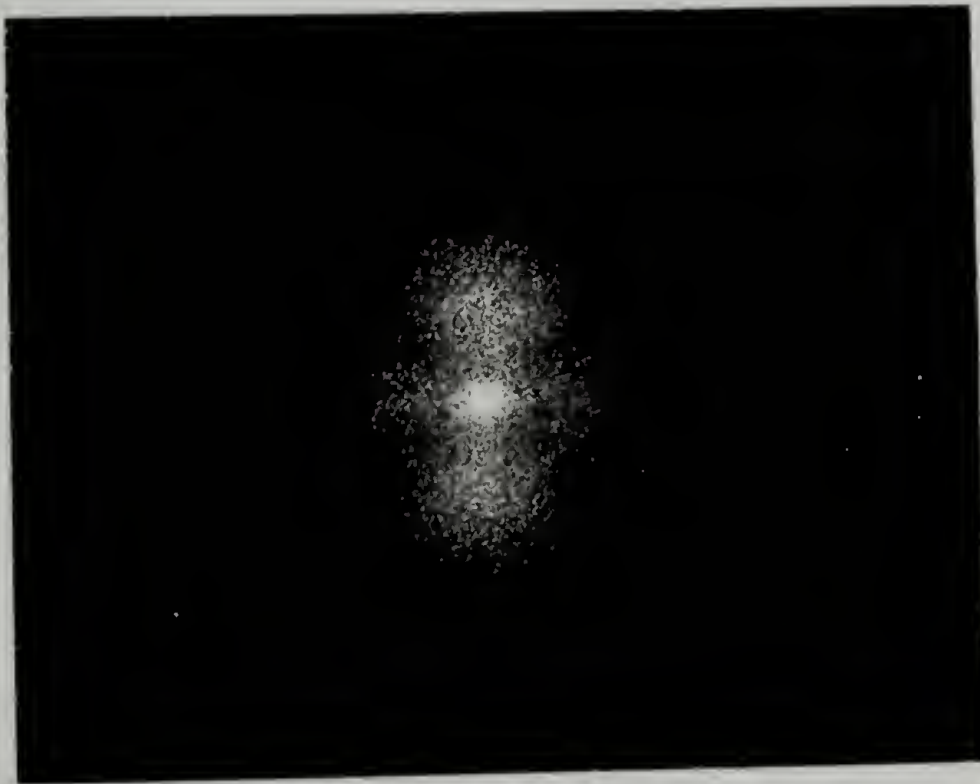


(c)

FIGURE III-22



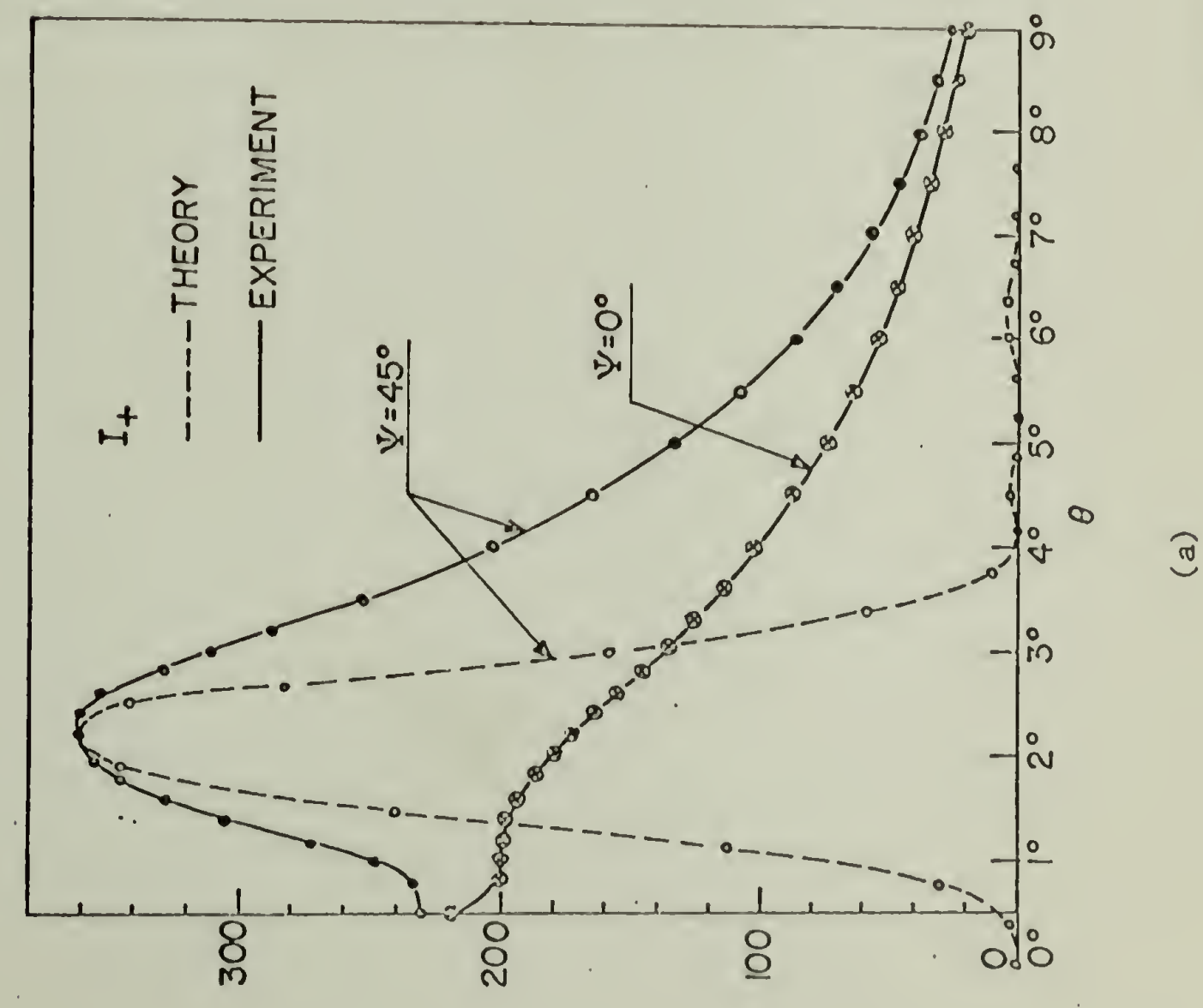
H_v



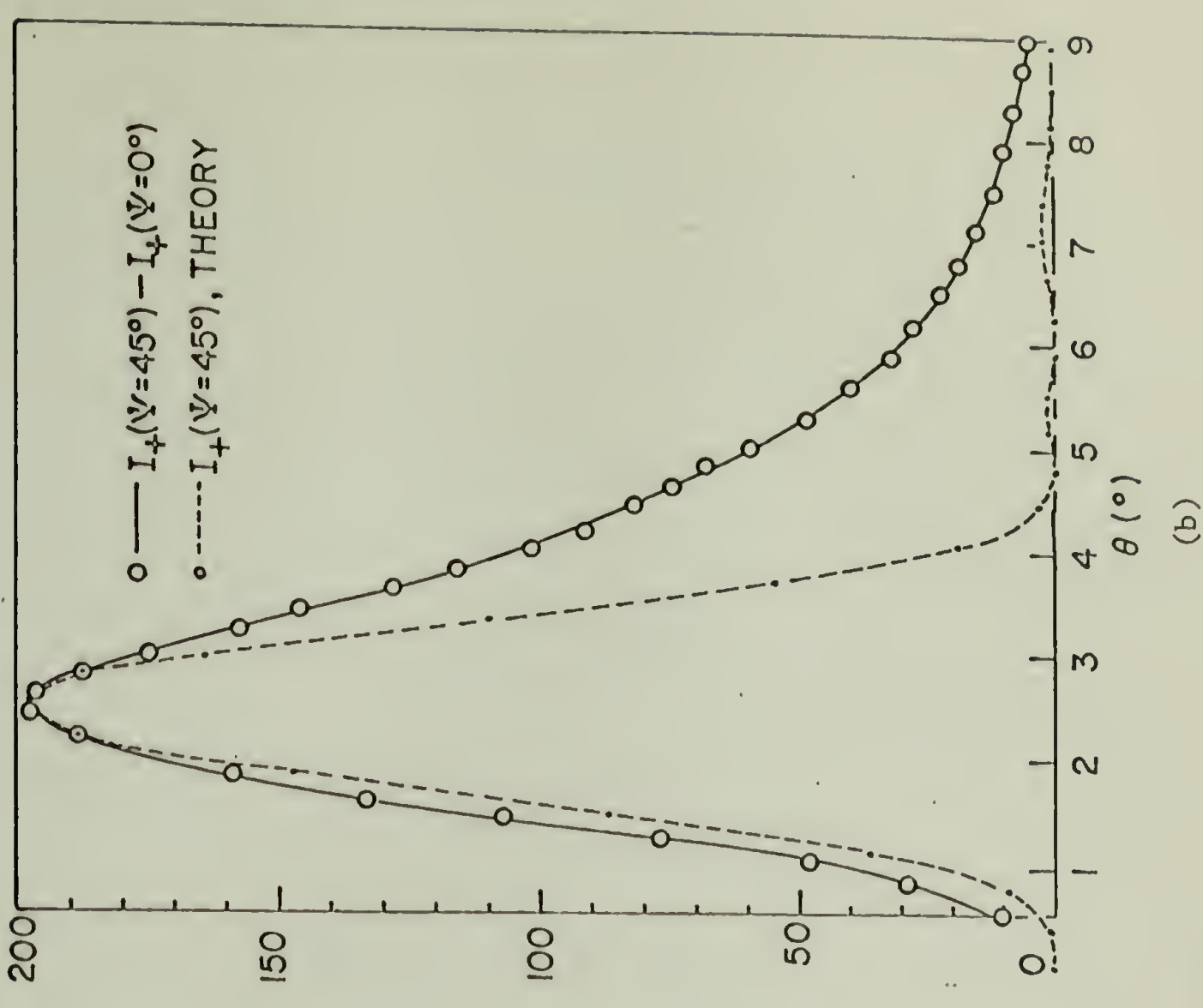
V_v

UNDEFORMED MDPE

FIGURE III-23



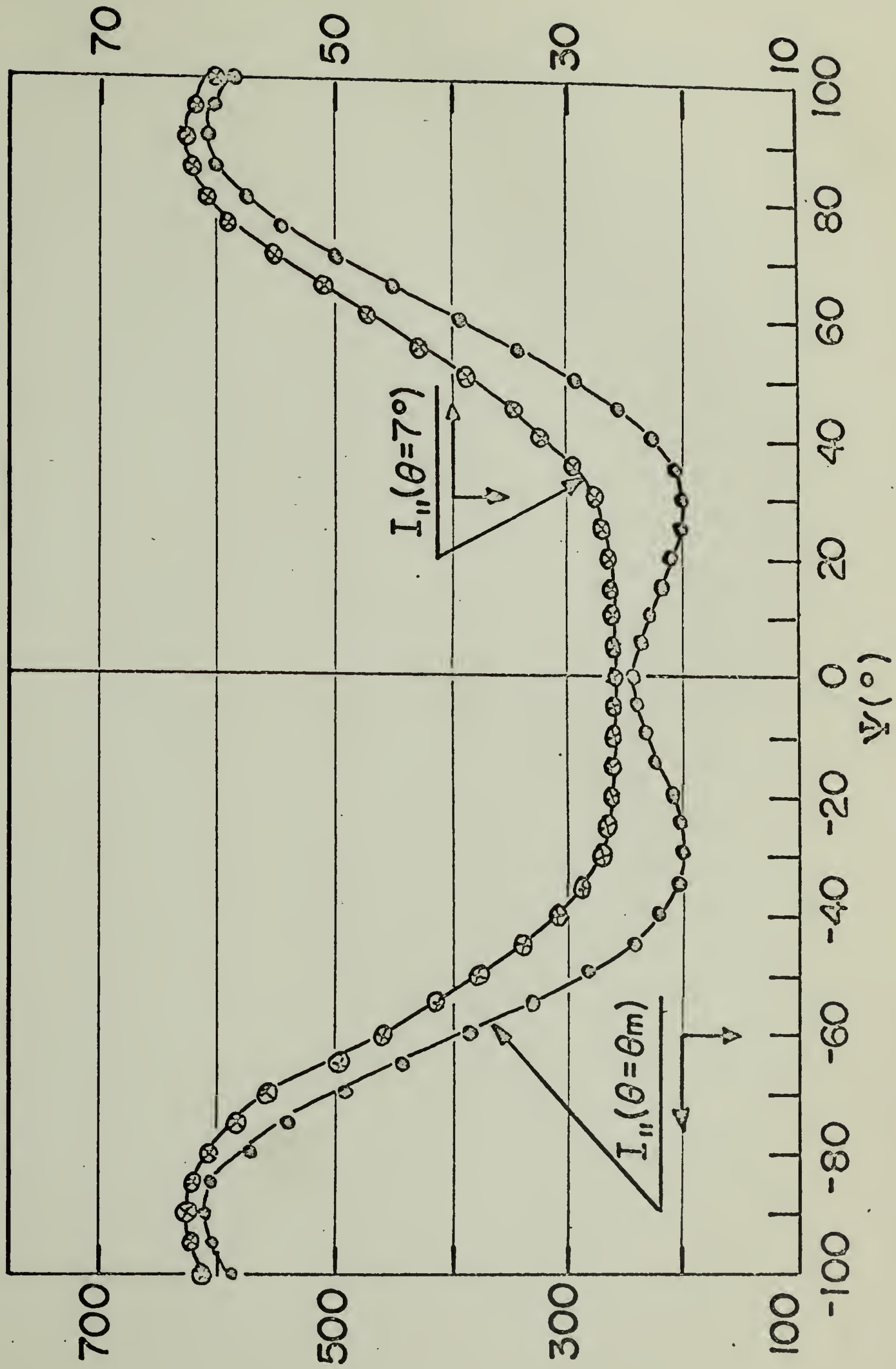
(a)

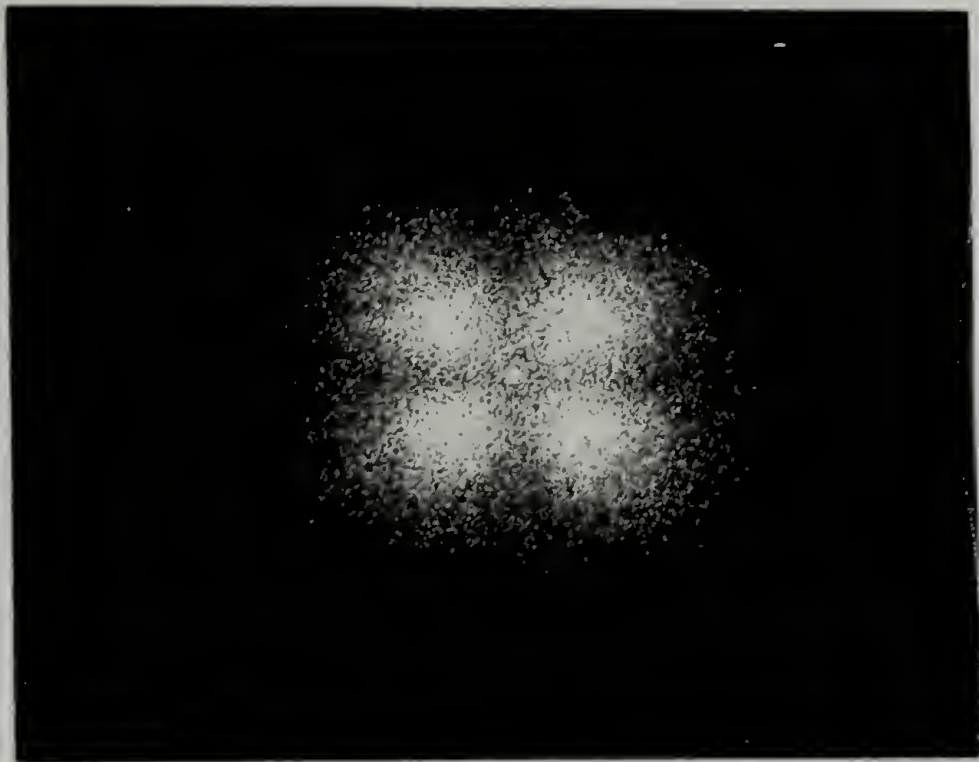


(b)

FIGURE III-24

FIGURE III-25





10 %



20 %

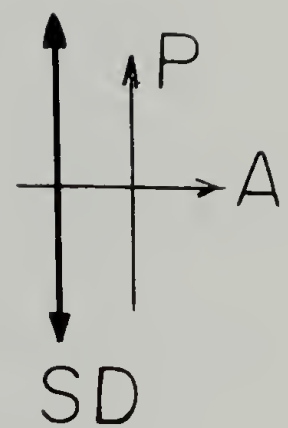


FIGURE III-26

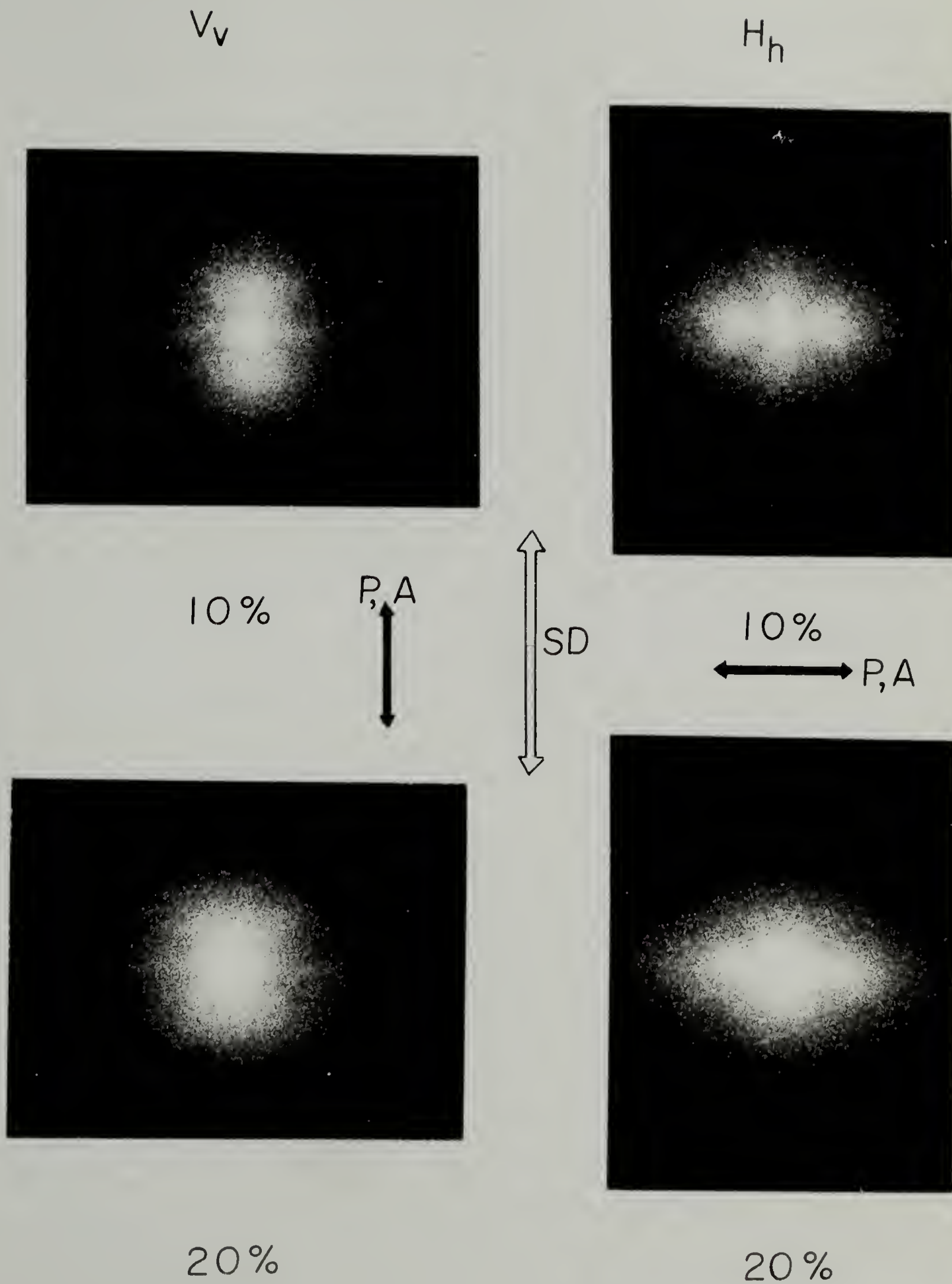


FIGURE III-27

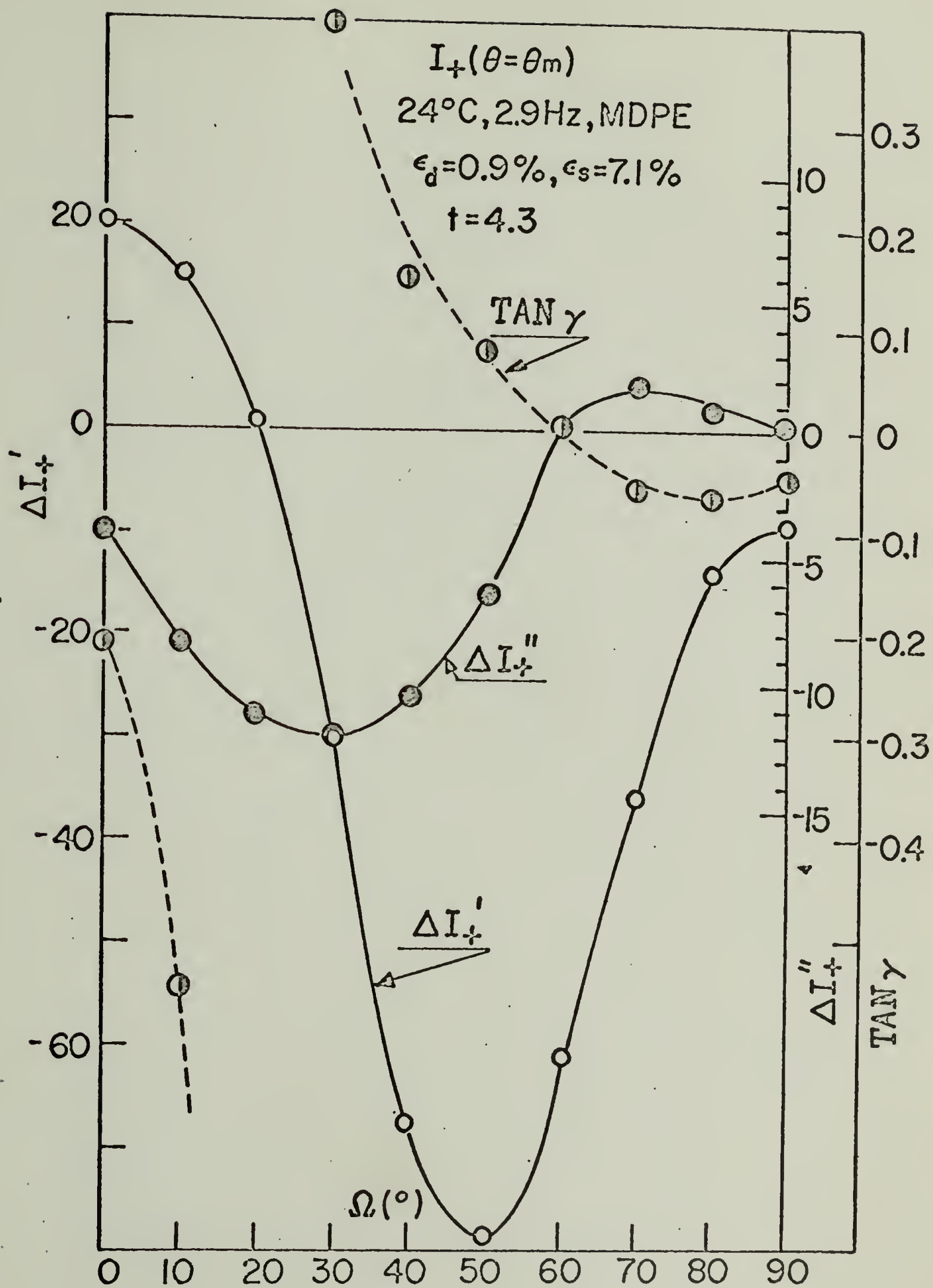


FIGURE III-28

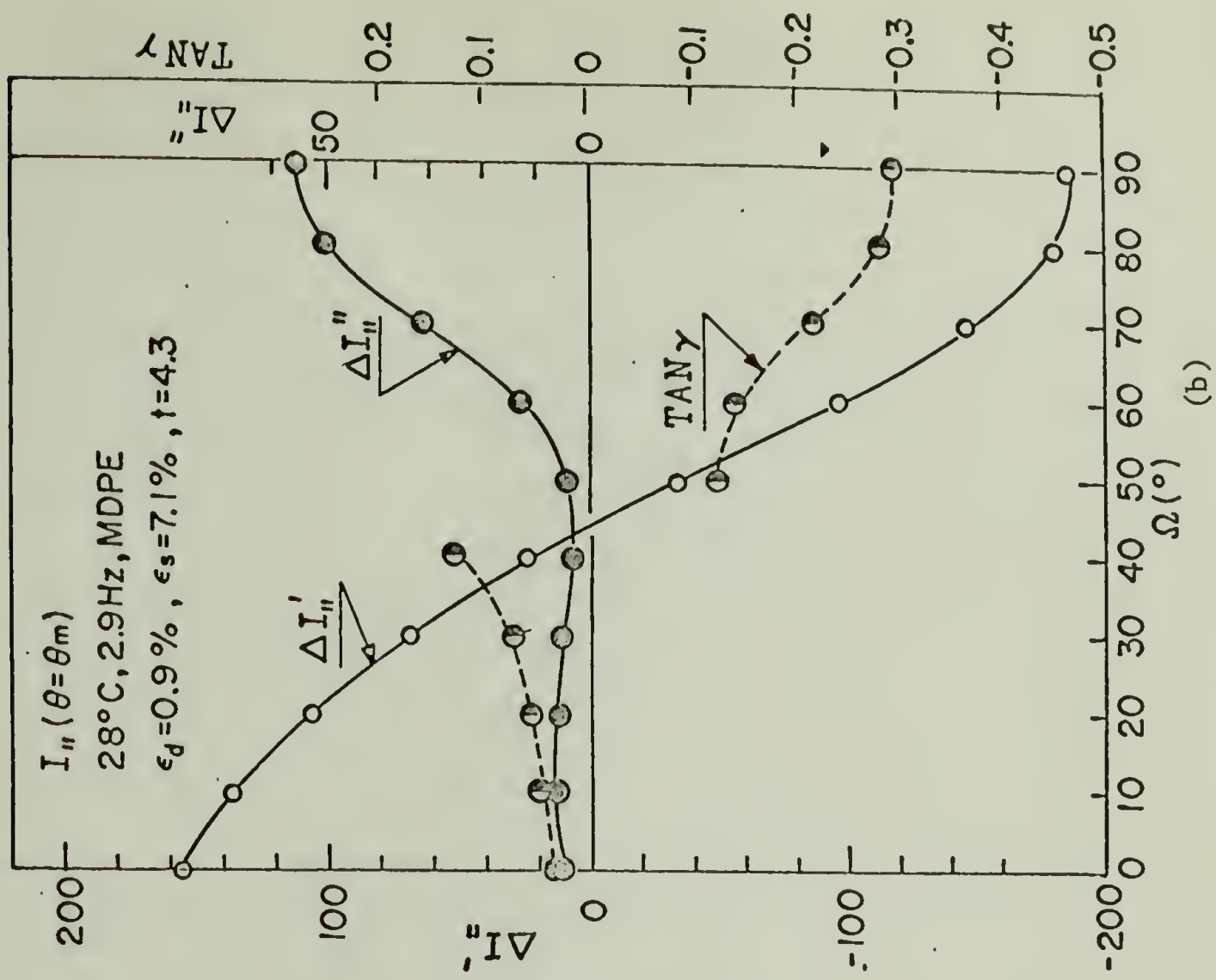
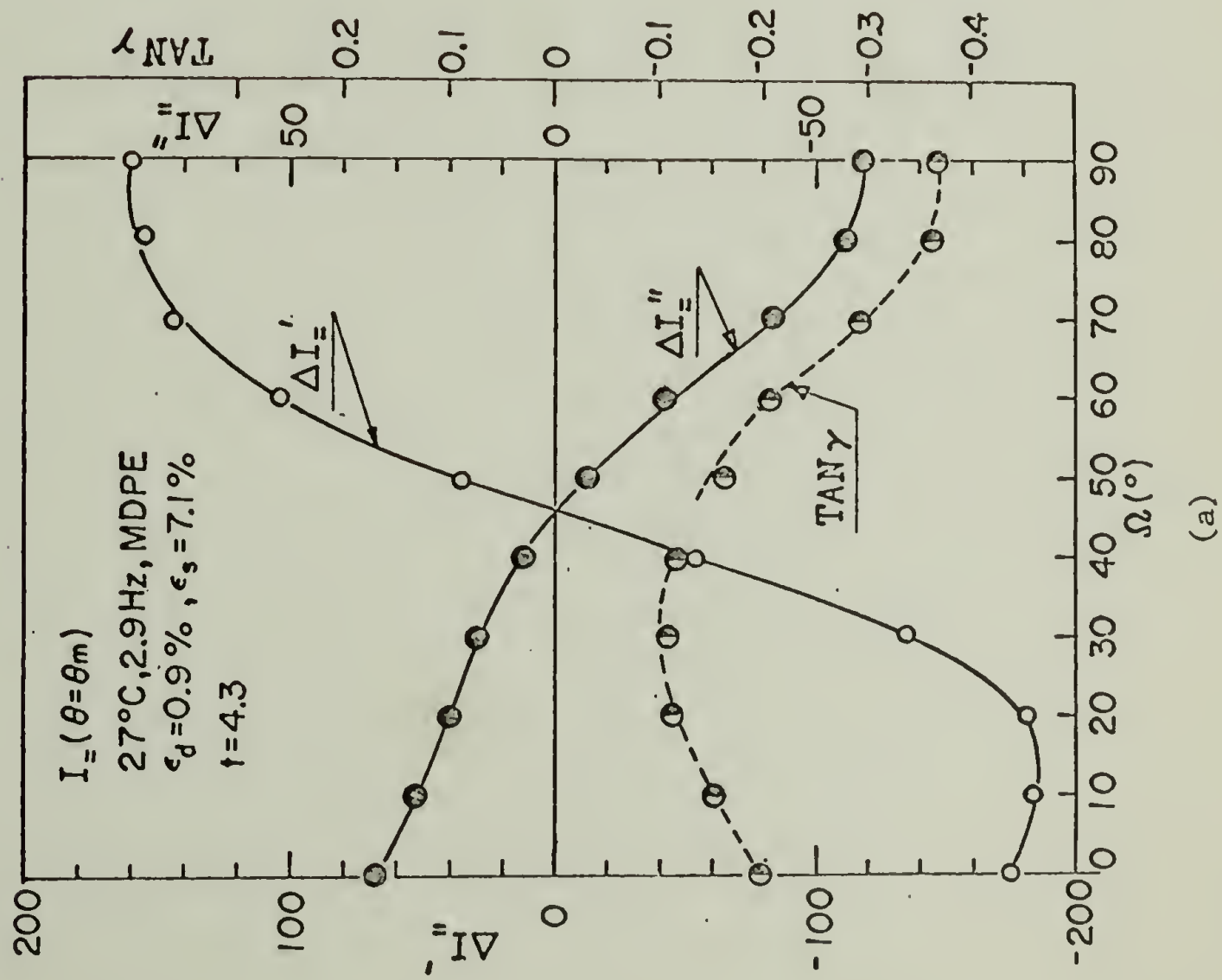


FIGURE III-29

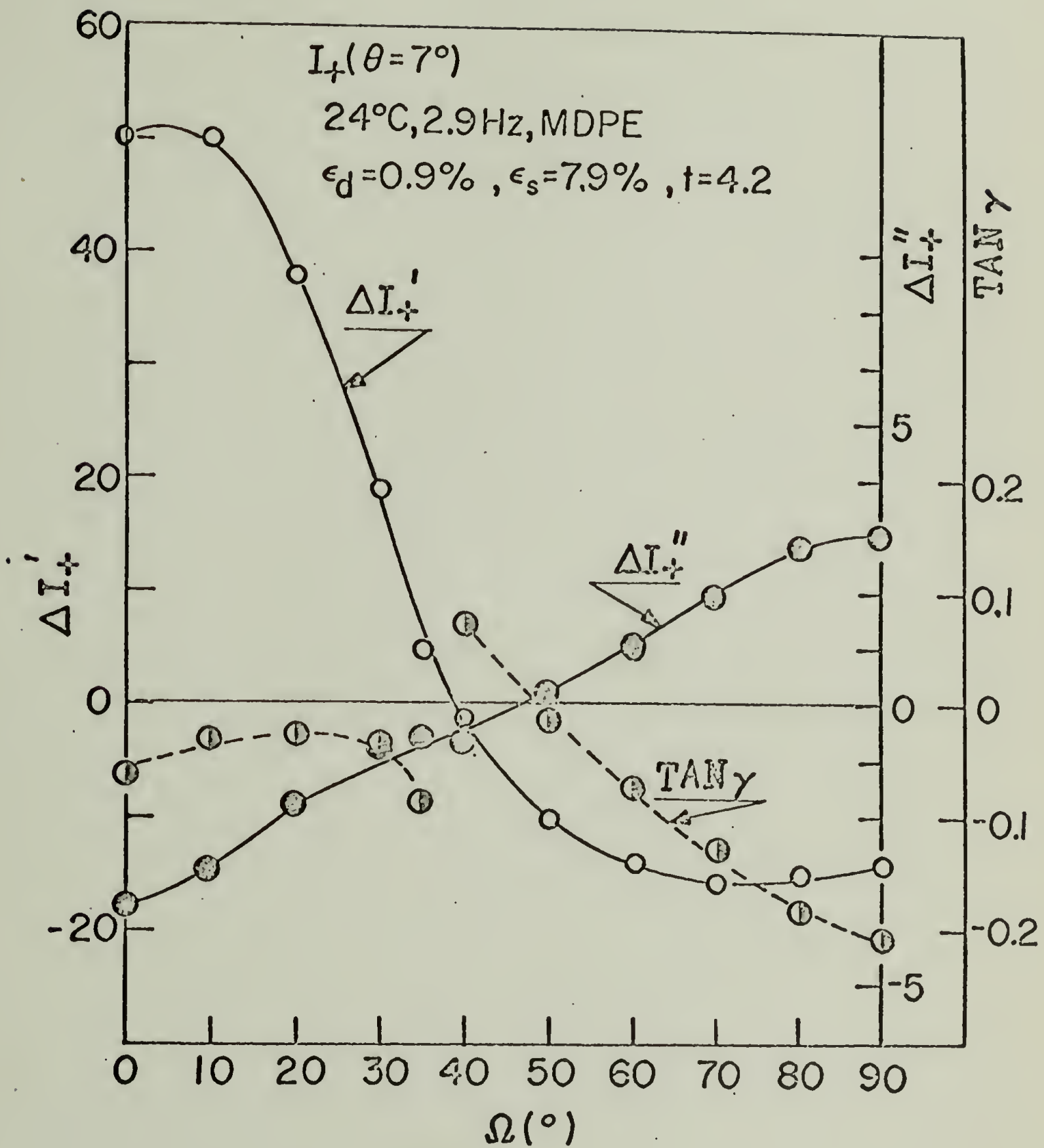
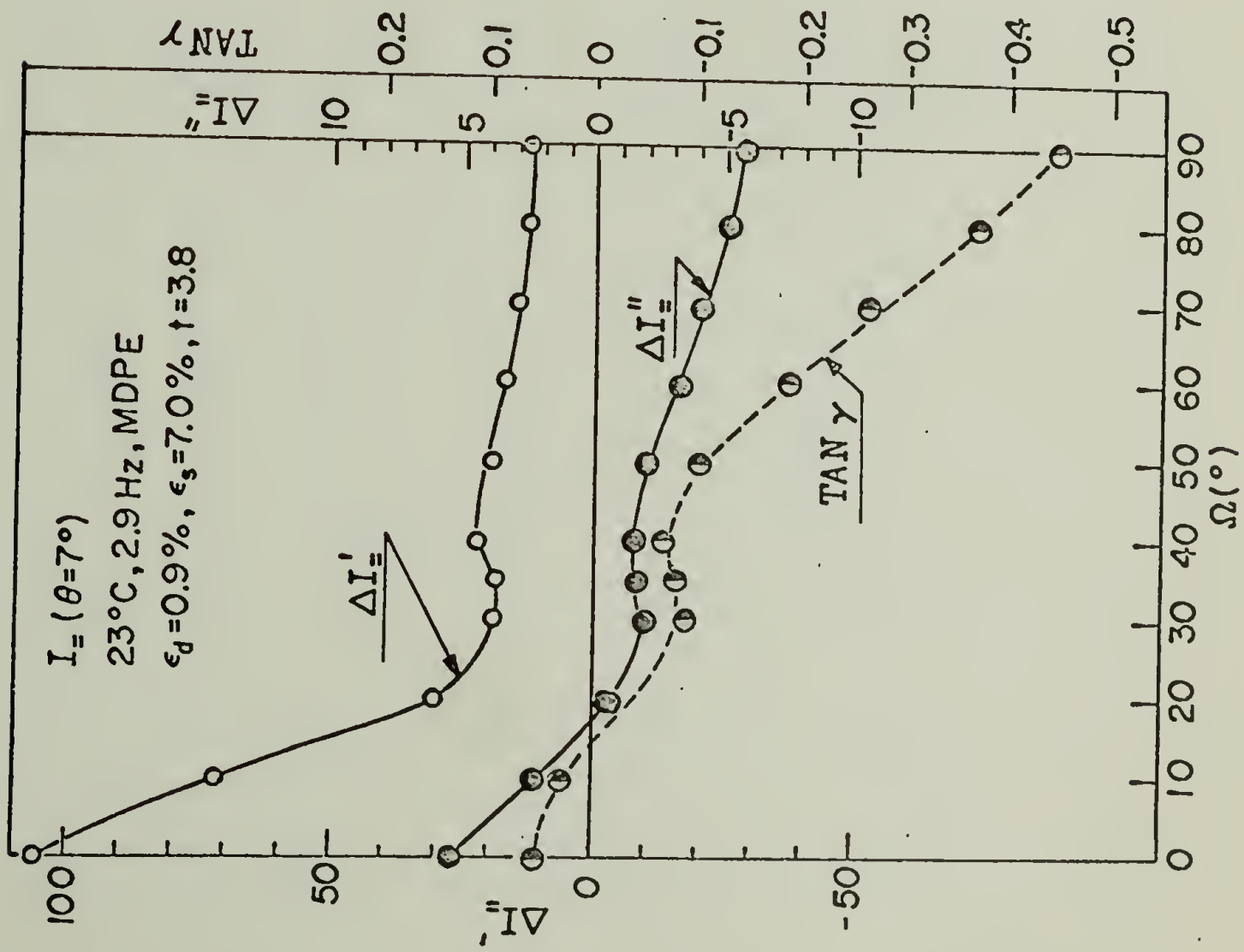
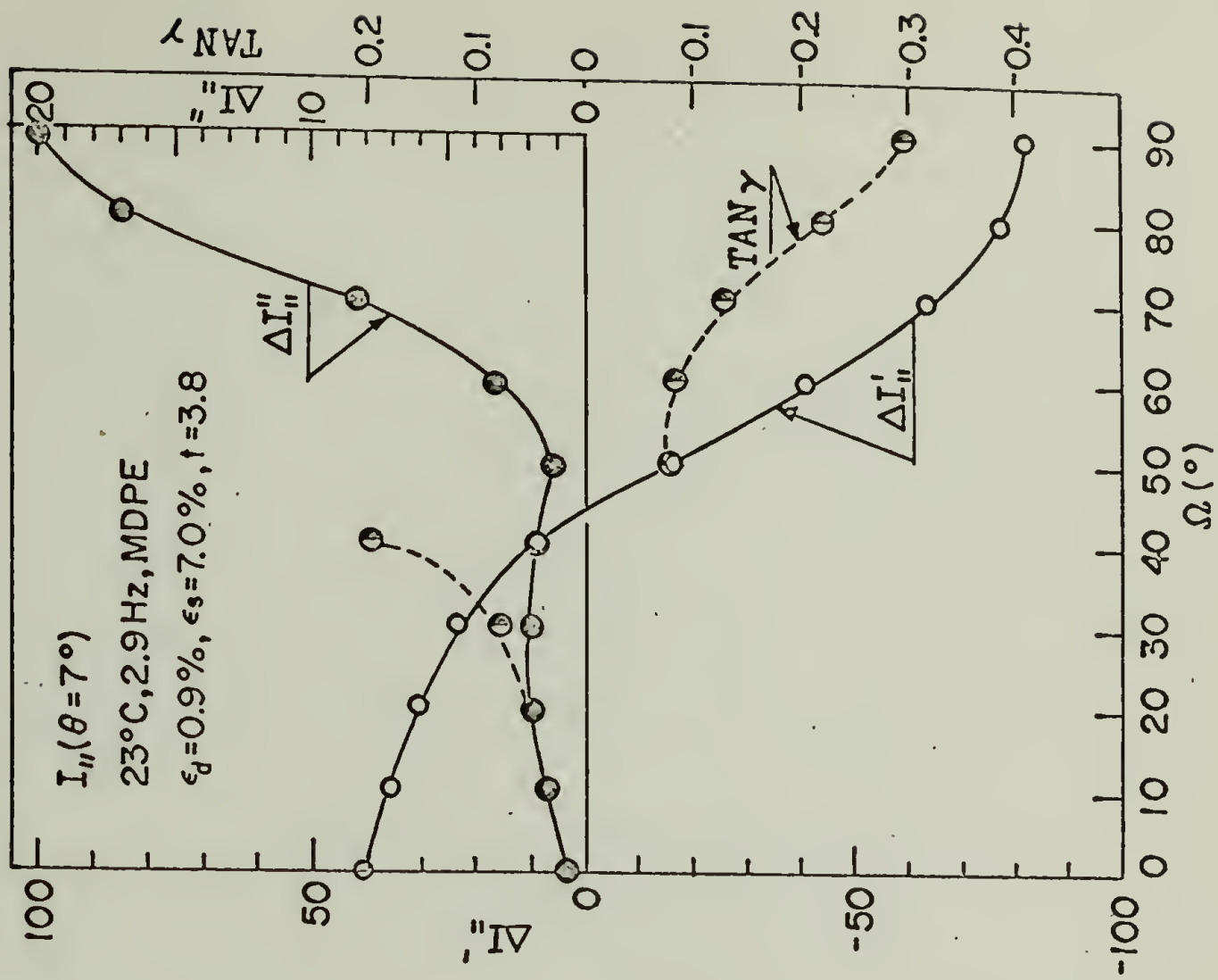


FIGURE III-30

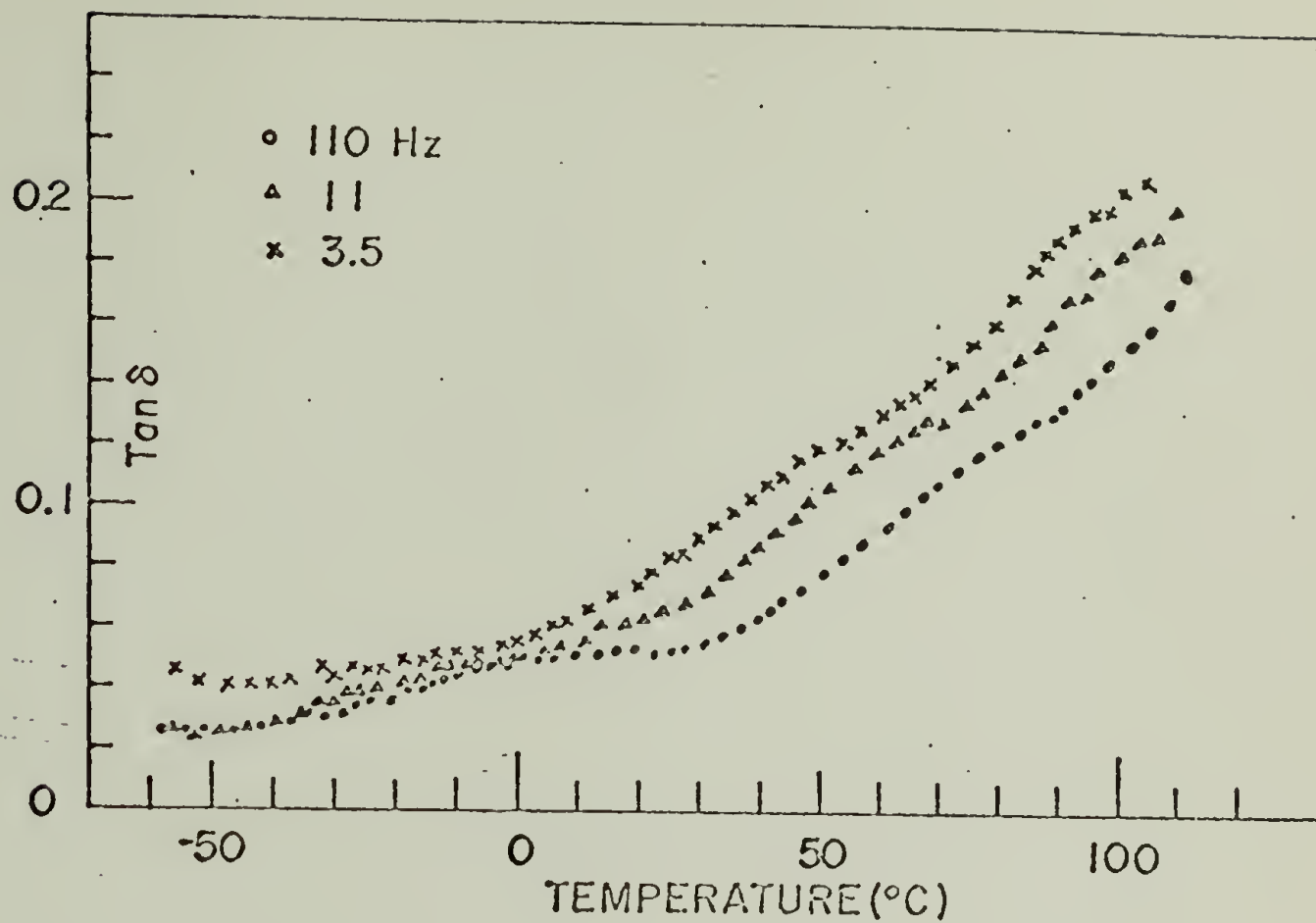


(a)

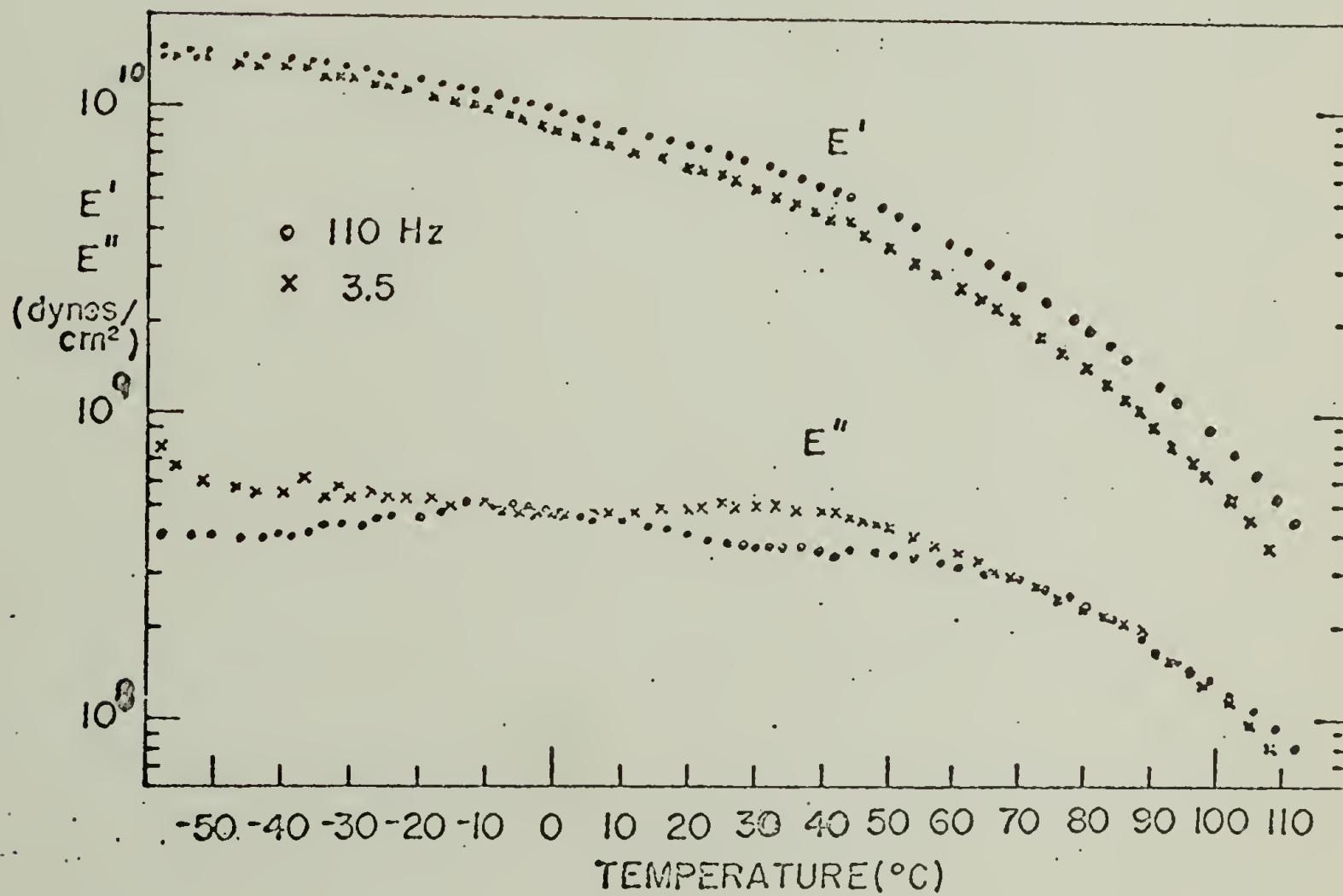


(b)

FIGURE III-31

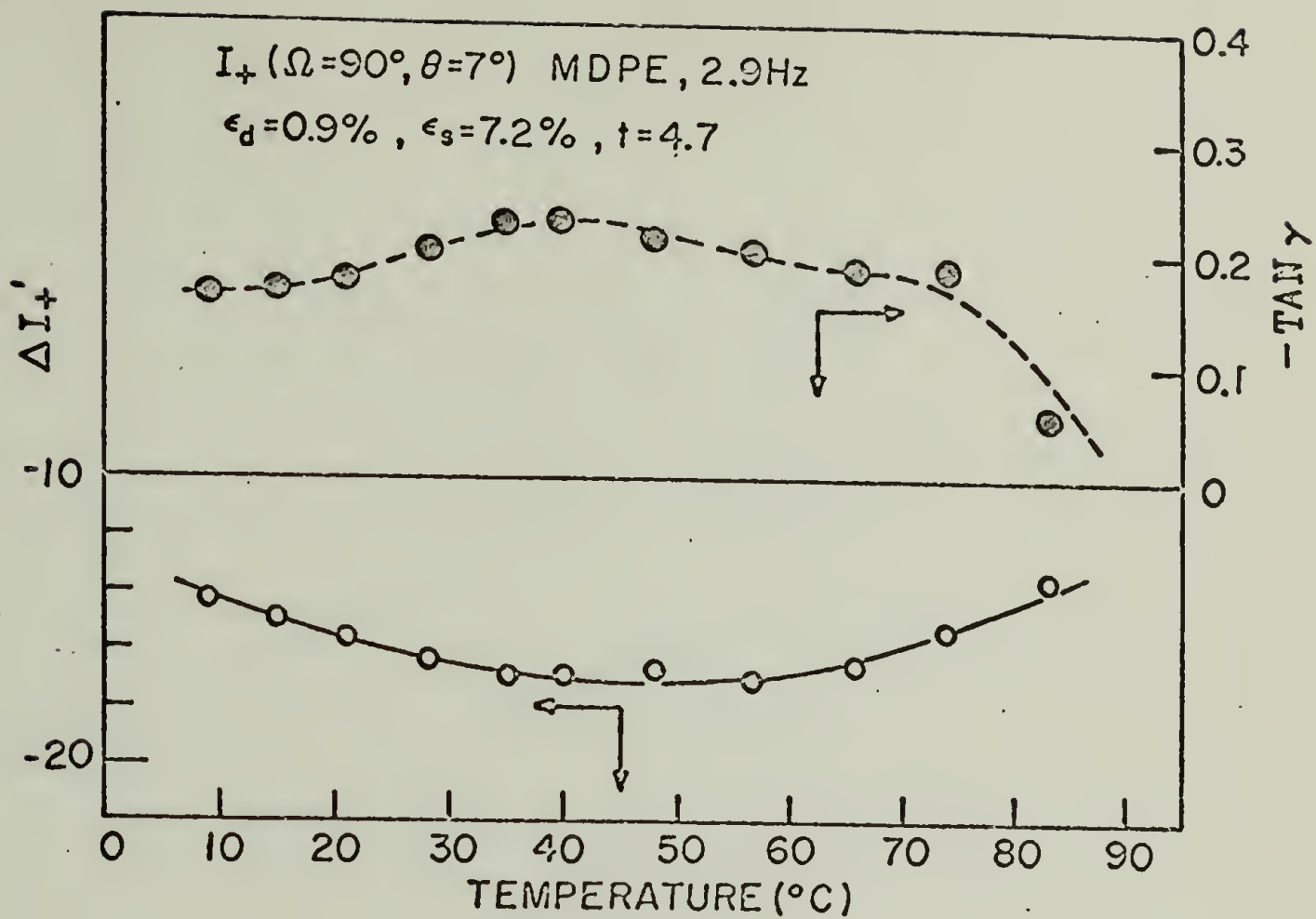


(a)

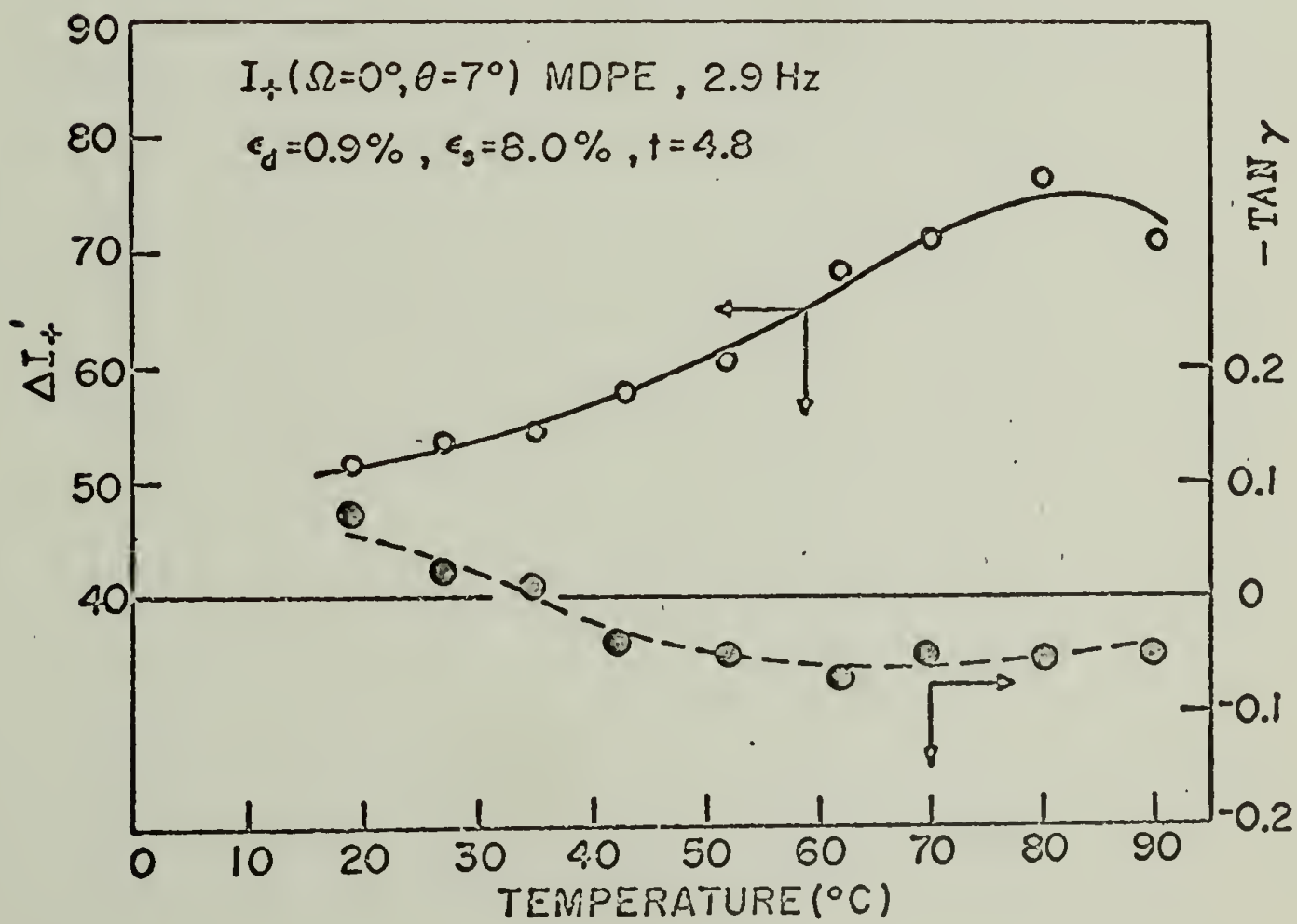


(b)

FIGURE III-32

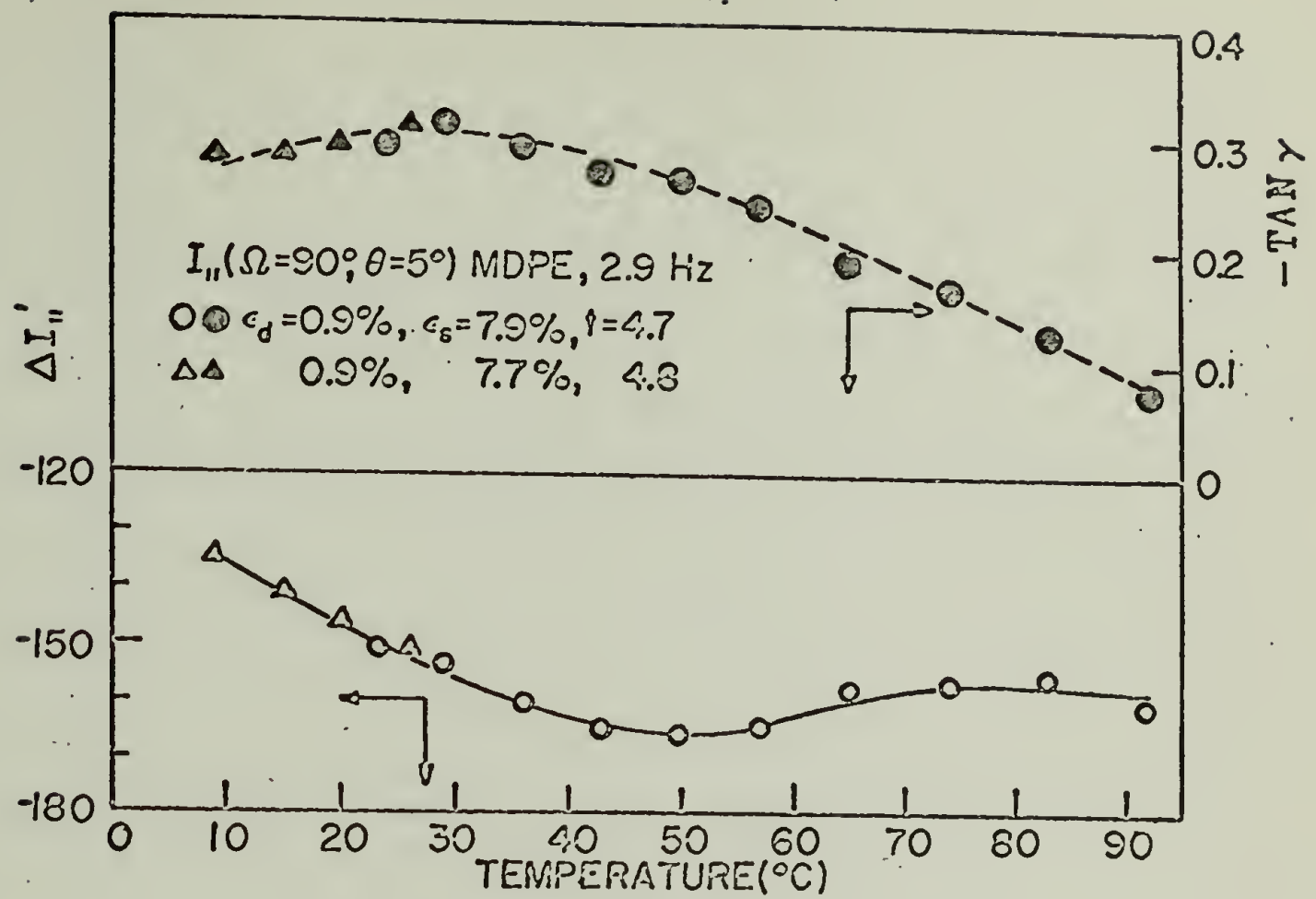


(a)

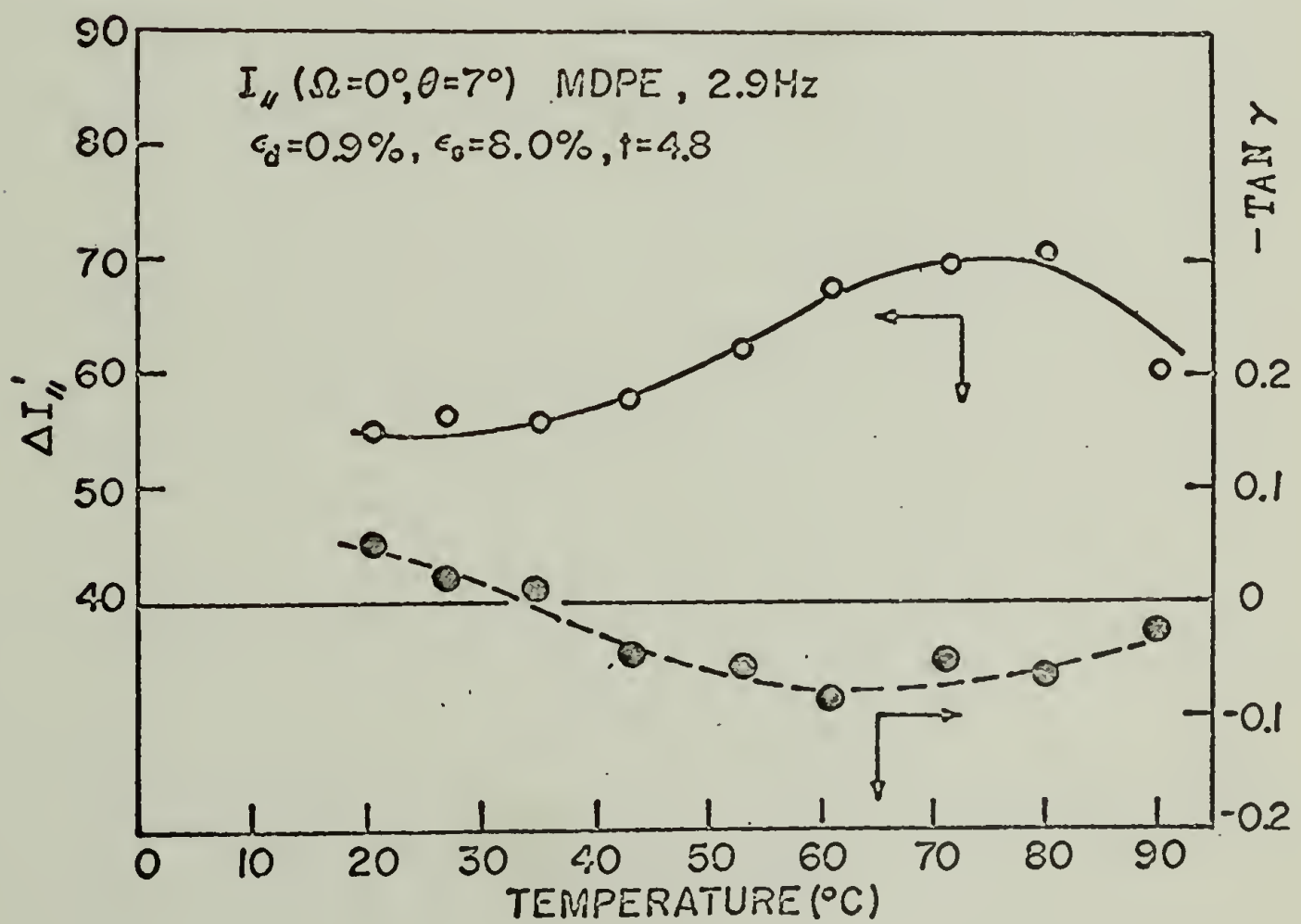


(b)

FIGURE III-33

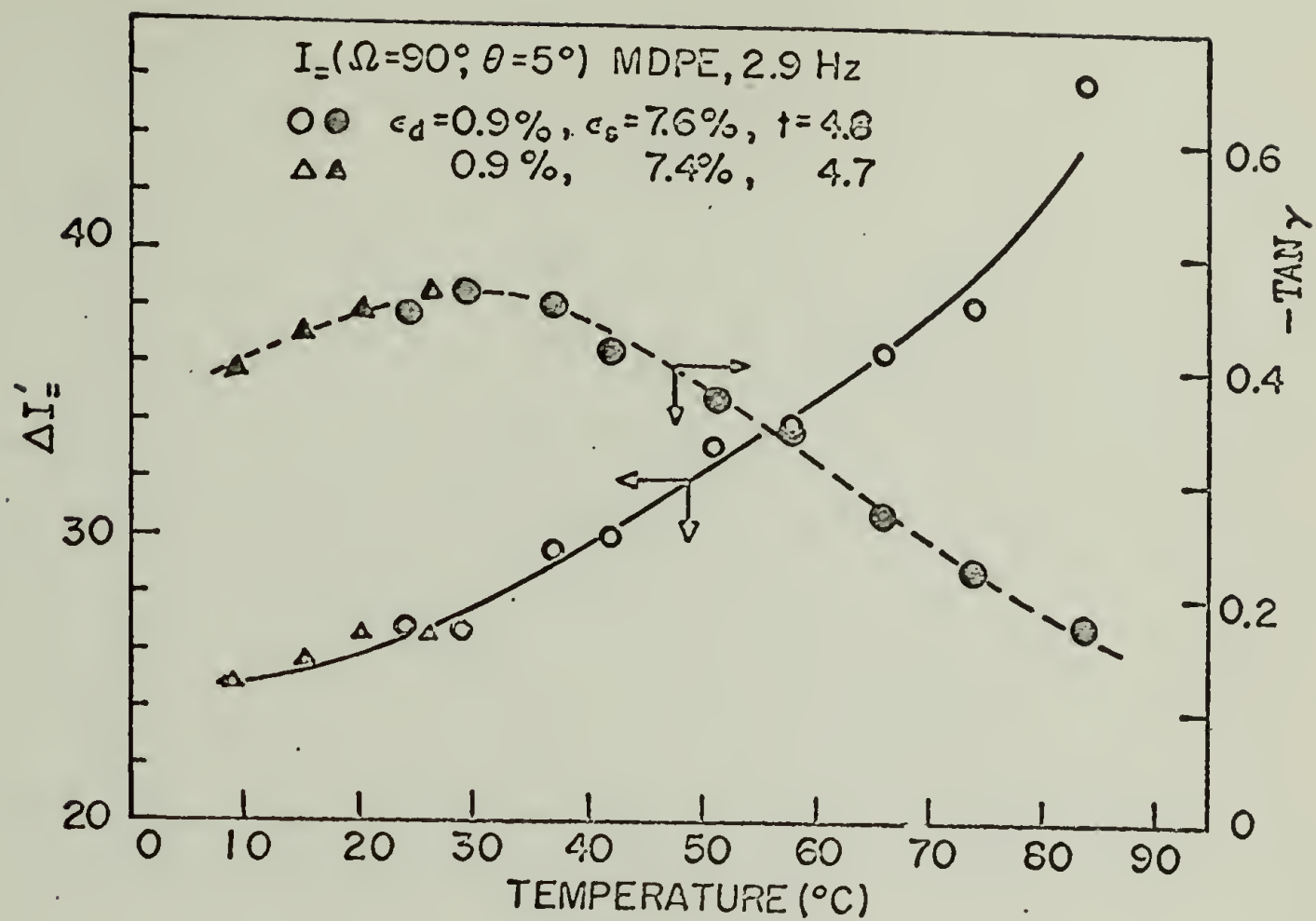


(a)

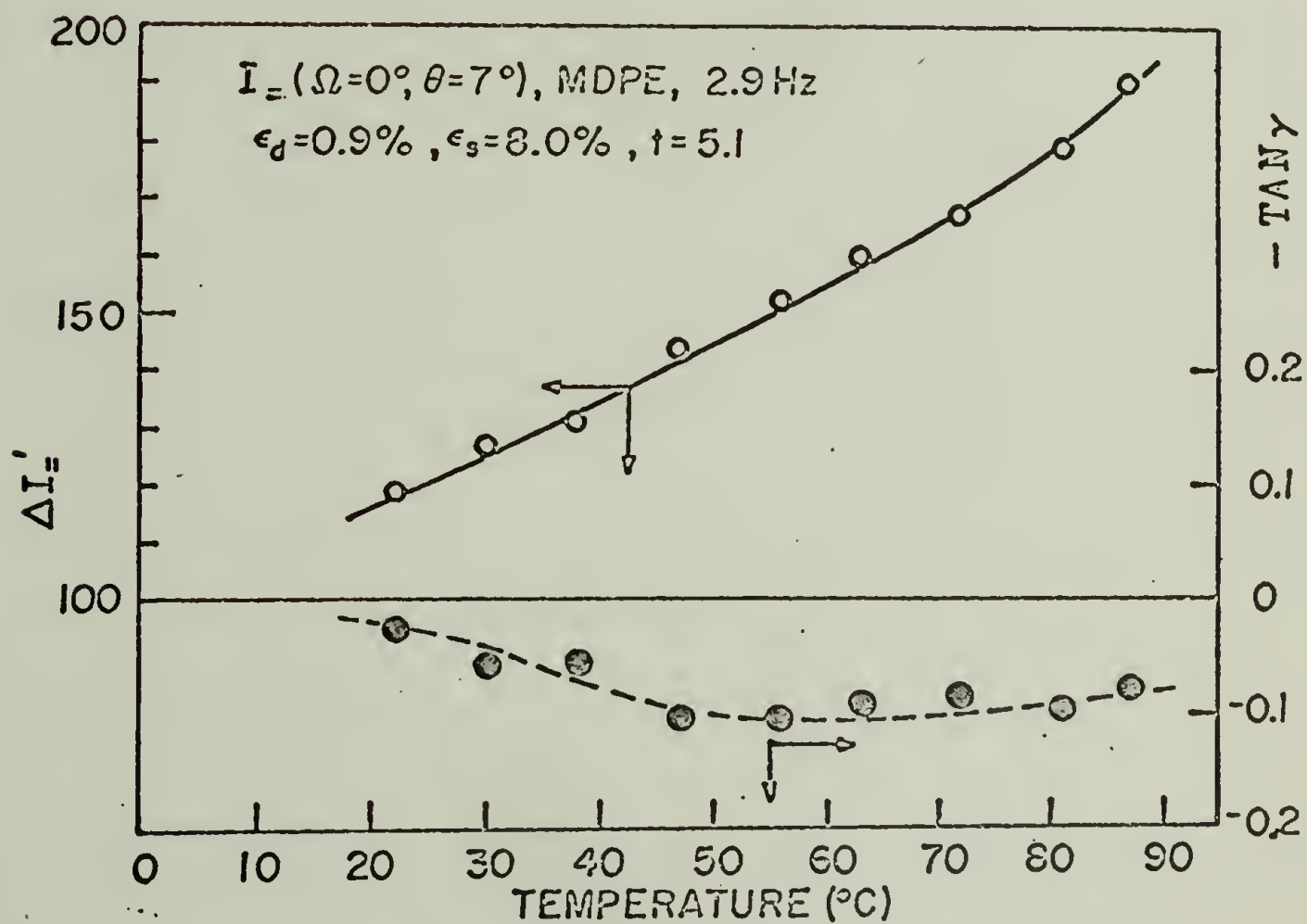


(b)

FIGURE III-34



(a)



(b)

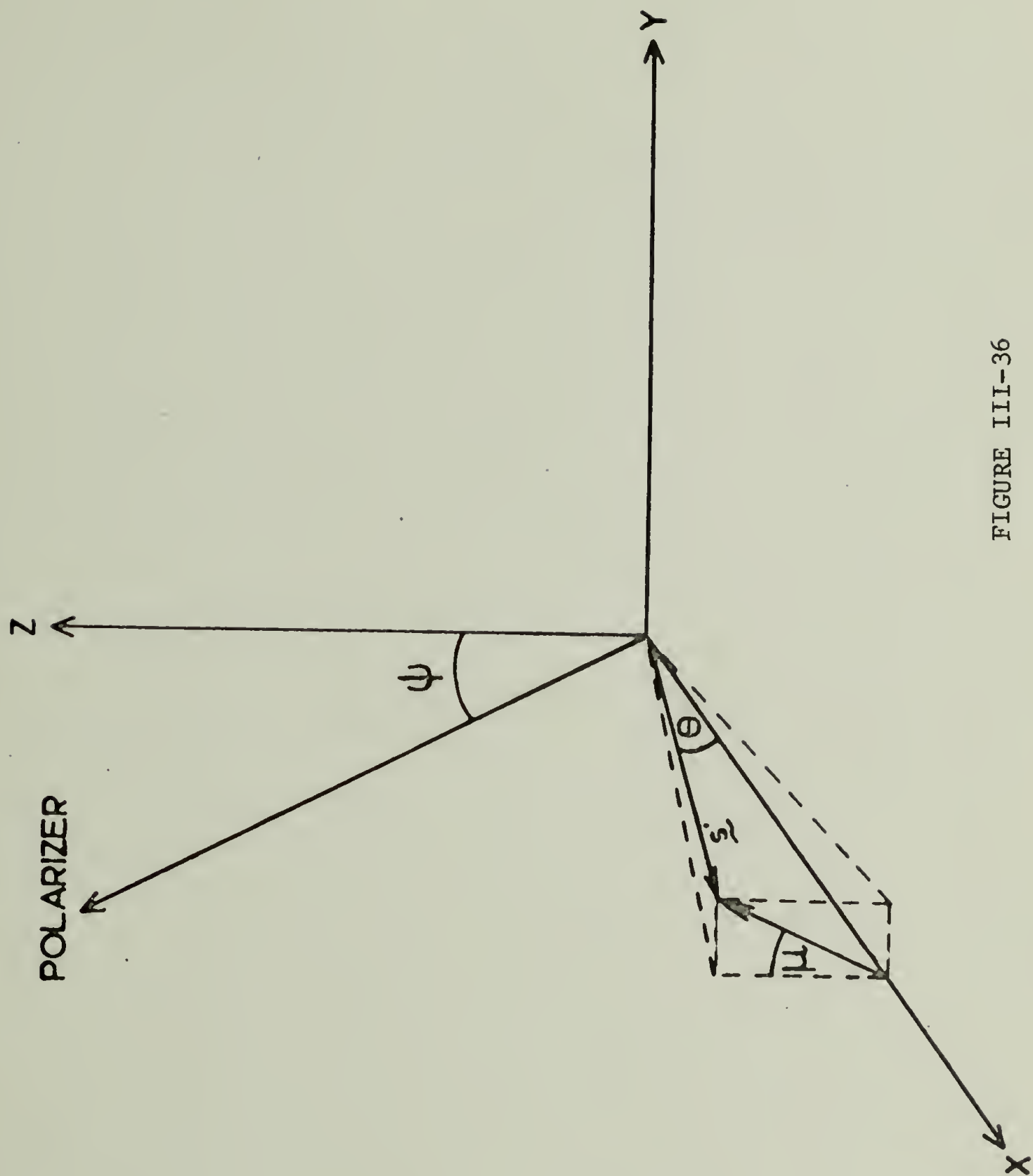


FIGURE III-36

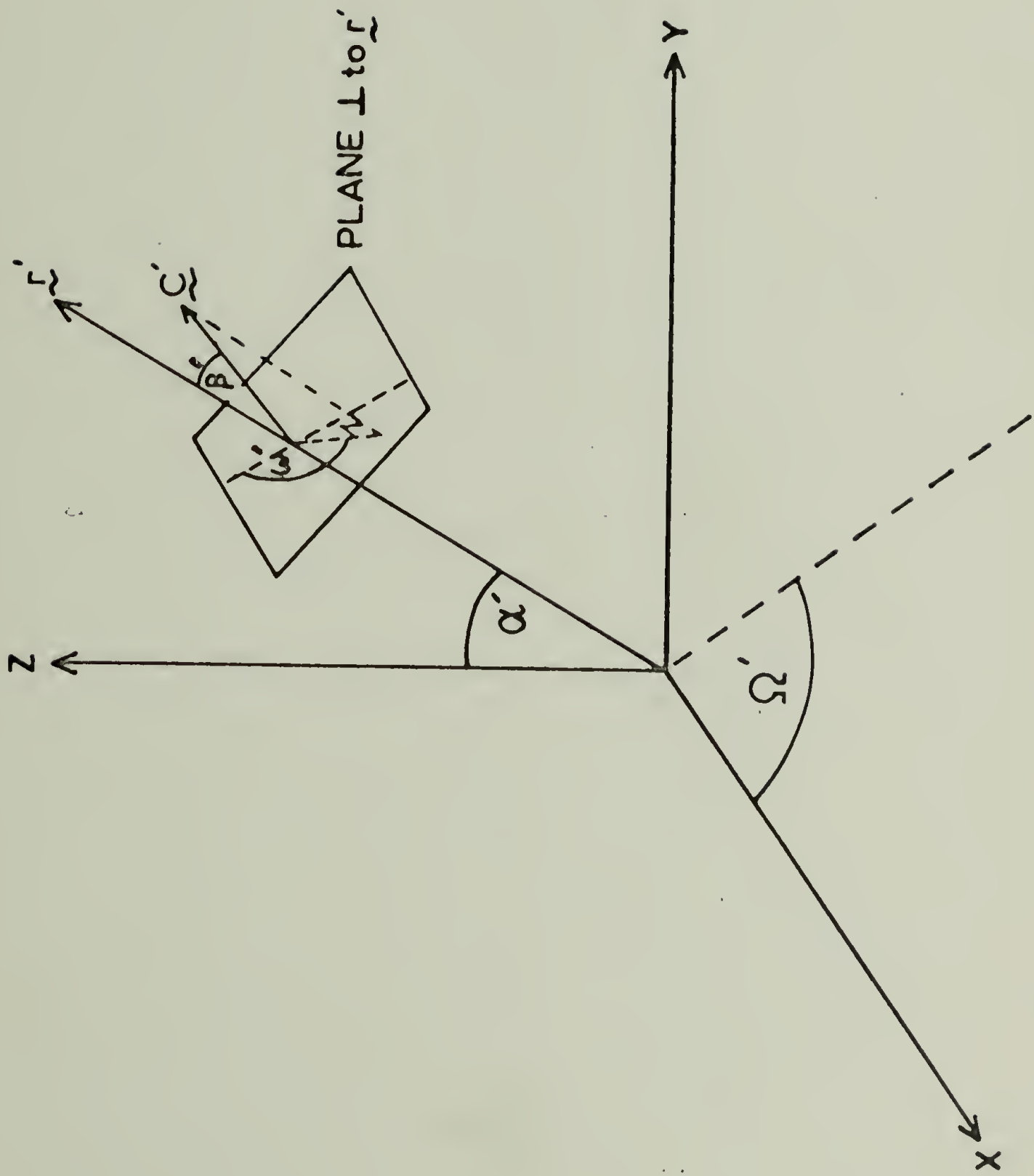
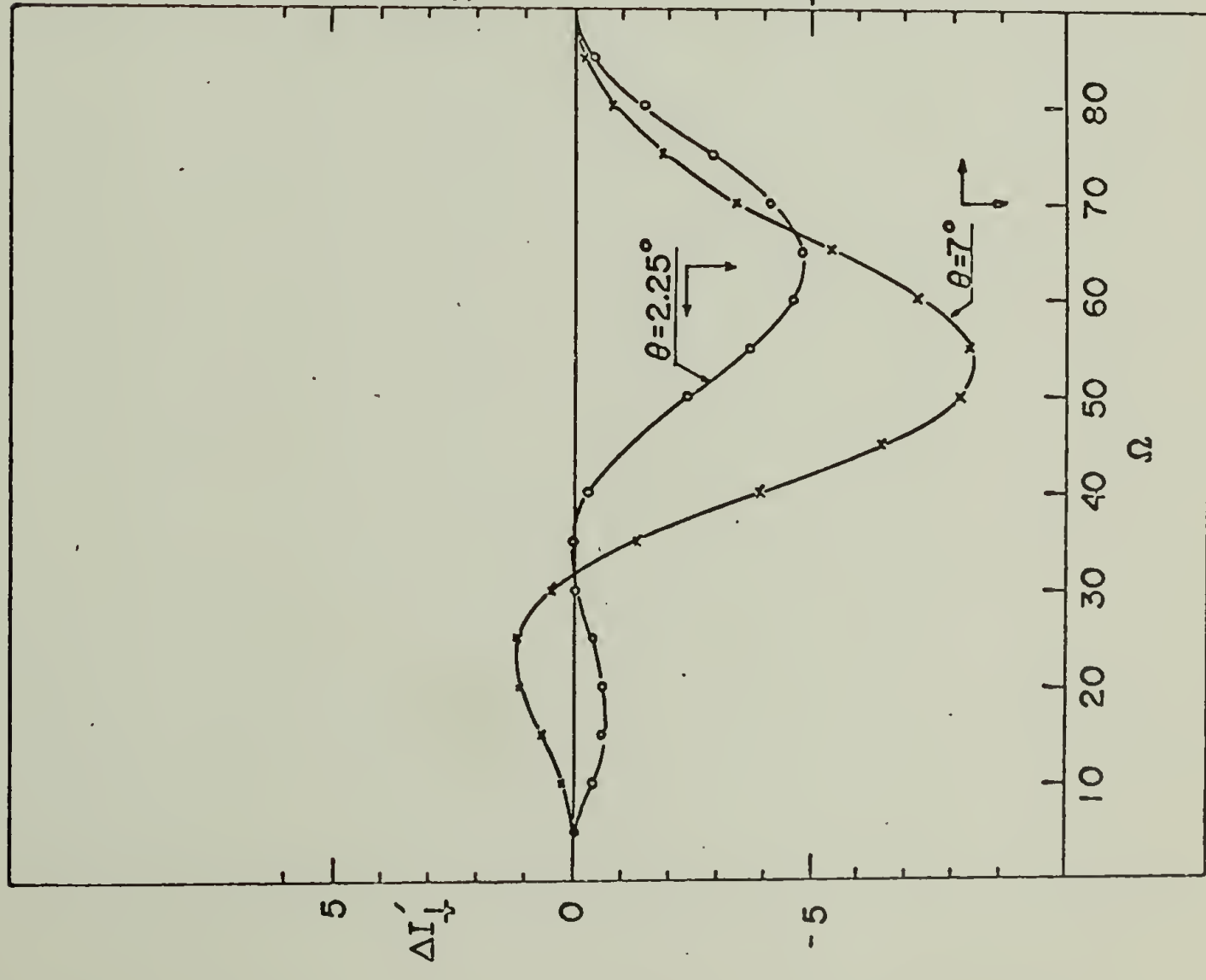
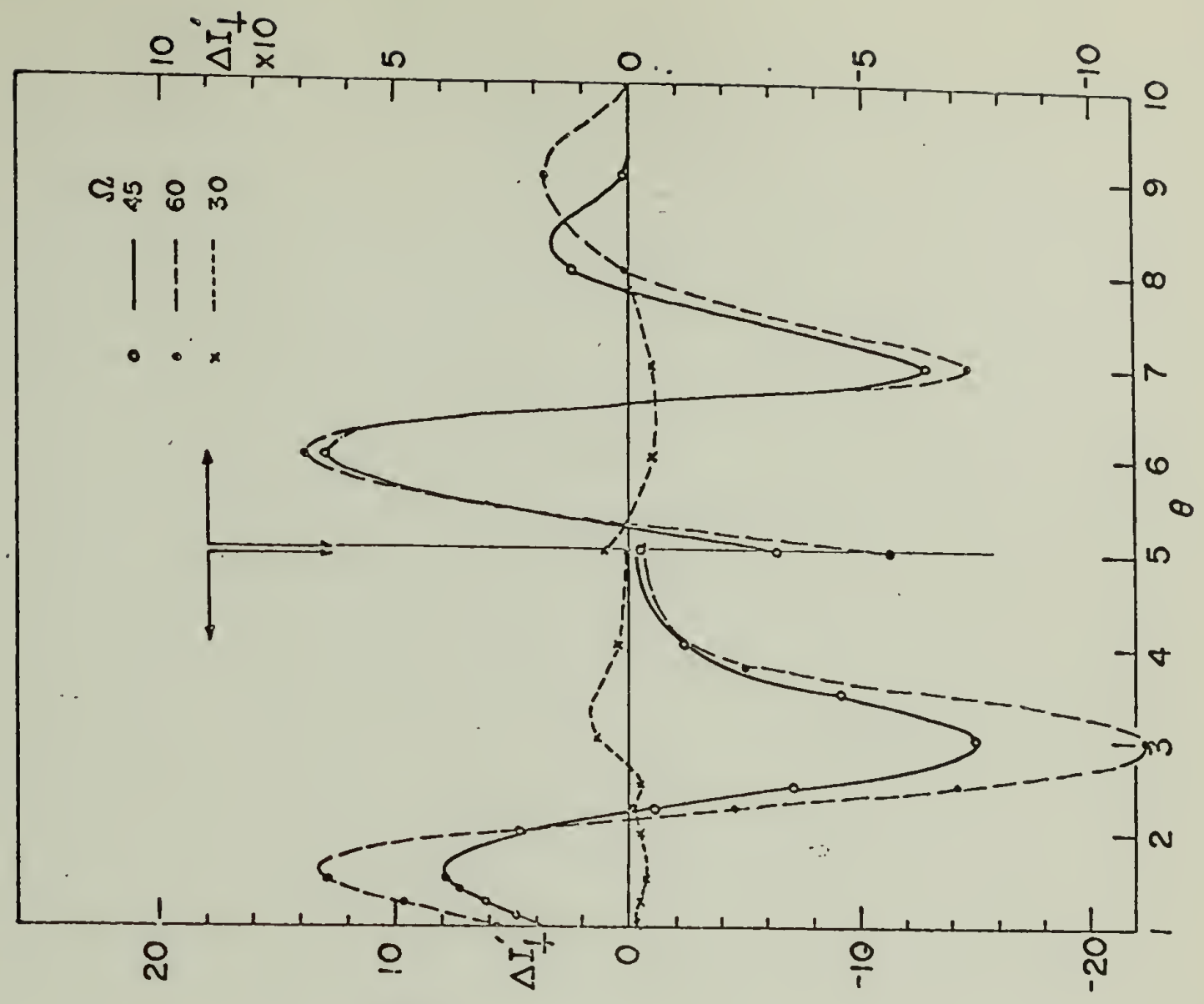


FIGURE III-37



(a)



(b)

FIGURE III-38

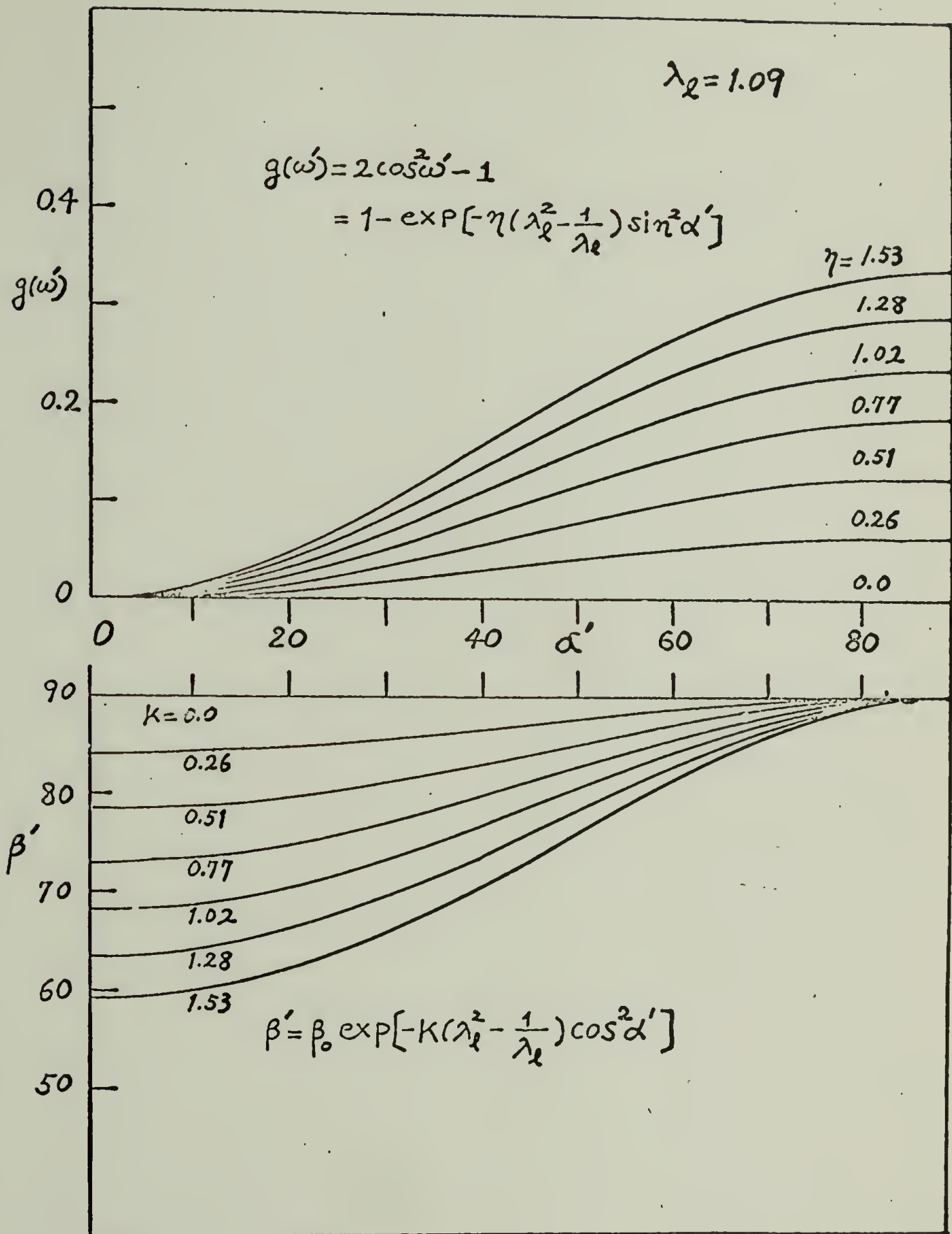


FIGURE III-39

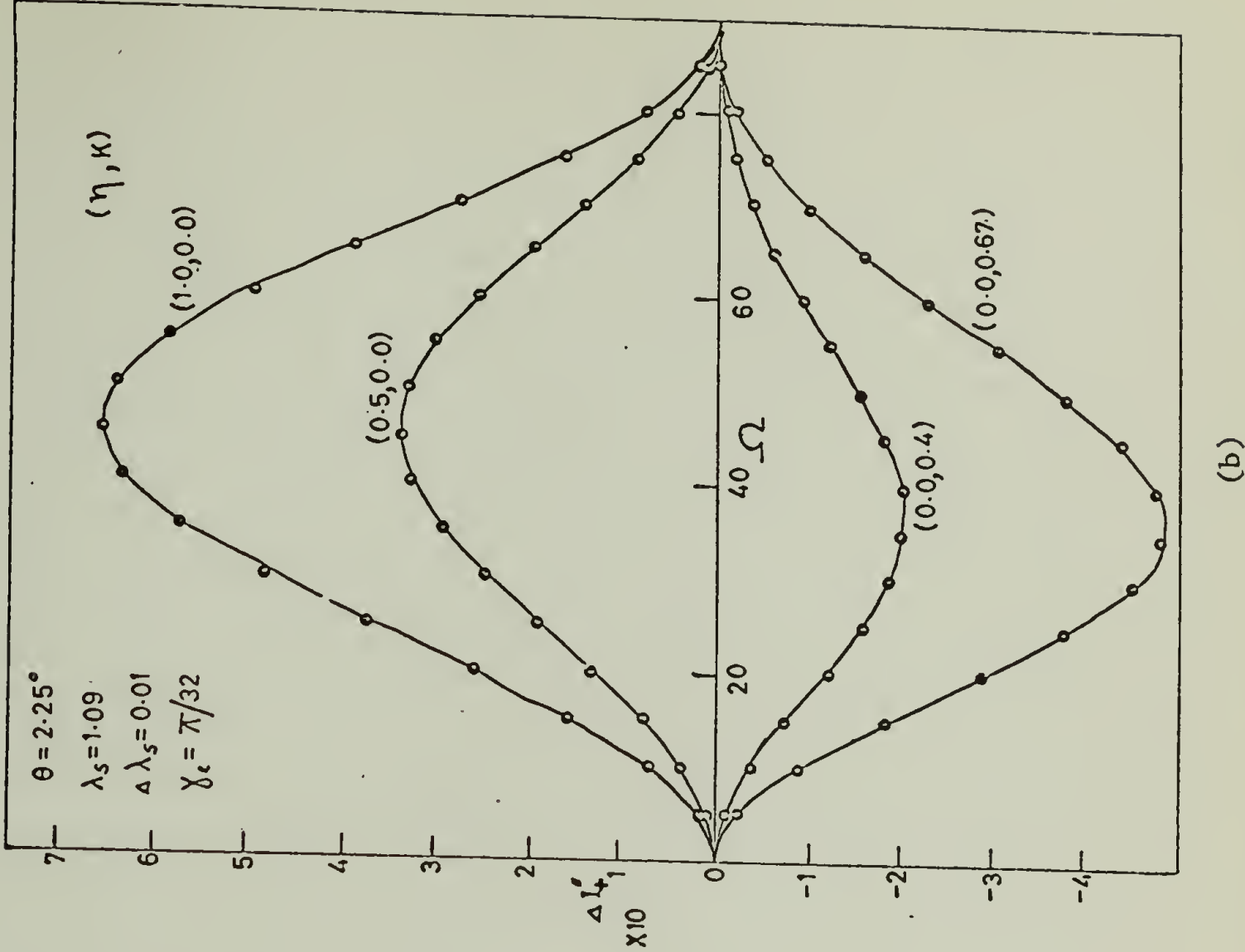
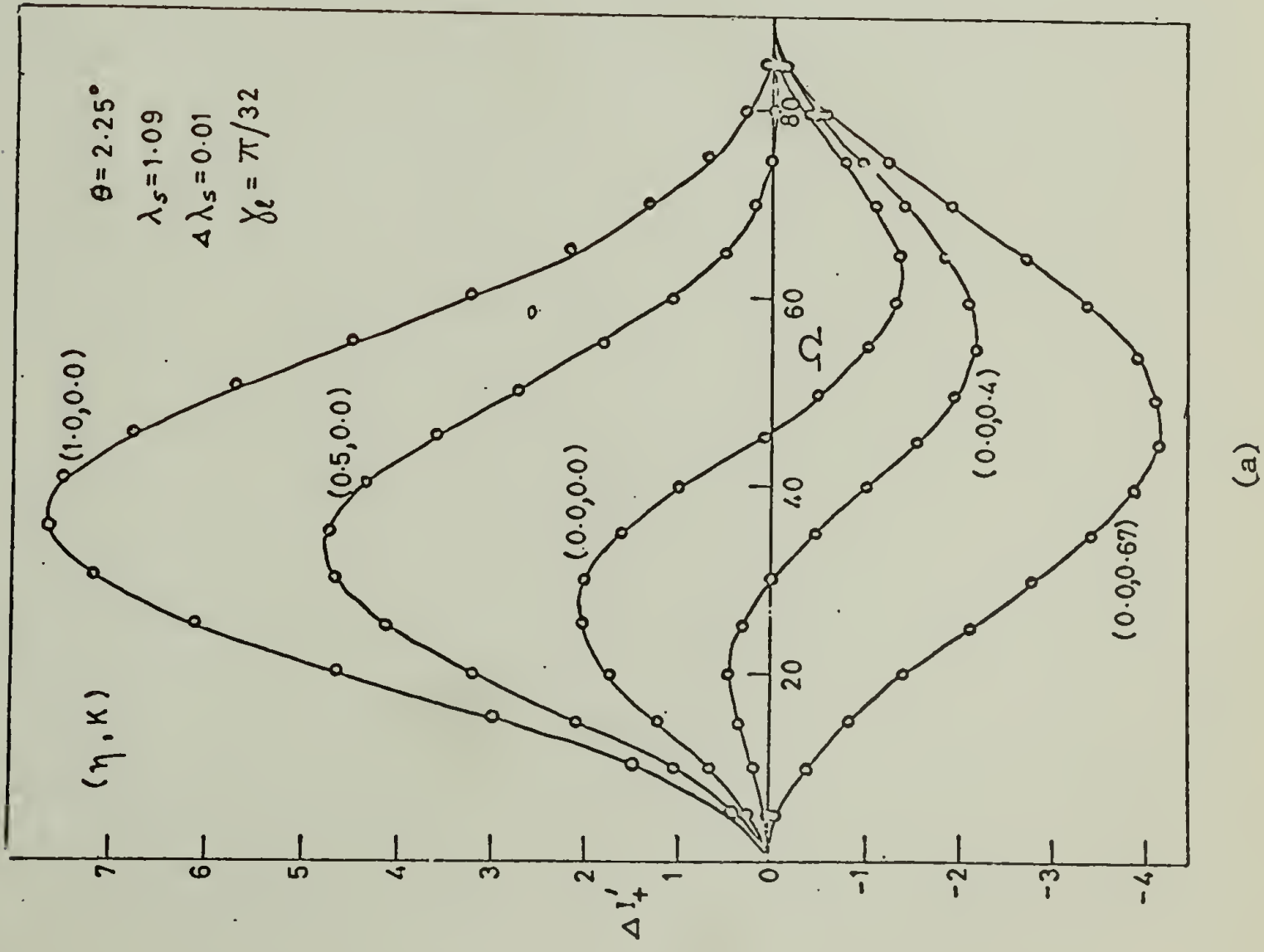
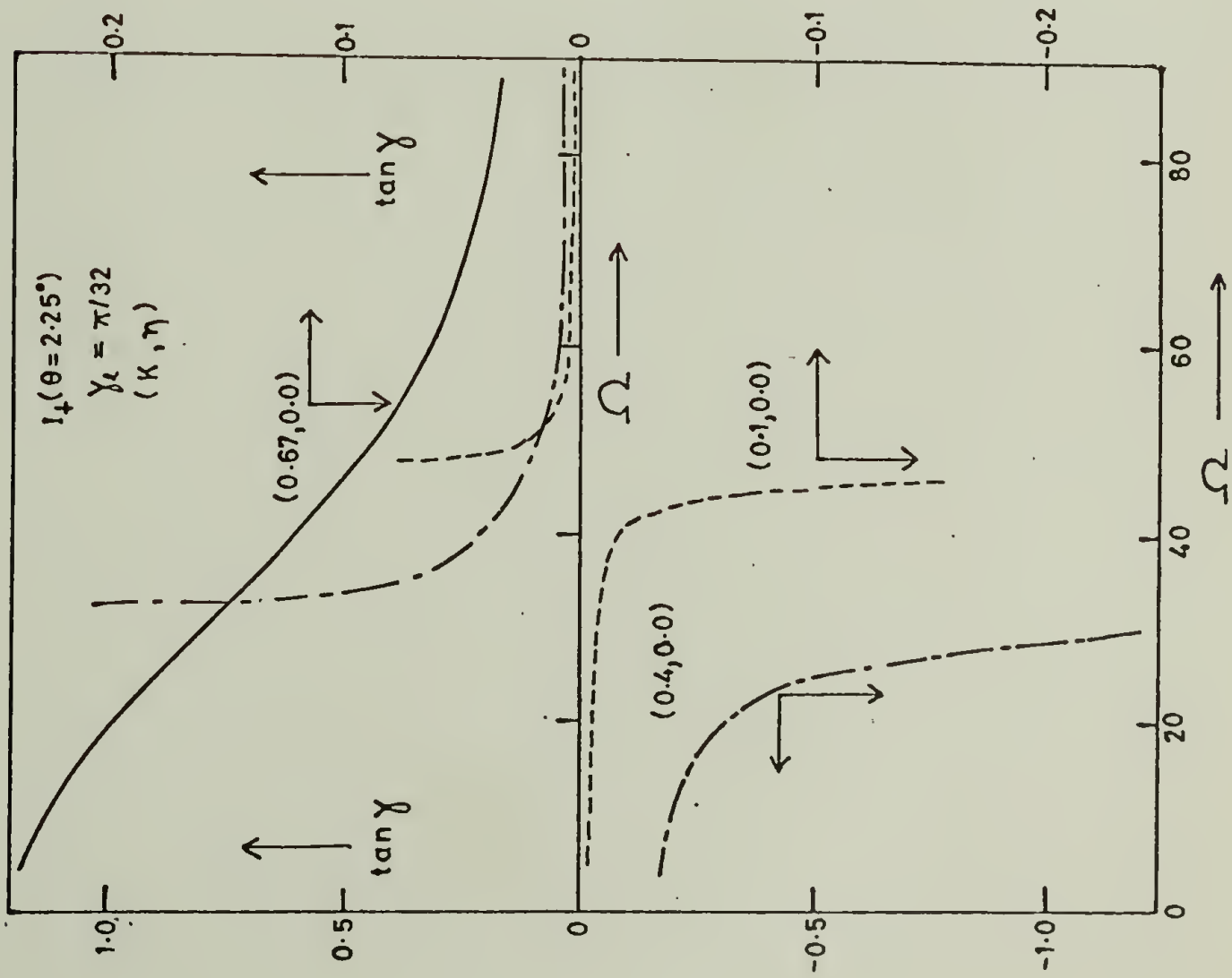
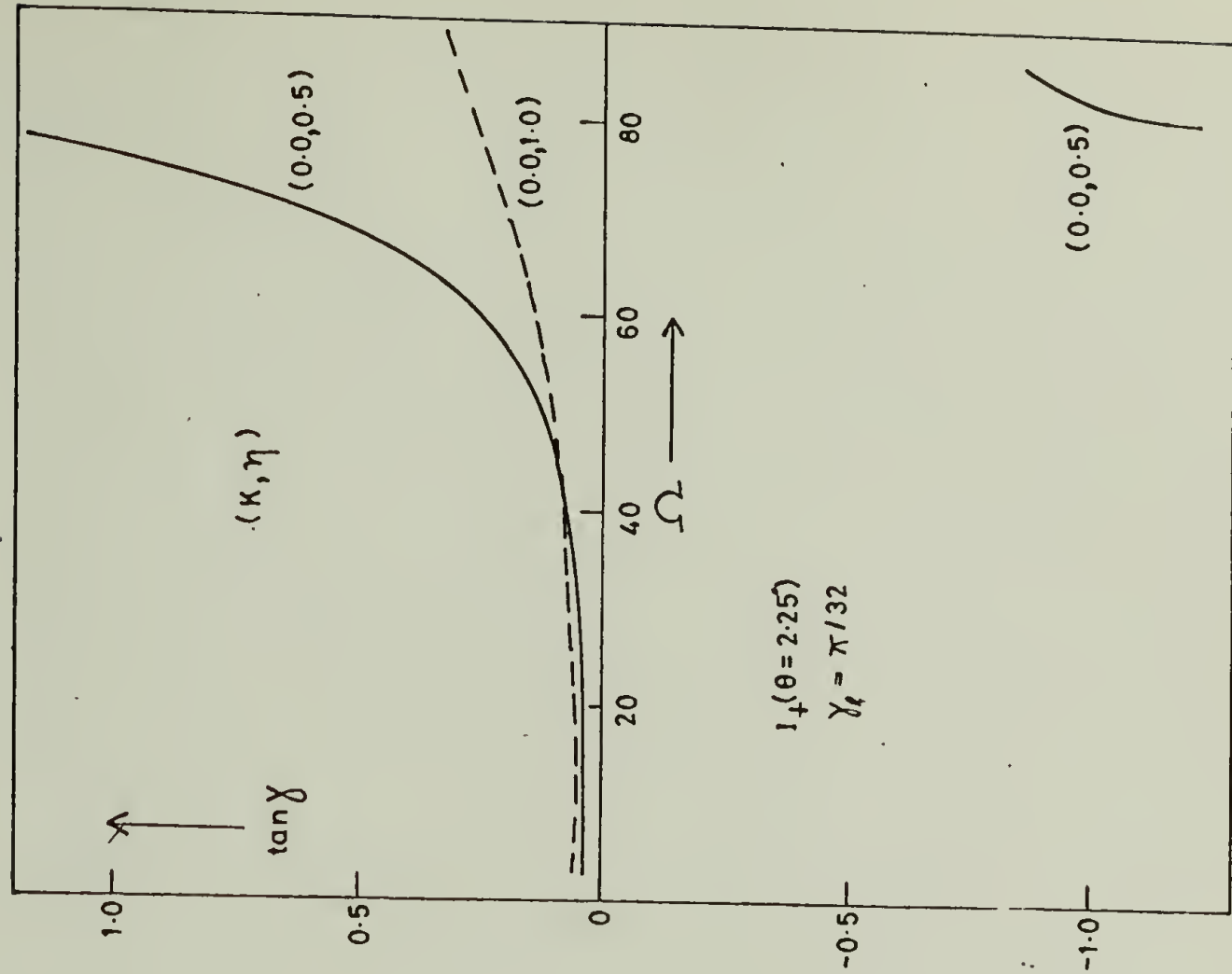


FIGURE III-40



(a)



(b)

FIGURE III-41

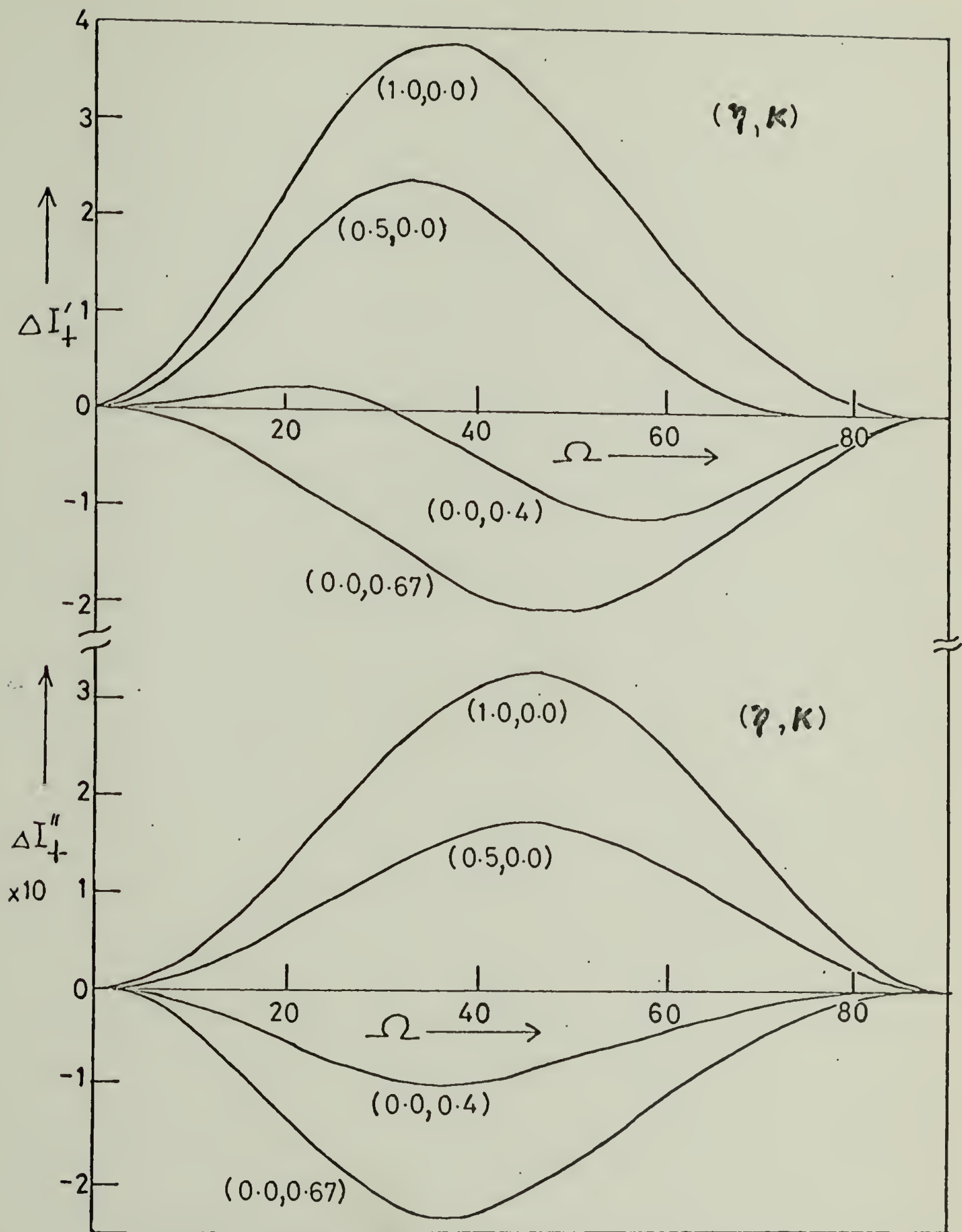


FIGURE. III-42

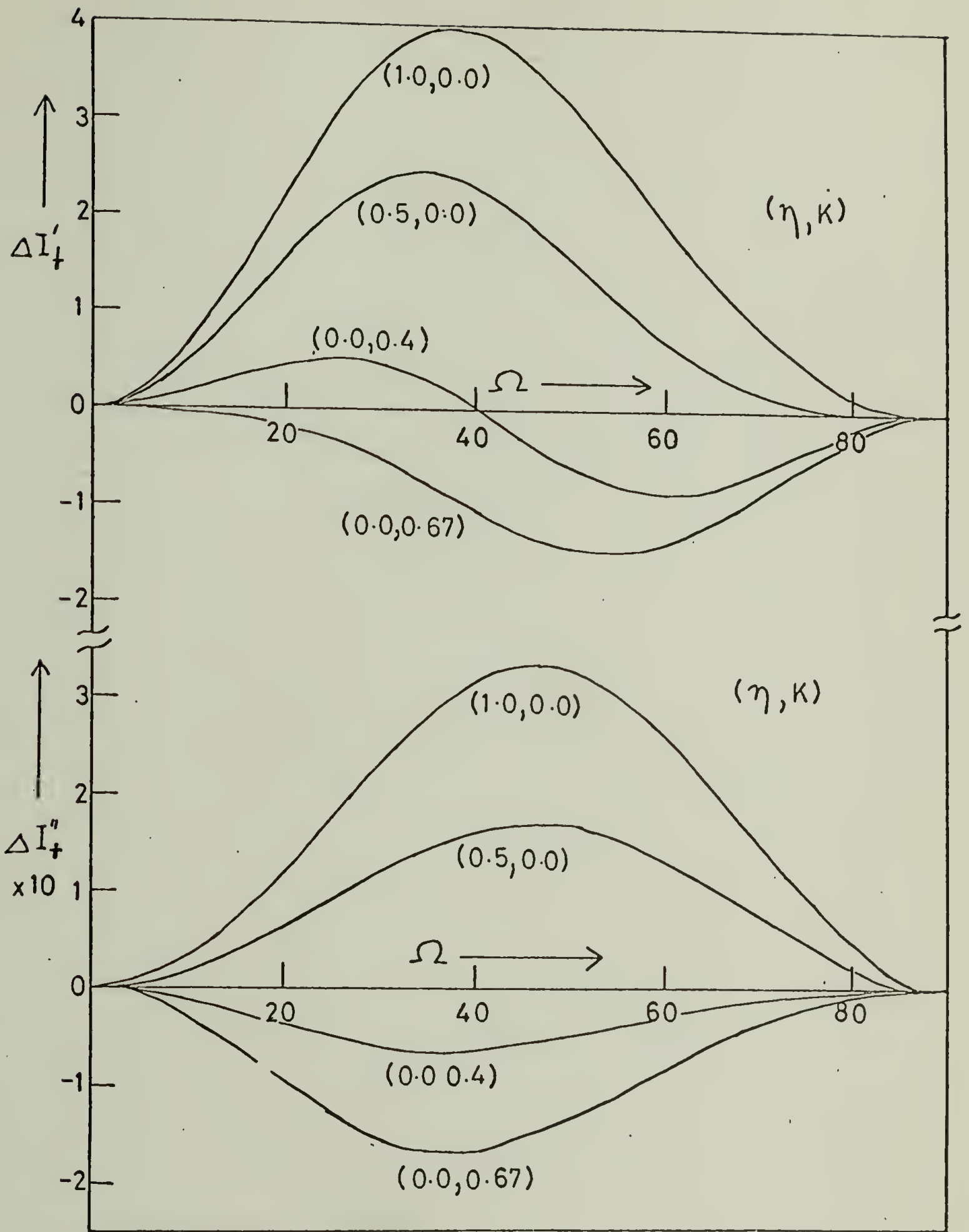
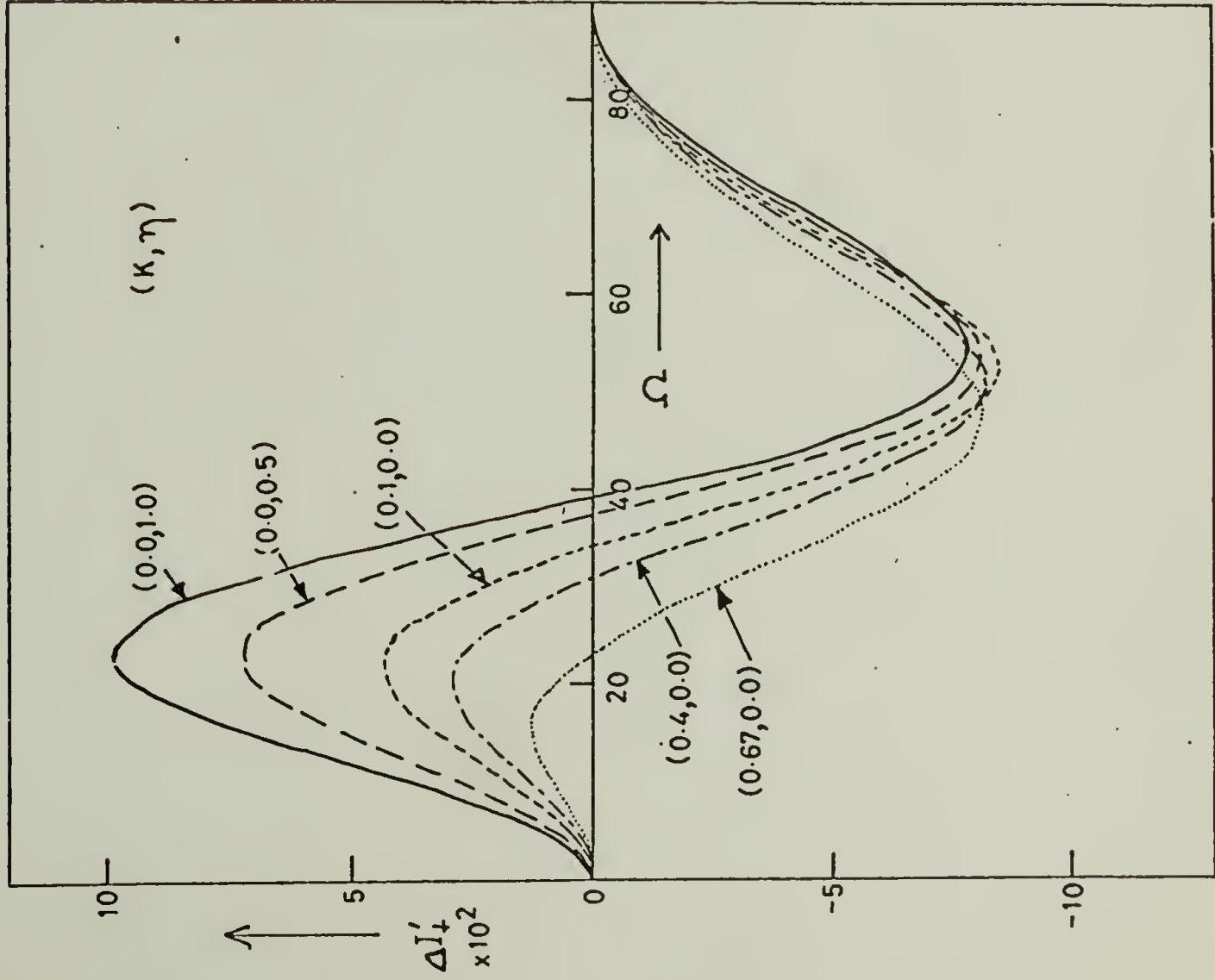
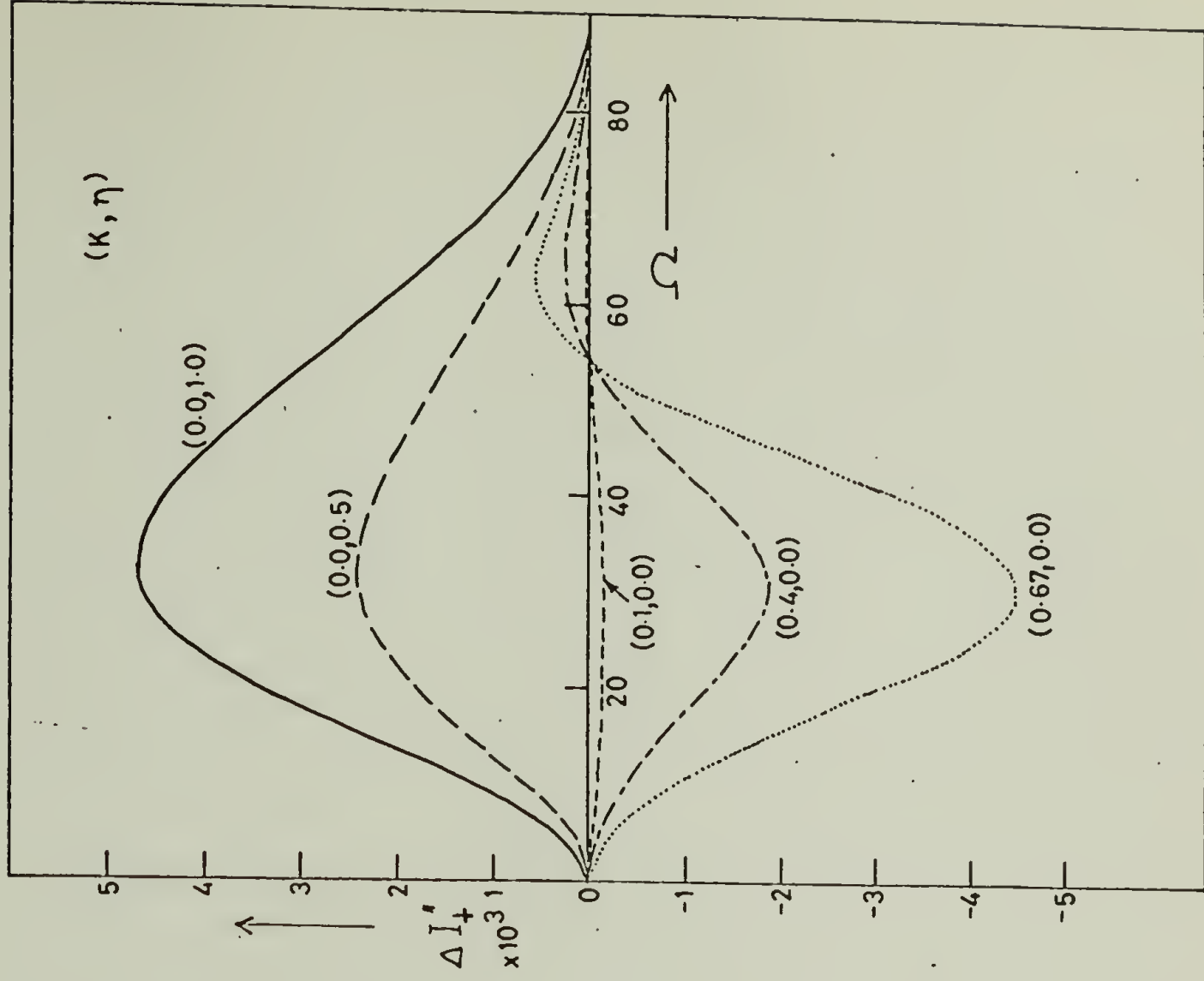


FIGURE III-43.



(a)



(b)

FIGURE III-44

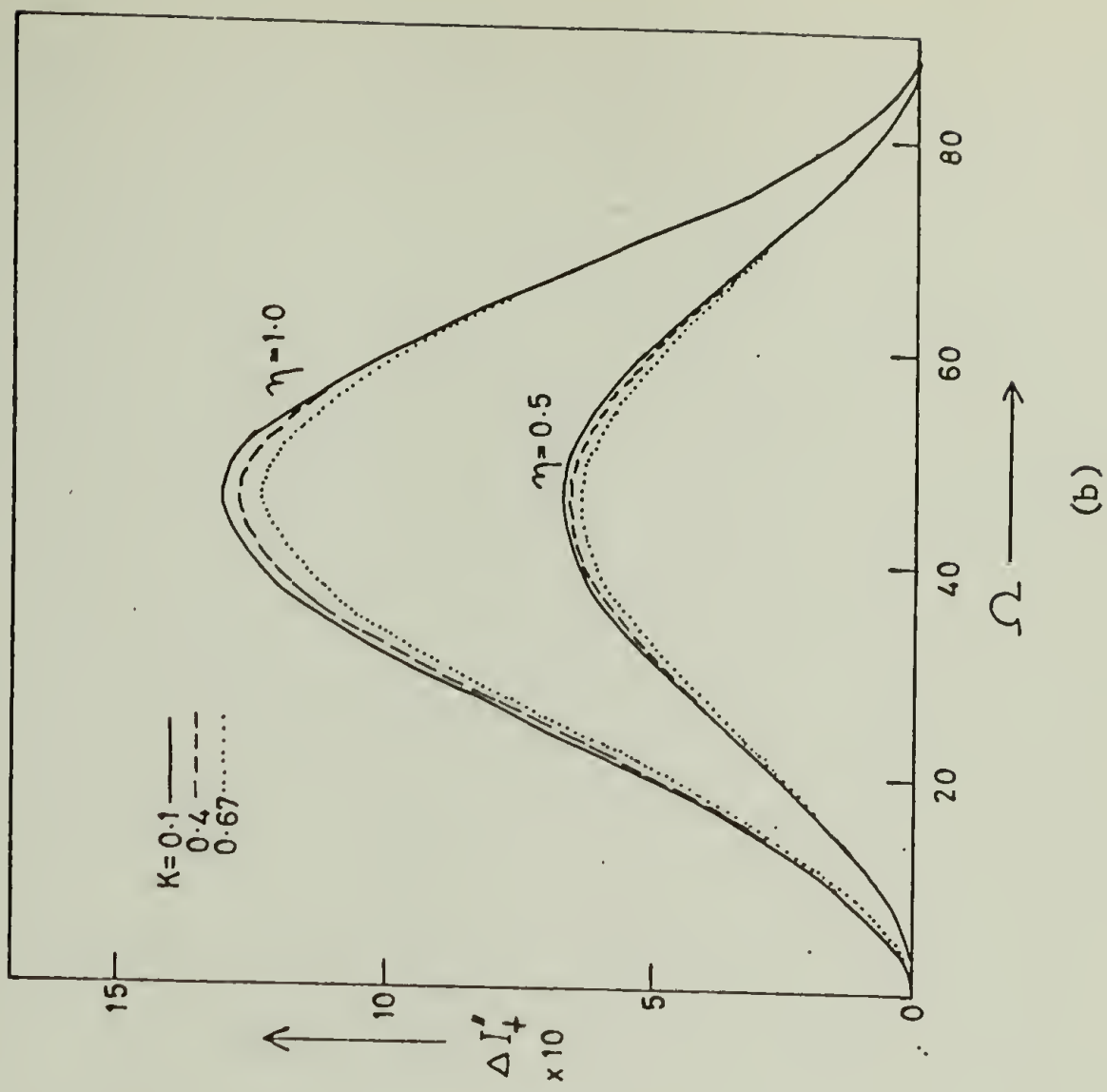
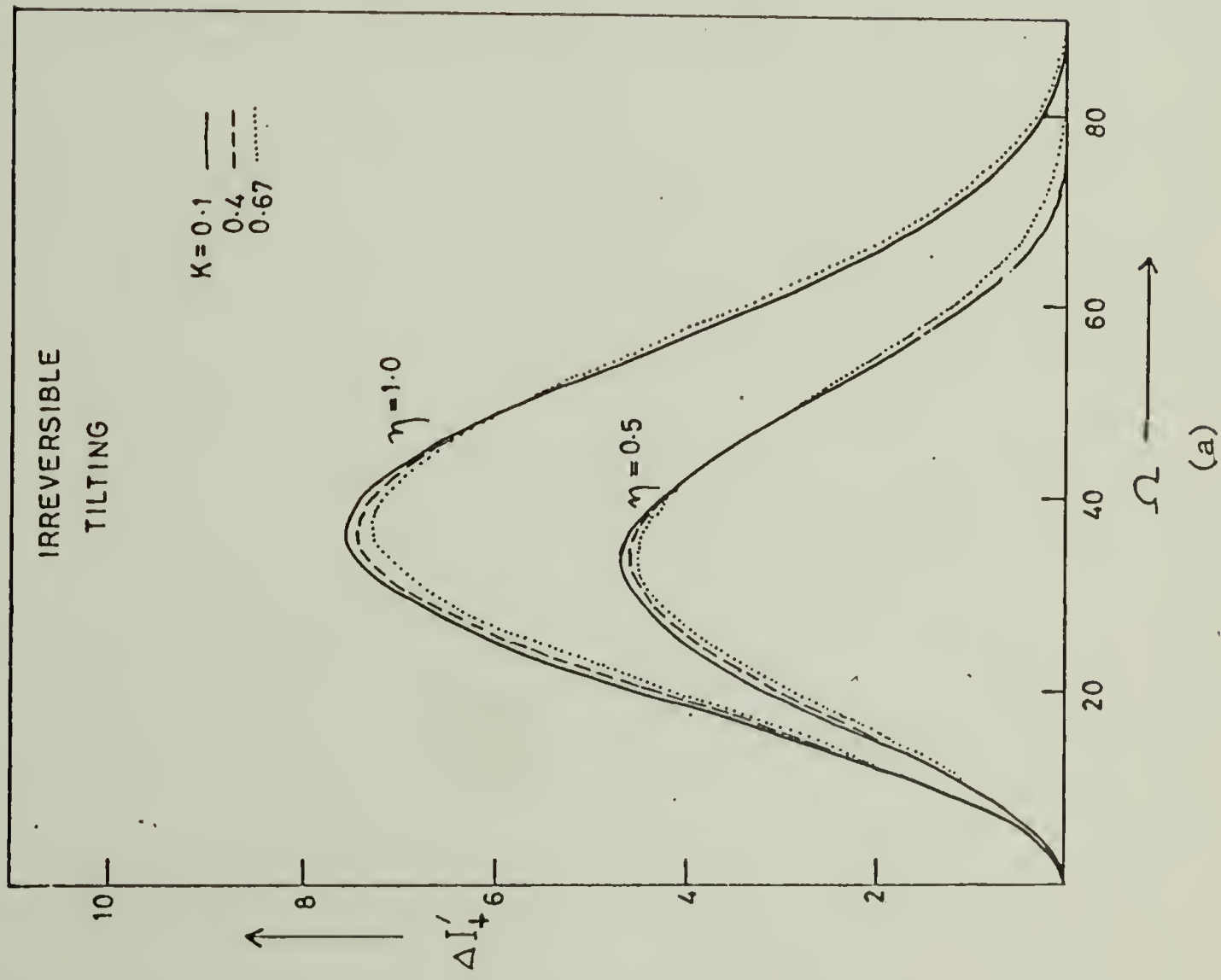


FIGURE III-45

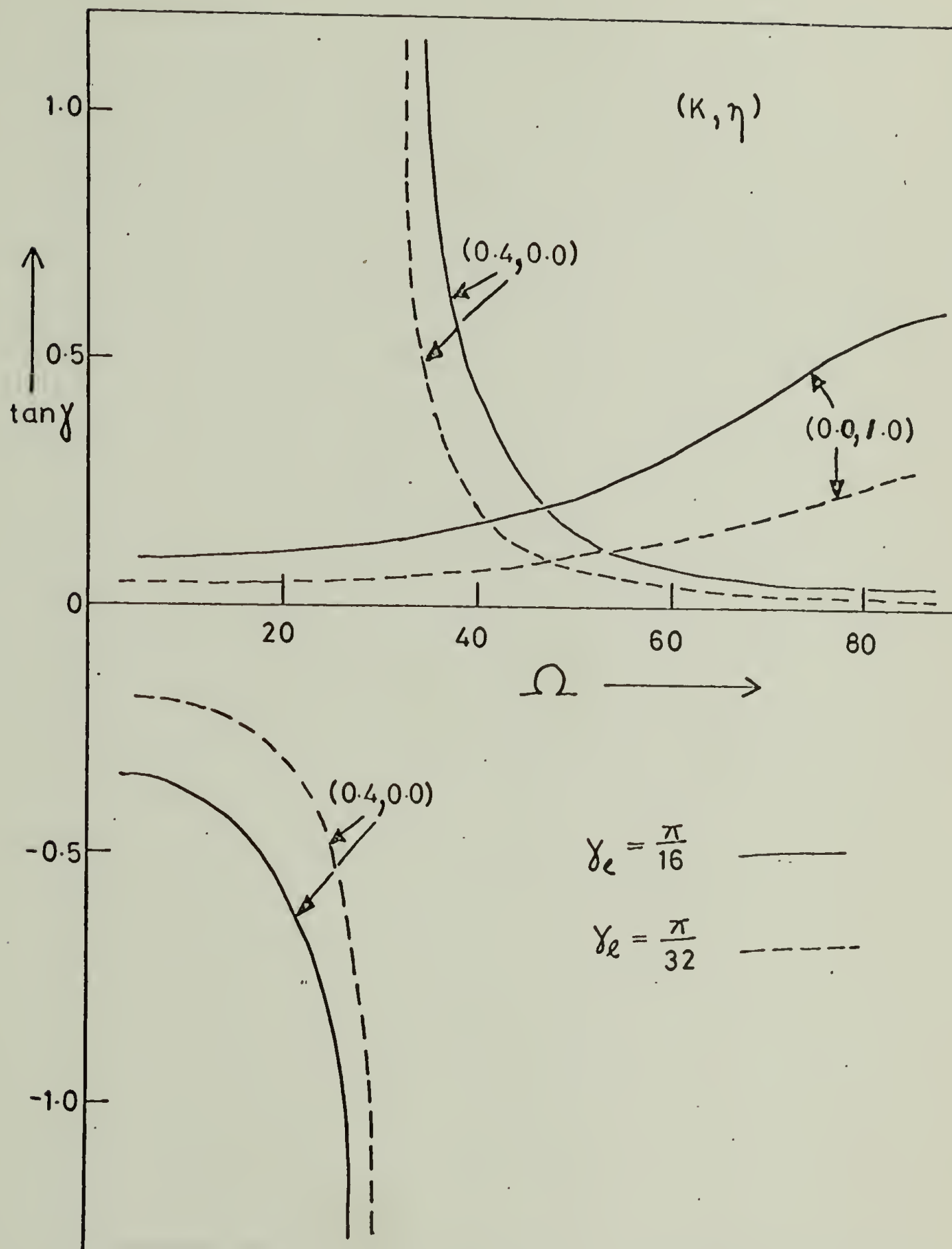


FIGURE III-46

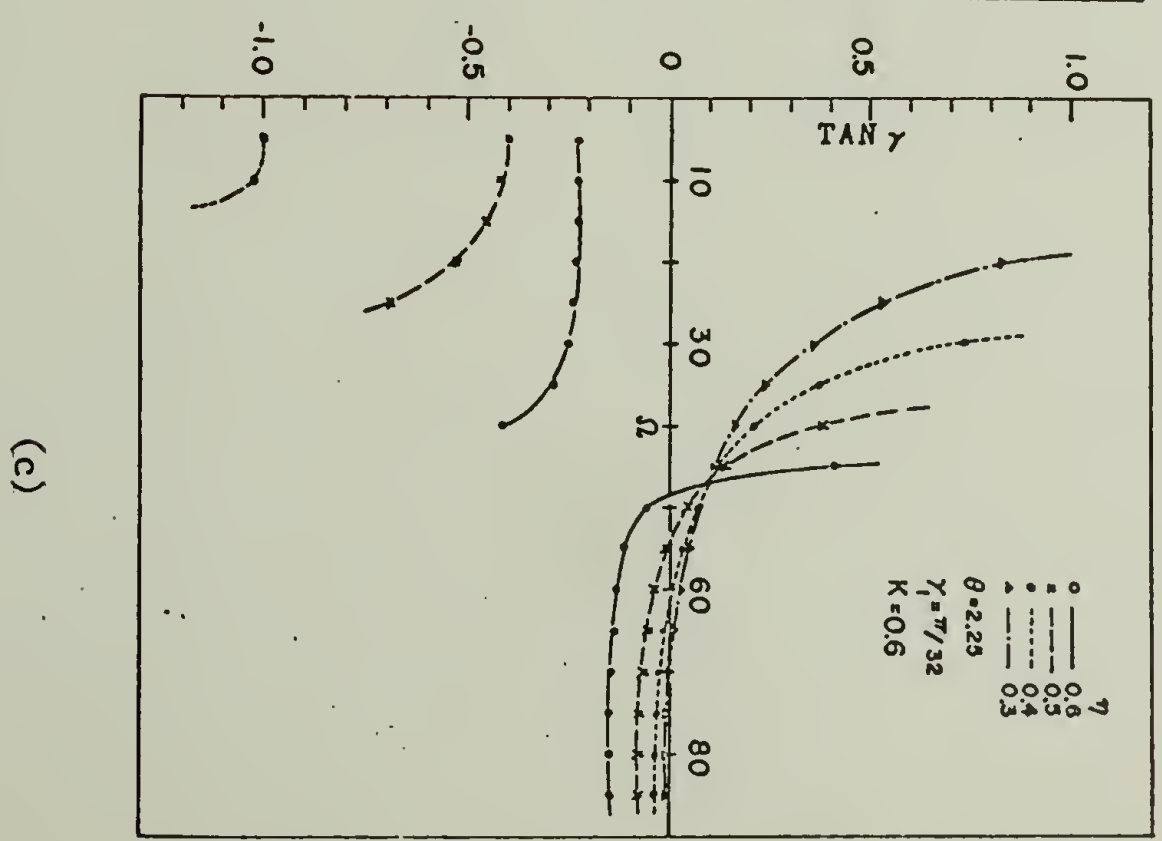
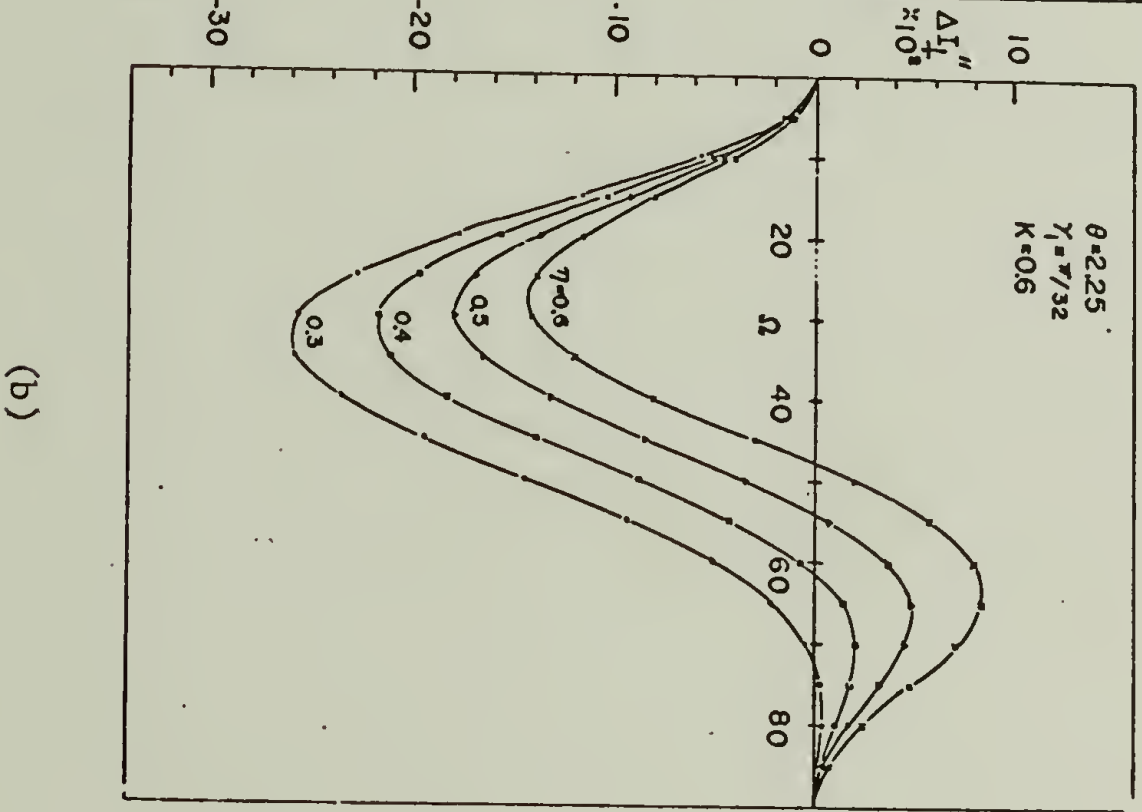
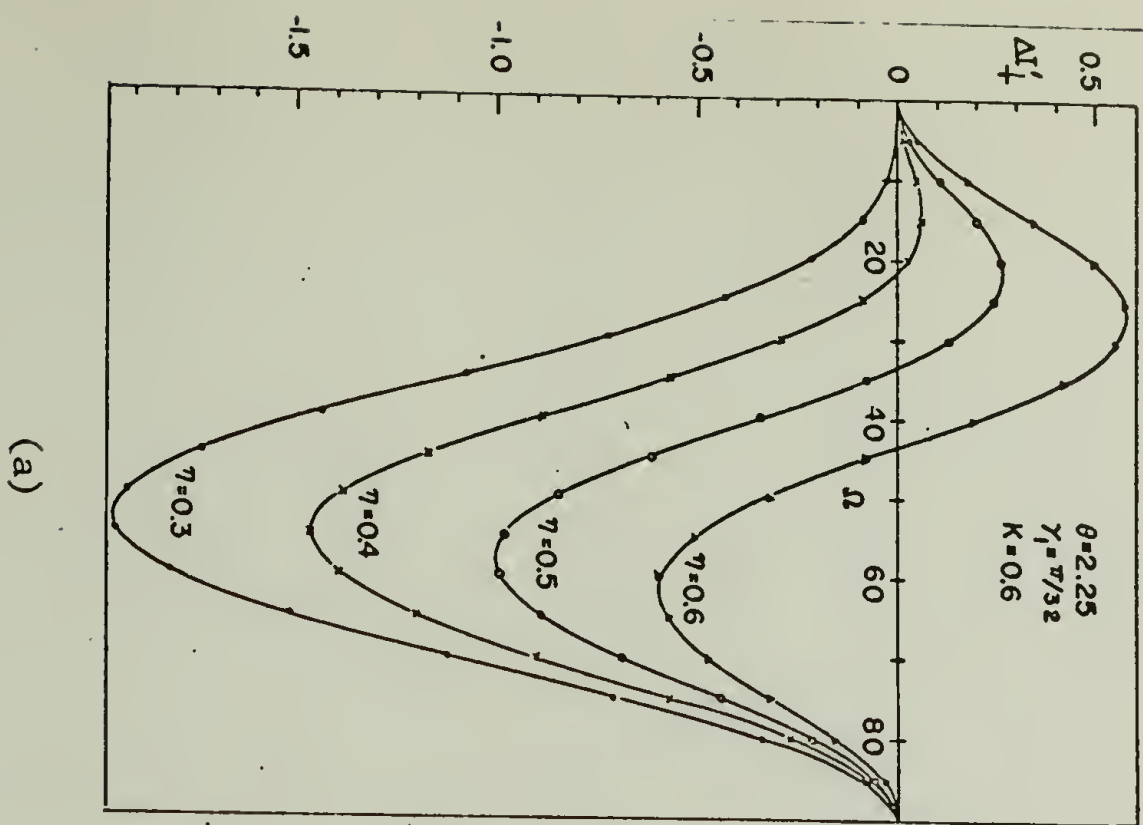


FIGURE III-47

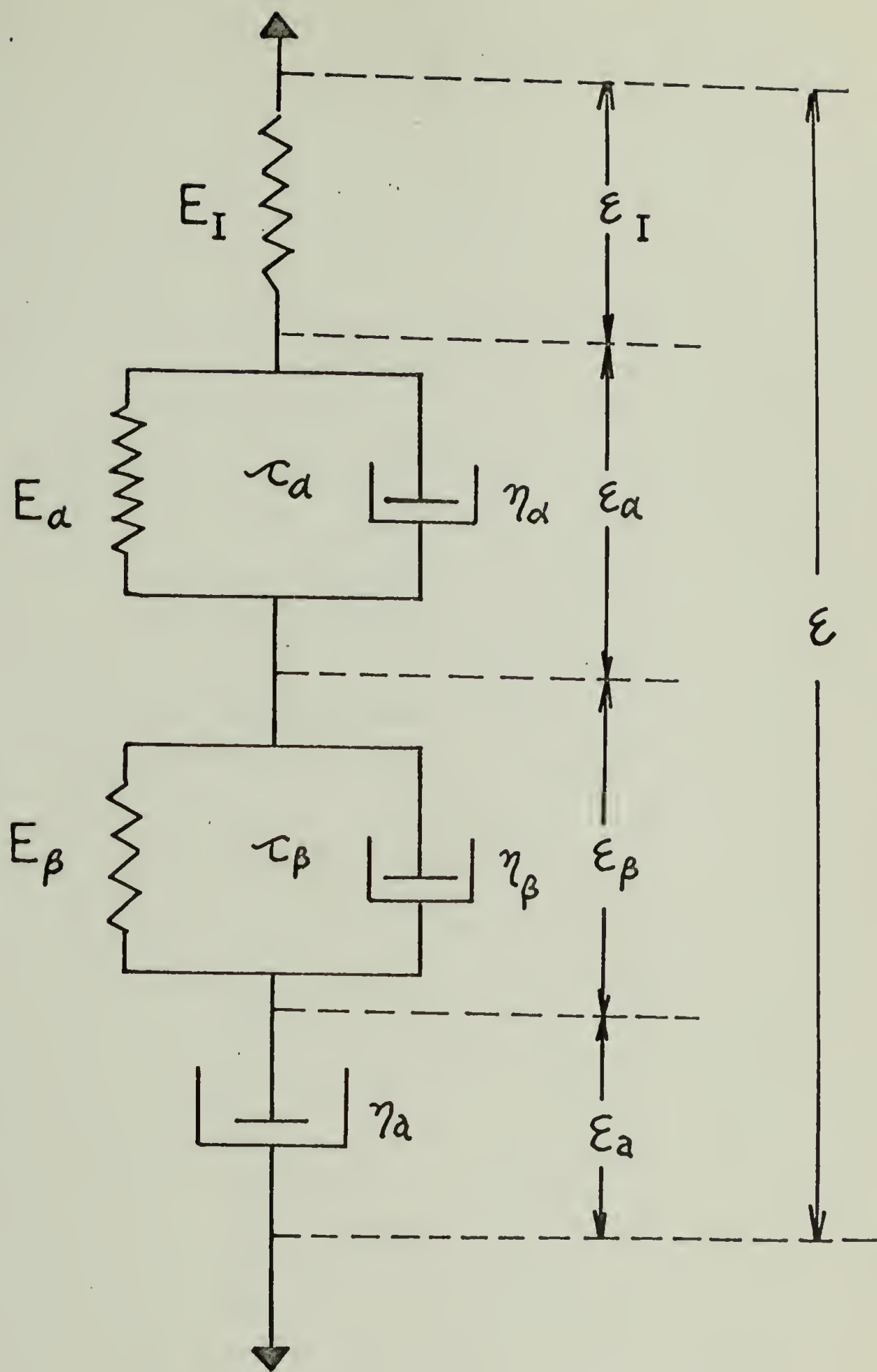


FIGURE III-48

LOG E' and LOG E'' (dynes/cm²)

-100

-50

0

50

100

TEMP. (°C)

E'

E''

Q

FIGURE IV-1(a)

○ 110 C.P.S.
⊖ 11
● 3.5

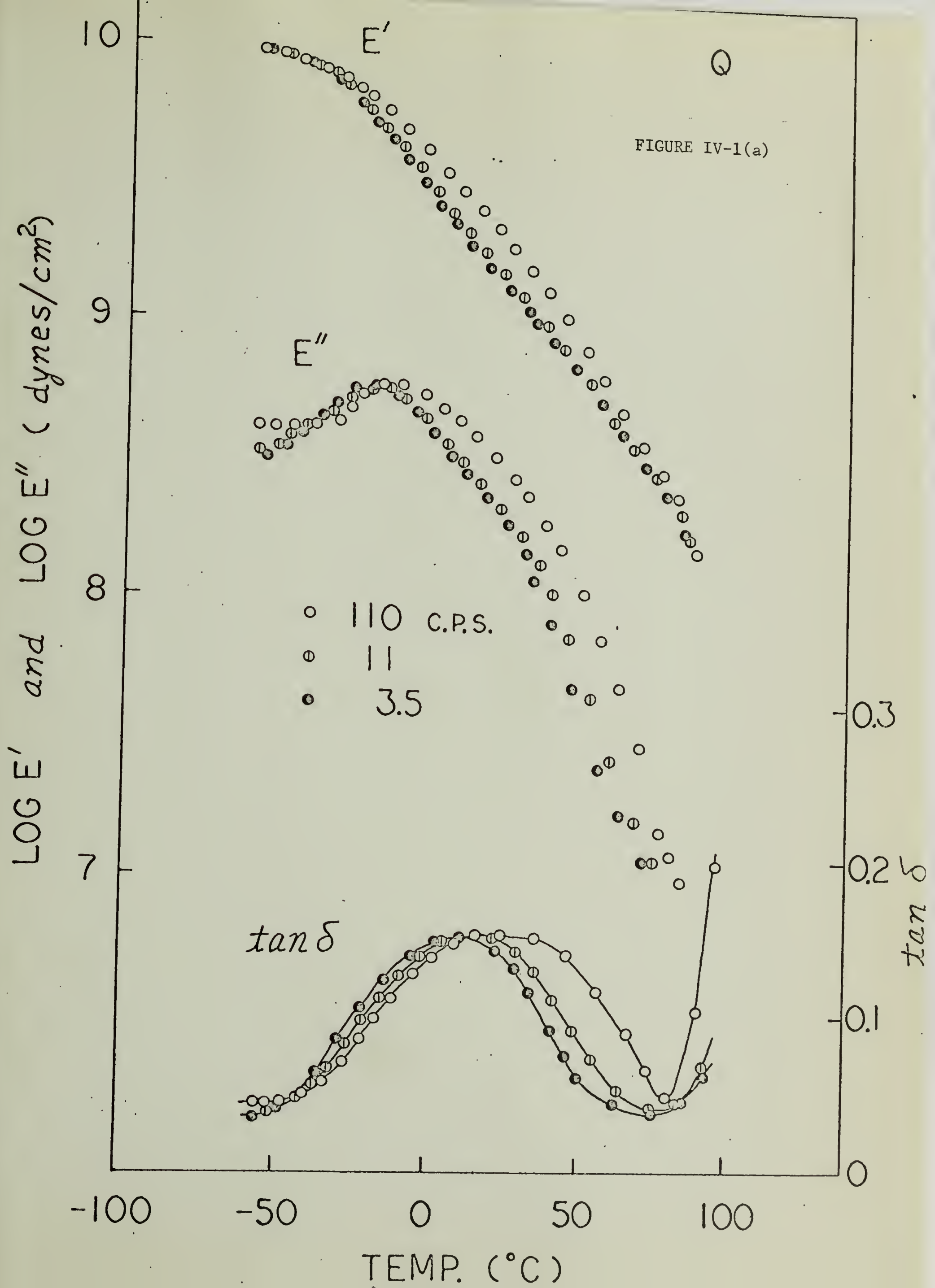
$\tan \delta$

0.3

0.2
 $\tan \delta$

0.1

0



LOG E' and LOG E'' (dynes/cm²)

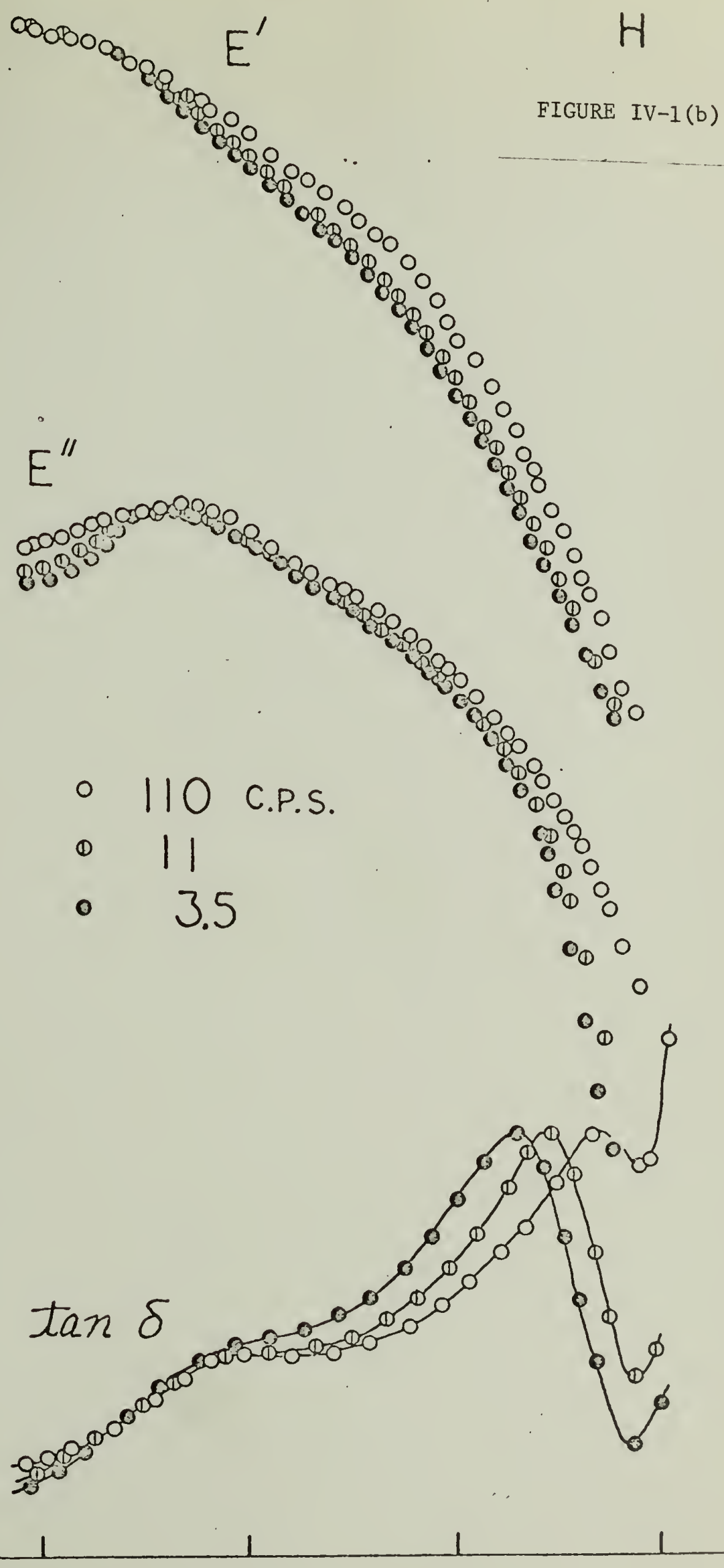


FIGURE IV-1(b)

- 110 C.P.S.
- ⊖ 11
- 3.5

tan delta

tan delta

TEMP. (°C)

HV PATTERNS OF STRETCHED SAMPLES

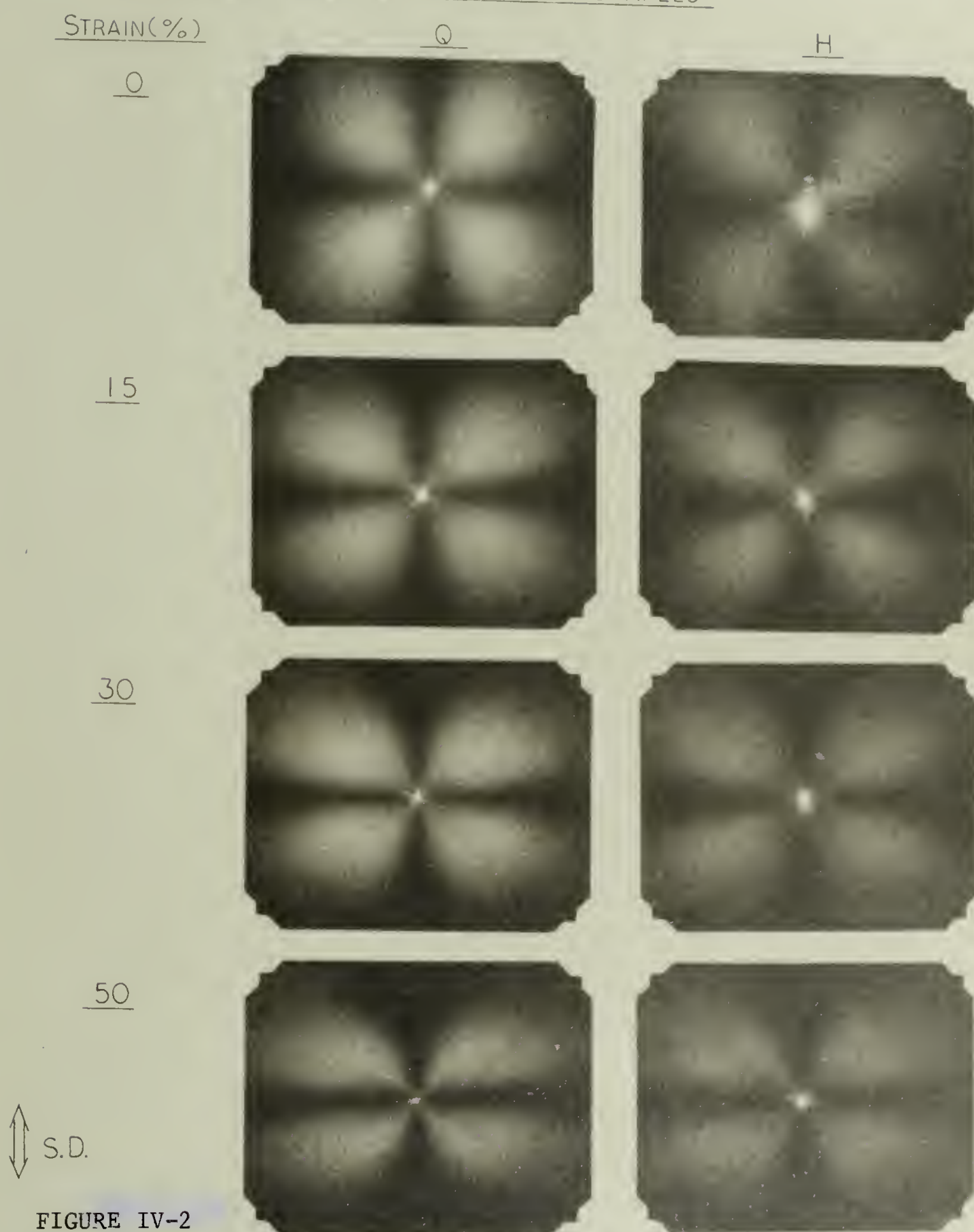


FIGURE IV-2

SCATTERING ANGLE (°)

10 20 30 40 50

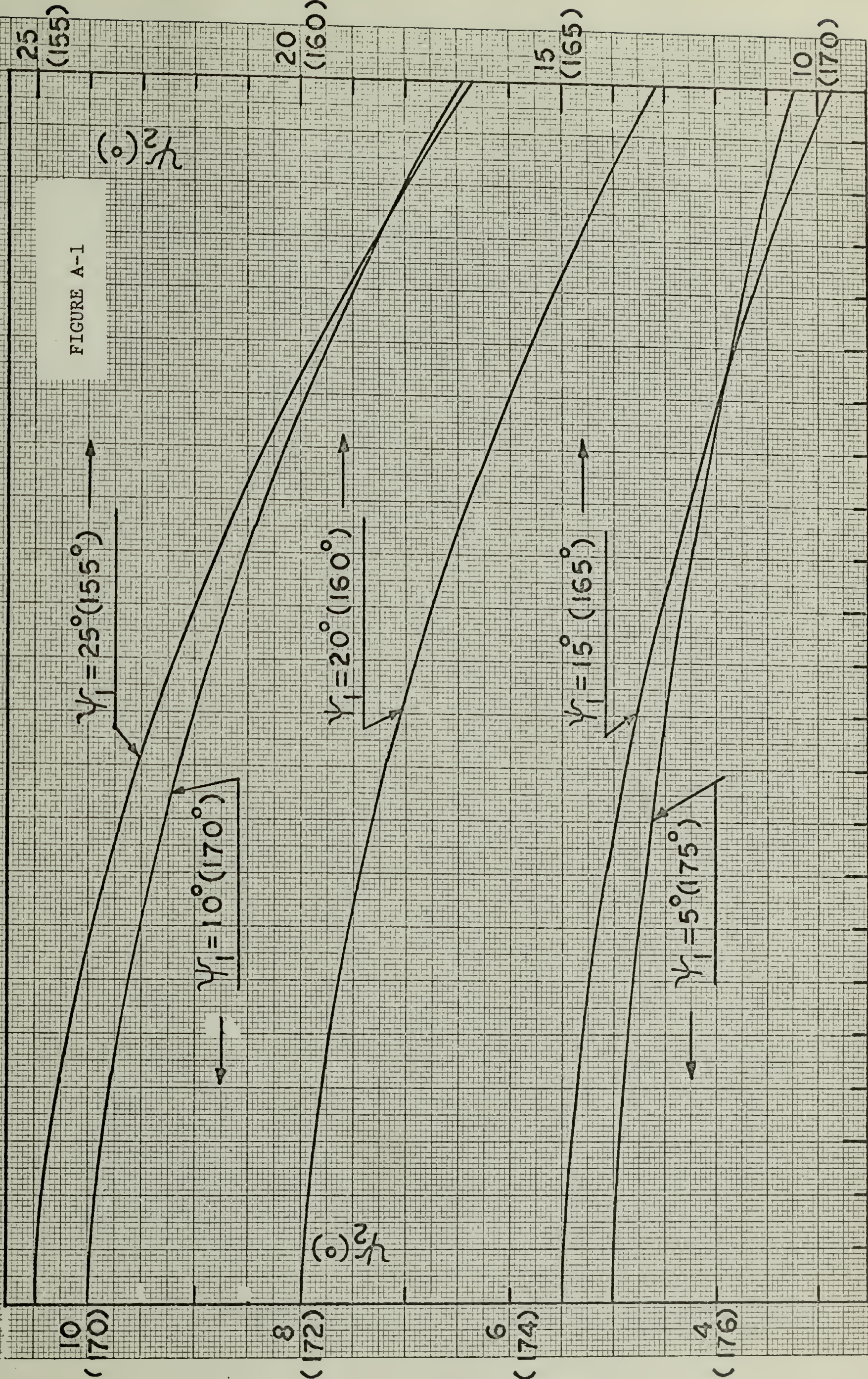


FIGURE A-1

SCATTERING ANGLE (°)

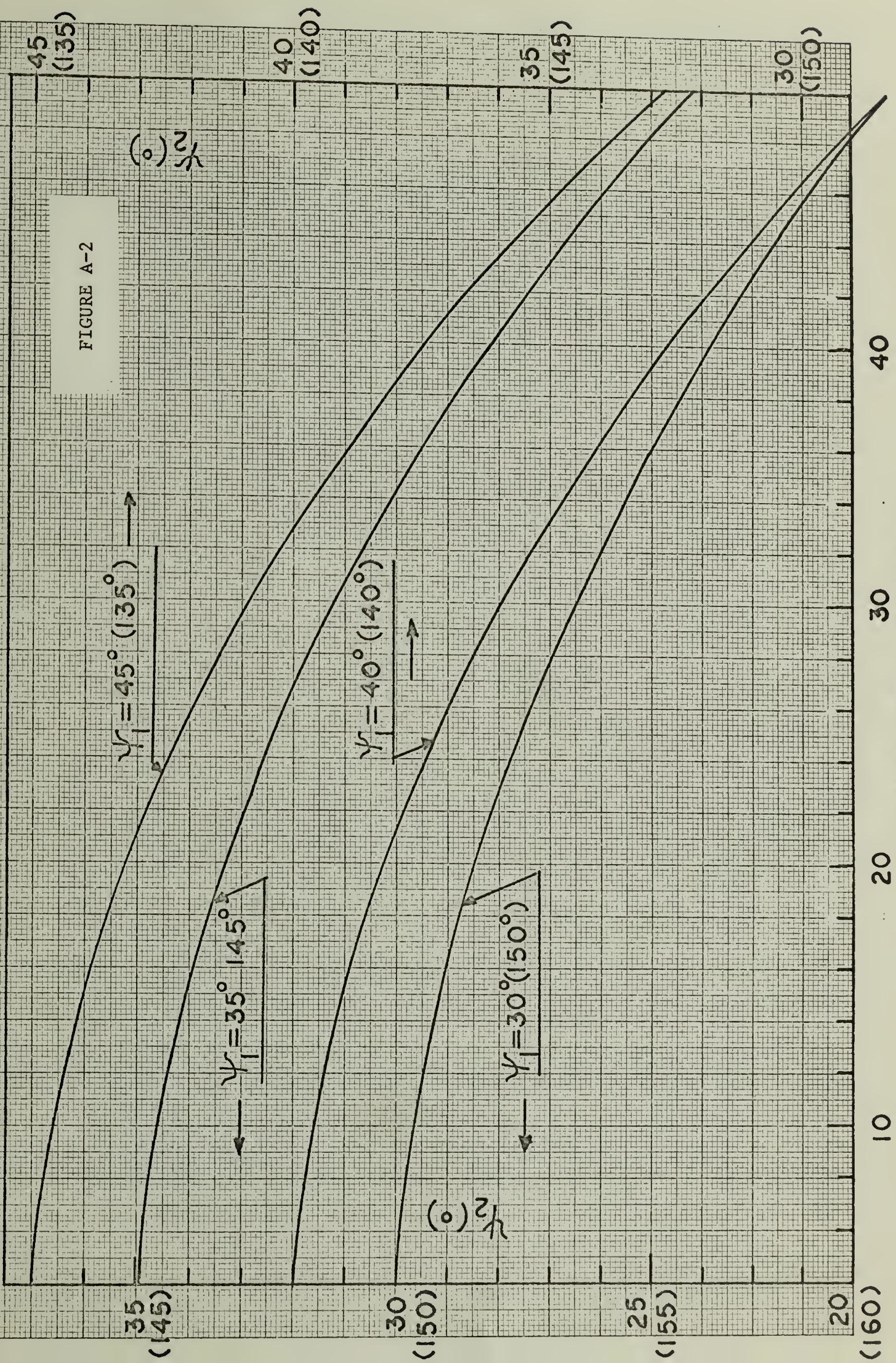


FIGURE A-2

SCATTERING ANGLE(°)

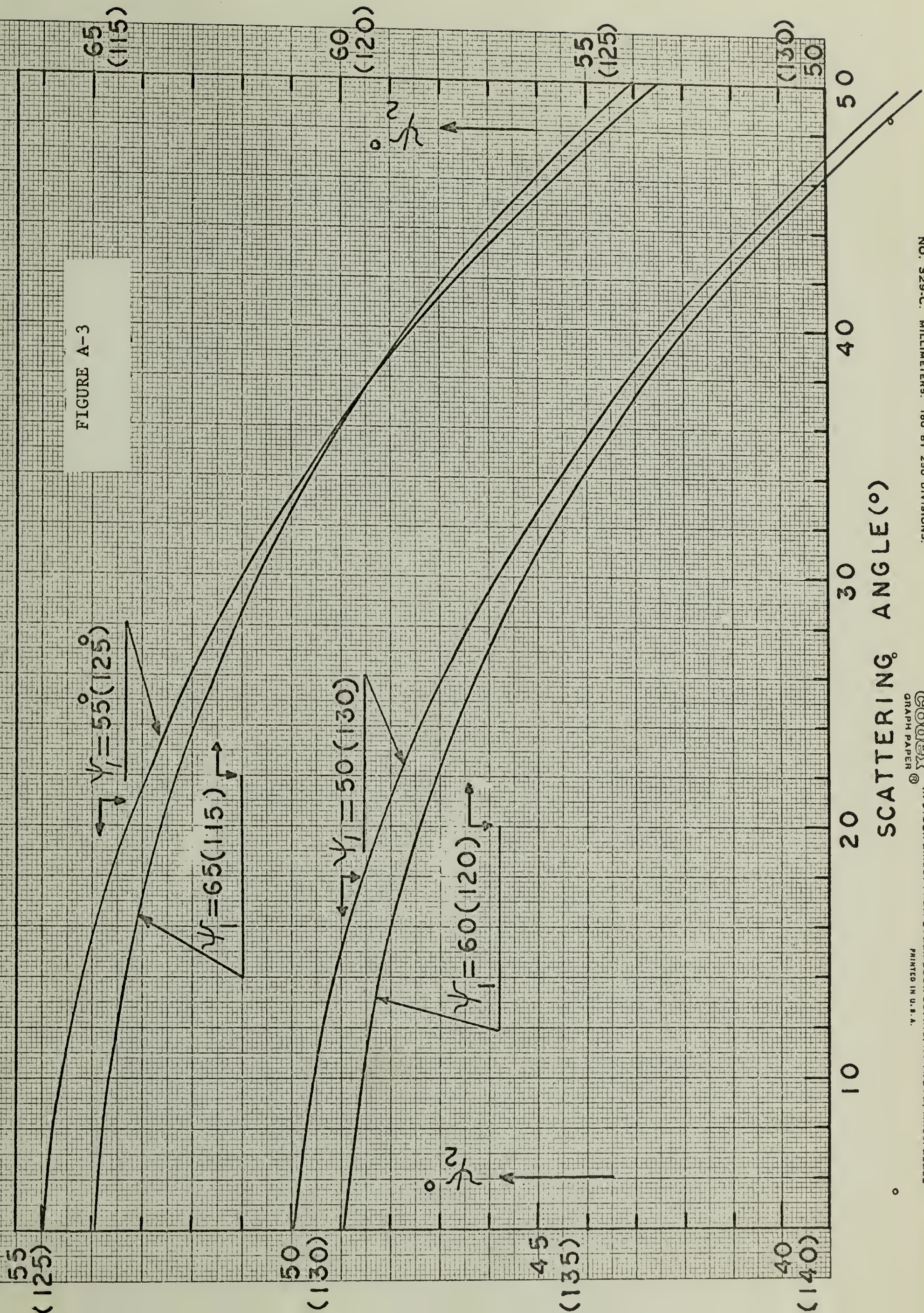


FIGURE A-3

SCATTERING ANGLE(°)

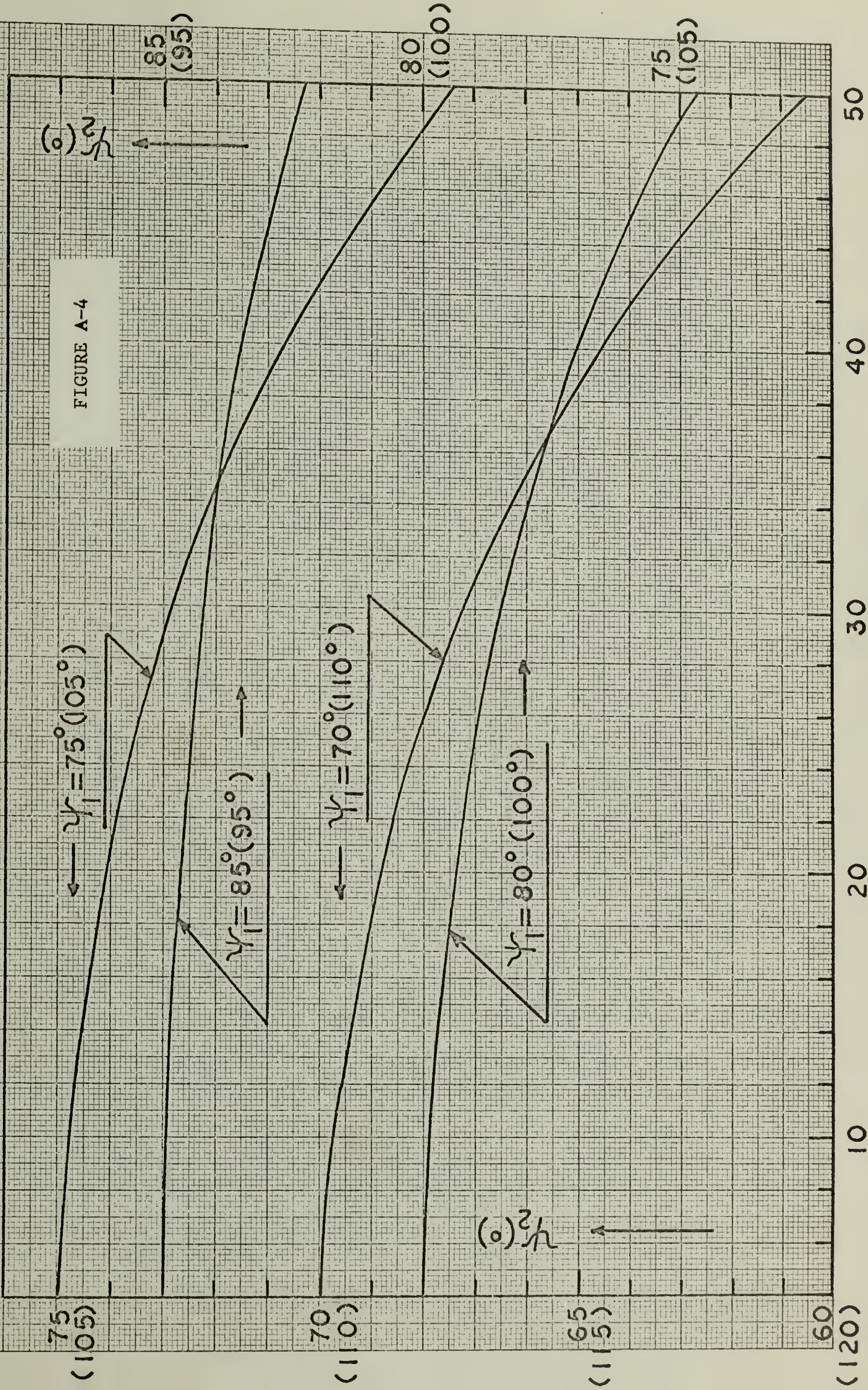


FIGURE A-4

A P P E N D I X I

THE RELATIONSHIP BETWEEN ψ_1 AND ψ_2 IN I_+ AND $I_{||}$
 SCATTERING IN LIGHT SCATTERING THEORY AND
 EXPERIMENT ACCORDING TO THE NEW DEFINITION OF $\vec{0}$ VECTOR

Prins et. al.¹⁸ proposed a new relationship between polarization direction of polarizer (ψ_1) and analyzer (ψ_2) with respect vertical direction of the apparatus (Z-direction) (see Fig. I-1). According to their definition a vector $\vec{0}$ which is a unit vector along polarization direction of the analyzer is defined as follows.

1) $\vec{0}_{||}$ is unit vector parallel through the plane of \vec{t}_p (unit vector along polarization direction of the polarizer) and \vec{s}' (unit vector along scattered beam), and is perpendicular to \vec{s}' .

2) $\vec{0}_+$ is unit vector perpendicular to the plane of \vec{t}_p and \vec{s}' .

An advantage of using the new relationship between ψ_1 and ψ_2 over the conventional relationship used in this work (see Part I) is that in the new relationship, I_+ scattering is independent of the density fluctuations and only depends upon the orientation fluctuations, while in the conventional relationship it depends upon both (see Part I).

Since the geometry of their apparatus¹⁸ is different from that of our apparatus, the relationships between ψ_1 and ψ_2 according to the new definition are recalculated for our experimental system shown in Fig. I-1, and are given by

$$\tan(\psi_2)_{||} = \tan \psi_1 \cdot \cos \theta \quad (A1)$$

$$\tan (\psi_2)_+ = - 1 / (\tan \psi_1 \cdot \cos \theta) \quad (A2)$$

where $(\psi_2)_{||}$ and $(\psi_2)_+$ are the values of ψ_2 for $I_{||}$ and I_+ scattering intensity, respectively.

Numerical calculations for the values of $(\psi_2)_{||}$ and $(\psi_2)_+$ are carried out as a function of scattering angle θ and polarizer angle ψ_1 , the results of which are shown in Figs. A1, A2, A3 and A4. From the figures it is shown that the difference of the values of $(\psi_2)_{||}$ and $(\psi_2)_+$ between the new definition and the conventional definition is negligible when the scattering angle is less than 10° but is significant when the scattering angle is large.

In Figs. A1 to A4, the ordinate scale shown in the parentheses shows the value of ψ_2 for ψ_1 greater than 90° . The value of $(\psi_2)_{||}$ and $(\psi_2)_+$ are given by

$$(\psi_2)_{||} = \psi_2 \quad (A3)$$

$$(\psi_2)_+ = \psi_2 + 90^\circ \quad (A4)$$

where ψ_2 can be read for a given set of θ and ψ_1 from the figures.

A P P E N D I X II

FORTRAN COMPUTER PROGRAMS FOR THE CALCULATIONS
OF LIGHT SCATTERING THEORIES

Each program given by appendices II-1 to II-7 is for numerical calculations of the following theories;

- II-1. Program for I_+ scattering from unoriented systems having non-random orientation fluctuations.
- II-2. Program for $I_{||}$ scattering from unoriented systems having non-random orientation fluctuations.
- II-3. Program for scattering of light from oriented systems having non-random orientation fluctuations.
- II-4. Program for scattering of light from the disordered spherulites with radial disorder in spherulite anisotropy.
- II-5. Program for scattering of light from the disordered spherulites with angular disorder in spherulite anisotropy.
- II-6. Program for scattering of light from the deformed disordered spherulites.
- II-7. Program for the dynamic light scattering from spherulites.

PROGRAM LIGHTS

```

C HASHIMOTO NON-RANDOM FLUCTUATION TWO-DIMENSIONAL THEORY, UNORIENTED
C SYSTEM INTENSITY DISTRIBUTION FOR IX SCATTERING, MODEL 4 IS USED.
C DEFINITIONS
C CD=FIRST TERM IN EQ.(17)
C CO=2ND TERM IN EQ.(17), CH=3RD TERM IN EQ.(17)
C ALPHA=AVERAGE SQUARE OF POLARIZABILITY FLUCTUATIONS
C DELTA=AVERAGE SQUARE OF ANISOTROPY OF SCATTERING ELEMENTS
C DCD=DENSITY CORRELATION DISTANCE, OCD=ORIENTATION CORRELATION DISTANCE
C RAD=RADIUS OF DOMAIN STRUCTURE, CT=TOTAL IX SCATTERING INTENSITY
C OCD1=ORIENTATION CORRELATION DISTANCE WITHIN THE DOMAIN
C OCD2=ORIENTATION CORRELATION DISTANCE OUTSIDE THE DOMAIN
      DIMENSION THI(30),CTTA(30),T(40)
100 READ 10,ALPHA,DELTA,DCD,OCD1,OCD2,RAD
10 FORMAT(6F11,8)
      PRINT 20,ALPHA,DELTA,DCD,OCD1,OCD2,RAD
20 FORMAT(2X,6HALPHA=,F11.9,2X,6HDELTA=,F11.9,2X,4HDCD=,
1 F11.9,2X,5HOCD1=,F11.9,2X,5HOCD2=,F11.9,2X,4HRAD=,F11.9,2X)
      PRINT 30
30 FORMAT(2X,5HTHETA,4X,4HBETA,4X,4HTHIA,6X,2HCO,12X,2HCD,12X,
1 2HCH,12X,2HCT)
      IF(ALPHA)99,5,5
5 THETA=0.0
15 BETA=0.0
8 I=0
      DO 45 J=1,30
      THI(J)=0.0
45 CTTA(J)=0.0
      THIA=0.0
6 THIA=THIA*3.14159/180.0
      I=I+1
      BETAR=BETA*3.14159/180.0
      THETAR=THETA*3.14159/180.0
      X1=SINF(THIA)
      X2=COSF(THIA)
      X3=COSF(THETAR)
      X4=SINF(THETAR)
      X5=(DCD*3.14159*X4/5.46E-05)**2
      U01=(OCD1*2.0*3.14159*X4)/5.46E-05
      U02=(OCD2*2.0*3.14159*X4)/5.46E-05
      XEXP1=EXP(-U01**2/4.0)
      XEXP2=EXP(-U02**2/4.0)
      X7=SINF(2.0*THIA)
      X8=THIA*2.0*BETAR
      X9=4.0*BETAR
      X10=COSF(X8)
      X11=SINF(X8)
      X14=RAD*5.46E-05/(3.14159*2.0*X4)
      X15=COSF(2.0*THIA)
      XK1=X1**2*X2**2*(1.0-X3)**2
      W=2.0*3.14159*RAD*X4/5.46E-05
      CD=3.14159*ALPHA*XK1*DCD**2*EXP(-X5)
      A0=0.5*(X2**2*X3**2*X1**2)
      A2=0.5*X7*(1.0-X3)*(X1*X10+X3*X2*X11)
      X16=COSF(X9)
      X17=SINF(X9)

```



```

A4=0.5*{(X15*(X1**2-X2**2*X3**2)*X7**2*X3)*X16*
1 (X2**2*X3**2*X1**2)*X17)
X18=OCD1**2*XEXP1
X19=OCD2**2*XEXP2
C01=0.5*AU*(X18*(2.0*3.14159-1.0)*X19)
NO=1
KODE=0
CALL BES(NO,W,KODE,RESULT,T)
C02=A2*((2.0*OCD1**2*(1.0-XEXP1)/U01**2*X18*0.5)+
1 (2.0*OCD2**2*(1.0-XEXP2)/U02**2*X19*0.5))
C04=A4*((48.0*OCD1**2*(XEXP1-1.0*U01**2/4.0)/U01**4+
18.0*OCD1**2*(1.0-XEXP1)/U01**2*0.5*X18)+
2 (48.0*OCD2**2*(XEXP2-1.0*U02**2/4.0)/U02**4+
38.0*OCD2**2*(1.0-XEXP2)/U02**2*0.5*X19))
C0=(C01+C02+C04)*DELTA*0.25
CH=(3.14159*0.5)*DELTA*XK1*X14*RESULT
CT=CD+C0+CH
PRINT 40,THETA,BETA,THIA,C0,CD,CH,CT
40 FORMAT(2X,F5.2,4X,F5.2,3X,F5.2,2X,
1 E14.5,3X,E14.5,3X,E14.5,3X,E14.5)
THI(1)=THIA
CTTA(1)=CT
THIA=THIA*5.0
IF(THIA#90.0)6,6,7
7 CALL GRAPH2(THI,CTTA)=1,5HSMALL,4HAUTO,16HINTENSITY PLOT,,,
1 6HTHIA,,,21HINTENSITY MODEL4 IX,,,3)
BETA=BETA*45.0
IF(BETA#90.0)8,8,11
11 THETA=THETA*2.0
IF(THETA#20.0)15,15,12
12 GO TO 100
99 STOP
END
C3 UCSD BES BESSEL FUNCTION

```

PROGRAM LIGHT2

C HASHIMOTO NONRANDOM FLUCTUATION, TWO DIMENSIONAL THEORY, UNORIENTED
 C SYSTEM, INTENSITY DISTRIBUTION FOR T(PARALLEL) SCATTERING.
 C MODEL 4 IS USED.

C DEFINITIONS,

C CD=FIRST TERM IN EQ.(18)

C CO=2ND TERM IN EQ.(18), CH=3RD TERM IN EQ.(18)

C ALPHA=AVERAGE SQUARE OF POLARIZABILITY FLUCTUATIONS

C DELTA=AVERAGE SQUARE OF ANISOTROPY OF SCATTERING ELEMENTS

C DCD DENSITY CORRELATION DISTANCE

C CCD1=ORIENTATION CORRELATION DISTANCE WITH IN THE DOMAIN

C CCD2=ORIENTATION CORRELATION DISTANCE OUTSIDE THE DOMAIN

DIMENSION THI(60), CTTA(60)

100 READ 10, ALPHA, DELTA, DCD, CCD1, CCD2

10 FORMAT(5F11.8)

PRINT 20, ALPHA, DELTA, DCD, CCD1, CCD2

20 FORMAT(2X, 6HALPHA=, F11.9, 2X, 6HDELTA=, F11.9, 2X, 4HDCD=,

1 F11.9, 2X, 5HCCD1=, F11.9, 2X, 5HCCD2=, F11.9, 2X)

PRINT 30

30 FORMAT(2X, 5HTHETA, 4X, 4HBETA, 4X, 4HTHIA, 6X, 2HCO, 12X, 2HCD, 12X,

1 2HCH, 12X, 2HCT)

IF (ALPHA) 99, 5, 5

5 THETA=0.0

15 BETA=-45.0

8 I=0

DO 45 J=1, 30

THI(J)=0.0

45 CTTA(J)=0.0

THIA=0.0

6 THIAI=THIA*3.14159/180.0

I=I+1

BETAI=BETA*3.14159/180.0

THETAI=THETA*3.14159/180.0

X1=COSE(THIAI)

X2=SINE(THIAI)

X3=COSE(THETAI)

X4=SINE(THETAI)

X5=X1**2

X6=X2**2

X7=X3**2

X8=X1**3

X9=1.0+X3

X10=X2**3

XK1=(X5+X6*X3)**2

XK2=X5**2

XK3=X7*X6**2

XK4=X6*X5*X3

XK5=X2*X8*X9

XK6=X10*X1*X3*X9

XK7=X6*X5*X9**2

QO=XK2+XK3-2.0*XK4+XK7

X11=COSE(2.0*BETAI)

X12=SINE(2.0*BETAI)

X13=COSE(4.0*BETAI)

X14=SINE(4.0*BETAI)

XK8=XK2-XK3

A7

```

XK9=XK5+XK6
XK10=XK2+XK3-2.0*XK4-XK7
XK11=XK6-XK5
Q2=2.0*X11*XK8-2.0*X12*XK9
Q4=X13*XK10+2.0*X14*XK11
IC=XK2+XK3+XK7
UC=CCD1*2.0*3.14159*X4/5.46E-05
UD=UCD*2.0*3.14159*X4/5.46E-05
UR=CCD2*2.0*3.14159*X4/5.46E-05
X14=EXP(-UD**2/4.0)
X15=EXP(-UC**2/4.0)
X16=EXP(-UR**2/4.0)
X17=CCD**2*0.5*X14
X18=CCD1**2*0.5*X15
X19=CCD2**2*0.5*X16
X20=1.0-X15
X21=1.0-X16
X22=UC**2*0.25
X23=UR**2*0.25
X24=CCD1**2/UC**2
X25=CCD1**2/UC**4
X26=CCD2**2/UR**2
X27=CCD2**2/UR**4
CD=2.0*3.14159*XK1*ALPHA*X17
CO1=CO*(X18-X19)
CO2=J2*((2.0*X24*X20-X18)-(2.0*X26*X21-X19))
CO4=Q4*(48.0*X25*(X22-X20)-8.0*X24*X20+X18)-
1 (48.0*X27*(X23-X21)-8.0*X26*X21+X19)
CO=DELTA*(CO1+CO2+CO4)/8.0
CH=0.25*3.14159*DELTA*IC*X19
CT=CD+CO+CH
PRINT 40,THETA,BETA,THIA,CO,CD,CH,CT
40 FORMAT(2X,F5.2,4X,F5.2,3X,F6.2,2X,
1 E14.5,3X,E14.5,3X,E14.5,3X,E14.5)
THI(1)=THIA
CTTA(1)=CT
THIA=THIA+5.0
IF (THIA-180.0)6,6,7
7 CALL GRAPH2(THI,CTTA,-1,5HSMALL,4HAUTO,16HINTENSITY PLOT.,
1 6HTHIA.,21HINTENSITY MODEL4 I=.,3)
THETA=THETA+2.0
IF (THETA-20.0)15,15,12
12 GO TO 100
99 STOP
END

```

PROGRAM LIGHT3

C HASHIMOTO/NONRANDOM ORIENTATION FLUCTUATION THEORY FOR
 C TWO-DIMENSIONAL AND ORIENTED SYSTEM.
 C INTENSITY FOR I(CROSS) SCATTERING DENSITY CONTRIBUTION IS NOT INCLUDED
 C INTENSITY ARE CALCULATED UNDER A CONDITION OF $\text{THI} = \text{OMEGA}$.

DIMENSION THI(60),CTTA(60)

100 READ 10,DELTA,DO,D,SIGMA,RHO

C DO=ORIENTATION CORRELATION DISTANCE ALONG THE DOMAIN.

C D=ORIENTATION CORRELATION DISTANCE FOR THE DIRECTION OTHER THAN

C DOMAIN AXES.

C SIGMA=ANISOTROPY PARAMETER FOR SHAPE OF CORRELATED REGION

C IN ORIENTATION

C RHO=ORIENTATION PARAMETER FOR OPTIC AXES.

10 FORMAT(5F11.8)

110 PRINT 20,DELTA,DO,D,SIGMA,RHO

20 FORMAT(2X,6HDELTA=,F11.9,2X,3HDO=,F11.9,2X,2HD=,

1 F11.9,2X,6HSIGMA=,F11.9,2X,4HRHO=,F11.9,2X)

PRINT 30

30 FORMAT(2X,5HTHETA,4X,4HBETA,4X,4HTHIA,6X,

1 6HRANDOM,12X,4HXNON,12X,5HTOTAL)

C RANDOM=SCATTERING DUE TO RANDOM ORIENTATION FLUCTUATIONS.

C XNON=SCATTERING DUE TO NONRANDOM ORIENTATION FLUCTUATIONS

C TOTAL=TOTAL SCATTERING INTENSITY.

120 IF (DELTA) 99,5,5

5 THETA=0.0

15 BETA=0.0

8 I=0

130 DO 45 J=1,30

140 THI(J)=0.0

45 CTTA(J)=0.0

THIA=0.0

6 THIA=THIA*3.14159/180.0

150 I=I+1

160 BETAR=BETA*3.14159/180.0

170 THETAR=THETA*3.14159/180.0

180 Y1=COSE(2.0*THIAR)

Y2=SINF(2.0*THIAR)

Y3=COSE(4.0*THIAR)

Y4=SINF(4.0*THIAR)

Y5=SINF(THIAR)

190 Y6=COSE(THIAR)

Y7=Y5**2

Y8=Y6**2

Y9=Y7*Y8

Y10=Y5*Y6

200 Y11=COSE(THETAR)

Y12=1.0*Y11

Y13=1.0-Y11

Y14=Y12**2

Y15=Y13**2

210 PH0=Y9*Y14

PH2=PH0+(Y8*Y11-Y7)**2

PH3=(1.0-Y11**2)*Y9

PH11=(Y7-Y8*Y11)*Y10

PH12=PH11*Y13

PH4=PH0-(Y8*Y11-Y7)**2


```

PH13=PH11*Y12
220 A00=4.0*(PH2+2.0*RHO*(PH3*Y1-PH12*Y2))
221 A02=4.0*(PH2+2.0*RHO*(PH3*Y1-PH12*Y2))*Y1
222 A20=2.0*(2.0*PH3+RHO*((2.0*PH0+PH2)*Y1-2.0*PH13*Y2))
223 A22=2.0*RHO*PH2+2.0*(PH3*Y1-PH12*Y2)+
1      RHO*(PH4*Y3-2.0*PH13*Y4)
224 A221=RHO*(PH4+2.0*PH2*Y3)+2.0*(PH3*Y1+PH12*Y2)
225 A40=2.0*(PH4+2.0*RHO*(PH3*Y1+PH12*Y2))
226 A42=2.0*RHO*PH3+PH4*Y1-2.0*PH13*Y2
227 A421=PH4*Y1+2.0*PH13*Y2+2.0*RHO*(PH3*Y3+PH12*Y4)
228 A60=2.0*RHO*(PH4*Y1+2.0*PH13*Y2)
229 A62=RHO*PH4
230 A621=RHO*(PH4*Y3+2.0*PH13*Y4)
231 XH=2.0*3.14159*SINF(THETAR)/0.364
232 Z0=-(XH*D0)**2/4.0
233 Z=-(XH*D)**2/4.0
234 T=EXP(-Z)
235 T0=EXP(-Z0)
236 F11=T
      F12=(T-1.0)/Z
      F13=2.0*(T-1.0-Z)/Z**2
      F14=6.0*(T-1.0-Z-Z**2/2.0)/Z**3
      F15=24.0*(T-1.0-Z-Z**2/2.0-Z**3/6.0)/Z**4
      F16=120.0*(T-1.0-Z-Z**2/2.0-Z**3/6.0-Z**4/24.0)/Z**5
      F17=720.0*(T-1.0-Z-Z**2/2.0-Z**3/6.0-Z**4/24.0-Z**5/120.0)/Z**6
237 F110=T0
      F120=(T0-1.0)/Z0
      F130=2.0*(T0-1.0-Z0)/Z0**2
      F140=6.0*(T0-1.0-Z0-Z0**2/2.0)/Z0**3
      F150=24.0*(T0-1.0-Z0-Z0**2/2.0-Z0**3/6.0)/Z0**4
      F160=120.0*(T0-1.0-Z0-Z0**2/2.0-Z0**3/6.0-Z0**4/24.0)/Z0**5
      F170=720.0*(T0-1.0-Z0-Z0**2/2.0-Z0**3/6.0-
1      Z0**4/24.0-Z0**5/120.0)/Z0**6
238 HG01=F110
      HG1=F11
239 F230=-F130+2.0*F120
      HG02=F230
240 F23=-F13+2.0*F12
      HG2=F23
241 F250=-3.0*F150+4.0*F140
      F240=-2.0*F140+3.0*F130
      F350=-1.0*F250+2.0*F240
      HG03=F350
242 F25=-3.0*F15+4.0*F14
      F24=-2.0*F14+3.0*F13
      F35=-1.0*F25+2.0*F24
      HG3=F35
243 F260=-4.0*F160+5.0*F150
      F270=-5.0*F170+6.0*F160
      F360=-1.5*F260+2.5*F250
      F370=-2.0*F270+3.0*F260
      F470=-F370+2.0*F360
      HG04=F470
244 F26=-4.0*F16+5.0*F15
      F27=-5.0*F17+6.0*F16
      F36=-1.5*F26+2.5*F25

```

$F37 = -2.0 * F27 + 3.0 * F26$
 $F47 = -F37 + 2.0 * F36$
 $HG4 = F47$
245 $F33 = T$
 $HG5 = F33$
 $F330 = T0$
 $HG05 = F330$
246 $F21 = T * (1.0 + Z)$
 $HG6 = F21$
 $F210 = T0 * (1.0 + Z0)$
 $HG06 = F210$
 $F34 = -0.5 * F24 + 1.5 * F23$
 $F45 = -F35 / 3.0 + 4.0 * F34 / 3.0$
 $HG7 = F45$
247 $F340 = -0.5 * F240 + 1.5 * F230$
 $F450 = -F350 / 3.0 + 4.0 * F340 / 3.0$
 $HG07 = F450$
248 $F38 = 7.0 * (Z + 6.0) * F37 / (4.0 * Z) - 21.0 * F36 / (2.0 * Z)$
 $F39 = 8.0 * (Z + 7.0) * F38 / (5.0 * Z) - 56.0 * F37 / (5.0 * Z)$
 $F48 = -4.0 * F38 / 3.0 + 7.0 * F37 / 3.0$
 $F49 = -5.0 * F39 / 3.0 + 8.0 * F38 / 3.0$
 $F58 = -3.0 * F48 / 4.0 + 7.0 * F47 / 4.0$
 $F59 = -F49 + 2.0 * F48$
 $F69 = -0.6 * F59 + 1.6 * F58$
 $HG8 = F69$
249 $F380 = 7.0 * (Z0 + 6.0) * F370 / (4.0 * Z0) - 21.0 * F360 / (2.0 * Z0)$
 $F390 = 8.0 * (Z0 + 7.0) * F380 / (5.0 * Z0) - 56.0 * F370 / (5.0 * Z0)$
 $F480 = -4.0 * F380 / 3.0 + 7.0 * F370 / 3.0$
 $F490 = -5.0 * F390 / 3.0 + 8.0 * F380 / 3.0$
 $F580 = -3.0 * F480 / 4.0 + 7.0 * F470 / 4.0$
 $F590 = -F490 + 2.0 * F480$
 $F690 = -0.6 * F590 + 1.6 * F580$
 $HG08 = F690$
2491 $F46 = -2.0 * F36 / 3.0 + 5.0 * F35 / 3.0$
 $F57 = -0.5 * F47 + 1.5 * F46$
 $HG9 = F57$
2492 $F460 = -2.0 * F360 / 3.0 + 5.0 * F350 / 3.0$
 $F570 = -0.5 * F470 + 1.5 * F460$
 $HG09 = F570$
250 $XK1 = 0.5 * (D0 ** 2 * HG01 - D ** 2 * HG1)$
251 $XK2 = XH ** 2 * (D0 ** 4 * HG02 - D ** 4 * HG2) / 16.0$
252 $XK3 = XH ** 4 * (D0 ** 6 * HG03 - D ** 6 * HG3) / 384.0$
253 $XK4 = XH ** 6 * (D0 ** 8 * HG04 - D ** 8 * HG4) / (2.0 ** 7 * 120.0)$
254 $XK5 = SIGMA * XH ** 2 * (D ** 6 * HG5 - D0 ** 6 * HG05) / 8.0$
255 $XK6 = 0.5 * SIGMA * (D ** 4 * HG6 - D0 ** 4 * HG06)$
256 $XK7 = SIGMA * XH ** 4 * (D ** 8 * HG7 - D0 ** 8 * HG07) / 128.0$
257 $XK8 = SIGMA * XH ** 8 * (D ** 12 * HG8 - D0 ** 12 * HG08) / (2.0 ** 9 * 336.0)$
258 $XK9 = D ** 2 * HG1 / 2.0$
259 $XK10 = -SIGMA * XH ** 2 * D ** 6 * HG5 / 8.0$
 $XK71 = SIGMA * XH ** 6 * (D ** 10 * HG9 - D0 ** 10 * HG09) / (2.0 ** 7 * 30.0)$
260 $Y16 = COSF(2.0 * BETAR)$
 $Y17 = COSF(4.0 * BETAR)$
 $Y18 = COSF(6.0 * BETAR)$
270 $X1 = 0.5 * A00 * XK1$
 $X2 = A20 * Y16 * XK2$
 $X3 = A40 * Y17 * XK3$


```
X4=A60*Y18*XK4
280 X5=0.5*A02*XK5
X6=A22*Y16*XK6
X7=A221*Y16*XK7
X8=A42*Y17*XK5
X9=A421*Y17*XK71
290 X10=A62*Y18*XK7
X11=A621*Y18*XK8
X12=A00*XK9
X13=A02*XK10
300 RANDOM=3.14159*(X12+X13)*DELTA/16.0
C DELTA=AVERAGE SQUARE OF ANISOTROPY OF SCATTERING ELEMENTS
310 XNCON=DELTA*(X1+X2+X3+X4+X5+X6+X7+X8+X9+X10+X11+0.0)/16.0
320 TOTAL=RANDOM+XNCON
330 PRINT 40,THETA,BETA,THIA,RANDOM,XNCON,TOTAL
40 FORMAT(2X,F6.2,4X,F6.2,3X,F6.2,2X,
1 E14.5,3X,E14.5,3X,E14.5)
340 THI(I)=THIA
350 CTTA(I)=TOTAL
360 THIA=THIA+5.0
370 IF(THIA-90.0)6,6,7
7 CALL GRAPH2(THI,CTTA,-1,5HSMALL,4HAUTO,
1 16HINTENSITY PLOT...,6HTHIA...,
2 14HINTENSITY I=...,3)
380 BETA=BETA+90.0
390 IF(BETA-90.0)8,8,11
11 THETA=THETA+2.0
400 IF(THETA-20.0)15,15,12
12 GO TO 100
99 STOP
410 END
```

FTN5.48

03/28/70

PROGRAM LIGHT6

C SCATTERING OF LIGHT FROM DISORDERED SPHERULITE IN TERMS OF
 C SPHERULITE ANISOTROPY IN RADIAL DIRECTION.
 C R IS THE RADIUS OF SPHERULITE, A IS THE CORRELATION DISTANCE
 C IN RADIAL DIRECTION.
 C DELTA IS RATIO OF AVERAGE SQUARE OF THE ANISOTROPY FLUCTUATIONS
 C TO THAT OF SPHERULITE ANISOTROPY.
 C HVP AND HVIM ARE THE HV SCATTERING DUE TO PERFECT SPHERULITE
 C AND THAT DUE TO THE RADIAL DISORDERS, RESPECTIVELY.
 C HVT IS THE TOTAL HV SCATTERING.

DIMENSION THET(100), W(100), HVP(100), HVIM(100)

DIMENSION HVT(100), T(200), TI(200)

DIMENSION XHVP(100), XHVI(100)

DIMENSION DIIN(100)

DO 700 J=1,100

THET(J)=0.0

W(J)=0.0

HVP(J)=0.0

HVIM(J)=0.0

HVT(J)=0.0

XHVP(J)=0.0

XHVI(J)=0.0

DIIN(J)=0.0

700 CONTINUE

READ 100, AK, BETAZ, R, WAVE

100 FORMAT(4F20.8)

PRINT 110, AK, BETAZ, R, WAVE

110 FORMAT(2X, 3HAK=, F20.6, 3X, 6HBETAZ=, F20.8,

1 3X, 2HR=, F20.8, 3X, 5HWAVE=, F20.8)

1000 DO 200 I=1,60

READ 210, THET(I), DIIN(I)*

210 FORMAT(F10.4, F20.6)

PRINT 220, THET(I), DIIN(I)

220 FORMAT(2X, 7HTHETAR=, F10.4, 2X, 12HINTEGRATION=, E20.6)

200 CONTINUE

PI=3.14159

DO 900 I=1,60

THETR=THET(I)*PI/180.0

SITH=SINF(THETR)

COTH=COSF(THETR)

SITH2=SITH**2

COTH2=COTH**2

W(1)=2.0*PI*R*SITH/WAVE

Y=W(1)

W4=Y**4

R4=R**4

CALL BES(0, Y, 0, AJ0, T)

CALL BES(1, Y, 0, AJ1, T1)

XHVP(1)=(2.0-2.0*AJ0-Y*AJ1)**2*R4/W4

900 CONTINUE

230 READ 250, DELTA

250 FORMAT(F8.3)

PRINT 260, DELTA

260 FORMAT(2X, 6HDELTA=, F8.3)

IF (DELTA) 999, 970, 270

270 AMU=45.0

* Numerical value were obtained according to the program by

W.Chu (see ref. 35)


```

AMUR=AMU/180.0*PI
SIMU=SINF(AMUR)
SIMU2=SIMU**2
T1=AMU+BETAZ
TIR=T1*PI/180.0
TIR2=2.0*TIR
SITIR2=SINF(TIR2)
DO 500 I=1,60
  THETR=THEI(I)*PI/180.0
  SITH=SINF(THETR)
  COTH=COSE(THETR)
  SITH2=SITH**2
  COTH2=COTH**2
  XNUM=COTH2
  DENOM=COTH2+SITH2*SIMU2
  CORC2=XNUM/DENOM
  COEF=AK*CORC2*SITIR2**2
  HVP(I)=COEF*XHVP(I)
  XHVI(I)=COEF*D1IN(I)
500 CONTINUE
  DO 600 I=1,60
    HVIM(I)=DELTA*XHVI(I)
    HVT(I)=HVP(I)+HVIM(I)
    PRINT 300,THEI(I),W(I),HVP(I),HVIM(I),HVT(I)
300 FORMAT(2X,7HTHEIAR=,F6.2,2X,2HW=,F8.4,
1      2X,4HHVP=,E15.6,2X,5HHVIM=,E15.6,2X,
2      4HHVT=,E15.6)
600 CONTINUE
610 CALL GRAPH2(W,HVP,-1,5HSMALL,4HAUTO,11H1HVP PLOT...,3HW...,
61111HINTENSITY...,3)
612 CALL GRAPH2(W,HVIM,-1,5HSMALL,4HAUTO,12H1HVIM PLOT...,3HW...,
61311HINTENSITY...,3)
614 CALL GRAPH2(W,HVT,-1,5HSMALL,4HAUTO,11H1HVT PLOT...,3HW...,
61511HINTENSITY...,3)
  GO TO 230
970 GO TO 1000
999 STOP
END

```

C3 UCSD BES

BESSEL FUNCTION

PROGRAM LIGHT7

C THE LIGHT SCATTERING BY DISORDERD SPHERULITES IN TERMS OF
 C THE ANISOTROPY IN ANGULAR DIRECTION.
 C R=RADIUS OF THE SPHERULITE. C=THE CORRELATION DISTANCE IN ANGULAR
 C DIRECTION. DELTA=RATIO OF THE AVERAGE SQUARE OF THE ANISOTROPY
 C FLUCTUATIONS TO THAT OF AVERAGE SPHERULITE ANISOTROPY.
 C HVP,HVIM AND HVT ARE THE HV SCATTERING FOR THE PERFECT SPHERULITE,
 C THE TERM DUE TO ANGULAR DISORDERS AND TOTAL HV SCATTERING.

DIMENSION AMU(20),THET(30),EINT11(30),EINT21(30)

DIMENSION XHV(20,30),W(30),T(200),T1(200)

DIMENSION HVP(20,30),HVIM(20,30),HVT(20,30)

DIMENSION XIHVP(30),XIHVIM(30),XIHVT(30)

DIMENSION XIHVT1(30)

DO J=1,19

DO I=1,30

AMU(I)=0.0

THET(J)=0.0

EINT11(J)=0.0

EINT21(J)=0.0

XHV(I,J)=0.0

W(J)=0.0

HVP(I,J)=0.0

HVIM(I,J)=0.0

HVT(I,J)=0.0

XIHVP(J)=0.0

XIHVIM(J)=0.0

XIHVT(J)=0.0

XIHVT1(J)=0.0

1 CONTINUE

PI=3.14159

READ 100,AK,BETAZ,R,WAVE

100 FORMAT(4F20.6)

PRINT 110,AK,BETAZ,R,WAVE

110 FORMAT(2X,3HAK=,F20.6,3X,6HBETAZ=,F20.8,

13X,2HR=,F20.6,3X,5HWAVE=,F20.8)

1000 READ 1001,ZAMU,THE,DINT1,DINT2

1001 FORMAT(2F10.2,2E20.6)

IF (THE) 999,2000,2000

2000 J=THE

22 THET(J)=THE

THETR=THET(J)*PI/180.

COTH=COSH(THETR)

COTH2=COTH*COTH

SITH=SINH(THETR)

SITH2=SITH*SITH

W(J)=R*2.0*PI*SITH/WAVE

EINT11(J)=DINT1

EINT21(J)=DINT2

Y=W(J)

W4=Y**4

CALL BES(0,Y,0,AJ0,T)

CALL BES(1,Y,0,AJ1,T1)

XHVP=(2.0-2.0*AJ0-Y*AJ1)**2/W4

2001 I=1

8000 AMU(I)=ZAMU

AMUR=AMU(I)*PI/180.0

* Numerical values were obtained according to the program by
 W.Chu (see ref. 35)


```

      T1=AMU(1)+BLTAZ
      TIR=2.0*T1*PI/180.0
      S1TIR=SINF(TIR)
      S1TIR2=S1TIR**2
      COTIR=COSE(TIR)
      COTIR2=COTIR**2
      COMU=COSE(AMUR)
      SIMU=SINF(AMUR)
      SIMU2=SIMU*SIMU
      DENOM=SQRT(COTH2+S1TH2*SIMU2)
      CORO=COTH/DENOM
      CORO2=CORO*CORO
      COEF1=AK*CORO2
      X11=S1TIR2*EINT11(J)*COEF1
      X12=COTIR2*EINT21(J)*COEF1
      XHV(I,J)=X11+X12
      HVP(I,J)=AHVP*S1TIR2*COEF1
      PRINT 502,AMU(1),THET(J),EINT11(J),EINT21(J)
502  FORMAT(2X,4HAMU=,F6.2,3X,5HTHET=,F6.2,3X,6HEINT11=,E20.6,3X,
1  6HEINT21=,E20.6)
      ZAMU=ZAMU+5.0
      IF(ZAMU-45.0)900,900,950
900  I=I+1
      GO TO 8000
950  GO TO 1000
999  READ 250,DELTA
250  FORMAT(F10.5)
      PRINT 260,DELTA
260  FORMAT(2X,6HDELTA=,F10.5)
      IF(DELTA)9999,265,270
265  GO TO 1000
270  DO 300 I=1,10
      DO 300 J=1,15
      HVIM(I,J)=DELTA*XHV(I,J)
      HVT(I,J)=HVIM(I,J)+HVP(I,J)
300  CONTINUE
      DO 400 I=1,10
      DO 400 J=1,15
      PRINT 500,AMU(1),THET(J),W(J),HVP(I,J),HVIM(I,J),HVT(I,J)
500  FORMAT(3HAMU=,F6.2,2X,7HTHET=,F6.2,2X,2HW=,F8.4,
12X,4HHVP=,E15.6,2X,5HHVIM=,E15.6,2X,4HHVT=,E15.6)
400  CONTINUE
      DO 700 K=1,15
      XIHVP(K)=HVP(10,K)
      XIHVIM(K)=HVIM(10,K)
      XIHVT(K)=HVT(10,K)
      XIHVT1(K)=HVT(1,K)
700  CONTINUE
      CALL GRAPH2(W,XIHVP,-1,5HSMALL,4HAUTO,11HIHVP PLOT...,
13HW...,11HINTENSITY...,3)
      CALL GRAPH2(W,XIHVIM,-1,5HSMALL,4HAUTO,12HIHVIM PLOT...,
13HW...,11HINTENSITY...,3)
      CALL GRAPH2(W,XIHVT,-1,5HSMALL,4HAUTO,11HIHVT PLOT...,
13HW...,11HINTENSITY...,3)
      CALL GRAPH2(W,XIHVT1,-1,5HSMALL,4HAUTO,12HIHVT1 PLOT...,
13HW...,11HINTENSITY...,3)

```

GO TO 999

9999 STOP

END

C3 UCSD DES

BESSEL FUNCTION

3

PROGRAM LIGHTS

```

C  HV-SCATTERING BY DEFORMED-DISORDERED-SPHERULITES WITH ANGULAR
C  DISORDER IN ORIENTATION (MODEL II) WHICH ALLOWS AN ANGULAR
C  DEPENDENCE OF THE MAGNITUDE OF ORIENTATION FLUCTUATIONS.
C  PROGRAMED BY HASHIMOTO
  DIMENSION THET(20), AMU(20), W(20), PHI1(200), FPH1(200)
  DIMENSION PHI2(200), FPH2(200), GGA(200), PRUD1(200)
  DIMENSION PRUD2(200), BSUM1(200), BSUM2(200), EINT11(20), EINT21(20)
  DIMENSION BAL1(200), CAL1(200), BAL2(200), CAL2(200)
  DIMENSION XIP(20,20)
  DIMENSION THET1(20), AMU1(20), EINT1(20), EINT2(20)
  DIMENSION XI1(20,20), XI2(20,20)
  DIMENSION RAYP(20,20), RAYU(20,20), GRAYP(20,20), GRAYU(20,20)
  DIMENSION HV(20,20), GHV(20,20)
  DIMENSION RHV1(20), RHV2(20)
  1 READ 100, AK, BETAZ, RAMDA
100 FORMAT(3F20,8)
  PRINT 101, AK, BETAZ, RAMDA
101 FORMAT(2X, 3HAK=, F20.8, 5X, 6HBETAZ=, F20.8, 5X, 6HRAMDA=, F20.8)
  2 READ 102, C, R, WAVE
C  C IS ANGULAR CORRELATION DISTANCE IN RADIAN, R IS THE RADIUS
C  OF SPHERULITE IN CM., WAVE IS WAVE LENGTH IN MEDIUM IN CM,
C  RAMDA IS EXTENSION RATIO OF SPHERULITE ALONG STRETCHING DIRECTION.
102 FORMAT(3F20,8)
  PRINT 103, C, R, WAVE
103 FORMAT(2X, 21H CORRELATION-DISTANCE=, F14.8, 3X, 18H SPHERULITE RADIUS=,
1F14.8, 3X, 12H WAVE LENGTH=, F14.8)
  PI=3.14159
  DO 3 II=1,19
  DO 3 NN=1,10
  DO 3 LL=1,200
  AMU(II)=0.0
  AMU1(II)=0.0
  THET(NN)=0.0
  THET1(NN)=0.0
  W(NN)=0.0
  PHI1(LL)=0.0
  PHI2(LL)=0.0
  FPH1(LL)=0.0
  FPH2(LL)=0.0
  GGA(LL)=0.0
  PRUD1(LL)=0.0
  PRUD2(LL)=0.0
  BSUM1(LL)=0.0
  BSUM2(LL)=0.0
  BAL1(LL)=0.0
  CAL1(LL)=0.0
  BAL2(LL)=0.0
  CAL2(LL)=0.0
  EINT1(NN)=0.0
  EINT2(NN)=0.0
  EINT11(NN)=0.0
  EINT21(NN)=0.0
  XIP(II,NN)=0.0
  XI1(II,NN)=0.0
  XI2(II,NN)=0.0

```

```

RAYP(II,NN)=0.0
RAYU(II,NN)=0.0
GRAYP(II,NN)=0.0
GRAYU(II,NN)=0.0
HV(II,NN)=0.0
GHV(-II,NN)=0.0
RHV1(NN)=0.0
RHV2(NN)=0.0
3 CONTINUE
I=1
ZAMU=0.0
25 AMU(I)=ZAMU
AMUR=AMU(I)*PI/180.0
COMU=COSF(AMUR)
SIMU=SINF(AMUR)
SIMU2=SIMU*SIMU
COMU2=COMU*COMU
DENOM1=SQRTF(SIMU2+COMU2*RAMDA**4)
SIGA=SIMU/DENOM1
COGA=COMU*RAMDA**2/DENOM1
SI2GA=2.0*SIGA*COGA
CO2GA=COGA*COGA-SIGA*SIGA
J=1
THE=1.0
22 THET(J)=THE
THETR=THET(J)*PI/180.0
COTH=COSF(THETR)
COTH2=COTH*COTH
SITH=SINF(THETR)
SITH2=SITH*SITH
DENOM=SQRTF(COTH2+SITH2*SIMU2)
CORO=COTH/DENOM
CORO2=CORO*CORO
W(J)=R*2.0*PI*SITH/WAVE
X=(R*2.0*PI*SITH/WAVE)*(DENOM1/RAMDA)
K=1
PH1=0.0
10 PH11(K)=PH1
COPH1=COSF(PH11(K))
TERM1=X*COPH1
ATERM=(COSF(ATERM1)-1.0)/(ATERM1*ATERM1)
BTERM=SINF(ATERM1)/ATERM1
FPH1(K)=ATERM+BTERM
700 SIPH1=SINF(PH11(K))
SI2PH1=2.0*SIPH1*COPH1
CO2PH1=COPH1*COPH1-SIPH1*SIPH1
SI2AL1=SI2PH1*CO2GA+CO2PH1*SI2GA
SIAL1=SIPH1*COGA+COPH1*SIGA
SIAL12=SIAL1*SIAL1
COAL1=COPH1*COGA-SIPH1*SIGA
COAL12=COAL1*COAL1
RAM2=RAMDA*RAMDA
RAM4=RAM2*RAM2
DENOM2=SIAL12+RAM4*COAL12
BAL1(K)=RAM2*SI2AL1/DENOM2
CAL1(K)=(RAM4*COAL12-SIAL12)/DENOM2

```



```

      L=1
      PH2=0.0
10  PH12(L)=PH2
      CPH2=COSF(PH12(L))
      TERM2=X*CPH2
      CTERM=(COSF(TERM2)-1.0)/(-TERM2*TERM2)
      DTERM=SINF(TERM2)/TERM2
      FPH2(L)=CTERM*DTERM
1400 SIPH2=SINF(PH12(L))
      SI2PH2=2.0*SIPH2*CPH2
      CO2PH2=CPH2*CPH2-SIPH2*SIPH2
      SI2AL2=SI2PH2*CO2GA+CO2PH2*SI2GA
      SIAL2=SIPH2*COGA+CPH2*SIGA
      SIAL22=SIAL2*SIAL2
      COAL2=CPH2*COGA-SIPH2*SIGA
      COAL22=COAL2*COAL2
      RAM2=RAMDA*RAMDA
      RAM4=RAM2*RAM2
      DENOM3=SIAL22+RAM4*COAL22
      BAL2(L)=RAM2*SI2AL2/DENOM3
      CAL2(L)=(RAM4*COAL22-SIAL22)/DENOM3
      PHI12=ABSF(PHI1(K)-PHI2(L))
      IF(PHI12-PI)5,5,6
5  GGA(L)=EXPF(-PHI12/C)
      GO TO 7
6  GGA(L)=EXPF((2.0*PI-PHI12)/C)
7  PROD1(L)=GGA(L)*BAL2(L)*BAL1(K)*FPH1(K)*FPH2(L)*SIAL12
      PROD2(L)=GGA(L)*CAL2(L)*CAL1(K)*FPH1(K)*FPH2(L)*SIAL12
      DPH=2.0*PI/150.0
      PH2=PH2+DPH
      DIFF=PH2-2.0*PI
      IF(DIFF)8,8,9
8  L=L+1
      GO TO 10
9  SUM1=0.0
      SUM2=0.0
      DO 11 M=1,L
      IF(M-1)12,12,13
12  SUM1=SUM1+0.5*(PROD1(M+1)*PHI2(M+1))
      SUM2=SUM2+0.5*(PROD2(M+1)*PHI2(M+1))
      GO TO 11
13  SUM1=SUM1+0.5*(PROD1(M+1)+PROD1(M))*DPH
      SUM2=SUM2+0.5*(PROD2(M+1)+PROD2(M))*DPH
11  CONTINUE
      BSUM1(K)=SUM1
      BSUM2(K)=SUM2
      PH1=PH1+DPH
      IF(PH1-2.0*PI)14,14,15
14  K=K+1
      GO TO 16
15  DINT1=0.0
      DINT2=0.0
      DO 17 N=1,K
      IF(N-1)18,18,19
18  DINT1=DINT1+0.5*(BSUM1(N+1)*PHI1(N+1))
      DINT2=DINT2+0.5*(BSUM2(N+1)*PHI2(N+1))

```

```

      GO TO 17
19  DINT1=DINT1+0.5*(BSUM1(N+1)+BSUM1(N))*DPH
    DINT2=DINT2+0.5*(BSUM2(N+1)+BSUM2(N))*DPH
17  CONTINUE
    EINT11(J)=DINT1
    EINT21(J)=DINT2
    PUNCH 501, AMU(I), THE1(J), EINT11(J), EINT21(J)
501  FORMAT(2F10.5, 2E20.6)
    PRINT 502, AMU(I), THE1(J), EINT11(J), EINT21(J)
502  FORMAT(2X, 4HAMU=, F6.2, 3X, 5HTHE1=, F6.2, 3X, 6HEINT11=, E20.6, 3X,
1  6HEINT21=, E20.6)
    COEF1=AK*CORO2
    XI11=COEF1*EINT11(J)
    XI21=COEF1*EINT21(J)
    XI1(I,J)=XI11-XI21
52  THE=THE+1.0
    IF (THE-10.0) 20, 21, 21
20  J=J+1
    GO TO 22
21  ZAMU=ZAMU+5.0
    IF (ZAMU-90.0) 23, 23, 24
23  I=I+1
    GO TO 25
24  GO TO 999
999  READ 5010, ZAMU1, THE1, DINT1, DINT2*
5010  FORMAT(2F10.5, 2E20.6)
    IF (THE1) 3000, 4000, 4000
4000  IF (ZAMU1-0.0) 4001, 4001, 4002
4001  I=1
    GO TO 5000
4002  IF (ZAMU1-4.0) 4003, 4003, 4004
4003  PRINT 6000
6000  FORMAT(2X, 14HMISTAKE IN AMU)
    GO TO 5000
4004  IF (ZAMU1-9.0) 4005, 4005, 4006
4005  I=2
    GO TO 5000
4006  IF (ZAMU1-14.0) 4007, 4007, 4008
4007  I=3
    GO TO 5000
4008  IF (ZAMU1-19.0) 4009, 4009, 4010
4009  I=4
    GO TO 5000
4010  IF (ZAMU1-24.0) 4011, 4011, 4012
4011  I=5
    GO TO 5000
4012  IF (ZAMU1-29.0) 4013, 4013, 4014
4013  I=6
    GO TO 5000
4014  IF (ZAMU1-34.0) 4015, 4015, 4016
4015  I=7
    GO TO 5000
4016  IF (ZAMU1-39.0) 4017, 4017, 4018
4017  I=8
    GO TO 5000
4018  IF (ZAMU1-44.0) 4019, 4019, 4020

```

* Programs for numerical calculations of these are not shown here.
 These were calculated in a manner similar to the calculations
 of EINT11(J) and EINT21(J) in this program.


```

4019 I=9
      GO TO 5000
4020 IF (ZAMU1-49,0) 4021,4021,4022
4021 I=10
      GO TO 5000
4022 IF (ZAMU1-54,0) 4023,4023,4024
4023 I=11
      GO TO 5000
4024 IF (ZAMU1-59,0) 4025,4025,4026
4025 I=12
      GO TO 5000
4026 IF (ZAMU1-64,0) 4027,4027,4028
4027 I=13
      GO TO 5000
4028 IF (ZAMU1-69,0) 4029,4029,4030
4029 I=14
      GO TO 5000
4030 IF (ZAMU1-74,0) 4031,4031,4032
4031 I=15
      GO TO 5000
4032 IF (ZAMU1-79,0) 4033,4033,4034
4033 I=16
      GO TO 5000
4034 IF (ZAMU1-84,0) 4035,4035,4036
4035 I=17
      GO TO 5000
4036 IF (ZAMU1-89,0) 4037,4037,4038
4037 I=18
      GO TO 5000
4038 I=19
      GO TO 5000
5000 AMU1(I)=ZAMU1
      AMUR1=AMU1(I)*PI/180,0
      SIMU1=SINF(AMUR1)
      SIMU12=SIMU1*SIMU1
      J=THE1
      THET1(J)=THE1
      THETR1=THET1(J)*PI/180,0
      COTH1=COSF(THETR1)
      COTH12=COTH1*COTH1
      SITH1=SINF(THETR1)
      SITH12=SITH1*SITH1
      DENOM1=SQRT(COTH12+SITH12*SIMU12)
      CORO1=COTH1/DENOM1
      CORO12=CORO1*CORO1
      COEF11=AK*CORO12
      EINT1(J)=DINT1
      EINT2(J)=DINT2
      XI1(I,J)=COEF11*EINT1(J)
      XI2(I,J)=COEF11*EINT2(J)
      PRINT 5020,AMU1(I),THET1(J),EINT1(J),EINT2(J)
5020 FORMAT(2X,5HAMU1=,F6,2,2X,6HTHET1=,F6,2,2X,
1 5HINT1=,E20,6,2X,5HINT2=,E20,6)
      GO TO 999
3000 READ 7000,GO,SIGMA
7000 FORMAT(2F7,3)

```

```
      PRINT 7100, G0, SIGMA
7100 FORMAT(2X, 3HGU=, F7.3, 5X, 6HSIGMA=, F7.3)
      IF (G0) 9999, 9999, 7200
7200 DO 7300 I=1, 19
      DO 7300 J=1, 9
      RAYU(I, J) = G0 * XI1(I, J) + (1.0 - G0) * XI2(I, J)
      RAYP(I, J) = G0 * SIGMA * XIP(I, J)
      HV(I, J) = RAYU(I, J) + RAYP(I, J)
7300 CONTINUE
      PRINT 7400
7400 FORMAT(1X, 3HAMU, 4X, 5HTHETA, 4X, 1HW, 9X, 12HHV INTENSITY, 14X, 4HRAYP)
C RAYP SHOWS AN EFFECT OF ANGULAR DEPENDENCE OF MAGNITUDE OF
C ORIENTATION FLUCTUATION TO HV SCATTERING INTENSITY.
      DO 7600 IJ=1, 19
      DO 7600 JK=1, 9
      PRINT 7700, AMU(IJ), THET(JK), W(JK), HV(IJ, JK),
1 RAYP(IJ, JK)
7700 FORMAT(F5.1, 3X, F4.1, 2X, F6.3, 2(2X, E20.8))
7600 CONTINUE
      DO 7800 LM=1, 9
      RHV1(LM) = HV(1, LM)
      RHV2(LM) = HV(10, LM)
7800 CONTINUE
      CALL GRAPH2(THET, RHV1, -J, 5HSMALL, 4HAUTO,
1 19HHV PLOT FOR MU=0., 6HTHET, 11HINTENSITY, 1, 3)
      CALL GRAPH2(THET, RHV2, -J, 5HSMALL, 4HAUTO,
1 20HHV PLOT FOR MU=45., 6HTHET, 11HINTENSITY, 1, 3)
      GO TO 3000
9999 STOP
      END
```


PROGRAM DLS2

```

C THE DYNAMIC LIGHT SCATTERING FROM THREE DIMENSIONAL SPHERULITES
C ACCORDING TO DEFORMATION MODEL OF VAN AARTSEN WITH PHASE
C LAG INTRODUCED INTO TILTING AND TWISTING OF THE LAMELLAE,
C P1=RAMDA, RAMDA=EXTENSION RATIO OF SPHERULITES, BZ=BEIJAR ZERO
C P2=RAMDA+DELTA RAMDA
C G=K, RAN=
C D=PHASE ANGLE OF LOCAL STRAIN TO EXTERNAL STRAIN,
C EXT31, EXT32, EXT21 AND EXT22 ARE THE SPHERULITIC STRAIN,
C EXT41, EXT42, EXT51, EXT52 ARE LOCAL STRAIN,
  DIMENSION Y1(101), Y2(101), Z1(30,30), Z2(30,30)
  COMPLEX D, EXT41, EXT42, EXT51, EXT52, XP1
  COMPLEX XP2, EXP1, EXP2, BTA1, BTA2, GOM1
  COMPLEX GOM2, DIV1, DIV2, Z1, Z2
  COMPLEX SUMZ1, SUMZ2, AHV1, AHV2, HV1
  COMPLEX HV2, DELHV
  DO 300 J=1,101
  DO 300 I=1,30
    Y1(J)=0.0
    Y2(J)=0.0
    Z1(I)=(0.0,0.0,0.0)
    Z2(I)=(0.0,0.0,0.0)
300 CONTINUE
  READ 700, AK
700 FORMAT(F20.8)
  PRINT 710, AK
710 FORMAT(2X,3HAK=,F20.8)
  1 READ10, P1, P2, AZG1, DAZ, AZMA, Q
  10 FORMAT(2F6.3,3F6.2)
  PRINT110, P1, P2, Q
110 FORMAT(2X,3HP1=,F6.3,5X,3HP2=,F6.3,5X,2HQ=,F6.2)
  50 READ 51, D
  51 FORMAT(C(F3.1,F10.5))
  PRINT 52, D
  52 FORMAT(2X,2HD=,C(F3.1,F10.5))
105 READ 88, BZ, Q, RAN
  88 FORMAT(3F10.2)
  PRINT89, BZ, Q, RAN
  89 FORMAT(2X,3HBZ=,F10.2,5X,2HQ=,F10.2,5X,4HRAN=,F10.2)
1000 READ 100, U
  100 FORMAT(F6.2)
  PRINT120, U
  120 FORMAT(2X,2HU=,F6.2)
  IF(U)999,105,2000
2000 EXT31=P1
  EXT32=P2
  EXT21=SQRTF(Q/P1)
  EXT22=SQRTF(Q/P2)
  PI=3.14159
  2 AZG=AZG1
  PRINT500
500 FORMAT(4X,2HMU,6X,9HHV2(REAL),8X,14HHV2(IMAGINARY),
  13X,13HDELTA I PRIME,5X,14HDELTA I DPRIME,4X,
  212HABS(DELTA I),7X,10HTAN(GAMMA))
  3 AZ=AZG/360.0*2.0*PI
  SIAZ=SINF(AZ)

```

N.B. Following statements are added in
between the statements of
COMPLEX HV2, DELHV and DO 300 J=1,101 ;

{ DIMENSION DHVS(2)
EQUIVALENCE (DELHV, DHVS)

```
COAZ=COSF(AZ)
SIAZ2=SIAZ*SIAZ
COAZ2=COAZ*COAZ
ARG1=EXT21**2*SIAZ2*EXT31**2*COAZ2
ARG2=EXT22**2*SIAZ2*EXT32**2*COAZ2
USTAR1=U*SQRTF(ARG1)
USTAR2=U*SQRTF(ARG2)
XNUM1=EXT31*COAZ
XDEN1=EXT21*SIAZ
XRAT1=XNUM1/XDEN1
DELTA1=ATANF(XRAT1)
XNUM2=EXT32*COAZ
XDEN2=EXT22*SIAZ
XRAT2=XNUM2/XDEN2
DELTA2=ATANF(XRAT2)
AL=0.0
DA=5.0/360.0*2.0*PI
DO 12 I=1,19
RHO1=0.0
RHO2=0.0
DO 9 J=1,21
SIAL=SINF(AL)
COAL=COSF(AL)
SIAL2=SIAL*SIAL
COAL2=COAL*COAL
X1=RHO1*COSF(DELTA1)*SIAL
X2=RHO2*COSF(DELTA2)*SIAL
X22=X2*X2
X12=X1*X1
B=1.0
5 CNT=2.0
TERM1=X1/2.0
AJ1=TERM1
6 DN1=CNT
CNT=CNT+2.0
DEN=CNT*DN1
FAC1=X12/DEN
FACA1=B*FAC1
TERM1=TERM1*FACA1
AJ1=AJ1*TERM1
TER1=ABSF(TERM1)
DIF1=1.E+06*TER1
IF(DIF1)7,7,200
7 GO TO 6
200 CNT=2.0
TERM2=X2/2.0
AJ2=TERM2
250 DN1=CNT
CNT=CNT+2.0
DEN=CNT*DN1
FAC2=X22/DEN
FACA2=B*FAC2
TERM2=TERM2*FACA2
AJ2=AJ2*TERM2
TER2=ABSF(TERM2)
DIF2=1.E+06*TER2
```



```

      IF(DIF2)210,210,8
210  GO TO 250
      8  AR1=RH01*SINF(DELTA1)*COAL
        AR2=RH02*SINF(DELTA2)*COAL
        Y1(J)=SINF(AR1)*AJ1*RH01**2
        Y2(J)=SINF(AR2)*AJ2*RH02**2
        RH01=RH01+0.05*USTAR1
        RH02=RH02+0.05*USTAR2
      9  CONTINUE
        SUMY1=0.0
        SUMY2=0.0
        DO11 M=1,9
          SUMY1=SUMY1+4.0*Y1(2*M)+2.0*Y1(2*M+1)
          SUMY2=SUMY2+4.0*Y2(2*M)+2.0*Y2(2*M+1)
      11  CONTINUE
        AMP1=0.05*USTAR1/3.0*(Y1(1)+SUMY1+4.0*Y1(20)+Y1(21))
        AMP2=0.05*USTAR2/3.0*(Y2(1)+SUMY2+4.0*Y2(20)+Y2(21))
        TAN1=EXT21*SIAL/(EXT31*COAL)
        TAN2=EXT22*SIAL/(EXT32*COAL)
        ALPR1=ATANF(TAN1)
        ALPR2=ATANF(TAN2)
        BZERO=BZ/360.0*PI*2.0
        EXT41=EXT31
        EXT42=EXT31*(EXT32-EXT31)*CEXP(D)
        EXT51=SQRTF(Q/EXT41)
        EXT52=CSORT(Q/EXT42)
        XP1=EXT41**2-EXT51**2
        XP2=EXT42**2-EXT52**2
        COALP1=GOSF(ALPR1)
        COALP2=GOSF(ALPR2)
        SIALP1=SINF(ALPR1)
        SIALP2=SINF(ALPR2)
        COALP12=COALP1**2
        COALP22=COALP2**2
        SIALP12=SIALP1**2
        SIALP22=SIALP2**2
        EXP1=CEXP(-G*XP1*COALP12)
        EXP2=CEXP(-G*XP2*COALP22)
        BTA1=BZERO*EXP1
        BTA2=BZERO*EXP2
        GOM1=1.0*CEXP(-RAN*XP1*SIALP12)
        GOM2=1.0*CEXP(-RAN*XP2*SIALP22)
        DIV1=(1.0+3.0*CCOS(BTA1)**2+GOM1*CSIN(BTA1)**2)
        DIV2=(1.0+3.0*CCOS(BTA2)**2+GOM2*CSIN(BTA2)**2)
        Z1(I)=SIALP1*COALP1*DIV1*AMP1*SIAL
        Z2(I)=SIALP2*COALP2*DIV2*AMP2*SIAL
        AL=AL+DA
      12  CONTINUE
        SUMZ1=(0.0,0.0,0.0)
        SUMZ2=(0.0,0.0,0.0)
        DO 13 N=1,8
          SUMZ1=SUMZ1+4.0*Z1(2*N)+2.0*Z1(2*N+1)
          SUMZ2=SUMZ2+4.0*Z2(2*N)+2.0*Z2(2*N+1)
      13  CONTINUE
        AHV1=DA/3.0*(Z1(1)+SUMZ1+4.0*Z1(18)+Z1(19))
        AHV2=DA/3.0*(Z2(1)+SUMZ2+4.0*Z2(18)+Z2(19))

```

```

      HV1=AK*AHV1**2/USTAR1**6
      HV2=AK*AHV2**2/USTAR2**6
      DELHV=HV2-HV1
      * [ ABSDEL=CABS(DELHV)
        ANGDEL=CANG(DELHV)
        TANGAMA=ATANF(ANGDEL)
        PRINT 15,AZG,HV2,DELHV,ABSDEL,TANGAMA
15    FORMAT(2X,F6.2,2X,C(E15.6,E15.6),2X,C(E15.6,E15.6),
12X,E15.6,2X,E15.6)
        AZG=AZG+DAZ
        IF(AZG-AZMA)3,3,16
16    GO TO 1000
999  STOP
      END

```

* N.B.

These two statements are replaced by following statements;

```

{ DHVR = DHVS(1)**
  DHVI = DHVS(2)**
  TANGAMA = DHVS(2)/DHVS(1)

```

** DHVR and DHVI are the real and imaginary part of the
complex H_V dynamic light scattering intensity (DELHV)

